Diversity and drivers of coral reef cryptofauna communities

Margaux Steyaert
Somerville College
University of Oxford

A thesis submitted for the degree of
Doctor of Philosophy
Hilary Term 2023

Supervised by:

Catherine Head
Michael Bonsall
Emma Ransome

Declaration

I declare that the work presented in this thesis is wholly my own work, under the supervision of Dr Catherine Head (Institute of Zoology, ZSL London / University of Oxford), Prof. Michael Bonsall (University of Oxford) and Dr Emma Ransome (Imperial College London).

This thesis is submitted in fulfilment of the requirements for the degree of Doctor of Philosophy in Zoology (DPhil) at the University of Oxford. No part of this thesis has been accepted, or is concurrently being submitted, for any degree, diploma, certificate or other qualification in this University or elsewhere.

Margaux Steyaert

Somerville College

Student number : 602891

January 2023

Word count: 47,470 (excluding title page, abstract, acknowledgments, table of contents, list of figures, list of tables, bibliography and Appendix)

Abstract

Tropical coral reefs are exceptionally biodiverse ecosystems, and many species within reefs remain undiscovered, undescribed or under-studied. This is especially true of organisms living hidden within the cavities and crevices of the reef matrix, the cryptofauna. Cryptofauna, and the cryptobenthic communities they form, make up a significant portion of animal diversity within coral reefs and play functional roles vital for reef productivity and trophodynamics. Globally, coral reefs are experiencing degradation due to climate-change and direct human impacts, and face mass biodiversity loss by the end of the 21st century. To predict the impacts of projected climate change on coral reefs, we must have a comprehensive understanding of the baseline diversity and composition of the communities they harbour. This thesis explores the diversity and drivers of cryptobenthic communities across the remote and protected Chagos Archipelago Marine Protected Area (MPA)(Central Indian Ocean), an important scientific reference site for the wider Indian Ocean due to its near-pristine status and minimal local human impacts. Standardised artificial substrates named Autonomous Reef Monitoring Structures (ARMS) were deployed across three reefs in 2018 and retrieved in 2019 and 2021 to collect image and genetic data on cryptobenthic communities.

Little research has been conducted on cryptobenthic communities in the Chagos Archipelago, and we have a poor understanding of their biodiversity across the MPA in comparison to other reefs of the Indo-Pacific. Here, a rich and highly diverse community of coral reef organisms is recovered using multi-marker (COI, 18S) metabarcoding, and significant spatial and temporal variability in the metazoan community composition of three reefs is observed. However, only 3-4% of the 18,436 COI sequence variants identified are assigned to species level. With high confidence I identify 168 fully described species, but 95% of these are not represented in online museum records which hold specimen collected from the archipelago. This indicates that the archipelago's reef biodiversity is likely far higher than presently understood. However, less than half of the species known to inhabit the archipelago have representative sequences in this study's classifier, which is used to assign taxonomy to sequences , highlighting how the current paucity of references databases hinders metabarcoding studies of cryptofauna.

Studies integrating biological and physical components of reef habitats are needed to understand how cryptobenthic communities may respond to shifts in environmental conditions. I show how ocean-facing and lagoonal reefs differ in environmental conditions, using seven *in-situ* environmental variables, and how this is reflected in the community composition of sessile cryptobenthic organisms. Internal waves are detected across ocean-facing reefs and found to maintain lower temperature conditions, and findings demonstrate the importance of using *in-situ* data, rather than *ex-situ* satellite-based data. Calcifying organism abundance significantly correlates with lower temperature profiles of ocean-facing reefs, but fleshy macroalgal abundance is associated with more variable profiles of pH and dissolved oxygen in a lagoonal habitat. Overall, results highlight habitat preferences of sessile invertebrate and algal groups within year-old communities and suggest which may be more resilient to climate-change induced increases in temperature and pH conditions.

All artificial substrates used to study coral reefs have inherent biases, and it is important to determine what those biases are when using them to study natural reefs. I compare sessile communities recovered on ARMS against those on dead tabular *Acropora sp.* coral, a common species in the archipelago, to help understand these biases. I find similar abundances of sponges, soft-tube worms and ascidians on both substrates, but that ARMS may significantly overestimate natural abundances of calcifying invertebrates and under-estimate those of hard corals, turf and crustose coralline algae. I also compare communities recovered, using metabarcoding, on ARMS versus those from filtered water samples (environmental DNA) collected in the vicinity. I find eDNA sampling may be a poor proxy for studying motile invertebrates, but valuable for studying sponges, as it detects 17 out of 20 most abundant sponge species as well as an additional 9 species not detected on ARMS.

Finally, I explore the use of fluorescence imaging to study ARMS sessile communities, and record 35 hard coral colonies on average per m^2 across study sites. I find overall coral abundance is equal between lagoonal and ocean-facing reefs, but that coral abundance in the lagoonal reef is higher on the undersides of ARMS plates than on top of them, a pattern not observed across ocean-facing reefs and potentially driven by higher sedimentation occurring in the lagoon. This study highlights how fluorescence imaging may be a valuable additional method for the study of cryptobenthic assemblages on ARMS and I recommend its integration within the ARMS toolkit.

In summary, this thesis significantly advances the knowledge of cryptobenthic communities of the Chagos Archipelago MPA, highlights its importance as a biodiverse scientific reference site, and furthers our understanding

of the ARMS methodology. Whilst further work will be needed to fully characterise cryptofauna biodiversity across these reefs, findings presented in this thesis provide a baseline for future studies of these complex communities across the Indian Ocean region.

Funding

For funding, major thanks are extended to the Bertarelli Programme in Marine Sciences for funding my university fees, stipend and research costs. Thanks also to Somerville College and the Marya Antonina Czalicka Fund for funding a postgraduate course in bioinformatics which was of great help for this thesis.

Acknowledgments

Firstly, I'd like to thank my supervisors Catherine Head, Emma Ransome and Michael Bonsall for their advice, guidance and support throughout this thesis. Catherine, thank you for entrusting this project to me, and giving me the opportunity to explore a new side of coral reef diversity. It was a pleasure diving and travelling with you! Emma, thank you for agreeing to be my supervisor halfway through this project, I'm so glad to have joined your team and look forward to more ARMS brainstorming in the future. Mike, thank you for all your support at Oxford, organising trips to the other side of the world isn't the easiest so thank you for helping me get there (and back!) and for overseeing this project.

I'd like to thank our collaborators from Stanford University, Prof. Rob Dunbar, Dr David Mucciarone, Alexy Khrizman and Dr Mathilde Lindhart. It was great to meet you all, and a pleasure to work with you in the field and on our research paper. Thank you for teaching me about the physics and chemistry of coral reefs, I've learned so much through working with you. What a team!

I want to say thank you to Nadia Santo-Domingo for your friendship and guidance since the pandemic – thank you for teaching me how to identify sessile critters, and for agreeing to work with me on all the sponges I've collected throughout this project.

I want to say a big thank you to Rosie Dowell, Nick Dunn and Hannah Wood for helping me in the field, collecting and processing ARMS on a boat is tough, smelly and really tiring and I literally couldn't have done it without you! Rosie and Nick, thank you for your friendship and help throughout this PhD, and for being awesome dive buddies, may our underwater adventures continue. I also want to say thanks to Bry Wilson, another important dive buddy, thank you for inviting me to work with you in the field.

Thank you to Dada Gotelli, Kevin Hopkins and Chris Yesson, who have provided tremendous support for this project at the Institute of Zoology (IoZ) at ZSL, both in the labs and in the offices. Doing barcoding and metabarcoding through a pandemic was not easy, so thank you so much for all your help.

I'll be forever grateful to have had the privilege to work in the Chagos Archipelago MPA, it really is one of the most beautiful and special places on earth. Thank you to Rachel, Emma and Sharmin, without whom we wouldn't have expeditions to this remarkable part of the world. Thank you for all your help and kindness.

Thanks also to the crews of the Grampian Frontier and the Grampian Endurance, without whom the ARMS would not have made it out of the water in the first place. Their support for science on expeditions was crucial.

I would like to thank the Bertarelli Programme in Marine Sciences for funding this project and for awarding me a stipend extension when the pandemic hit.

Finally, I would like to thank my friends, my family and my partner Kai, your support means the world. Thank you, Manon and Kai, for being my rocks, I love you both very much. My parents are the best, thank you for helping me through my seemingly never-ending studies, I love you both, bisous.

I'd like to dedicate this thesis to all my grandparents, who taught me to be creative and love the ocean in the first place. As oceanographers, ship captains and artists, you continue to inspire me to explore and study the ocean, and all the wonderful and beautiful things that inhabit it.

Far and away, the greatest threat to the ocean, and thus to ourselves, is ignorance. But we can do something about that.

- *Dr Silvia Earle*

How can a creature that spends all of its time underwater smell so bad?

- *Spongebob Squarepants*

And remember, science is hard!

- *Professor Rob Dunbar*

COVID-19 Impact Statement

Field sampling was interrupted in March 2020 due to travel restrictions imposed by the Covid-19 global pandemic, resulting in the abrupt cancelling of field research and therefore no samples were retrieved across sample sites that year. Instead, samples intended for collection in 2020 were retrieved in March 2021, and those meant to be retrieved in 2021 were instead collected in October 2022. The analysis of samples collected in late 2022 was not carried out in time for the submission of this thesis. As such, this impacts Chapter 2, which aimed to study community succession over a three-year period. In addition, lab work was postponed and delayed in 2020 and 2021 as access to laboratories at the Institute of Zoology (ZSL, London) was restricted and the delivery of consumables was delayed. This has resulted in the barcoding of invertebrate samples to be incomplete and therefore presented in the Appendix section of this chapter instead of the main body of this thesis.

Contents

List of Figures

List of Tables

CHAPTER 1

Introduction

1.1 Coral reefs

Biological diversity positively correlates with the structural and compositional complexity of natural ecosystems (Kovalenko et al., 2012). The 'habitat heterogeneity hypothesis' puts forward the argument that a complex habitat caters for the needs of many species by providing varied environmental resources, and that habitat heterogeneity increases the number of ecological niches available, which in turn promotes speciation and ultimately sustains high biological diversity (Pierre & Kovalenko, 2014; Stein et al., 2014). This concept has been widely discussed and tested across terrestrial ecosystems (reviewed in Tews et al., 2004), and to some extent across marine ecosystems (Cox et al., 2021; Nash et al., 2013; Gratwicke & Speight, 2005).

Modern coral reefs are shallow marine habitats dominated by structurally complex scleractinian corals. The 3D structure which corals form with their skeletal structures, deemed the reef matrix, in turn provides habitat for highly biodiverse reef-associated assemblages of vertebrate, invertebrate and microbial organisms. Whilst estimated to cover an area of just ~300,000km^2 globally (0.1-0.5% of ocean floor)(Spalding et al., 2001), coral reefs are exceptionally productive systems (Crossland et al., 1991).

This is especially true of tropical coral reefs, which occur within nutrient poor warm waters, and yet harbour dense and biodiverse communities (Knowlton et al., 2010; Reaka-Kudla, 1997; Small & Spoon, 1998). Estimates of total species richness within coral reef ecosystems range between 550,000 and 1,330,000, with many metazoan groups still to be discovered or described (Fisher et al., 2015).

A total of 128 countries are bordered by coral reef ecosystems and 108 million people live within 5km of a coral reef, a figure which has rapidly increased over the last two decades (Wong et al., 2022). Coral reefs ecosystems provide a myriad of direct and indirect ecosystem services to humankind (Woodhead et al., 2019), such as providing food, revenue and cultural value. In the age of the Anthropocene, coral reefs face imminent threats such as habitat degradation and biodiversity loss directly caused by humankind (Hughes et al., 2017). Around the globe, reefs are already experiencing the impacts of climate change with increasingly frequent instances of high mortality bleaching events (Hughes et al., 2003). Some studies predict shallow coral reefs found within at-risk areas, such as the tropics, could ultimately undergo phase shifts into microbialised or algal and sponge-dominated states (Bell et al., 2018; Loh & Pawlik, 2014; Bell et al., 2013; Pawlik et al., 2013). As climate change increasingly impacts and threatens coral reefs around the globe, the need to thoroughly assess the biological diversity of these ecosystems upon which humankind depend on has never been so urgently needed.

1.2 Coral reef cryptofauna

The network of cavities and recesses within reef matrices have been estimated to account for up to two-thirds of the total volume of coral reef habitats (Ginsburg, 1983). The communities of organisms living within this hidden framework are referred to as ‘cryptofauna’ or ‘cryptobenthos’ and include taxa spanning almost all major animal groups (Reaka-Kudla, 1997; Kobluk, 1988). Cryptofauna can be found associated with both live and dead coral communities, and coral rubble, and can be classified as either motile or sessile.

Motile benthic invertebrates are highly diverse within reef matrixes (reviewed in Gibson et al., 2011). These organisms hail from a variety of taxonomic groups including arthropods, annelids, gastropods, echinoderms, platyhelminths as well as nemertean, nematode, hemichordate and sipunculid worms

(Goldberg, 2013). These taxa are found across a range of micro-habitats within the reef matrix as facultative or obligate coral-dwellers (Britayev et al., 2017; Molodtsova et al., 2016), or living within other sessile invertebrates (García-Hernández et al., 2019; Henkel & Pawlik, 2011).

As highly diverse communities, mobile macrofaunal (>500um) and meiofaunal (40um-500um) invertebrates carry out many functional roles within coral reef ecosystems as deposit/filter feeders, herbivores, carnivores/predators and corallivores (Glynn and Enochs, 2011; Gibson et al., 2011). For example, obligate coral-dwelling decapods such as coral guard crabs (Trapeziidae) and snapping shrimps (Alpheidae) can protect adult coral hosts from corallivores (Pratchett, 2001), and maintain coral health by actively removing sediment (Stewart et al., 2006). Other macroinvertebrate such as urchins and herbivorous crabs help to regulate algal growth (Francis et al., 2019; Klumpp & Pulfrich, 1989), whilst crustaceans such as shrimp contribute to the breakdown of organic detritus such as fish faeces (Rothans & Miller, 1991) and coral mucus (McCloskey, 1970). Ultimately, many cryptofauna taxa are an important food source to invertivorous reef fish (Kramer et al., 2013; Leray et al., 2013). Furthermore, the density of mobile cryptofauna on reefs has been shown to be very high. For example, Klumpp et al. (1988) recorded up to 570 cryptic crustaceans and molluscs per m^{-2} of reef space whilst 160 decapod per m^{-2} of dead coral head surface was recorded by Head et al. (2018).

Sessile groups inhabiting intra-reef cavities often include filter and suspension-feeding organisms such as sponges, colonial or solitary ascidians, bryozoans, bivalved molluscs and tubed polychaete worms, as well as foraminifera and algal groups such as fleshy red and brown macroalgae and crustose coralline algae (CCA). Most of these groups are also often found on exposed reef surfaces (Kornder et al., 2021; Higgins et al., 2019). However, the composition of sessile cryptobenthic communities is known to be significantly different than those found on exposed reef surfaces (Kornder et al., 2021). Sessile groups can play an important role in shaping cryptic cavity habitats for the wider cryptobenthic community as bioeroders or reef-builders. For example, cryptic sponges can support coral colonies by acting as a ‘glue’, holding weakened or broken coral colonies to the reef frame (Biggs, 2013; Wulff, 1984; Goreau & Hartman, 1966) or provide macroinvertebrates and small fish with breeding grounds and spaces in which to inhabit and shelter away from predators (García-Hernández et al., 2019; Tyler & Bohlke, 1972). Bivalves can also act as bioeroders as they bore into reef substrate (e.g., lithophagine

bivalves)(Glynn & Manzello, 2015), or as habitat providers in the case of giant clams (Neo et al., 2015). Coralline crustose algae can often be found within reef cavities (Scheffers et al., 2010) and have been shown to increase the structural integrity of the reef matrix as well as promote larval recruitment of coral recruits (Gómez-Lemos et al., 2018). Other groups such as bryozoans, foraminiferans and serpulid worms are also important framework-building organisms and contribute significantly to overall reef accretion (Mallela, 2007). Thanks to sessile organisms and the diversity of microbes which they harbour, reef cavities are powerhouses of primary productivity (Kramer et al., 2014; de Goeij et al., 2013). For example, sponges play a key role in benthic-pelagic coupling and have been suggested to account for up to 90% of nutrient cycling within DOM reincorporation pathways on tropical coral reefs (Rix et al., 2016; de Goeij et al., 2013).

1.3 How and why cryptofauna are understudied

Despite dominating metazoan reef diversity and biomass, both mobile and sessile cryptofauna are understudied in comparison to more conspicuous reef groups such as hard corals and fish (Brandl et al., 2019). A simple literature search across academic research of the last 20 years highlights this bias (Figure 1.1). Studies focusing on reef functioning (Bellwood et al., 2019), morphological traits (Zawada et al., 2019) and overall coral reef ecology (Williams et al., 2019) have often focused on fish or hard corals. For instance, many cryptofauna are calcifiers but groups such as bryozoans are often left out of reef carbonate budget studies as well as literature on reef biomineralization (Lange et al., 2020; Januchowski-Hartley et al., 2017; Perry & Morgan, 2017). Within cryptobenthic communities, many studies have focused on cryptobenthic fish and their diversity (Brandl et al., 2018), their role within reef trophodynamics (Depczynski et al., 2003) and the factors which drive their composition (Ahmadia et al., 2018; Coker et al., 2018).

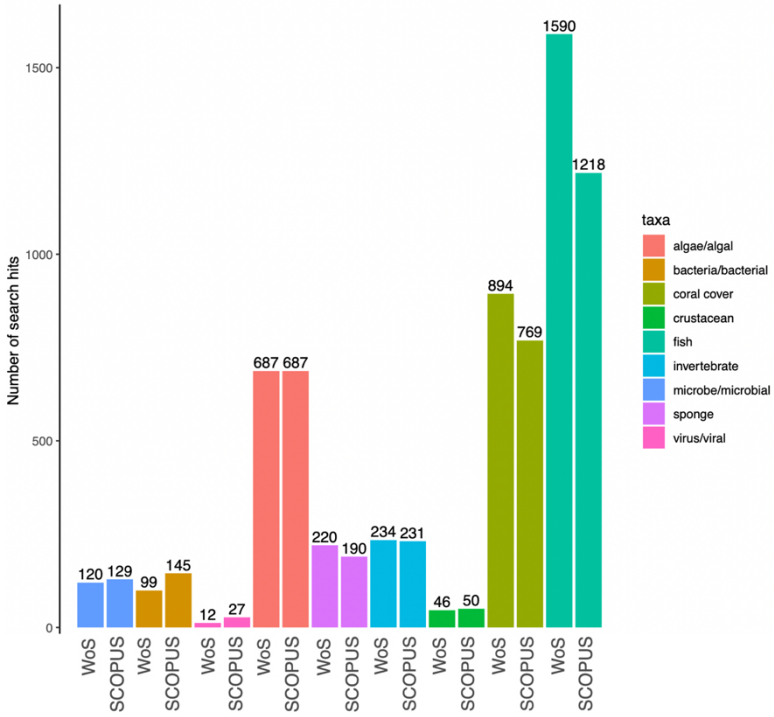

Figure 1.1. Bar chart summarising the number of research articles focused on individual taxonomic groups across coral reef communities in the last 20 years. Systematic searches were carried out across both Web of Science (WoS) and SCOPUS search engines and had to include the term 'coral AND reef' as well as 'monitoring' or 'indicator' or 'assessment' for each taxa of choice. For algae, microbes and viruses, the terms 'algal', 'microbial' and 'viral' were also searched for. Numbers above each bar indicate the total number of search hits for which these terms were found within the title or keywords.

There are several reasons why invertebrate cryptofauna are understudied in comparison to other metazoan groups on coral reefs. Firstly, cryptofauna are often small and live in close association with the reef matrix so observing or collecting them *in-situ* is more difficult than larger organisms found on exposed reef surfaces or in the water column. Cryptofauna can also be camouflaged or burrowed within reef surfaces, meaning conventional photo or video-based survey methods are not likely to recover their presence. Cryptofauna communities are also highly speciose, and often harbour many rare and regionally specific species (Head et al., 2018; Takada et al., 2007). Identifying specimens across cryptofauna communities requires the expertise of multiple taxonomists and can be labour intensive. For some groups, such as nematode worms and microgastropods, classical morphology-based methods alone can fall short for group identification (Middelfart et al., 2016). There is also an imbalance

in the availability of taxonomic identification guides for different cryptobenthic groups (Costello et al., 2010) with crustaceans having some of the highest numbers of guides per geographical region (*n* = 14), compared to bryozoans and platyhelminthes for which there are much fewer (*n* = 2). Overall, the number of taxonomic studies has increased since the mid-2000s (Costello, 2015a) but our need for taxonomic expertise is also rapidly increasing as we race to characterise ecosystems facing major species extinction (Costello et al., 2015b).

Cryptofauna are also under-represented within biomonitoring initiatives. Major global frameworks for coral reef observations and monitoring include the Global Coral Reef Monitoring Network (GCRMN), the Global Ocean Observing System (GOOS) and the Group on Earth Observations' Biodiversity Observation Network (GEO-BON)(Pereira et al., 2013). Essential Ocean Variables (EOVs) were created by GOOS to simplify and streamline ocean observations and are spread across Physics, Biochemistry and Biology & Ecosystems categories, with EOVs in the latter category focused on measuring the biomass, distribution and composition of individual taxonomic groups (Miloslavich et al., 2018; Pereira et al., 2013). Currently, hard coral cover and composition, fleshy algal cover, as well as fish abundance and diversity are the top three EOVs used for monitoring and reporting coral reef health (Obura et al., 2019). One proposed but currently undeveloped EOV focuses on benthic invertebrates. First proposed in 2017 as 'Invertebrate Abundance and Distribution', this EOV has since been renamed to 'Benthic Invertebrates' but is still under development and lacks a specification sheet otherwise available for all other EOVs within the Biology and Ecosystems category (GOOS Meeting Reports).

The future of coral assemblages across reefs will likely be determined by species-specific responses or vulnerabilities to local stressors (Camp et al., 2018). This is likely to be the same for cryptobenthos, as taxa groups have been shown to respond differently to changes in the environment. For example, sponge communities may be more resilient than other sessile groups to increased sedimentation (Cummings et al., 2020; Biggerstaff et al., 2017) or ocean warming and acidification under future climate change scenarios (Bennett et al., 2018; Bennett et al., 2017). In fact, it has been shown that increased OA can be a strong driver of sponge-mediated erosion of the reef matrix (Stubler et al., 2014). Ascidians, another common group within cryptobenthic communities, can smother and overgrow corals (Littler & Littler, 1995), and have been shown to increase in abundance on degraded reefs (Roth et al.,

2018) and following bleaching events (Tebbett et al., 2019). Several lab and field studies report varied effects of decreased pH on the abundance and mortality rates of ascidian communities, with most suggesting these organisms could benefit from elevated CO_2 levels (Peck et al., 2015; Dupont & Thorndyke, 2009; but see Fabricius et al., 2014). Like for other calcifying marine taxa, ocean acidification also poses a risk to bryozoan communities by reducing growth rates and increasing skeletal dissolution (Durrant et al., 2013). However, it has also been shown that whilst colony growth is reduced or halted at high temperatures, the reproductive success of adults and the swimming ability and recruitment success of larvae remains resistant (Pecquet et al., 2017; Pistevos et al., 2011). Furthermore, as asexually reproducing colonial organisms, bryozoans may have the phenotypic plasticity to adapt to acidifying conditions by balancing metabolic investments (Swezey et al., 2017). Fabricius et al. (2014) and Plaisance et al. (2021) found that increased pH conditions can lead to significant declines across both motile and sessile taxa, and that loss of habitat complexity resulted in significant reductions of macro-invertebrate groups such as crustaceans and some echinoderms.

1.4 Studying cryptofauna on live or dead coral

Various methods can be used to collect coral reef cryptofauna including direct sampling from live coral colonies (Enochs, 2012), dead coral heads (Head et al., 2015; Plaisance et al., 2011), coral rubble (Wolfe et al., 2021), epilithic algal matrix and sediment (Kramer et al., 2013), or from artificial devices and recruitment plates (Monroy-Velasquez et al., 2020; Zimmerman et al., 2004). Live hard coral colonies can harbour abundant communities of motile cryptofauna, likely due to the trophic benefits conferred to organisms from the host coral (Enochs, 2012). Although the habitat structure and conditions conferred by a living branching coral hosts differ significantly from those of deep-set cryptic cavities of the reef matrix, several studies have shown that cryptofauna density and diversity can be as high or higher within cavities or within dead coral rubble than on live coral hosts (Stella et al., 2022; Enochs et al., 2011).

Dead coral colonies and coral rubble, which arises from the breakdown of the skeletal structure of dead hard corals and form loose deposits on the reef floor, can also harbour diverse cryptobenthic communities (reviewed in Wolfe et al., 2021), and can be colonised by cryptofauna as soon as 2-4

weeks (Takada et al., 2007). Many studies have used dead coral colonies or coral rubble to collect and study cryptofauna (Head et al., 2018; Takada et al., 2016; Head et al., 2015; Kramer et al., 2014). The study of dead coral cryptofauna can be standardised to some extent by ensuring the same weight of substrate is collected, or by placing rubble deposits in mesh bags or baskets of specific sizes (Enochs et al., 2011; Takada et al., 2007). Valles et al. (2006), developed Standard Monitoring Units for Recruitment of Fishes (SMURFS), which use coral rubble, mesh, and plastic containers to trap cryptobenthic fish. More recently, Rubble Biodiversity Samplers, which are 3D printed coral rubble models, were developed to study rubble communities and associated organisms in a standardised manner (Wolfe & Mumby, 2020).

1.5 Artificial structures and materials for studying cryptofauna

Artificial materials and structures have long been used to study ecological trends and processes within coral reef ecosystems. Settlement plates are a common tool used to assess the rate of settlement and survival of hard coral recruits (Mundy, 2000; Dunstan & Johnson, 1998; Harrison & Wallace, 1990), fish grazing behaviour and pressure (Ayalon et al., 2010), sedimentation (Babcock & Smith, 2002), calcium carbonate accretion (Johnson et al., 2022) and invertebrate recruitment (Higgins et al., 2019; Luter et al, 2016). Recently, Levy et al., (2023) showed how ceramic tiles with 3D printed grooves and micro-ridges can be used to collect data on cryptobenthic communities using environmental DNA sampling. Large reef structures composed of artificial materials are also now employed to aid the restoration and conservation of reef ecosystems (reviewed in Higgins et al., 2022), by providing additional substrate for the settlement of coral recruits and increased habitat heterogeneity for fish and invertebrates. Artificial substrates intended for the collection of marine cryptofauna can be classed as dendritic (e.g., branching-like) or crevice-like, and it has been shown that both types can harbour different assemblages of macrofauna (Carreira-Flores et al., 2021).

One of the advantages of artificial structures for the study of cryptofauna is the non-destructive aspect of the method; no live or dead natural substrate needs to be removed or detached from the reef matrix. Several studies have shown that most cryptofauna found on natural surfaces will colonise and recruit onto artificial devices also (Plaisance et al., 2011; Yakovis et al., 2007). Other advantages of artificial

devices and substrates include increased standardisation for sample collection as the shape of size of structures can be more easily regulated. There are also disadvantages to using artificial structures and man-made materials for the study of cryptobenthic communities. Firstly, different materials used to build artificial structures can have their own inherent biases when it comes to the recruitment and attachment of organisms, due to differences in density or rugosity (Randall et al., 2021; Mallela et al., 2018; Salinas de León, 2011; Harriott & Fisk, 1987). Although durable materials (e.g., polyvinyl chloride plastic, 3D printed concrete and flax-based polylactic acid) can positively influence hard coral recruitment and extent of live cover by sessile communities, others such as ceramic and porous concrete can yield significantly less sessile recruitment than observed on natural substrates (Leonard et al., 2022). Another disadvantage is the time required for communities to colonise and develop on artificial substrates, which can range from 3 months to several years depending on the structure used and study objectives (Baronio & Bucher, 2008; Pearman et al., 2018). The use of artificial structures means that data cannot be obtained instantaneously, and studies employing such devices must be planned in advance and deployment times standardised in order to gather comparable data (Obst et al., 2020).

1.6 Autonomous Reef Monitoring Structures

Autonomous Reef Monitoring Structures (ARMS) are artificial structures used for the collection and study of marine benthic organisms. They were first described by Zimmerman et al. (2004) as a tool for collecting cryptofauna, and were originally composed of concrete plates, PVC pipes and mesh bags containing coral rubble, and weighed over 30kg. These artificial devices were then re-designed and deployed by the Census of Marine Life's CReefs Program (Knowlton et al., 2010). Currently, these instruments are composed of 9 stacked polyvinyl chloride (PVC) plates (23.5cm x 23.5cm) with alternating 'open' and 'closed' gaps created by the addition of PVC crossbars, which together can be attached to the reef matrix using a larger base plate (Figure 1.2). Coral rubble is no longer included in the makeup of ARMS. These tiered devices are larger and provide more micro-habitat complexity than single-plate or simpler-designed artificial settlement devices such as Calcification Accretion Units (CAUs)(Johnson et al., 2022). Overall, these devices were created to systematically collect and assess cryptobenthic biodiversity from marine systems.

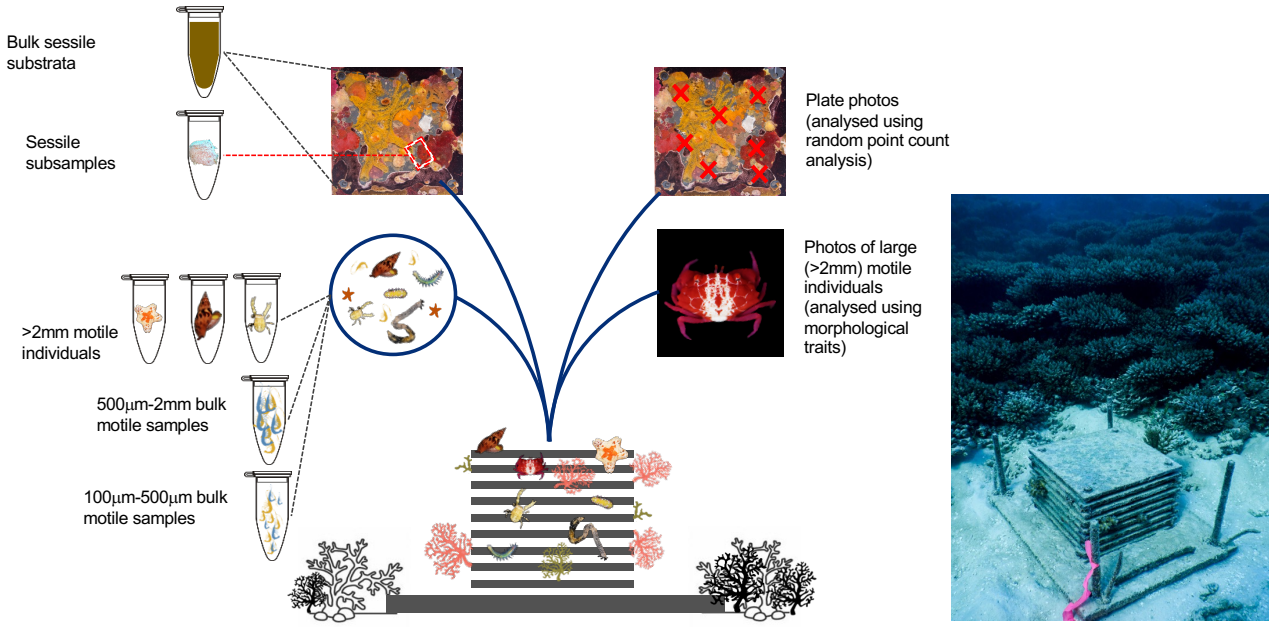

Figure 1.2. Graphic summarising ARMS processing steps including the fractioning of motile and sessile communities destined for either image-based (right-hand side of graphic) or genetic analysis (left hand side of graphic). A photograph of an ARMS *in-situ* on a reef studied in this thesis is also provided.

A series of standardised field and laboratory protocols for the deployment, collection, processing of image and genetic data from ARMS are available for researchers to use from the Global Ocean ARMS Project website (https://naturalhistory.si.edu/research/global-arms-program). Broadly, these recommend first separating motile organisms from sessile communities, and fractioning the former into size classes (>2mm, 500um-2mm, 100-500um). Whilst the larger class of mobile organisms (>2mm) should be photographed and individually barcoded, the two smaller classes (500-2mm, 100-500um) should be metabarcoded. The sessile communities inhabiting ARMS plates should first be photographed for downstream image-based community analysis, and then scrapped, homogenised, and analysed using metabarcoding. Tissue samples from sessile specimens can also be photographed and individually vouchered as is done for >2mm motiles. A range of genetic regions can be targeted based on the target community of choice, but standardised protocols recommend the barcoding of the full Folmer region of the cytochrome oxidase I (COI) mitochondrial gene, and short fragments of the COI and 18S rRNA genes for metabarcoding analyses.

Leray et al. (2015) first provided field and laboratory protocols for the barcoding and metabarcoding analysis of ARMS data. Ransome et al. (2017) then provided recommendations for the collection and processing of ARMS community samples intended for metabarcoding, to better standardise biodiversity estimations using metabarcoding. Since then, Chang et al. (2020) has demonstrated successful application of Nanopore sequencing, using the MinION platform, to expedite the barcoding of motile macro-invertebrates from ARMS. Recently, Nichols et al. (2021) compared ARMS and water samples to show the potential of environmental sampling for studying cryptobenthic communities and Casey et al. (2021) reaffirmed the importance of multi-marker metabarcoding for analysing ARMS communities. Whilst Ransome et al. (2017) first showed that ARMS plate image-analysis could be used to supplement community metabarcoding, David et al. (2019) showed how image analysis alone could recover significant patterns of ARMS sessile cryptobenthos across regions and environmental gradients. Since then, Steyaert et al. (2022a)(Chapter 5) demonstrated the potential of fluorescence imaging for studying coral and cryptobenthic organisms on ARMS.

According to the last online publication by the Global Ocean ARMS Project's website in 2019, almost 1900 ARMS have been deployed across marine systems since 2006 (https://naturalhistory.si.edu/research/global-arms-program/get-involved). To date, 35 research articles utilising modern ARMS to collect, study and publish data on marine ecosystems have been published, with more studies released every year (Table 1.1). Whilst ARMS have been deployed across temperature and cold-water regions (Obst et al., 2020; Pennesi & Danovaro, 2017), almost all studies so far have focused on tropical coral reef ecosystems (Table 1.1). An average of 20 ARMS are deployed per study, for an average of 26 months (Table 1.1), with Obst et al. (2020) reporting data from the greatest number of ARMS (134), followed by Pearman et al. (57). Morphological analysis has been the most used method for studying ARMS (19 studies), followed by metabarcoding (18 studies), barcoding (13 studies), whilst plate photo analysis has been the least popular method (9 studies). Lastly, 83% of ARMS-based studies so far are open access.

Table 1. Summary of current ARMS published literature, methods used; P = plate image analysis, B = barcoding, M = metabarcoding, Mo = morphological identification, along with the number of ARMS, length of ARMS deployment (months), number of sites, region of study, open access status (OA), and additional comments (e.g., mesocosm or mock community-based studies).

Authors	Year	Method	ARMS	Deployment	Sites	Region	OA	Comments
Steyaert et al.	2022	P	9	36	3	Chagos Archipelago	Yes	
Villalobos et al.	2022	B, M	33	12, 38, 72	4	Red Sea	Yes	
Sundberg et al.	2022	M	16	4	16	Sweden	Yes	
Reid et al.	2022	M	3	36	3	Palmyra Atoll	Yes	
Steyaert et al.	2022	P	9	36	3	Chagos Archipelago	No	
Ip et al.	2022	B, M	12	24	4	Singapore	Yes	
Vicente et al.	2022	B, Mo	36	24	2*	Hawaii	No	*mesocosm
Longenecker	2022	Mo	1	24	1	Hawaii	Yes	
Vicente et al.	2022	Mo, P	6	24	*	Hawaii	Yes	*mesocosm
Coneo-Gomez et al.	2022	Mo	4	6, 8, 12, 18	1	Colombia	Yes	
Timmers et al	2021	B, M, Mo	12	24	*	Hawaii	Yes	*mesocosm
Nichols et al.	2021	M	6	23	2	Hawaii	Yes	
Plaisance et al.	2021	B, Mo	36	24, 30	2	Papua New Guinea	Yes	
Casey et al.	2021	M	9	12	2	Indonesia	Yes	
Longenecker	2021	Mo	1	12	1	Hawaii	Yes	
Longenecker	2021	Mo	1	34	1	Hawaii	Yes	
Palomino-Alvarez et al.	2021	Mo, P	8	12	2	Mexico	Yes	
Yang et al.	2021	Mo	na	12	na	Korea	na	
Pearman et al.	2020	Mo	54	12-14	18	Black Sea, Mediterranean, Red Sea, Baltic Sea, Biscay	Yes	
Timmers et al.	2020	B, M, Mo	12	24	*	Hawaii	Yes	*mesocosm
Chang et al.	2020	M	12	24	4	Singapore	Yes	
Obst et al.	2020	M, Mo, P	134	mixed	86	Europe	Yes	
Servis et al.	2020	B, Mo	na	24	3	Palmyra Atoll	No	
Carvalho et al.	2019	M	66	24	22	Red Sea	Yes	
Hazeri et al	2019	Mo	24	24	3	Indonesia	Yes	
David et al.	2019	Mo, P	36	16	12	mixed	Yes	
Pearman et al.	2019	M	57	24-36	19	Red Sea	Yes	
Pearman et al.	2018	B, M	33	24	11	Red Sea	Yes	
Ransome et al.	2017	M, P	3	24	1	French Polynesia	Yes	
Leray & Knowlton	2017	B, M, Mo	na	na	na	Florida	Yes	*mock com.
Pennesi & Danovaro	2017	Mo	10	13	3	North Adriatic Sea	No	
Al-Rshaidat et al.	2016	B, M	6	16	2	Red Sea	Yes	
Hurley et al.	2016	Mo, P	18	24	3	Hawaii	No	
Pearman et al.	2016	M, Mo, P	9	12	3	Red Sea	Yes	
Leray & Knowlton	2015	B, M	18	6	6	Florida	Yes	
Plaisance et al.	2011	B	15	12	2	Indo-Pacific, Caribbean	Yes	

One of the main goals for ARMS-based studies is to establish global baselines of cryptobenthic diversity. Several ARMS studies have recorded and characterized the biodiversity of crustaceans across tropical regions. Plaisance et al (2011) identified 525 species by co-analysing dead coral and ARMS across the Indo-Pacific, demonstrating the usefulness of ARMS to standardise and expedite the collection of cryptic invertebrates from different geographical regions. Studies such as Hurley et al. (2016) and Hazeri et al. (2019) used ARMS to collect brachyuran and anomuran crabs across shallow and mesophotic reefs of the Red Sea and Indonesia, but their findings highlighted the difficulty of identifying such taxa to species level using a morphometric approach alone. Servis et al. (2020) combined morphological identification with barcoding of the 16S and COI genes to present novel data on brachyuran crabs from the Palmyra Atoll in the Central Pacific.

Others have presented new records of species from multiple cryptofauna taxa, such as annelids, cnidarians and platyhelminths across reefs of New Mexico (Palomino-Alvarez et al., 2021), and Colombia (Coneo-Gómez et al., 2022). Studies by Ken Longenecker presented new records of amphipod species in Hawai'i (Longenecker, 2021a), and discovered new species from this taxonomic group (Longenecker, 2022; Longenecker, 2021b) using ARMS as his collection tool. Fewer studies have focused on sessile cryptobenthos, but Vicente et al. (2022) showed ARMS to be a valuable for the study of cryptic sponges using barcoding, providing 150 new records for these under-studied taxa and increasing the known sponge fauna of the Hawaiian Islands by 2.5-fold.

Metabarcoding, whereby high-throughput sequencing is used to identify multiple species from mixed community and environmental samples, is gaining popularity for the study and biomonitoring of diverse ecosystems (Makiola et al., 2020). Several ARMS-based studies have utilised metabarcoding to characterise cryptobenthic communities and their associated microbiomes across tropical regions such as the Red Sea (Villalobos et al., 2022; Carvalho et al., 2019; Pearman et al., 2019; Pearman et al 2018; Pearman et al., 2016; Al-Rshaidat et al., 2016), Hawaiian Islands (Timmers et al., 2021; Timmers et al., 2020), Palmyra Atoll (Reid et al., 2022) and Singapore (Ip et al., 2022), as well as temperate waters of Florida and Virginia (Leray & Knowlton, 2015), and Korea (Yang et al., 2021).

The highly standardised format of ARMS, and the protocols used to process samples from them, ensures that data can be compared across spatial and temporal scales. Indeed, several studies have used ARMS to compare the diversity of cryptobenthic communities across reefs within specific regions (Villalobos et al., 2022), or across wider latitudinal or longitudinal gradients (Pearman et al., 2018). This has led to studies investigating the relationship between cryptobenthic communities and natural environmental conditions (Steyaert et al., 2022b; David et al., 2019; Pearman et al., 2018). Plaisance et al. (2021) used ARMS in an experimental set up across sites with varying pH conditions and found that whilst motile cryptofauna abundance and diversity decreased in lower pH sites, the response of individual gastropods and crustacean taxa varied across test conditions. Using a mesocosm set-up, Timmers et al. (2021) found that increases in combined temperature and pH conditions led to subtle shifts in composition within cryptobenthic communities, and not community collapse as was predicted. Findings from these studies highlight the complex and non-linear responses of cryptobenthic taxa to differences in physical-chemical conditions and demonstrate the need to investigate whole communities as well as individual taxonomic groups.

Thanks to developments in the ARMS method these devices are useful biomonitoring tools. Recently, Sundberg et al. (2022) showed how ARMS can be used to monitor the threat of invasive species. Pennesi & Danovaro (2017) explored how ARMS microphytobenthos could be used as indicator taxa to monitor nutrient levels and changes in environmental conditions. To effectively monitor change in benthic communities over time, large numbers of ARMS across multiple locations must be co-analysed. A new network comprised of ARMS across 20 European observatories, named ARMS-MBON, was announced in 2020 following an initial 30-month phase (Obst et al., 2020). This initiative combines efforts across international teams and centralised the genetic analysis of ARMS as well as the management and storage of resulting datasets. The pilot study worked to establish standards across ARMS sampling and analysis steps and now aims to expand the network of observatories across European waters. No such initiative has yet been set up for the biomonitoring of tropical coral reefs using ARMS.

1.7 Advantages and disadvantages of the ARMS method

Studies so far have shown that ARMS are well suited for the study of marine benthic communities, including those found on coral reefs, but several limitations remain for the ARMS method. Firstly, the use of artificial materials, such as PVC in the case of ARMS, carries its own inherent biases (Sanabria-Fernandez et al., 2018; Chase et al., 2016). Whilst the benefits of using standardised devices with simple designs are clear, surprisingly few studies have directly compared ARMS communities with those found on natural reef surfaces (but see Nichols et al., 2021; Plaisance et al, 2011).

There are strengths and weakness to both image-based and genetic analyses. Image-based analyses can recover the abundance of cryptobenthic groups, or even the biovolume of individual groups if using 3D methods (see Kornder et al., 2021), but are constrained by image-resolution and taxonomic expertise. Genetic approaches, including both metabarcoding and barcoding, can recover immensely large and detailed datasets from ecological samples, but are limited by still incomplete reference databases (Hestetun et al., 2020), meaning large portions of sequence data collected are left un-identifiable. Metabarcoding is also subject to biases along laboratory and bioinformatics workflows and resulting community estimates can be greatly influenced by primer bias (van der Loos, 2021) as well as error-filtering, clustering, and curation parameters for sequence processing (Antich et al., 2021; Alberdi et al., 2019). Advances in automated image processing, e.g., the use of machine-learning algorithms for benthic analysis (Chen et al., 2021; Gonzalez-Rivero et al., 2020), and the improvement of reference databases will no doubt eventually reduce these limitations. For the latter, the Moorea Biocode Project (https://ocean.si.edu/ecosystems/coral-reefs/moorea-biocode-project), and the Sponge Barcoding Project (https://www.spongebarcoding.org/), are example of initiatives trying to tackle the paucity of genetic reference libraries for understudied cryptobenthic groups.

ARMS are an exciting new tool for the study of cryptobenthic reef communities, and many future avenues remain for this field. ARMS are gradually being used across global coral reefs, and whilst regions such as the Red Sea are now relatively well characterised (Villalobos et al., 2022; Pearman et al., 2018), no studies to date have presented ARMS data (image or genetic) for the Indian Ocean region, which hosts a diverse array of coral reef ecosystems. Many ARMS have been deployed and collected

across the globe, but it is unclear how many have been retrieved, processed, and analysed beyond those reported in research articles.

Metabarcoding of ARMS communities can inform on the breadth of biodiversity within reef ecosystems, but ARMS could also be an advantageous tool for the study of cryptobenthic microbiomes and their response to the environment, for example using molecular techniques such as metabolomics and metatranscriptomics. Quantifying the biomass of individual cryptofauna taxa collected on ARMS, for example using length-weight relationships (Wolfe et al., 2020), would allow for the study of community and food-web dynamics across reefs.

Finally, as Obst et al. (2020) said, “There is a need to move beyond episodic metabarcoding studies and build up time-series of genetic data”. The greatest attribute of the ARMS method is the collection of standardised genetic data across multiple time points and locations, but different choices in metabarcoding bioinformatic pipelines mean diversity estimates across studies are not easily compared. Studies characterising cryptobenthic communities from individual regions, such as this thesis, are important for building local knowledge but meta-analyses of ARMS are now also needed to investigate community trends across anthropogenic and climate-induced impacts. Large meta-analyses combining and co-analysing data from 100s, and eventually 1000s of ARMS, should now become a priority.

1.8 Study site: The Chagos Archipelago Marine Protected Area

Overall, studies of invertebrates along gradients of habitat complexity and ‘health’ are lacking within undisturbed ecosystems (Tews et al., 2004). As many coral reefs are found within the vicinity of human populations, disentangling the effects of direct human impacts (e.g., intensive and destructive fishing practices, coastal infrastructure, chemical and noise pollution) with impacts from global climate change (e.g., extreme weather events, ocean acidification, warming) can be difficult (He & Silliman, 2019). The Chagos Archipelago, a remote set of islands and atolls located along the southern tip of the Laccadives-Maldives-Chagos ridge (Central Indian Ocean)(Figure 1.3), harbours highly biodiverse tropical coral reefs (Sheppard et al., 2013). Following the forced removal of inhabitants in the 1970s, and later the

establishment of a large no-take Marine Protected Area (MPA) in 2010 (Koldewey et al., 2010), the archipelago has little to no direct human impacts, especially along the central (Great Chagos Bank) and northernmost atolls (Peros Banhos, Salomon)(Sheppard et al., 2012). The Chagos Archipelago MPA is the focus of this thesis, and all data presented henceforth were collected within the archipelago between 2018 and 2022.

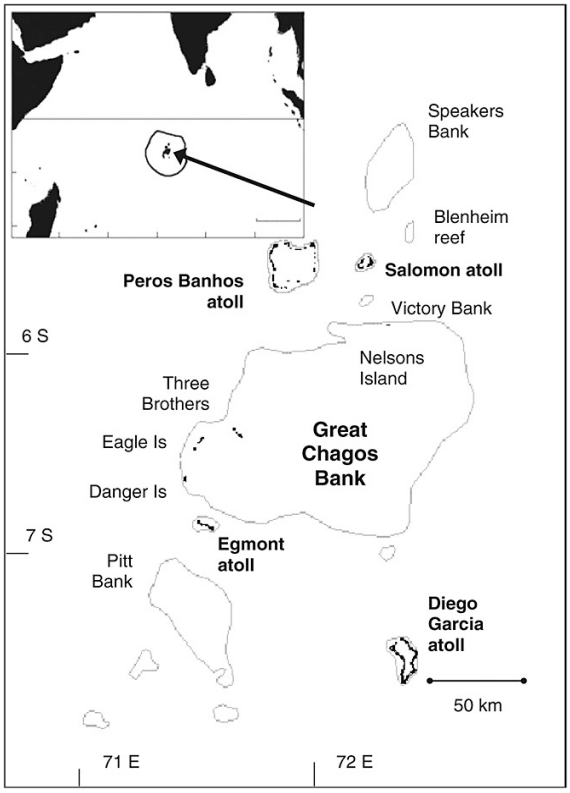

Figure 1.3. Map of the Chagos Archipelago Marine Protected Area (Central Indian Ocean) with islands outlined in black and all major atolls and banks outlined in light grey, obtained from Sheppard et al., (2012). The outline of the MPA within the Central Indian ocean is visible in the inserted map in the top left of the graphic.

Due to its remoteness and the limited direct human impacts, the archipelago acts as a rare reference site for pelagic and coral reef biodiversity and ecology of the Indian Ocean (reviewed in Hays et al., 2020; Sheppard et al., 2012). Long term monitoring of the diversity, cover and composition of scleractinian corals has undergone there since the 1970s (Sheppard et al., 2013). Approximately 300 reef-building scleractinian coral species have been recorded in the MPA (https://chagosinformationportal.org/corals), including the endemic brain coral species *Ctenella chagius*.

High mortality bleaching events took place across the archipelago in 1998 (Sheppard et al., 2013) and again in 2015 and 2016 (Head et al., 2019). Coral mortality was high following both bleaching events, with coral cover diminishing to 10% following the 1998 events, and again falling from 30% in 2012 to 12% in 2016 (Head et al., 2019). Several coral communities across the archipelago have faced substantial declines over time, with reductions of component species by 90-100% in some parts, leading to ecological extinctions amongst local assemblages (Sheppard et al., 2020). However, reefs of the archipelago have been shown to recover faster than other sites across the Indian Ocean (Sheppard & Sheppard, 2019). Subsequent work has explored the trajectories and patterns of reef recovery (Lange et al., 2022; Lange et al., 2020; Samoilys et al., 2018), as well as the key role of sea bird nutrients in coral reef recovery pathways (Benkwitt et al., 2019).

The Chagos Archipelago also host large numbers and high biodiversity of vertebrates. For example, the biomass of reef fish within the MPA has been found to be very high and up to by several orders of magnitude higher than estimates recorded elsewhere in the Indian Ocean (Graham, 2010), instead resembling most closely to estimates observed in unfished regions of the Pacific Ocean (Williams et al., 2011). Several studies have since explored reef fish assemblage structure across the MPA (Samoilys et al., 2018; Darling et al., 2017), as well as shark behaviour (Curnick et al., 2020), distribution (Dunn et al., 2019) and diversity (Dunn et al., 2022). It has been estimated that 39-51% of egg clutches laid by hawksbill turtles in the south-west Indian Ocean have occurred in the Chagos Archipelago MPA (Mortimer et al., 2020), and the MPA is classed as a globally significant turtle breeding site for hawksbill turtles (Mortimer & Donnelly, 2008) and green turtles (Seminoff, 2004). Manta rays also common across the MPA, which provides key habitats for manta feeding (Harris et al., 2021). Islands of the Chagos Archipelago MPA also host regionally important breeding sea bird populations, including 197,500 pairs of sooty terns, 22,871 red-footed boobies, 1,632 tropical shearwaters and 50,780 lesser noddies (Carr et al., 2021). In turn, these seabird populations play a key role in providing nutrient subsidies for reefs across the archipelago (Benkwitt et al., 2019; Graham et al., 2018).

Fewer studies have been conducted on non-coral marine invertebrates in the Chagos Archipelago MPA. The diversity and abundance of decapods on dead coral heads has been shown to be high across

the region (Head et al., 2018a; Head et al., 2018b; Head et al., 2015). Sea cucumber populations in the MPA were found to be impacted by illegal harvesting in 2006, with low population numbers observed in northern atolls compared to populations near Diego Garcia which were more abundant, with the military base on this atoll providing an apparent deterrent for such activities (Price et al., 2010). Localised outbreaks of *Acanthaster planci* (crown-of-thorns starfish), a predator of scleractinian corals, were observed in 2012 and 2013 but no major outbreaks have been reported since (Roche et al., 2015). The benthic community composition of reefs before the 2015/2016 bleaching events were recently studied by Pilly et al., (2022). Whilst focusing mostly on exposed surfaces, this study found that sponges were higher in abundance on reefs at a depth 20-25m compared to reefs at 5-10m, but that this pattern was observed across some, but not all, atolls of the MPA. Museums such as the Natural History Museum (London), the Florida Museum of Natural History and the Smithsonian's Natural Museum of Natural History have invertebrate specimen from the Chagos Archipelago in their archives, from field collections dating back to 1905 (https://collections.nmnh.si.edu/search/iz/). These include many coral specimen, but also molluscs, decapods, echinoderms, sipunculid worms and ascidians.

1.9 Thesis aims

This thesis investigates the diversity, composition, and potential drivers of coral reef cryptobenthic communities of the Chagos Archipelago Marine Protected Area (MPA). This thesis also explores the potential bias of Autonomous Reef Monitoring Structures (ARMS), employed here to study cryptobenthic communities from natural communities and evaluates other non-destructive genetic and image-based methods.

In Chapter 2 (first data chapter), I used multi-marker metabarcoding to study spatiotemporal patterns of diversity and composition in motile and sessile cryptobenthic communities from three shallow reefs. To do so, I collected ARMS from each sampling site in 2019 and 2021, following a one and three-year deployment and processed samples following standardised protocols. This chapter presents novel data and highlights the exceptional diversity of these remote protected reefs and is the first to metabarcode cryptobenthic communities in this region. I also carried out barcoding of large motile specimens collected on ARMS in 2019, and present 111 novel voucher sequences in the Appendix section of this

chapter. This chapter is part of an ongoing effort aiming to fill the knowledge gaps for cryptofauna of this region, and the wider Indian Ocean.

In Chapter 3, I investigated the composition and abundance of sessile organisms on ARMS alongside *in-situ* and *ex-situ* environmental parameters, to determine how differences in environmental profiles may be driving community patterns across sampling sites. I used image analysis to collect data on the percentage cover of major sessile cryptobenthic groups on ARMS recruitment plates collected in 2019. At the same time, colleagues from Stanford University recorded a suite of *in-situ* environmental parameters including temperature, pH, salinity, photosynthetic available radiation (PAR), wave height and flow velocities, as well as *ex-situ* temperature and wave height data in 2019. This chapter aimed to integrate analyses of both biological and physicochemical components of reef ecosystems and has since been published in the journal Frontiers in Marine Sciences, which I led as first author.

Using non-destructive sampling methods is important for limiting the impact of scientific exploration on coral reef ecosystems. However, communities recovered on ARMS must be critically compared to those inhabiting the local reef matrix if we are to understand if, and how, these devices may bias the study of cryptobenthic taxa in highly diverse regions such as the Chagos Archipelago MPA. In Chapter 4, I ground truthed cryptobenthic communities found on ARMS collected in 2021 by comparing them to those on nearby tabular coral (*Acropora sp.*) using image analysis. I also explored the potential of environmental DNA (eDNA) sampling, another non-destructive sampling method, for the detection and study of cryptobenthic taxa. For this I used multi-marker metabarcoding to recover communities from ARMS collected in 2021 as well as filtered sea water samples collected adjacent to each ARMS and compared the findings of each approach.

In Chapter 5, I explored the use of fluorescence imaging for studying ARMS sessile communities. I determine the recruitment density of juvenile hard corals and present observations of fluorescence patterns across adult coral colonies and sponge specimens on ARMS collected in 2021. This short study has been published as a Note article in the journal Corals Reefs, which I led as first author.

CHAPTER 2

Multi-marker metabarcoding reveals spatiotemporal patterns of cryptobenthic diversity across the Chagos Archipelago MPA

Margaux Steyaert[1,2], Emma Ransome[3], Michael Bonsall[1], Nicholas Dunn[2,3], Rosalie Dowell[2,3], Jake Williams[2,3], Kevin Hopkins[2] and Catherine Head[1,2]

[1] Department of Biology, University of Oxford, Oxford, OX1 3SZ, United Kingdom

[2] Institute of Zoology, Zoological Society of London, London, NW1 4RY, United Kingdom

[3] Department of Life Sciences, Imperial College of London, London, SL5 7PY, United Kingdom

This chapter is not submitted to any academic journal

2.1. Abstract

Tropical coral reefs are degrading rapidly and characterising the diversity of these ecosystems across scales of human impacts is needed to understand how reefs are responding to increasing environmental and ecological change. One of the largest components of coral reef eukaryotic diversity, the cryptobenthic community, remains understudied and under-reported. Cryptobenthic communities within tropical coral reefs are highly diverse, both in size and taxonomy, but their inherent association with the reef matrix renders them difficult to study. Here, a multi-marker metabarcoding approach was used to study cryptobenthic communities collected from artificial devices, Autonomous Reef Monitoring Structures (ARMS), across three shallow reefs of the remote and protected Chagos Archipelago Marine Protected Area (MPA), Central Indian Ocean. Each site was sampled in 2019 and 2021 following a 1 and 3-year deployment of ARMS units and the composition and diversity of eukaryotes within and between sites, as well as across sampling years, was assessed. Targeting both the 18S v4 region and a 314 bp region of the cytochrome oxidase I (COI) gene, 21 metazoan phyla were recovered. Communities on ARMS were highly heterogeneous, and the composition and presence or absence of individual cryptobenthic groups were significantly determined by both spatial and temporal factors, with strong differences observed in community composition between ocean-facing and lagoon reef habitats. In the partitioning of multi-site β-diversity across ARMS, turnover (species replacement), accounts for ~93% of the dissimilarity observed between communities of different sampling years, and 76-94% of community dissimilarity observed within sites (amongst triplicate ARMS). Only 3.8-4.3% of the recovered COI sequence variants were assigned species-level taxonomy, with 240 species (of which 168 are fully described) identified using a highly conservative approach (BLAST identification with 100% query cover and 100% identity match). A comparison with specimen in online collections of three museums suggests that most of the diversity of cryptofauna detected here, using metabarcoding, are likely new records for the Chagos Archipelago. However, the paucity of our classifier, which uses up to date genetic reference information, limits our ability to detect over half of the known species in these museum collections, and therefore previously recorded in the archipelago. This study is the first to employ ARMS and metabarcoding to assess coral reef benthic diversity in the Chagos Archipelago MPA and as such provides a primary baseline for ongoing work within this region.

2.2. Introduction

It remains uncertain exactly how biodiverse eukaryotic communities of coral reef ecosystems are today. Whilst several methods can be employed to quantify and describe the diversity of natural systems, such as categorising communities by functional roles and traits, a key metric remains the analysis of species richness (Hughes et al., 2002; Whittaker et al., 2001). Current estimates of total species richness across coral reefs range between 550,000 to 1,330,000 (Fisher et al., 2015). Although these values can vary significantly depending on the method used to extrapolate estimates beyond the known number of species present (Caley et al., 2014), it is possible that up to ~74% of eukaryotic species on coral reefs remain to be discovered (Costello et al., 2015; Fisher et al., 2015,). Tropical coral reefs are particularly vulnerable habitats to climate-change induced warming and occur in narrow ranges of environmental conditions (Guan et al., 2015). With increasingly devastating high-mortality bleaching events occurring across the globe, researchers are working to understand how climate-induced habitat decline impacts or reconfigures reef communities. However, attempting to predict the impacts of climate-change or anthropogenic pressure on coral reefs when our baseline knowledge of their biodiversity is incomplete is clearly a limitation.

Regardless of the lack of convergence between total estimates of species richness across coral reefs, it is clear our knowledge of reef biodiversity is not only incomplete, but also disproportionate between taxonomic groups (Appeltans et al., 2012). Within metazoan reef communities, cryptobenthic fauna are perhaps the least understood, and yet form the largest part of diversity (Reaka-Kudla, 1997). These organisms include sessile groups such as encrusting and burrowing sponges, colonial ascidians and bryozoans, and mobile fauna such as arthropods, echinoderms, molluscs and worms, which can be associated with sessile taxa, as well as live, dead or rubble coral substrate. Sessile cryptobenthic groups play many functional roles within reef communities as habitat providers and nutrient cyclers (Folkers & Rombouts, 2020; Maldonado, 2016; Wulff, 2001). Certain groups such as sponges are also important ecosystem shapers by binding, stabilizing or dismantling the coral matrix (Wulff, 2016; Wulff, 2001), whilst others such as bryozoans contribute to the mineralization of the reef structure (Mallela et al., 2013). A total of 9,144 extant and accepted species of marine sponges have been described to date (WORMS, 2022), along with 3,135 ascidians (Ascidiacea World Database, 2022), and 6,032 bryozoan

species (WORMS, 2022). Mobile macro-invertebrates carry out many functional roles within coral reef ecosystems, which help to regulate algal growth (Francis et al., 2019; Klumpp & Pulfrich, 1989), break down detritus and ultimately serve as prey for reef invertivores (Kramer et al., 2013; Leray et al., 2013). Arthropods are currently believed to be the most speciose group of mobile cryptofauna with over 56,660 accepted marine species described to date, closely followed by molluscs (49,259 sp.), annelids (13,242 sp.), platyhelminthes (11,922 sp.), echinoderms (7,447 sp.), nematodes (6,244 sp.), nemerteans (1,317 sp.) as well as hemichordate and sipunculid worms (130 sp. and 157 sp. respectively) (WORMS, 2020).

Morphological identification of cryptobenthic groups can be time-consuming and labour-intensive, and requires highly specific taxonomic expertise, a field which is diminishing inversely with our need for it (Coleman, 2015; Paknia et al., 2015). The use of next-generation sequencing methods such as DNA metabarcoding allows researchers to collect genetic data across multiple samples simultaneously. In essence, metabarcoding aims to identify multiple taxonomic groups within individual samples by targeting genetic regions which provide high enough resolution to distinguish between target taxa. The more degenerate the PCR primers and the more universal the gene region targeted during PCR amplification, the more taxonomic groups can be detected and identified. Metabarcoding is now a wide-spread and popular method for the study of coral reef organisms and their associated microbes (Carvalho et al., 2019; DiBattista et al., 2019), and when combined with standardised sample collection protocols, can provide detailed snapshots of diversity from hyperdiverse cryptobenthic communities across geographical and environmental gradients (Ip et al., 2022; Villalobos et al., 2022; Pearman et al., 2020). Unassigned DNA reads can be cleaned, merged and clustered into sequence variants, which can then be compared across samples to compare ‘species’ richness and establish connectivity between sites, even if the sequence variants remain unidentified. In addition, the comparison of sequence reads against a reference sequence dataset allows the assignment of taxonomic identities across amplicon datasets.

The paucity of reference genetic databases is well-recognised, especially for under-studied groups such as marine cryptofauna, and often leads to low assignment rates at lower taxonomic ranks (e.g., genus and species; Villalobos et al., 2022). Whilst arthropods, molluscs and echinoderms are often the most studied mobile macro-invertebrate groups within reef ecosystems, it has been estimated that a large

portion of these groups still remains to be discovered and/or described on coral reefs (Fisher et al. 2015, Appletans et al., 2012). Several initiatives and projects are gradually filling in knowledge and reference dataset gaps (e.g., Moorea Biocode Project, Sponge Barcoding Project) (see review by Trivedi et al., 2016), and growing consensus is now emerging that using localised and curated reference datasets is necessary to improve assignment rates for metabarcoding data. For example, Ransome et al. (2017) found that employing a curated reference database composed of sequences collected from individuals local to their sampling sites increased taxonomic identification success from 5.1% to 38.6%. It is especially important that barcoding initiatives focus efforts on reef sites which remain pristine or removed from human impacts, to ensure that datasets are populated with both rare and common taxa, and to establish realistic baselines of coral reef diversity

Global initiatives are pushing for increased protection of the world's ocean (Maestro et al., 2019), but few places can be found on earth where tropical coral reefs occur with very limited human direct impacts such as the Chagos Archipelago Marine Protected Area (MPA). The Chagos Archipelago is a remote set of islands, banks and atolls found in the Central Indian Ocean approximately 1,820km east of the Seychelles and 500km south of the southern tip of the Maldives archipelago. Following a turbulent political history, and the forced removal of island inhabitants in the 1970s, the archipelago is now almost completely uninhabited, save for the Diego Garcia atoll in the southern part of the region. The archipelago was declared a large no-take Marine Protected Area (MPA) in 2010 (Koldewey et al., 2010), and although these reefs still suffer from climate-change induced warming (Head et al., 2019), direct human-led impacts which threaten coral reef ecosystems including coastal infrastructure, chemical and sound pollution, intense fishing practices (e.g., bottom-trawl, dynamite or longline fishing) are mainly absent.

The archipelago has long been a place for the study of hard coral taxonomy and ecology in the absence of direct human impact (Sheppard et al., 2013; Hays et al., 2020). A suite of research has also been conducted on seabird populations (Carr et al., 2020), fish diversity and community structure (Tickler et al., 2017), turtle migration (Mortimer et al., 2020), shark and manta ray behaviour and distribution (Dunn et al., 2022; Curnick et al., 2020; Harris et al., 2019), benthic communities across depth and environmental conditions (Steyaert et al., 2022b; Pilly et al., 2022; Head et al., 2018a), as well as on

the variability of in-situ physical parameters such as reef flow and roughness (Lindhart et al., 2021). Studies investigating the link between seabird populations and reef productivity across the archipelago have demonstrated the importance of limiting human impacts, in this case invasive rats, for overall reef functioning (Graham et al., 2018). However, few studies to date have been conducted on cryptobenthic communities of the archipelago (but see Steyaert et al., 2022a; Steyaert et al., 2022b; Head et al., 2018a; Head et al., 2018b; Head et al 2015). Cryptofaunal decapods living on dead coral colonies have been found to be exceptionally diverse in the MPA, with groups such as Galatheoidea (porcelain crabs and squat lobsters) being particularly abundant (Head et al., 2018b).

Here, we use multi-marker metabarcoding of two universal eukaryotic genetic regions (COI, 18S v4) to analyse the diversity of cryptobenthic communities collected from artificial devices, Autonomous Reef Monitoring Structures (ARMS), following a 1- and 3-year submersion on three shallow coral reefs of the Chagos Archipelago MPA. Our study objectives are as follows: i) to determine the richness and alpha diversity of ARMS motile and sessile communities across sampling sites and sampling collections, ii) assess the effect of site choice and length of ARMS deployment on the abundance of metazoan groups, and iii) explore spatiotemporal patterns of metazoan beta-diversity. We also aim to explore how represented Chagos Archipelago cryptofauna are in current genetic reference databases by assessing the taxonomy assignment success of our metabarcoding sequences. We expect to see high diversity and heterogeneity across sampling sites and sampling collections and expect to detect organisms across the tree of life. We also hypothesise that turnover (aka species replacement), rather than nestedness (aka species loss), will be high between sites, due to the likely additional detection of DNA signal originating from the surrounding environment, and as has been previously observed in other coral reef ARMS-based studies conducted over small spatial scales. Finally, we expect to find few sequence variants with genus or species-level assignment in our COI amplicon dataset, as cryptofauna of the Chagos Archipelago is under-studied and likely under-represented in current reference databases. This is the first metabarcoding study to look at cryptobenthic communities using metabarcoding in this region and provides a baseline for studying reef cryptofauna across the wider Indian Ocean basin.

2.3. *Methods*

2.3.1. Sampling sites

This study was conducted across the Peros Banhos and Salomon atolls of the Chagos Archipelago Marine Protected Area (MPA), Central Indian Ocean. Eighteen ARMS were deployed in 2018 across three shallow sites (7-12m depth)(*n* = 6 per site), near Moresby island (Peros Banhos, ocean-facing reef), Ile du Coin island (Peros Banhos, lagoon-facing reef) and Ile Anglaise island (Salomon atoll, ocean-facing reef) (see Figure 1; GPS coordinates in Appendix Table A.1). Triplicate ARMS were retrieved on SCUBA from each site following a 12-month deployment (March-April 2019), whilst another set of triplicate units were retrieved following a 36-month deployment (March-April 2021) from the same sites.

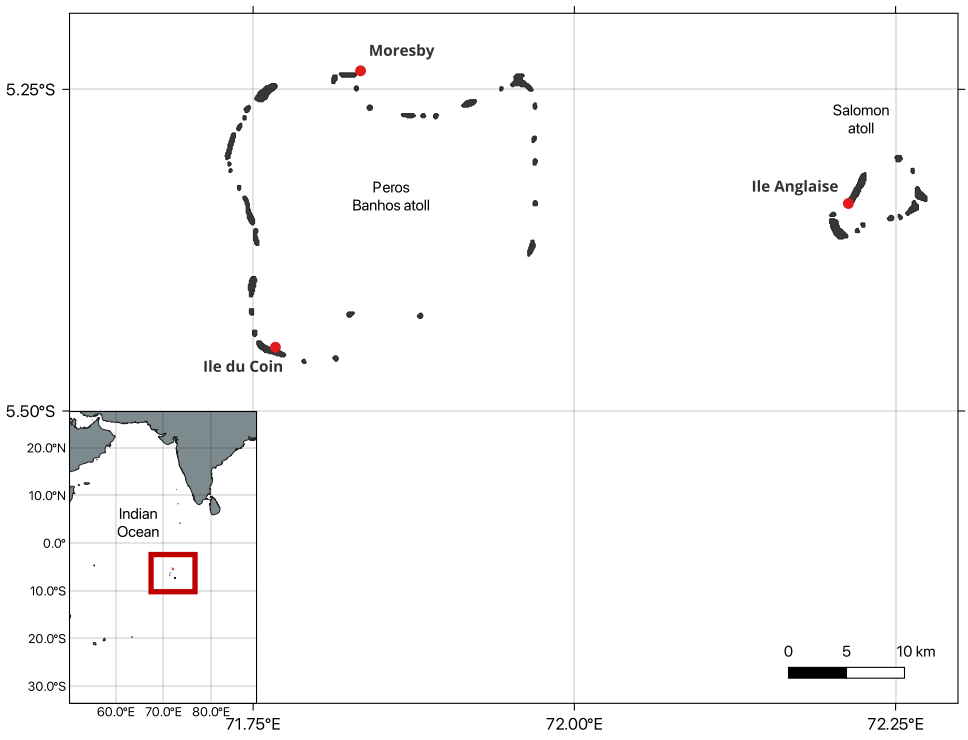

Figure 2.1. Map of the sampling sites across the Chagos Archipelago MPA, Central Indian Ocean. The smaller map shows the geographical position of the archipelago, whilst the larger map shows the Peros Banhos and Salomon atolls, which are located in the northern region of the MPA, along with the precise location of each ARMS study site by the islands of Moresby, Ile de Coin and Ile Anglaise (red dots).

For the retrieval of ARMS, a clear plastic bin was placed over each unit and secured flush against the base plate to minimise the loss of motile organisms. ARMS were then put inside a blacked out 96L bin and covered with seawater filtered through 40micron mesh and aerated using aquarium bubblers. Each unit was then disassembled, and mobile and sessile communities were separated and fractioned off using standardised protocols (Leray et al., 2015). ARMS plates were gently shaken within the filtered seawater to remove small motile organisms. Sessile communities were scrapped off each ARMS plate, and bulk homogenised together using a sterile kitchen blender, before being squeezed dry through 40µm nylon mesh. Each bulk mix was then briefly sprayed with 95-98% ethanol, squeezed dry again using 40µm nylon mesh, and then preserved in salt saturated DMSO buffer (3 x 50mL Falcon tubes). Mesh sieves were used to separate small motile organisms in the filtered seawater into two size fractions (100-500µm, 500µm to 2mm). These two bulk fractions were then also squeezed dried using 40µm nylon mesh and preserved in 95-98% ethanol. All sessile and motile fractions were then placed in -16 °C freezers for the remainder of field collection expeditions and then carried back to the Zoological Society of London (ZSL, London) using hermetic cooler boxes (transit times varied between 24-48 hours). Photographs of ARMS plates, and the preservation and photography of individual motile organisms larger than 2mm was also carried out but results from these samples are not presented here.

2.3.2. DNA metabarcoding

DNA was extracted from motile and sessile samples within months of each ARMS retrieval in 2019 and then again in 2021. Bulk motile fractions (100-500µm, 500µm -2mm) were decanted using MilliQ water and a sterile 100µm mesh sieve to separate tissue/specimens from inorganic matter, as recommended in Leray et al. (2015). Individual sessile samples were drained of DMSO buffer and briefly homogenised again using a sterile spatula in a sterile weighing boat. Decanted and drained motile and sessile samples were then weighed, and up to 8g per sample was used for DNA extraction using QIAGEN's DNeasy PowerMax Soil kits following manufacturer's protocols, with the addition of an extended overnight lysis step at 56°C, in a shaking incubator. DNA concentration was then quantified across individual samples using the QuBit dsDNA High Sensitivity assay kit, following the manufacturer's protocol.

Both cytochrome oxidase I (COI) and 18S genes were targeted using universal primers with attached Illumina adapters (on 5' ends). The mlCOIintF/jgHCO2198 primer pair was used to target a short (313bp) region of the COI gene (Leray et al., 2013), whilst the TarEukFWD1/TarEukREV3 primer pair was used to target the V4 region (270-387bp) of the 18S gene (Stoeck et al., 2010). For COI, PCR reactions were conducted in triplicates, in 20µL volumes including 2µL of DNA, 0.5µL of both forward and reverse primers, 4µL of 5X HOT FIRPol Blend Master Mix (12.5mM $MgCl_2$) and 13µL of PCR-grade H_2O, and with an initial denaturation step at 95°C for 15 minutes, followed by 35 cycles of 95°C for 30 seconds, 55°C for 30 seconds, 72°C for 1 minute, and a final extension at 72°C for 7 minutes. For 18S, PCR reactions were conducted in triplicates, in 20µL volumes including 2µL of DNA, 0.5µL of both forward and reverse, 4µL of 5X HOT FIRPol Blend Master Mix (12.5mM $MgCl_2$) and 13µL of PCR-grade H_2O, and with an initial denaturation step at 95°C for 15 minutes, followed by 30 cycles of 95°C for 30 seconds, 50°C for 45 seconds, 72°C for 1 minute, and a final extension at 72°C for 7 minutes. All amplicon PCRs also included a negative control, where sterile molecular grade water was used instead of sample DNA. To check for successful amplification, PCR triplicates were pooled and run on a 1.5% agarose gel by mixing 2µL of DNA pooled product and 2µL loading dye for 30-50 minutes at 100V, alongside a 50bp HyperLadder ladder and a negative PCR control. DNA products were then cleaned using Agencourt Ampure XP beads and a magnetic plate, following an in-house protocol.

Samples were individually dual-indexed in second-round PCR reactions using Nextera XT DNA Library Preparation Kit indexes (v2 set 2, 500-cycles, Illumina) in 40µL reactions including 25µL of Kapa HiFi Hotstart polymerase, 10µL of PCR-grade water and 5µL of cleaned DNA product, with an initial denaturation step at 95°C for 4 minutes, followed by 8 cycles of 95°C for 30 seconds, 55°C for 30 seconds and 72°C for 30 seconds, and a final extension at 72°C for 5 minutes. A total of 56µL of index PCR products per sample was then cleaned using a magnetic bead clean up step, using Agencourt Ampure XP beads and an in-house protocol. Clean index PCR products were checked on a TapeStation platform (Agilent) using the TapeStation D1000 HS reagent kit. Cleaned index DNA products for each sample were then quantified using dsDNA High Specificity QuBit reagent kit and QuBit machine, using manufacturer's protocols. COI and 18S DNA samples were then pooled separately based on individual sample concentrations, and pooled samples were quantified using dsDNA Qubit reagents and Qubit machine (as mentioned previously), using the manufacturer's protocol. A total of 10µL of pooled

samples were denatured using 10µL of 0.2N NaOH. A PhiX standard was prepared by adding 2µL of 10nM PhiX, 3µL of H_2O and 5µL of 0.2N NaOH. A total of 980µL of HT1 buffer was then added to each denatured pooled sample, and then diluted to 3.5 pM, whilst 825µL of HT1 buffer was added to 175µL of 20pM denatured PhiX. Then, 950µL of 3.5 pM sample library and 50µL of 3.5 pM PhiX were mixed. MiSeq v2 (500-cycles) reagent cartridges were then prepared, loaded, and run on a MiSeq sequencer (Illumina). In 2019, both COI and 18S samples were run on the same cartridge, whilst in 2021 COI and 18S samples were run on separate cartridges alongside additional environmental samples (see Chapter 4). The final pool concentrations and protocols followed for preparing and loading the sequencing cartridge and reagents was identical for both sequencing runs.

2.3.3. Bioinformatics

A custom bioinformatics pipeline was used to run the merging, error-filtering (DADA2, Callahan et al., 2016), clustering (VSEARCH, Rognes et al., 2016), curation (LULU, Frøslev et al., 2017) and taxonomy assignment of COI and 18S sequence datasets (Williams et al., *manuscript in preparation*). For both datasets, the *filterAndTrim* function's truncLen parameter was set to 240 bp for both forward and reverse reads, maxN was set to 0, maxEE was set to (2,2) and truncQ was set to 2. For the core sample inference function *dada*, the pooling parameter was set to 'pseudo-pool' for both amplicon datasets. The trimLeft parameter was set to (20,18) for 18S amplicons and (26, 26) for COI amplicons, to trim away primer sequences. For both 18S and COI, three sets of sequence variants were obtained. Exact Sequence Variants (ESVs) were obtained directly from the final DADA2 pipeline for both COI and 18S datasets. Both COI and 18S ESVs were then clustered into OTUs separately using VSEARCH with a similarity threshold set to 0.97. These were then curated using LULU to produce curated OTUs (cOTUs), with all parameters left as default except for match rate at 0.84 for COI and match rate at 0.90 for 18S, following recommendations made by Brandt et al. (2019). The cOTU cluster representative sequences was chosen as the OTU with the highest abundance of reads.

IDTAXA (Murali et al., 2018) was then used to assign taxonomy to sequence variants, using the SILVA r138 dataset for 18S data (Quast et al., 2013), and a custom COI classifier was created using full MIDORI (v248)(Leray et al., 2018) and BIOCODE reference datasets (Williams et al., *manuscript in preparation*). To reduce the total number of sequences and the computational demand of training and

using our MIDORI-BIOCODE classifier, terrestrial orders with more sequences than the largest marine order, Decapoda (*n* = 52,385), were randomly subsampled to the same number of sequences present in Decapoda. Subsampled terrestrial orders included Aranea, Hemiptera, Coleoptera, Hymenoptera, Lepidoptera, Diptera. Both 18S and COI datasets were formatted for the IDTAXA algorithm prior to taxonomy assignment, and the assignment threshold minimum was set to 30. The BLAST algorithm was also used to assign taxonomy to the COI metabarcoding dataset against our MIDORI-BIOCODE classifier to determine species-level assignments with the highest possible threshold (100% query cover, 100% identification match).

Species identified using a high confidence BLAST threshold were then compared against online specimen records from the Chagos Archipelago at the Natural History Museum (London) (Natural History Museum, 2014), the Smithsonian National Museum of Natural History, which has a collection of 468 specimen (incl. 200 species) from the archipelago (https://collections.nmnh.si.edu/search/iz/), and the Florida Museum's Invertebrate Zoology collection, which includes collections of molluscs sampled between 1977 and 1994 across rubble, coral reef and lagoonal slopes of the Diego Garcia atoll (http://specifyportal.flmnh.ufl.edu/iz/).

2.3.4. Statistics

All statistical analyses were carried in R (R Core Team) using RStudio (version 2022.02.03)(RStudio Team, 2022). A custom function was used to format the DADA2 bioinformatics pipeline output to be usable with R package "phyloseq" v 1.40.0 (McMurdie & Holmes, 2013), which was used to handle and subset sequence variants. All plots presented were created using the "ggplot2" package (version 3.3.6)(Wickham, 2016).

The extent of sequencing depth and coverage across samples was checked using the *rarecurve* function in vegan (version 2.6.2)(Oksanen et al., 2013), using an interval of 100. The number of singletons across sequence variant datasets (ESVs, cESVs, cOTUs) was then counted across all samples, as well as motile and sessile samples separately, and were not removed from the datasets. Samples were then rarefied using the *rarefy_even_depth* function within the phyloseq package. Following this, the number and proportion of cOTUs shared between motile and sessile fractions, as

well as between sampling sites, were calculated and visualised using the web-based DeepVenn program (Hulsen et al., 2008), which produces are-proportional Venn diagrams.

Estimates of total cOTU richness, along with respective standard errors, and high/low confidence intervals, were then calculated across ARMS samples using the "breakaway" package (version 4.7.6)(Willis & Bunge, 2015). Breakaway uses the frequency ratios of sample counts (aka reads) to predict the unobserved count and estimate total richness of species (in this case sequence variants)(Willis & Bunge, 2015). Due to the internal normalisation step, un-rarefied read counts were used to perform this analysis across both COI and 18S samples. The effect of sampling year and sampling site on the estimated cOTU richness of sessile and motile samples was then tested using the *betta* function, which uses a mixed-model approach to test for sample heterogeneity across covariates.

Phyloseq objects were then subsetted to only include metazoan phyla, and the percentage and number of cOTUs with IDTAXA assignments were counted for each taxonomic rank. cOTUs were then grouped by order-level assignment across both COI and 18S datasets, and the estimated Shannon diversity of motile/sessile fractions and sites was calculated using the "DivNet" package (version 0.4.0)(Willis & Martin, 2018). DivNet calculates Shannon diversity using estimated richness to account for unobserved taxa/sequence variants. Similar to breakaway analysis, due to the internal normalisation of read counts, un-rarefied samples were used to perform this analysis. The effect of sampling year on fraction and site estimated Shannon diversity was then tested also using the *betta* function.

Nonmetric Multidimensional Scaling (NMDS) was performed on dissimilarity matrices of COI and 18S rarefied cOTUs separately using Jaccard distances (presence/absence), using the *metaMDS* function in the package "vegan" using 2 dimensions (*k*). The composition of ARMS communities across sampling years and sites was then visualised by plotting NMDS results and using 95% confidence ellipses around group centroids.

Beta-diversity (based on Jaccard distances) was calculated, and multiple-site dissimilarities were assessed with the package "betapart" (version 1.5.6)(Baselga & Orme, 2012) to determine the extent of community dissimilarity attributed to species turnover (aka species replacement) or nestedness (aka

species loss and gain). Rarefied samples were used for this analysis. The function *beta.multi* was used to calculate the value of overall beta diversity, as well as the fractions attributed to nestedness and turnover components, for communities across ARMS triplicates within sampling site and per year (e.g., between triplicate ARMS in Ile Anglaise in 2019). The function *beta.temp* was used to calculate the same three values, but between ARMS communities of individual sites across sampling years (e.g., between 2019 and 2021 ARMS communities in Ile Anglaise).

Multivariate generalised linear models (GLMs) were used to determine the effect of site, sampling year and the interaction between both variables on the community composition of metazoan orders, across rarefied COI and 18S datasets separately, using the package “mvabund” (version 4.2.1)(Wang et al., 2012). The function *manyglm* was used to run binomial multivariate models on a presence/absence matrix of order level taxa, using a complimentary log-log identity link to account for uneven distributions of 1’s (presence) and 0’s (absence) of groups, across sampling year and site, with interactive terms between both variables. Analysis of deviance tests were run using the function *anova.manyglm* to determine the statistical significance of the fitted model, as well as the individual effects of site, year, and their interaction, on overall community composition and the abundance of individual order level taxa. For this, the test statistic parameter was set to “LR” (likelihood ratio), correlation parameter was set to “I” and unadjusted resampling-based univariate and multivariate p-values were obtained. The relationship between the occurrence of COI cOTUs and groups of sites across years was then explored using indicator analyses with the package “indicspecies” (version 1.7.12)(de Caceres & Legendre, 2009). A total of 999 permutations were carried out. The number of indicator cOTUs with a genus or species-level assignment was then compared and discussed.

2.4. Results

2.4.1 Sequencing depth and richness of ARMS samples

A total of 10,435,435 COI reads and 8,670,128 18S reads were recovered following error-filtering and chimera- removal steps, with an average sampling depth of 249,356 COI sequences and 174,783 18S sequences across 2019 samples, and 279,991 COI sequences and 297,823 18S sequences across 2021 samples (see Appendix Tables A.2 & A.3 for DADA2 output). Sequencing failed for three COI samples from the 2021 dataset (ARMS 1 100-500micron, ARMS 1 500micron-2mm, ARMS 3 sessile), originating from site Ile Anglaise, and were therefore removed from subsequent analyses. A total of 18,426 COI cOTUs and 6,457 18S cOTUs were obtained following the clustering and curation of 52,471 COI Exact Sequence Variants (ESVs) and 21,061 18S ESVs. Approximately twice as many sequence variants were observed in motile samples then across sessile samples across both years, with 15,941 motile COI cOTUs and 5,462 motile 18S cOTUs compared to 8,299 sessile COI cOTUs and 3,109 sessile 18S cOTUs (Table 2.1). Few singletons were observed across curated and non-curated sequence variant datasets (Table 2.1).

Table 2.1. Summary of curated and non-curated sequence variants (ESV = Exact Sequence Variants, OTU = Operational Taxonomic Units) observed richness across all un-rarefied samples and fractions (motile and sessile) over both sampling years. The number of sequence variants with a total abundance of 1 (singletons) are listed in brackets (*).

Amplicon	Sequence variant	All samples	Motile fraction	Sessile fraction
COI	ESV	52,471 (*165)	42,036 (*202)	17,628 (*305)
	curated OTU (cOTU)	18,426 (*35)	15,941 (52)	8,299 (*142)
18S	ESV	21,061 (*442)	16,059 (*394)	8,617 (*244)
	curated OTU (cOTU)	6,457 (*47)	5,462 (*51)	3,109 (*40)

Sequencing effort differed among samples, but overall, rarefaction curves of observed curated Operational Taxonomic Units (cOTU) richness plateaued across COI and 18S samples, indicating that sufficient sequencing depth was achieved (Figure 2.2). Following a rarefaction step, read counts were rarefied to 56,783 per COI sample and 61,466 per 18S sample.

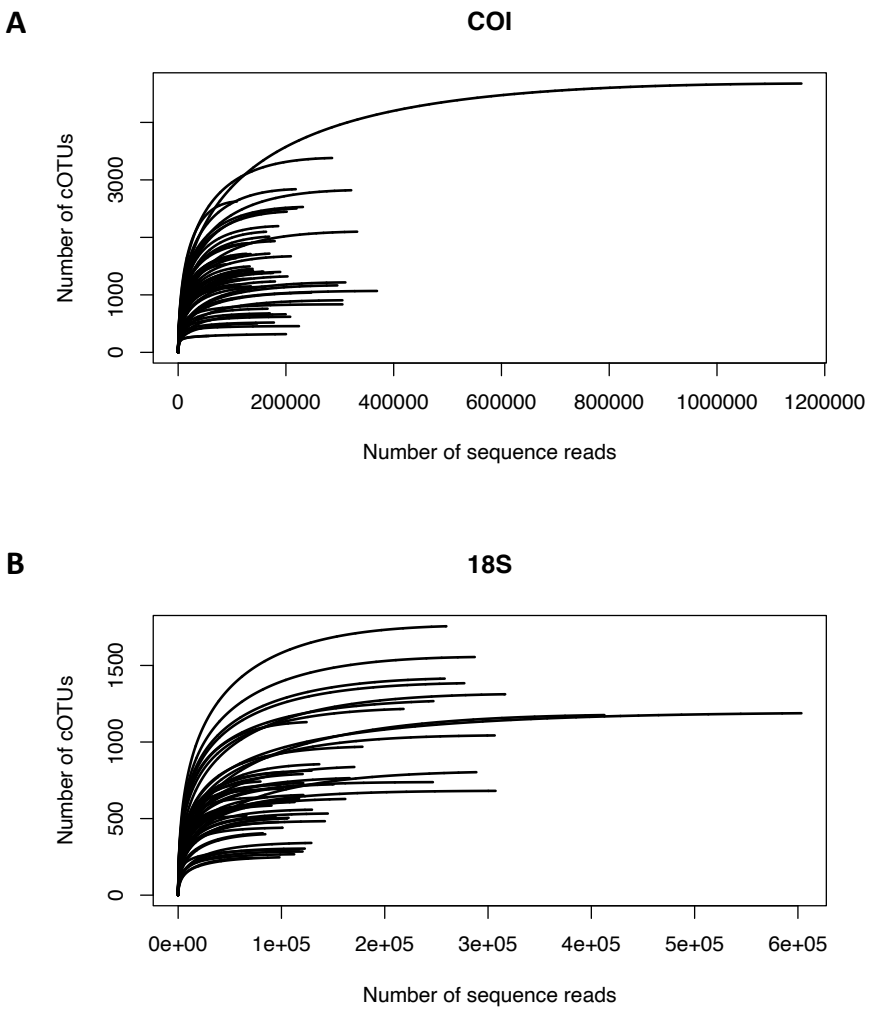

Figure 2.2. Rarefaction curves for individual metabarcoding samples across (A) COI and (B) 18S curated OTU (cOTU) datasets. Each plot depicts the relationship between the number of cOTUs detected as a function of the number of sequence reads per sample, with step size of 100 sequence reads.

Across rarefied samples, approximately a third of all cOTUs were found to be shared between motile and sessile fractions over both sampling years, with 31.9% of COI cOTUs and 33.6% of 18S cOTUs detected in both fractions (Figure 2.3). Overall, the proportion of 18S cOTUs (23.3% of all 18S cOTUs) found across all sites was almost double that of COI cOTUs (11.8%). For both amplicon datasets, Ile du Coin was found to have the highest proportion of unique COI (27.9%) and 18S cOTUs (22.6%), compared to Ile Anglaise and Moresby. On average across sites, 39.3% of COI cOTUs and 39.6% of 18S cOTUs were detected both in 2019 and 2021 samples (Figure 2.3). Samples collected in 2021 had more unique sequence variants than those collected in 2019, with 41.4% of 18S and 33.7% of COI cOTUs uniquely found in 2021 (Figure 2.3).

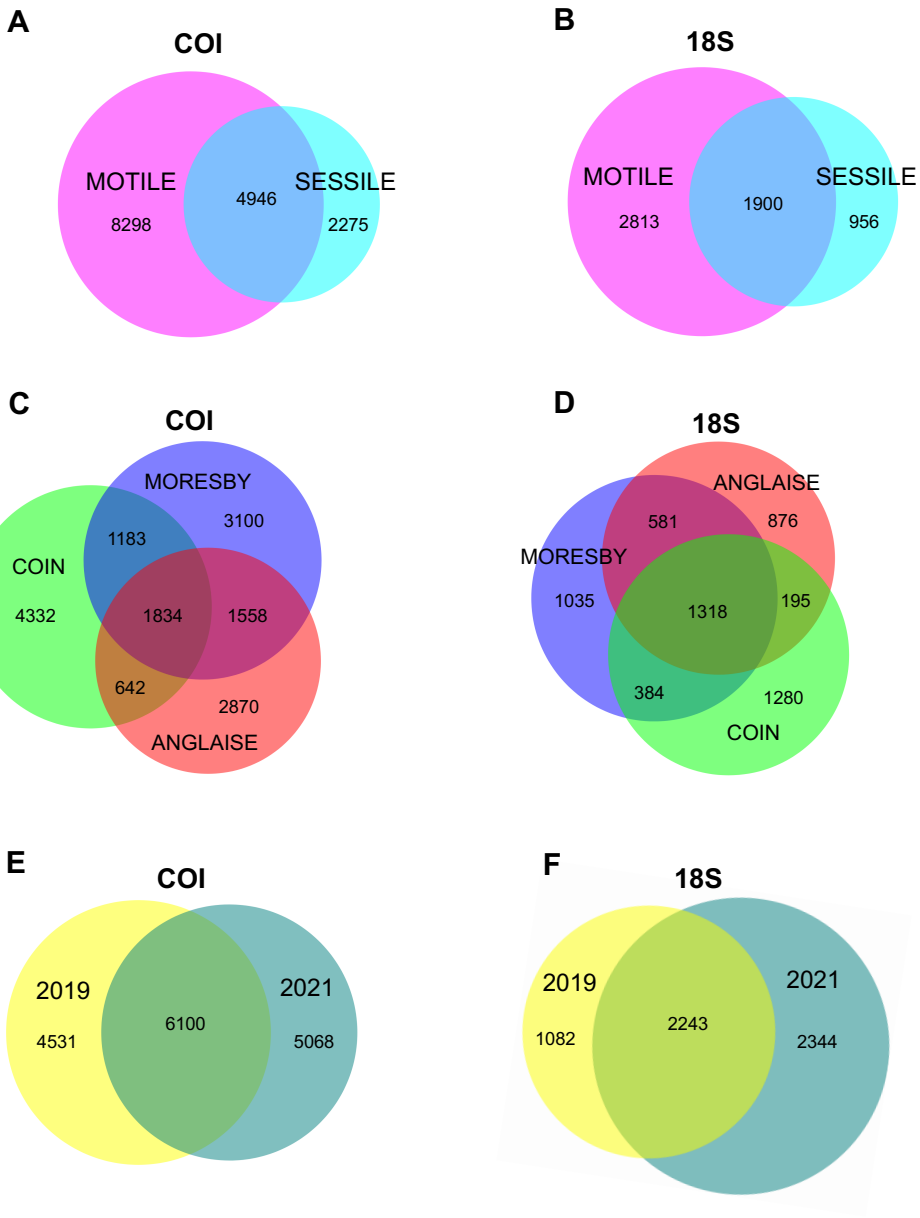

Figure 2.3. Venn plots displaying the number of COI and 18S cOTUs observed across A) B) motile and sessile fractions, C) D) across sampling sites, and E) F) across sampling years, following sample rarefaction.

Breakaway richness analyses estimated the presence of 60 more COI and 71 18s cOTUs than observed across all ARMS samples (Table 2.2). For both COI and 18S datasets, the estimated richness of all motile samples significantly increased between 2019 and 2021 samples by an estimate of 640 cOTUs (betta test, $p<0.05$*), whilst only the richness of sessile COI cOTUs, and not 18S cOTUs, was found to have significantly decreased over time, by an estimate of 376 cOTUs (betta test, $p<0.05$*) (Figure 2.4). No significant differences in the estimated richness of ARMS replicates across different sites, over both years, were observed for motile or sessile samples (betta test, $p>0.05$).

Table 2.2. Total estimated richness (breakaway analysis) across COI and 18S cOTUs, along with corresponding standard error (SE) values, and high and low confidence intervals, for samples across years and metabarcoding fractions.

	COI (cOTUs)				
Sample group	**Observed richness**	**Total estimated richness**	**SE**	**Confidence lower interval**	**Confidence higher interval**
All samples	18426	18486	15.93	18431	19173
2021	13927	13984	12.79	13933	14482
2019	11765	12021	67.99	11774	19167
100-500micron	13998	14103	22.37	14006	15405
500micron-2mm	7613	7738	25.65	7622	9389
sessile	8299	8480	35.96	8310	11391
2021 (100-500micron)	11281	11352	15.3	11288	12027
2021 (500micron-2mm)	5546	5555	3.15	5548	5594
2021 (sessile)	4957	5085	35	4963	7550
2019 (100-500micron)	7969	8224	54.51	7980	13757
2019 (500micron-2mm)	4147	4260	28.62	4154	6096
2019 (sessile)	6026	6039	3.91	6028	6100
	18S (cOTUs)				
Sample group	**Observed richness**	**Total estimated richness**	**SE**	**Confidence lower interval**	**Confidence higher interval**
All samples	6457	6528	27.61	6460	7993
2021	5334	5425	36.26	5338	7665
2019	3558	3602	13.76	3561	4109
100-500micron	4828	4832	2.13	4829	4851
500micron-2mm	2772	2780	3.02	2773	2816
sessile	3109	3119	7.48	3110	3259
2021 (100-500micron)	4122	4129	2.79	4126	4160
2021 (500micron-2mm)	2312	2369	17.86	2316	3152
2021 (sessile)	2434	2455	16.18	2435	2926
2019 (100-500micron)	2558	2563	2.46	2559	2587
2019 (500micron-2mm)	1287	1326	12.95	1290	1776
2019 (sessile)	1879	1908	10.21	1882	2204

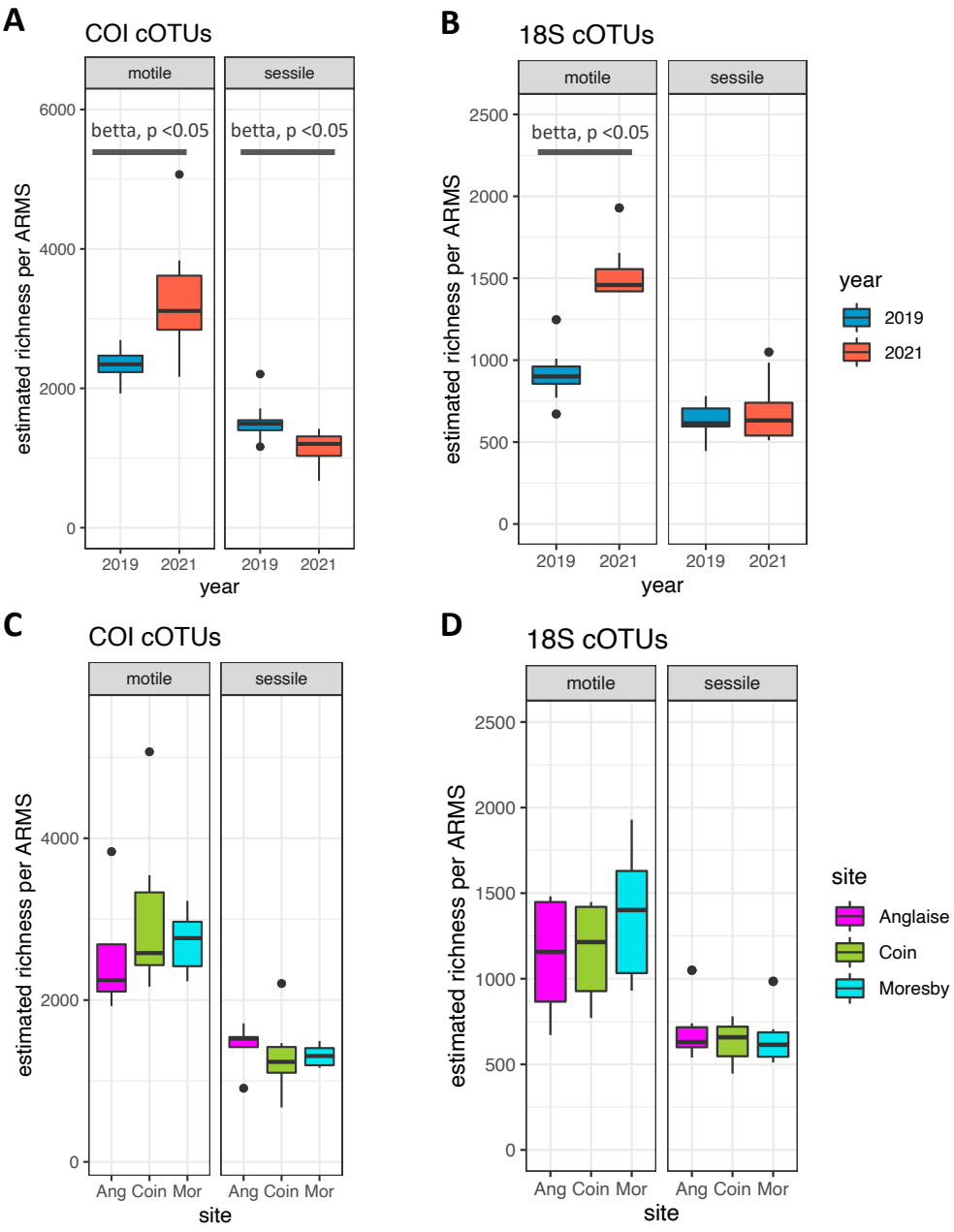

Figure 2.4. Boxplots of estimated richness (breakaway analysis) of (A) COI cOTUs in motile and sessile samples collected in 2019 (blue) and 2021 (red), (B) 18S cOTUs in motile and sessile samples collected in 2019 and 2021, (C) COI cOTUs in motile and sessile samples across Ile Anglaise (magenta), Ile du Coin (light green) and Moresby (turquoise) reef sites, and (D) 18S cOTUs in motile and sessile samples also across reef sites. Significant differences in the estimated richness (p-value<0.05, detected using betta tests of heterogeneity) of COI and 18S motile samples between sampling years, and of COI sessile samples between sampling years, were found, and are highlighted in each respective boxplot.

2.4.2 Community composition and taxonomy assignment success

A total of 32 phyla were identified across COI cOTUs and 33 phyla across 18S cOTUs, with 21 of these found in both amplicon datasets. When combined, a total of 21 metazoan, 5 plant, 4 fungi, 4 chromist and 8 protozoan phyla were identified across ARMS samples. Of the metazoan phyla, Arthropoda was found to have the highest number of both COI and 18S cOTUs as well as the highest number of sequence reads (Figure 2.5). Following arthropods, molluscs, cnidarians, sponges, echinoderms and chordates were then observed to have the highest number of COI cOTUs, in that order. For 18S, nematozoans, platyhelminthes, annelids, sponges and molluscs were observed to have high numbers of cOTUs, in that order. Sponges closely followed by arthropods have the highest sequence read abundance in the COI dataset, whilst annelids had the second highest abundance of reads in the 18S dataset (Figure 2.5).

After 12 months deployment (2019 collections), the top 10 most abundant cOTUs contributed 37.8% of total metazoan reads for that year, whilst after 36 months deployment (2021 collections) the top 10 cOTUs contributed 35.45% of total metazoan reads. In 2019, the most abundant cOTUs were an un-identified polychaete, followed by a shrimp (family = Hippolytidae) and an oyster (family = Ostreidae), in that order. In 2021, six of the top 10 must abundant cOTUs were sponges, including the top three cOTUs which identified as a demosponge (order = Poecilosclerida), *Oscarella* sp. and *Neofibularia hartmani*, in that order.

Estimated Shannon diversity at order level (DivNet analysis) was found to be significantly lower in 2021 sessile samples than in 2019 samples, across both COI and 18S cOTU datasets ($p<0.05$* for both)(Figure 2.6). Whilst no significant differences were observed between motile communities across sampling years in COI samples, the estimated Shannon diversity of motile 18S cOTUs was significantly higher in 2021 samples ($p<0.05$*)(Figure 2.6). Significantly higher diversity was observed in 2021 Ile du Coin 18S samples from than those from 2019 ($p<0.05$*), but no significant differences in Shannon diversity was observed between sampling years for any other sites.

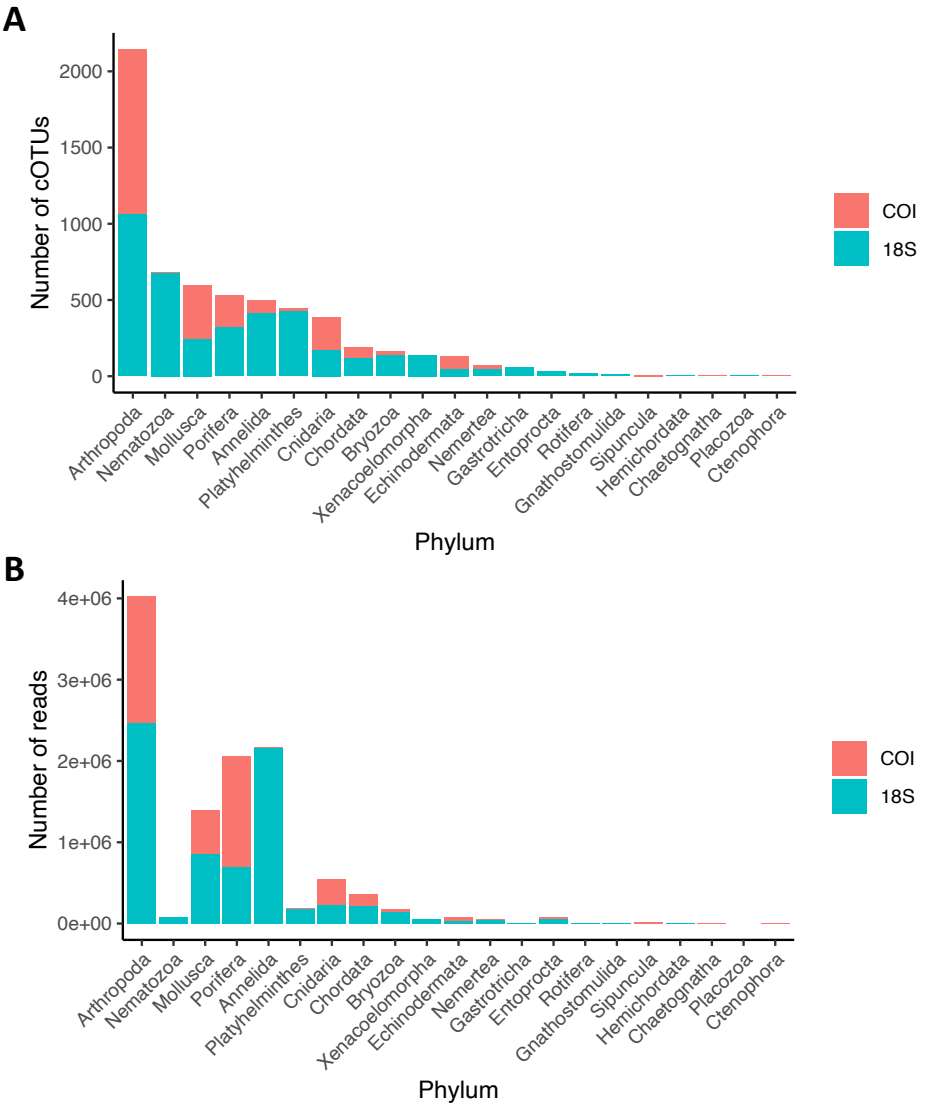

Figure 2.5. Stacked bar plots displaying (A) the total number of COI (red) and 18S (blue) cOTUs identified across metazoan phyla, and (B) the total number of COI (red) and 18S (blue) sequence reads detected across metazoan phyla, in all ARMS metabarcoding samples.

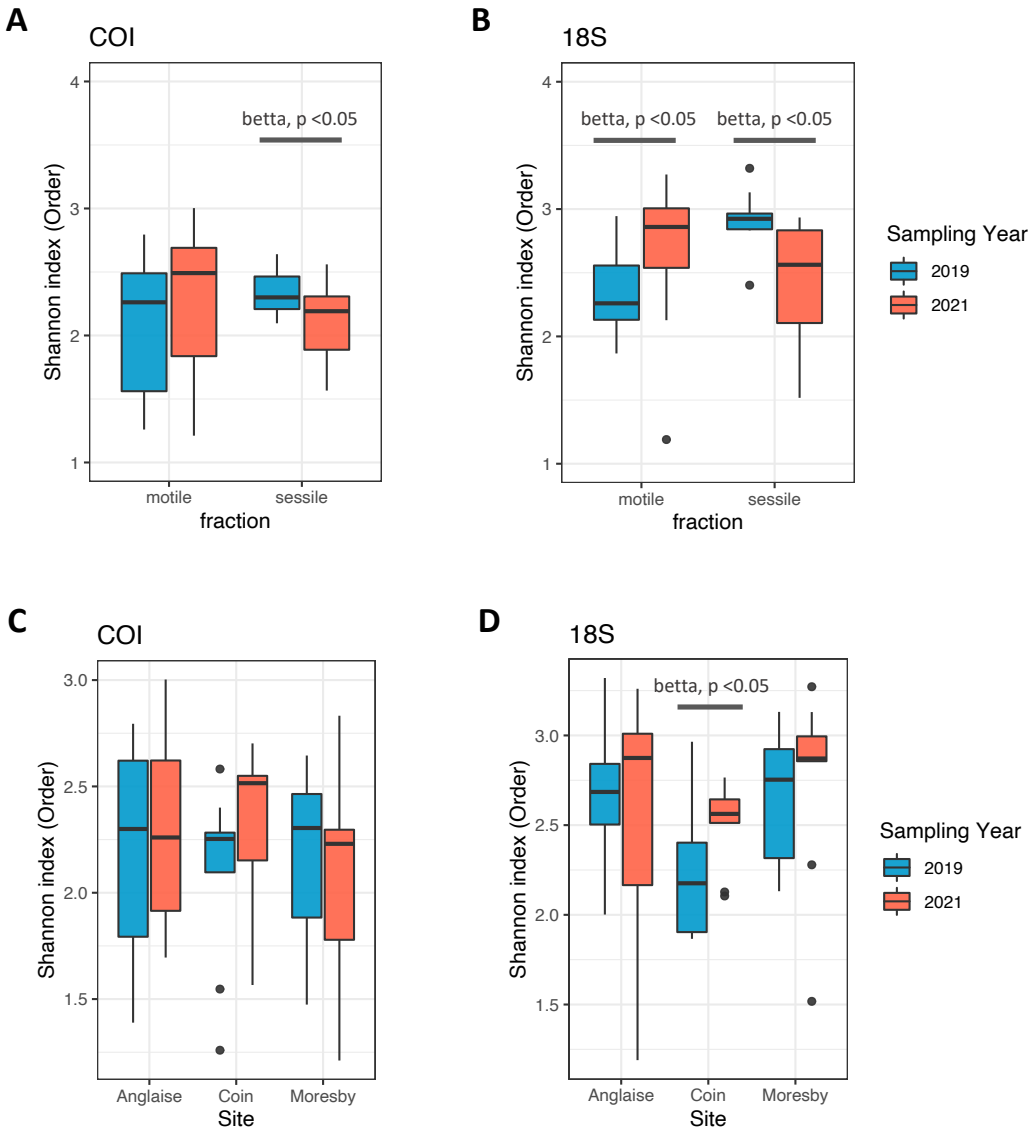

Figure 2.6. Boxplots of estimated Shannon diversity (breakaway analysis) of metazoan orders in ARMS samples over both 2019 (blue) and 2021 (red) sampling years, including (A) COI cOTUs in motile and sessile samples, (B) 18S cOTUs in motile and sessile samples, (C) COI cOTUs in samples from different sampling sites, and (D) 18S cOTUs in samples from different sites. Significant differences were detected between sampling years in the Shannon diversity values of sessile samples in both COI and 18S cOTU datasets (see subplots A and B), motile samples in the 18S cOTU datasets (see subplot B), and Ile du Coin (Coin) samples in the 18S cOTU dataset (see subplot D), indicated by the betta test p-values located in each respective boxplot.

Assignment success of sequence variants using IDTAXA (confidence at or above 30%) was high at domain level for both COI cOTUs (95.1% of sequence variants identified) and 18S cOTUs (91.3%)(Figure 2.7). For 18S, assignment success gradually drops across taxonomic ranks, with 38.4% of cOTUs assigned at order level across all samples. For COI, assignment success drops sharply after domain level, with only 15.9% of cOTUs assigned at phyla level and 3.8% of cOTUs assigned at species level. For both COI and 18S datasets, less unique taxa were identified from sessile samples, but a higher percentage of sequence variants in sessile samples were identified across taxonomic ranks than sequences variants in motile samples.

We also employed the BLAST approach to assign taxonomy to COI cOTUs and found the assignment success rate of this method to be only slightly higher than the IDTAXA method, with 26.1% of cOTUs successfully assigned at phyla level (medium coverage; 85% query cover, 85% percentage identity) and 4.3% of cOTUs assigned at species level (high coverage; 85% query cover, 97% percentage identity). For motile samples, 3.7% of cOTUs were assigned at species level (588 cOTUs, high coverage) and 23.9% at phyla level (3814, medium coverage). A slightly higher percentage of COI cOTUs in sessile samples are assigned at both species (4.9%) and phyla (28.0%) ranks using a BLAST approach.

A total of 488 COI cOTUs were found to have a species-level assignment using IDTAXA at or above 60% confidence (default high confidence, see Murali et al., 2018). The IDTAXA taxonomy assignment of these cOTUs closely matched with the species-level assignment given to them by the BLAST approach. Of these 488 cOTUs, 364 had exact matches with BLAST assignments, 122 had near/similar assignments (e.g., for OTU_6568 the IDTAXA assignment is "*Viriolopsis fallax*" and "unclassified_Viriolopsis" using BLAST), and only two had wrong assignments (e.g., for OTU_2314, IDTAXA assignment is *Boasia chierchiae* at 60.7% confidence, but *Creseis virgula* using BLAST with a query cover of 99% and identification match of 100%). On average across COI cOTUs with exact or near matching IDTAXA/BLAST assignments, the BLAST query cover was at 98.9% and identity match at 98.7%.

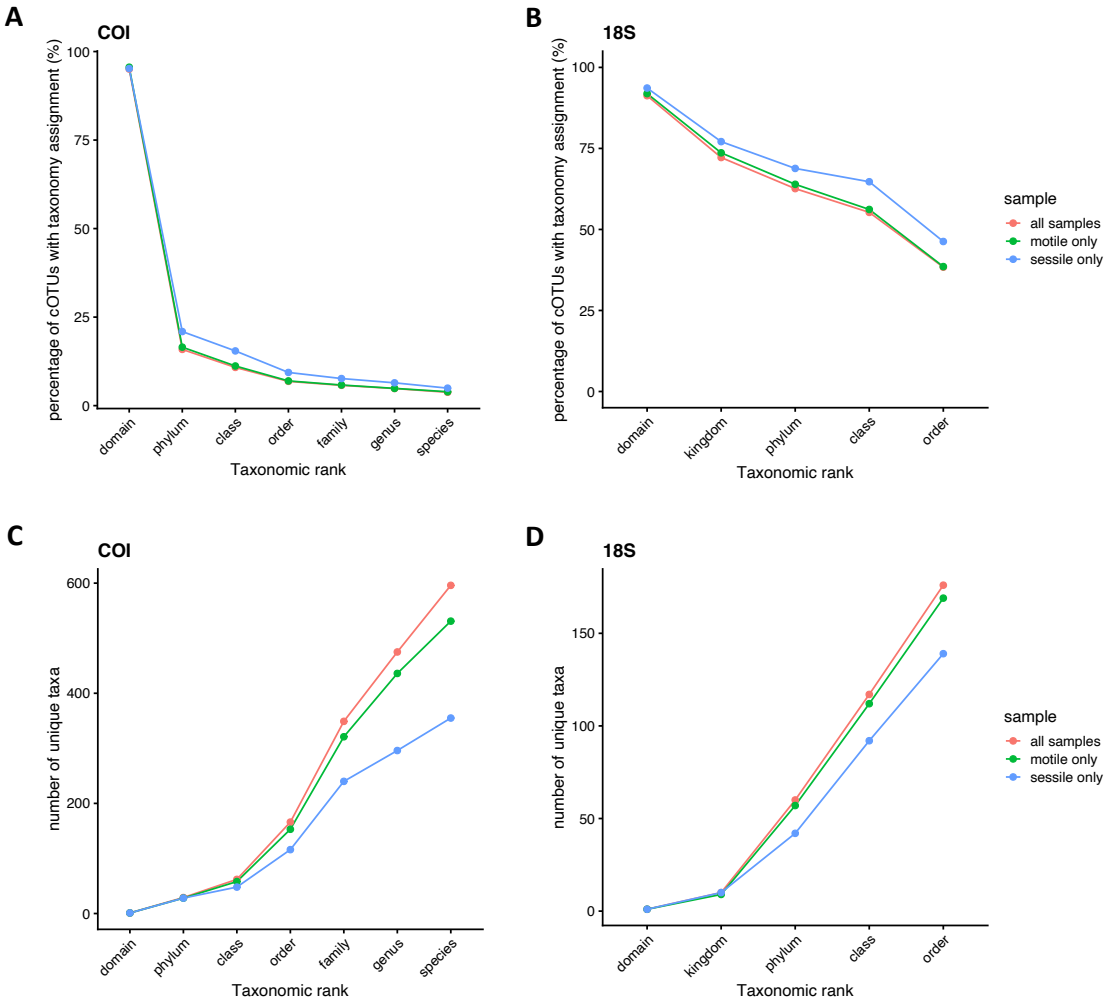

Figure 2.7. Plots of the taxonomy assignment success of cOTUs, using the IDTAXA assignment algorithm, across ARMS samples. The percentage of (A) COI cOTUs and (B) 18S cOTUs in either all samples (red), motile samples only (green) and sessile samples only (blue), is provided across taxonomic ranks. The number of unique taxa identified at each taxonomic rank across (C) COI cOTUs and (D) 18S cOTUs across all samples (red), motile samples only (green) or sessile samples only (blue) is also presented.

When using the most conservative approach possible (BLAST identification, 100% query cover, 100% identification match), we identified a total of 240 marine metazoan species, of which 168 are fully described (aka species name does not include identification numbers such as “Anomura sp. LPdivOTU90”)(Appendix Table A.4). These 168 species included 23 sponges, 17 gastropods, 15 decapods, 8 brittlestars and 5 sea cucumbers and 37 fish (Figure 2.8).

Figure 2.8. Images of some of the marine species identified on ARMS across the Chagos Archipelago MPA with high confidence using metabarcoding (BLAST assignment at 100% query cover and 100% identity match). From the top left across to the right; *Fusigobius neophytus, Octopus cyanea, Acanthaster planci, Callyspongia fallax, Goniobranchus vibratus, Maculotriton serriale, Palaemonella rotumana, Macrophiothrix longipeda, Holothuria scabra, Euplica ionida, Toxopneustes pileolus, Conchodytes meleagrinae*. Copyright references are provided for each image.

Only 14 species of the 168 described species identified using metabarcoding are represented in the online archives of the Natural History Museum of London (Natural History Museum, 2014), and only 6 are represented in the online archives of the Smithsonian National Museum of Natural History. Two high confidence cOTUs match with specimens in the Florida Museum's Chagos specimen collection. Finally, Head et al., (2018) identified 164 decapod species across dead coral heads in the Chagos Archipelago, and we find that only 3 of the 15 decapod species identified here are listed in their species list.

2.4.3 Spatiotemporal variability in metazoan community abundance and beta-diversity

Similar patterns of metazoan community composition, based on Jaccard dissimilarity of cOTUs with a metazoan phyla-level assignment, were observed across both 18S and COI datasets (Figure 2.9). Community composition of ARMS samples across years overlapped temporally (across years), but visible patterns of separation were seen spatially (between sampling sites), where samples from Ile du Coin (lagoonal site) clustered away from those of ocean-facing sites (Ile Anglaise, Moresby).

Across metazoan communities, and for both COI and 18S datasets, the majority of beta diversity (measured as Jaccard dissimilarity) observed between i) ARMS triplicates within sampling sites and per sampling year, or ii) across sampling years for each site, can be attributed to turnover (aka species replacement), rather than nestedness (species loss/gain) (Figure 2.10). On average in 2019, only 20.45% of COI cOTUs and 29.7% of 18S cOTUs were detected across all three triplicates within each site (Appendix Table A.7). On average in 2021, only 15.9% of COI cOTUs and 31.4% of 18S cOTUs were found present across all three triplicate ARMS within each site, although the low value of the former is likely due to the missing samples due to sequencing error (see Results section 2.4.1., Appendix Table A.7).

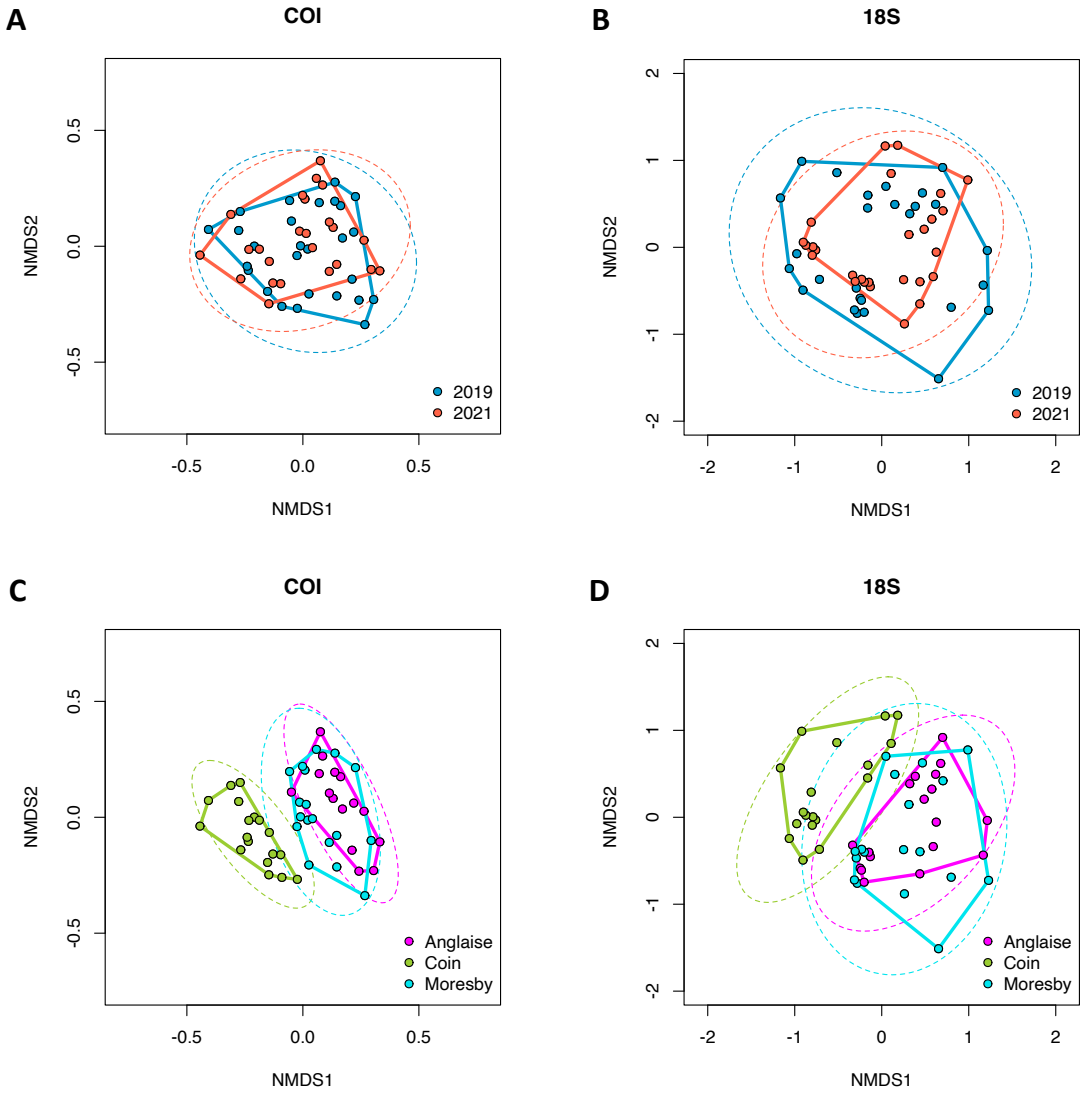

Figure 2.9. Non-metric dimensional plots (NMDS) comparing the community composition of metazoan (A) COI cOTUs and (B) 18S cOTUs from 2019 (blue) and 2021 (red) sampling collections, as well as the community composition of metazoan (C) COI cOTUs and (D) 18S cOTUs across Ile Anglaise (turquoise), Ile du Coin (magenta) and Moresby (light green) sampling sites. Distances between data points are based on Jaccard dissimilarities (presence-absence), and ellipses (dashed line) represent 95% confidence around group centroids, whilst solid lines represent the outer hull of points per group centroid.

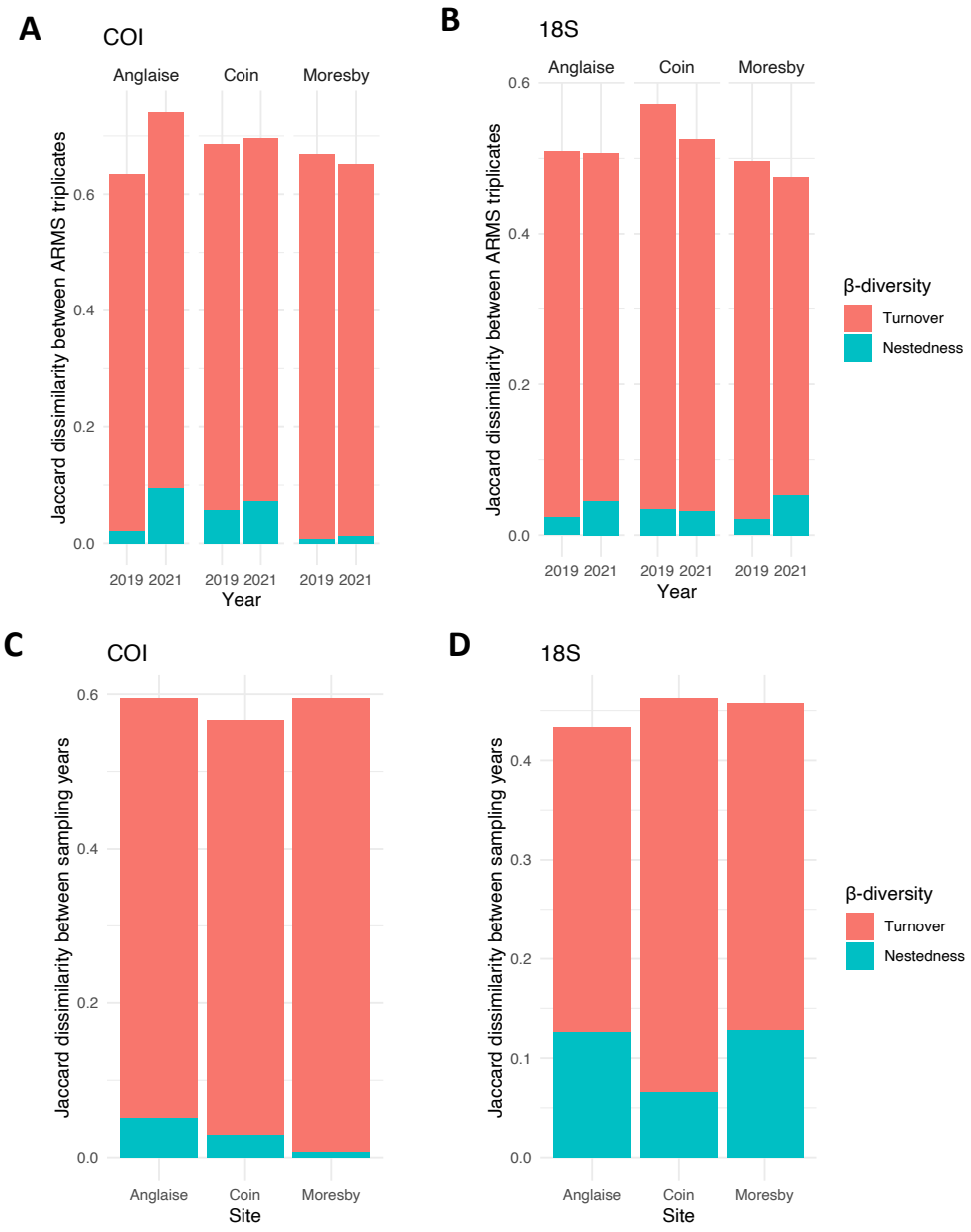

Figure 2.10. Stacked barplot displaying the fraction of beta-diversity (Jaccard dissimilarity, presence/absence) attributed to turnover or nestedness of metazoan cOTUs across ARMS triplicates within sites per sampling year for A) COI cOTUs and B) 18S cOTUs, and across sampling years (2019 vs 2021) per site for A) COI cOTUs and B) 18S cOTUs.

Overall, the dissimilarity between ARMS triplicates within each site was higher in the COI dataset than in the 18S dataset with mean dissimilarity distances of 0.68 and 0.51 respectively (Figure 2.10. **A** & **B**). Similarly, the dissimilarity between 2019 and 2021 samples for each individual site was higher in the COI dataset than in the 18S dataset, with respective distances of 0.59 and 0.45 (Figure 2.10. **C** & **D**). The proportion of dissimilarity attributed to turnover across triplicate ARMS per site and per sampling year was similar for both COI (93.63%) and 18S (93.02%) datasets. However, a higher proportion of the dissimilarity observed between sampling years across each site was attributed to turnover for COI samples (94.9% of dissimilarity) compared to 18S samples (76.14%), where nestedness plays a larger role in shaping beta-diversity (Figure 2.10).

Multivariate GLMs showed both site and year, as well as their interaction, had a significant effect on the composition of metazoan ARMS communities at order level for both COI and 18S datasets (where metazoan cOTUs were grouped based on their order level assignment)(ANOVA on multivariate GLM, Table 2.3).

Table 2.3. Output summary of multi-variate GLM on the effect of sampling sites, years and the interaction between both variables, on the composition of order-level taxa across COI and 18S metazoan communities.

Amplicon	Variables	Residual degrees of freedom	Dev	P-values
18S	(Intercept)	53		
	Site	52	370.1	0.001***
	Year	50	525.5	0.001***
	Site: Year	48	163.8	0.018*
COI	(Intercept)	50		
	Site	49	253.6	0.002**
	Year	47	604.5	0.001***
	Site: Year	45	205.0	0.003**

Site and sampling years, when interacting together, had a significant impact on the presence/absence of 7 metazoan orders in the COI dataset (out of 123) (Table 2.4), and 3 metazoan orders in the 18S dataset (out of 109) (Table 2.5) (see Appendix Tables A.5 & A.6 for full model outputs). For COI, this

included 2 demosponges (Biemnida, Bubarida), corrallimorphs (Corallimorphia), star fish (Valvatida), limpets (Siphonariida), and krill (Euphasiacea). For 18S, this included axinellid sponge (Axinellida) and soft corals (Actinaria).

Across both COI and 18S datasets, sampling site choice had a significant impact on the presence/absence of soft corals (Actinaria, Alcyonacea), bryozoans (Cyclostomatida) and nemertean worms (Monostilifera), with soft coral orders and bryozoans more frequently detected across ocean-facing sites (Moresby/Anglaise), and nemertean worms more frequently detected in the lagoon-facing site (Ile du Coin)(Tables 2.4 & 2.5). In the COI dataset alone, nudibranch (Nudibranchia), pteropod (Pteropoda), pleurobranchid (Pleurobranchida) and neogastropod (Neogastropoda) molluscs were less detected across ARMS in the lagoonal reef than in ocean-facing reefs (Table 2.4). The same pattern was observed for heart urchins (Spatangoida) and some copepods (Poecilostomatoida). On the other hand, hydrozoans (Anthoathecata) and polychaetes (Paraonidae, Eunicida) were present across more ARMS samples in the lagoonal reef than on ocean-facing reefs. In the 18S dataset alone, barnacles (Pygophora), bivalves (Limoida), siphonophores (Siphonophorae) and kinorhynchs (Cyclorhagida) were observed across more samples from ocean-facing sites, whilst nematodes (Triplonchida) and gnathostomulids (Bursovaginoidea, Filospermoidea) were more abundant in the lagoon-facing reef.

Sampling year alone also had a significant impact on the presence and absence of 17 orders in the COI dataset and 28 orders in the 18S dataset. Across both amplicon datasets, scleratinian corals (Scleractinia) and comb jellies (Platyctenida), were detected in significantly more 2021 samples than 2019 samples. In the COI dataset alone, calanoid copepods were detected in more 2021 than 2019 samples, whilst only bryozoans (Ctenostomatida) were detected more often in 2019. Furthermore, hydrozoans (Trachymedusae) and agelasid sponges (Agelasida) were only detected in 2021 samples. In the 18S dataset, aside from vetigastropods (Vetigastropoda), all orders whose presence/absence is determined by sampling year were found across more 2021 than 2019 samples, including sponges (Homosclerophorida, Bubarida) and tunicates (Stolidobranchia).

Table 2.4. Output summary of univariate GLMs of metazoan orders in the COI dataset with site, year, and both variables interacting. Only orders found to have a significant relationship with variables are displayed, indicated by a tick and green highlight, are displayed here. Full model output including p-values and test scores can be found in Appendix Table A.5.

Phylum	Order	Site * Year	Site	Year
Annelida	Eunicida		✓	
	Paraonidae		✓	
	Spionida		✓	
Arthropoda	Euphausiacea	✓		
	Amphipoda		✓	✓
	Sarcoptiformes			✓
	Tanaidacea			✓
	Isopoda		✓	
	Poecilostomatoida		✓	
Bryozoa	Ctenostomatida			✓
	Cyclostomatida		✓	
Chordata	Syngnathiformes		✓	✓
	Aplousobranchia			✓
	Gobiiformes			✓
	Lutjaniformes		✓	
Cnidaria	Corallimorpharia	✓		✓
	Trachymedusae		✓	✓
	Coronatae			✓
	Scleractinia			✓
	Actiniaria		✓	
	Alcyonacea		✓	
	Anthoathecata		✓	
Ctenophora	Platyctenida			✓
Echinodermata	Valvatida	✓		
	Aspidochirotida		✓	✓
	Amphilepidida		✓	
	Camarodonta		✓	
	Spatangoida		✓	
Mollusca	Siphonariida	✓		
	Triphoridae		✓	✓
	Littorinimorpha			✓
	Cerithiidae		✓	
	Heterostropha		✓	
	Neogastropoda		✓	
	Nudibranchia		✓	
	Pleurobranchida		✓	
	Pleurotomariida		✓	
	Pteropoda		✓	
Nematoda	Enoplida			✓
Nemertea	Monostilifera		✓	✓
Platyhelminthes	Polycladida	✓		
Porifera	Biemnida	✓		
	Bubarida	✓		
	Agelasida		✓	✓
	Polymastiida		✓	

Table 2.5. Output summary of univariate GLMs of metazoan orders in the 18S dataset with site, year, and both variables interacting. Only orders found to have a significant relationship with variables are displayed, indicated by a tick and green highlight, are displayed here. Full model output including p-values and test scores can be found in Appendix Table A.5.

Phylum	Order	Site * Year	Site	Year
Annelida	Haplotaxida		✓	✓
	Golfingiida			✓
	Phascolosomatiformes		✓	
	Aspidosiphonidormes		✓	
Arthropoda	Opiliones	✓	✓	
	Calanoida			✓
	Siphonostomatoida			✓
	Halocyprida			✓
	Facetotecta			✓
	Pygophora		✓	
Bryozoa	Cyclostomatida		✓	✓
	Tubuliporida		✓	✓
Cnidaria	Actiniaria	✓	✓	
	Alcyonacea		✓	✓
	Coronatae		✓	✓
	Carybdeida			✓
	Limnomedusae			✓
	Scleractinia			✓
	Siphonophorae		✓	
Ctenophora	Platyctenida			✓
	Cydippida			✓
Entoprocta	Loxosomatidae	✓	✓	
Gnathostomulida	Bursovaginoidea		✓	
	Filospermoidea		✓	
Lophophorata	Lingulida		✓	
Mollusca	Vetigastropoda			✓
	Ostreoida			✓
	Limoida		✓	
Nematozoa	Monhysterida			✓
	Araeolaimida			✓
	Chromadorida		✓	
	Triplonchida		✓	
Nemertea	Monostilifera		✓	
	Polystilifera		✓	
Platyhelminthes	Macrostomida			✓
Porifera	Axinellida	✓		✓
	Hadromerida		✓	✓
	Dendroceratida		✓	✓
	Homosclerophorida			✓
	Poecilosclerida			✓
	Verongiida			✓
	Bubarida			✓
	Haplosclerida			✓
	Tetractinellida		✓	
	Biemnida		✓	
Rotifera	Adinetida		✓	
Scalidophora	Cyclorhagida		✓	
Tunicata	Stolidobranchia			✓
	Enterogona		✓	

A total of 546 indicator cOTUs/species were identified within metazoan communities of the COI dataset for either ocean-facing or lagoonal reef habitat across individual, or both, sampling collections. Across both ocean-facing sites, and across both sampling collections, 39 cOTUs were identified as significant indicators of ARMS metazoan communities, including brittlestar *Ophiothrix trilineata*, sea anemone *Bunodeopsis medusoides*, annelid *Phyllodoce* sp. (aff. hawaiia HAW02) and soft coral *Ovabunda sp.* Across 2019 ARMS only, 13 COI cOTUs were found to be significant indicators of ocean-facing sites, including brittlestar *Breviturma doederleini*. Across 2021 ARMS only, 22 cOTUs were found to significantly associated with both sites, including 10 sponges, such as *Gelliodes wilsoni*, one *Plakortis* sp. and one *Petrosia* sp., as well as *Pavona* sp. coral and seven unidentified decapods. In the lagoon site alone, a total of 57 cOTUs were significantly associated with combined 2019 and 2021 ARMS metazoan communities. This includes demosponges *Tedania klausi* and *Iotrochota protea*, hydrozoan *Loxomitra mizugamaensis*, nematode *Cephalothrix cf. fasciculus* as well as gastropods *Amathina bicarinata*.

2.5. Discussion

Global losses in biodiversity threatens the stability of ecosystems world-wide and the services they provide to humanity (Cardinale et al., 2012; Diaz et al., 2006, Worm et al., 2006), and we now face losing species from tropical coral reefs before having fully assessed and understood their ecological roles (Bradshaw et al., 2009). Studies assessing patterns of coral reef benthic biodiversity across both spatial and temporal scales are not common but are urgently needed to understand how rapid environmental change will impact these habitats in different localities. Here, we present novel data on the biodiversity of cryptobenthic communities across reefs of the Chagos Archipelago Marine Protected Area (MPA). This study is the first to present metabarcoding data on benthic communities for the Chagos Archipelago MPA and explores how patterns of biodiversity differ over time and across different sites. Importantly, by using standardised collection tools, Autonomous Reef Monitoring Structures (ARMS), and following standardised protocols, we ensure our data is comparable and shareable with the wider research community.

2.5.1. High diversity across cryptobenthic communities

The diversity and small size of coral reef cryptofauna poses a significant challenge to morphology-based methods, and metabarcoding is a valuable and increasingly used method for the study of these organisms (Ip et al., 2022; Timmers et al., 2020; Carvalho et al., 2019). Using a multi-marker approach allows for a more comprehensive analysis of targeted communities (Clarke et al., 2017), as individual genetic regions have different rates of evolution, have different levels of representation in reference databases (Wangensteen et al., 2018), and universal primers used to target individual regions can carry certain biases (Sipos et al., 2007). Here, by targeting both COI and 18S genes, we recover the presence of organisms spanning 42 different phyla, across metazoan, plant, protist, fungi and chromist kingdoms. In total, our bioinformatics pipeline detects almost three times as many COI curated Operational Taxonomic Units (cOTUs)(18,426) than 18S cOTUs (6,457), but our rarefaction analysis and the results of our estimated richness calculations suggest that most of the diversity within our samples was captured. Both markers recover similar patterns of richness (number of sequence variants) and abundance (number of reads) across some metazoan groups, including arthropods, molluscs, sponges, cnidarians, echinoderms and chordates. However, metabarcoding of the COI region performed poorly however for the detection and identification of marine worms such as annelids, platyhelminthes and nematozoans, as well as for xenocoelomorphs. Similar proportions of genetic overlap between fractions, sites, and sampling years were also observed across both COI and 18S datasets, and both amplicons recovered similar patterns of estimated richness, Shannon diversity and overall community composition across samples. Overall, our findings suggest that whilst both genetic markers do not pick up the same set of organisms, they do detect the same overarching ecological patterns, as has been observed in other multi-marker metabarcoding marine studies (Wangensteen et al., 2018). We targeted the COI and 18S (v4) regions to recover eukaryotic diversity, and in particular metazoan communities, but the targeting of 16S, internal transcribed spacer (ITS) and 23S genetic regions could be used to recover the diversity of microbial, fungal and plant organisms from retrieved ARMS samples. Whilst the 16S gene has been previously used to study microbial communities from ARMS (Ip et al., 2022; Pearman et al., 2019), no studies to date have specifically targeted ARMS plant and fungal communities using metabarcoding.

2.5.2. Spatiotemporal factors result in high heterogeneity across samples

The rate of at which new marine benthic communities form on bare substrate depends on multiple factors including differences in larval settlement rates, growth rates and reproductive strategies of different colonising groups, as well as predator/grazing pressure and environmental factors (Gouezo et al., 2020; Osman et al., 2004; Duffy & Hay, 2000; Rodriguez et al., 1993). Here, we sampled the same reefs twice over a period of 3 years (once after 12 months, once after 36 months), and observed differences in richness, alpha and beta-diversity across benthic assemblages of different ages. On average, approximately a third of all COI and 18S cOTUs identified were detected in both one and three-year old ARMS communities. More unique cOTUs are observed in 2021 samples than in 2019 samples which appears to be driven by motile samples rather than sessile samples. Indeed, estimated richness increases within motile ARMS samples over time, whilst the estimated richness of sessile samples stays the same or reduces as communities age. The same patterns are observed across Shannon diversity estimates of metazoan communities, where sessile diversity estimates also significantly decreased over time. We hypothesise that as communities age, some sessile organisms become dominant across ARMS surfaces and increase disproportionally in biovolume in comparison to others, possibly leading to increased representation in extracted samples and ultimately across sequencing space (Elbrecht et al., 2017). In turn, as sessile organisms grow over time, more habitat complexity is provided for mobile organisms to inhabit, thereby increasing motile sample richness. To test our hypothesis, we would extend our current study by i) analysing of the diversity and abundance of larger motile organisms (>2mm) collected from the same ARMS, and ii) carrying out image-based analysis of the same ARMS plates to determine the percentage cover of sessile groups.

The length of ARMS deployment had a significant impact on the composition and the presence-absence of metazoan orders. Significantly more scleractinian corals were detected in 3-year-old communities versus 1-year-old communities, a pattern which is expected as hard corals are particularly slow growing in comparison to other sessile organisms. Higgins et al (2019) looked at benthic succession on diverse coral reefs in the Red Sea and found little hard coral recruitment on artificial substrates within a 13-month experiment, which they postulate could have been due to only capturing a single recruitment event. Here, by deploying ARMS over a 3-year period, we find that the abundance (number of reads) and diversity (number of cOTUs) of stony corals increase as communities age. We further explore the

recruitment patterns of hard corals on ARMS in Chapter 5. On the other hand, we see a significant reduction in bryozoan richness over time, which also fits expected patterns of recruitment for this group. Bryozoans readily colonise both natural and artificial surfaces in marine systems (Jackson and Hughes, 1985) and have been found to drive patterns of dissimilarity within young (7-13 month) benthic reef communities (Palomino-Alvarez et al., 2021; Higgins et al., 2019). Only one other ARMS study has investigated temporal changes in ARMS communities (Villalobos et al., 2022), but attributed most of the beta diversity observed to the occurrence of a bleaching event between ARMS field retrievals. Here we have presented observations of natural community succession over time in the absence of major environmental change.

Site choice also played an important and significant role in shaping cryptobenthic communities across ARMS in this study. Whilst the overall estimated richness of organisms was equal across sites, and the Shannon diversity remained mostly similar within each site between 2019 and 2021 samples, the composition of metazoan communities was significantly different across reefs. In particular, we observed large variations between the lagoon-facing reef (Ile du Coin) and the two ocean-facing reefs (Moresby, Ile Anglaise), with the former harbouring the most unique COI and 18S cOTUs and clustering away from communities of the other two sites. Whilst hydrozoans, nematode and polychaete worms were significantly more common in Ile du Coin, soft corals and several groups of molluscs including bivalves, nudibranchs and gastropods, were significantly more abundant on ARMS from ocean-facing reefs. Our indicator analysis suggests the potential habitat preference of certain species regardless of the age of ARMS communities, such as *Ovabunda sp.*, (soft coral), *Ophiothrix trilineata* (brittlestar) and *Bunodeopsis medusoides* (sea anemone) which were found highly associated with ocean-facing sites, or small snails *Petalochonchus keenae* and *Amathina bicarinate*, *Lysidice unicornis* (annelid) and multiple demosponges which were found in high association with the lagoonal reef site. Other ARMS studies have found that depth, distance from land, and cross shelf gradients can drive community patterns (Ip et al., 2022; Pearman et al., 2018).

Characterising the composition of beta-diversity across habitats is important as this information can be used to decide whether individual sites, or wider regions, must be prioritised for conservation purposes (Socolar et al., 2016). For example, if nestedness accounts for most of the beta-diversity observed

across habitats, then prioritising the conservation of sites with higher species richness may be valuable. On the other hand, if turnover is found to be the major component of observed beta-diversity, then a wider conservation effort encompassing a range of different sites may be needed. Here, we find almost all the beta-diversity observed between ARMS samples in this study can be attributed to turnover (aka species replacement), rather than nestedness (aka species loss). It is widely recognised that scales must be considered when studying the processes which influence species distribution and turnover in a certain habitat (Miyazawa et al., 2020; Chave, 2008). Several such processes include i) dispersal capabilities, ii) abiotic factors/climate, iii) species interaction and iv) habitat structure (McGill, 2010).

Environmental filtering can drive both nestedness and turnover components of beta-diversity within benthic marine ecosystems (Menegotto et al., 2019). Here, we hypothesise that differences in the exposure and physical-chemical profiles of ocean-facing reefs and sheltered lagoonal reefs likely contribute to the variation of community composition observed between sites in our analysis. For example, reefs located on the outside of atolls can be subject to higher wave action and lower temperatures, whilst reefs located within atolls and inside lagoons can experience variable tidal changes and increased sedimentation. However, as we do not present environmental data for our sampling sites in this study, the impact of abiotic factors on community composition observed on ARMS here remains an open question. An extension to this study would include an analysis of *in-situ* environmental parameters occurring across our reef sites to determine if, and how, cryptobenthic communities experience different abiotic conditions (see Chapter 2).

The dispersal abilities of species, and the barriers which hinders them, can also be important drivers of species turnover across marine ecosystems (Tosetto et al., 2022; Josefson et al., 2016). Our reef sites are spread across two atolls and are 25-50 km apart from each other (Figure 2.1). We know that prevailing currents move from east to west across the Chagos Archipelago MPA (Schott et al., 2009), but we have little knowledge of local currents within and between these two atolls over short time scales. Some cryptobenthic groups such as sponges can have very limited dispersal capabilities (Maldonado, 2006), whilst others such as echinoderms and crustaceans have higher dispersal capabilities due to their planktonic larval stages. It is possible that dispersal limitations drive species turnover across some, but not all, groups identified by our metabarcoding analysis. Pearman et al. (2020) investigated pan-

regional distributions of cryptobenthic communities using ARMS and found that the considerable overlap of sequence variants between motile and sessile fractions, which is also observed here in our study (Figure 2.3), renders it difficult to determine the extent of dispersal constraints for different taxa groups across local and regional scales. Further study on the abundance and diversity (e.g., using barcoding and image analysis) of individual taxonomic groups, as well as data on currents within the region would be needed to determine how connected our study sites are in the Chagos Archipelago MPA.

Whilst we observed overall differences between the composition of communities across sites, we also see high heterogeneity and high spatial turnover between ARMS triplicate sets (per site, per sampling year), with only an average ~ 24% of metazoan cOTUs (COI and 18S) found to be shared between all three units. We would expect the environmental conditions to be similar within sites, and that the proximity of ARMS triplicates (which are within ~5-10 meters of each other at each site) would result in little to no dispersal barriers across cryptobenthic groups. At very small spatial scales, habitat heterogeneity and inter-species processes such as predation/grazing and competition can significantly influence species distribution (Ellingsen et al., 2020). The standardised design of ARMS ensures that habitat structure as well as predation/grazing pressure should be equal amongst triplicates within individual sites, but competition could be an important driver for the resulting community assemblages across ARMS. Previous ARMS-based studies have also found that species turnover and community heterogeneity can be high at small spatial scales on coral reefs (Vicente et al., 2022; Villalobos et al., 2022). An extension to our study could include the analysis of cryptobenthic communities found on natural surfaces alongside those found on ARMS, to determine whether the local community heterogeneity observed on ARMS reflects that of *in-situ* communities (see Chapter 4).

2.5.3. Identifying species and spatiotemporal indicators

Low assignment success of amplicons is a wide-spread and well-recognised limitation in the current field of metabarcoding, as the taxonomic resolution of metabarcoding studies depends heavily on the quality and content of the reference dataset used to identify novel amplicon sequences (Richardson et al., 2018) and can also vary based on the method or algorithm used to assign taxonomy (Hleap et al., 2021). Using reference datasets which are composed of sequences from the same geographical region

as where metabarcoding data is collected, is important for improving taxonomy assignment success (Ransome et al., 2017). Here, we find that using two different assignment methods (IDTAXA, BLAST), and a reference dataset comprised of both Midori and BIOCODE reference sequences, we are still only able to assign 3.8-4.3% of COI cOTUs to species level. This is not surprising as BIOCODE reference sequences are from the islands of Mo'orea, in the Pacific Ocean, which highlights the need for curated and regional specific reference libraries from the Indian Ocean.

But how many of the species we identify with high confidence in our metabarcoding study have previously been recorded in the Chagos Archipelago? By comparing our findings to four separate records of cryptofauna from the Chagos Archipelago MPA (Natural History Museum of London archives, Smithsonian National Museum of Natural History, Florida Museum's online Invertebrate Zoology Collection and Head et al., (2018)), we find that most of the species we have identified with the highest confidence possible (BLAST 100% query cover and 100% identity match) are not represented in these specimen collections or not previously recorded within academic research. This highlights the extent to which the reef cryptobiome is understudied and unknown. But how represented is the known cryptofauna species record of the Chagos Archipelago within the reference dataset used in our study? Our COI classifier comprises 1,247,239 sequences, including 369,667 species, but we find that less than half of the species listed in official records (NHM/Smithsonian/Florida Museum/Head et al., (2018)) have representative COI barcode sequences. As such, we know for certain that our metabarcoding analysis is restricted by the paucity of our reference dataset.

Further work is now required, using both barcoding and morphological identification, to determine how much of the Chagos Archipelago's cryptobenthic communities remains undescribed or unrepresented in museum archives and zoological collections. The integration of barcode sequences from ARMS motile specimens (>2mm) into classifiers used to assign taxonomy to amplicons obtained from metabarcoding of the same ARMS, would undoubtedly increase assignment rates. Although not presented here, barcoding was undertaken for a portion of voucher motile specimens (>2mm) collected in 2019 (Appendix Section A.i). Whilst we were unable to integrate these into this current analysis due to delays relating to the pandemic, further work is now ongoing to barcode and identify motile and sessile voucher specimens from ARMS collected in 2019 and 2021.

2.5.4. Study limitations

We recognise there are several limitations to the study presented here. Firstly, our number of sampling collections per site is low (n = 2 over 3 years), meaning we are only able to compare ARMS communities between two time points. Our study originally intended on collecting ARMS across three time periods (2019, 2020, 2021), but we were not able to reach our sampling sites in 2020 due the global pandemic. We have since recovered ARMS from our three sampling sites in 2022 and will now look to include these results with findings presented here, to further our analysis of succession across cryptobenthic communities.

The sole use of metabarcoding to study ARMS cryptobenthic communities in this study carries several limitations. Firstly, due to the amplification bias of eukaryotic universal primers utilised in our study (Timmers et al., 2020; Elbrecht et al., 2018), we cannot confidently recover the abundance of sessile and motile organisms present on ARMS. Image-based analysis is a useful tool to recover the percentage cover and abundance of sessile organisms on ARMS plates (Vicente et al., 2022; David et al., 2019). We analyse images from ARMS recovered in 2019 in Chapter 3, but the comparison of image-based data from both 2019 and 2021 ARMS collection would help to further the analysis of community succession over time. For example, it would enable us to investigate whether some sessile taxa, or individual morphospecies, become dominant over time, and whether competition (in the form of overgrowth) is occurring between groups.

In this study, rarefaction is used in this study to account for unequal sequencing depth across samples for analyses which do not have an internal normalisation step (such as breakaway and DivNet, for the latter). The use of rarefaction is contested (McMurdie & Holmes, 2014), as it can introduce artificial variation by removing a random subset of information. Here, we chose to rarefy as all of our analyses are based on presence-absence, not read-based (e.g., NMDS and beta-diversity partitioning). We find that rarefying results in the loss of 15% of COI cOTUs and 12% of 18S cOTUs, but that patterns of overlap, community composition, indicator analysis and beta diversity partitioning remained the same as when the same analyses were run on raw data. Further work with the amplicon datasets presented here would include the exploration of the use of repeated rarefaction (Cameron et al., 2021), where

rarefaction and subsequent analyses are repeated 100s or 1000s of time, and which has been shown to be a good option for Jaccard-distance based analyses, such as the ones presented in this study.

Another limitation of using metabarcoding as our only method is the fact that some of the DNA signal recovered likely originates from organisms not present on ARMS devices. We see evidence of this through the detection of multiple fish species (Appendix Table A.4), many of them pelagic and larger than the ~1.5cm between ARMS recruitment plates. Extracellular DNA can be trapped within sponge tissue as water is filtered (Cai et al., 2022) and could also originate from the gut content of cryptofauna, or even trapped on benthic biofilms (Harrison et al., 2019). Whilst the detection of extracellular DNA from ARMS samples can help to provide a more rounded perspective of local reef diversity, it may be skewing our results of heterogeneity between ARMS triplicates (Appendix Table A.7).

2.5.5. Conclusion

The Chagos Archipelago MPA harbours highly diverse and productive marine and terrestrial habitats (Hays et al., 2020) which hold significant ecological importance for the wider Indian Ocean basin. However, few studies have utilised next-generation sequencing methods to study coral reefs in this region or focused on cryptobenthic organisms. Here, we present novel genetic data on the diversity of three shallow reefs across the archipelago and find that communities are highly heterogeneous across both locations and time. We observed high turnover across samples, even at very small spatial scales, but the drivers behind these community patterns remain unclear. Further work now needs to take place to determine how much of the reef diversity in the Chagos Archipelago MPA remains undiscovered, undescribed or un-represented in zoological collections or genetic reference databases. Even though assignment power remains limited by the slow improvement of reference datasets, there is an urgent need to publish and share metabarcoding data collected using standardised protocols across coral reef regions. Our study provides a baseline for future work on the diversity of cryptobenthic communities on the reefs of the Chagos Archipelago MPA, and through the use of standardised methods we ensure that our results are comparable with other studies employing the ARMS toolkit.

2.6. Author contributions

CH deployed ARMS in 2018, MS/RD/ND collected ARMS in 2019 and 2021. MS/RD/ND processed ARMS samples in 2019 and 2021. MS carried out lab work, with the help of KH who advised lab protocols and assisted with library prep and sequencing. MS and JW carried out bioinformatics, under the supervision of ER, using custom pipeline scripts created by JW. MS carried out statistical analyses and wrote this manuscript under the supervision and guidance of CH, ER and MB. CH, ER and MB all had inputs into this final draft.

CHAPTER 3

Remote reef cryptobenthic diversity: integrating Autonomous Reef Monitoring Structures (ARMS) and *in situ* environmental parameters

Margaux Steyaert[1,2*], Mathilde Lindhart[3], Alexandra Khrizman[4], Robert B. Dunbar[4], Michael B. Bonsall[1] , David A. Mucciarone[4], Emma Ransome[5], Nadia Santodomingo[6,7], Paige Winslade[8], Catherine E.I. Head[2,1]

[1] Department of Zoology, University of Oxford, Oxford, OX1 3SZ, United Kingdom
[2] Institute of Zoology, Zoological Society of London, London, NW1 4RY, United Kingdom
[3] Department of Civil and Environmental Engineering, Stanford University, Stanford, CA 94305, United States
[4] Department of Earth System Science, Stanford University, Stanford, CA 94305, United States
[5] Department of Life Sciences, Silwood Park Campus, Imperial College London, London, SL5 7PY, United Kingdom
[6] Department of Earth Sciences, The Natural History Museum of London, London, SW7 5BD, United Kingdom
[7] Institute of Earth Sciences, University of Lausanne, Geópolis, CH-1015, Lausanne, Switzerland
[8] School of Life Sciences, University of Essex, Colchester, CO4 3SQ, United Kingdom

This chapter has been published in the journal *Frontiers in Marine Sciences*

Steyaert, Margaux, et al. (2022). Remote reef cryptobenthic diversity: integrating Autonomous Reef Monitoring Structures (ARMS) and *in-situ* environmental parameters. *Frontiers in Marine Science*, 2460. https://doi.org/10.3389/fmars.2022.932375

3.1. Abstract

Coral reef sessile organisms inhabiting cryptic spaces and cavities of the reef matrix perform vital and varied functional roles but are often understudied in comparison to those on exposed surfaces. Here, we assess the composition of cryptobenthic taxa from three remote tropical reef sites (Central Indian Ocean) alongside a suite of *in situ* environmental parameters to determine if, or how, significant patterns of diversity are shaped by local abiotic factors. To achieve this, we carried out a point-count analysis of Autonomous Reef Monitoring Structure (ARMS) plate images and employed *in situ* instrumentation to recover long-term (12 months) profiles of flow velocity, wave heights, temperature, dissolved oxygen, and salinity, and short-term (3 weeks) profiles of light and pH. We recovered distinct environmental profiles between sampling sites and observed that ocean-facing reefs experienced frequent but short-lived cooling internal wave events, and that these were key in shaping *in situ* temperature variability. By comparing temperature and wave height profiles recovered using *in situ* loggers with *ex situ* models, we find that global satellite products either failed to recover site-specific profiles, or both over and under-estimated actual *in situ* conditions. We found that site choice and recruitment plate face (top or bottom) significantly impacted the percentage cover of bryozoans, gastropods, soft and calcified tube worms, as well as crustose coralline algae and fleshy red, brown and green encrusting macroalgae on ARMS. We observed significant correlations between the abundance of bryozoans, CCA and colonial tunicates with lower mean temperature and higher mean dissolved oxygen profiles observed across sites. Red and brown encrusting macroalgae abundance correlated significantly with medium to high flow velocity and wave height profiles but also higher pH and dissolved oxygen. This study provides a first insight into cryptobenthic communities in the Chagos Archipelago Marine Protected Area and adds to our limited understanding of tropical reef sessile communities and their associations with environmental parameters in this region. With climate change accelerating the decline of reef ecosystems, integrating analyses of cryptobenthic organisms and *in situ* physicochemical factors are needed to understand how reef communities, if any, may withstand the impacts of climate-change.

3.2. Introduction

Reef ecological studies often focus on the cover and composition of hard corals and fish species, but a large portion of diversity lies within benthic communities hidden in reef cryptic spaces (Klumpp et al., 1988; Appeltans et al., 2012; Leray and Knowlton, 2016). Scleractinian coral reefs are structurally diverse, with live and dead coral colonies forming a complex matrix of exposed surfaces and hidden cavities upon which many reef organisms rely. The surface area of hidden reef cavities significantly exceeds that of the exposed reef benthos, at times by a factor of eight (Scheffers et al., 2010), and can harbour highly diverse communities of sessile organisms including sponges, ascidians, bivalve molluscs, macroalgae, and annelids (Meesters et al., 1991; Richter et al., 2001). Many of these organisms are seldom seen on exposed reef surfaces, and the overall benthic biomass of these cryptic spaces is key for the cycling of nutrients and bacteria in tropical reef ecosystems (Scheffers et al., 2010; Pawlik and McMurray, 2020). These cavity communities and the environmental factors that influence their composition must therefore be considered when studying the functional outputs of coral reefs (de Goeij and Van Duyl, 2007; Kornder et al., 2021).

Our understanding of hidden sessile communities has advanced using genetic approaches, such as metabarcoding, in recent years (Vicente et al., 2021; Nichols et al., 2022). However, metabarcoding pipelines employing primers that target universal genetic regions have inherent sampling and amplification bias that currently limit our ability to quantify the abundance of taxonomic groups across marine benthic communities (van der Loos and Nijland, 2021). Image analysis has been a popular tool for estimating benthic cover, diversity, and recruitment success within cryptic cavities and surfaces of coral reefs (Scheffers et al., 2003; Scheffers et al., 2010; Kornder et al., 2021). Whilst molecular approaches such as metabarcoding can yield detailed information on the diversity of cryptobenthic organisms on autonomous reef monitoring structures (ARMS) (Pearman et al., 2018), image analysis enables researchers to estimate the percentage cover of individual taxa, therefore providing information on relative abundances on visible surfaces. In turn, such information can be used to study successional changes (Higgins et al., 2019) or estimate biovolume and biomass when images are converted to 3D photogrammetric modes (Kornder et al., 2021).

However, benthic organisms living in cryptic reef crevices are hard to access and photograph *in situ*, and thus, it is often challenging to study them without the risk of destroying or displacing the local reef matrix. ARMS were created to provide a standardised tool to both photograph and sample sessile and mobile reef cryptofauna for downstream image and genetic analysis (Zimmerman and Martin, 2004). These artificial devices are composed of stacked polyvinyl chloride (PVC) recruitment plates and have recently become a popular and successful way of studying cryptic reef invertebrates and their associated microbiomes (Al-Rshaidat et al., 2016; Pennesi and Danovaro, 2017; Carvalho et al., 2019; Pearman et al., 2019; Timmers et al., 2020; Cahyani, 2021; Steyaert et al., 2022). The standardised format of ARMS, along with widely available sampling and analysis protocols (Leray and Knowlton, 2015; Ransome et al., 2017), ensures that reef communities sampled across sites and regions can be compared using genetic or image-analysis methods (David et al., 2019; Obst et al., 2020; Pearman et al., 2020). Whilst a PVC material can bias the recruitment of benthic reef taxa (Mallela et al., 2017), and the short gaps between ARMS plates likely reduce predation/grazing pressure, the use of artificial recruitment devices such as ARMS is preferable to destructive sampling of the local reef matrix.

Abiotic factors such as water chemistry, wave exposure, currents, and tides have powerful influences on the shape, composition, and distribution of coral reef communities across multiple spatial scales (Gove et al., 2015; Steiner et al., 2018; Davis et al., 2021). Parameters such as temperature and light availability in part determine the recruitment success, calcification, and growth rate of benthic organisms, whilst dissolved oxygen and pH are intrinsically linked to metabolic productivity across reef systems. Climate change threats to coral reef ecosystems include warming and ocean acidification, both of which are predicted to significantly degrade coral reefs around the globe in the coming decades (IPCC, 2022). Field and lab-based studies have focused on the response of individual non-coral sessile groups to changes in temperature and pH, including sponges (Bell et al., 2018), ascidians (Peck et al., 2015), crustose coralline algae (CCA) (Kroeker et al., 2013; Cornwall et al., 2020), bryozoans (Pecquet et al., 2017), soft corals (Lopes et al., 2018), and fleshy encrusting macroalgae (Diaz-Pulido and Barrón, 2020; Ho et al., 2021). With newly developed methods furthering our ability to record *in situ* biogeochemical fluxes across benthic reef communities (Roth et al., 2019), studies are now needed to determine how cryptobenthic communities as a whole respond to combined stressors.

Physical factors such as current velocity and wave forcing are also important for shaping the structure of coral reefs (Lange et al., 2021), but benthic reef communities have been shown to have non-linear threshold responses to changes in these parameters (Gove et al., 2015). Our understanding of the combined effect of physical and environmental factors on whole sessile communities within cryptic reef cavities is limited (but see Scheffers et al., 2010 and Timmers et al., 2021). Recent ARMS studies looking at cryptobenthic diversity across environmental gradients have used remote sensing data sourced from satellites and publicly available geographic information system (GIS) rasters (Pearman et al., 2018; Pearman et al., 2019; Pearman et al., 2020). Findings from these studies suggest that sea surface temperature (SST) is a key driver of bacterial communities (Pearman et al., 2019) and that a wide range of SST values negatively correlates with eukaryotic species richness (Pearman et al., 2020). Others could not determine whether spatial effects, determined by a lack of connectivity due to distance between sampling sites, or environmental conditions had an impact on ARMS sessile communities (David et al., 2019).

Indeed, global real-time products such as SST, altimetry-derived ocean currents, and modelled wave profiles are widely available and utilised to study large-scale trends across marine systems or as a substitute for *in situ* measurements when these are unavailable. However, the geographical resolution of satellite-based products is often coarse (one to tens of kilometres), and sea surface temperature products typically have longer temporal resolution than *in situ* loggers (Hu et al., 2021). In addition, there is often a disconnect between satellite microwave-based “skin” temperatures and actual water temperatures observed across several to tens of metres below the surface, due to the presence of vertical gradients and stratification (Pan et al., 2017). Internal wave events, which are characterised by intrusions of often cooler subsurface waters onto coral reefs, may be missed when relying on remote sensing models. For example, Colin and Johnston (2020), who compiled two decades of *in situ* temperature measurements from over 70 sites around the Republic of Palau, found that satellite-derived SST (sSST) was not able to capture an accurate picture of thermal variability on coral reefs due to the presence of internal waves. Internal waves are thought to be vital for bleaching mitigation (Safaie et al., 2018; Reid et al., 2019) and have been shown to reduce cumulative heat exposure by up to 88% on reefs across the Pacific during the 2015–2016 El Niño (Wyatt et al., 2020). On the other hand, when co-occurring with acidifying conditions, upwelling events can significantly increase reef bioerosion

(Wizemann et al., 2018). The impact of internal waves and upwelling events on coral, kelp fish, and marine vertebrates has been studied and discussed (Lesser et al., 2009; DeCarlo et al., 2021), but to our knowledge, not with respect to whole cryptobenthic reef communities.

Uninhabited, protected, and remote shallow coral reefs are rare, but provide a unique opportunity to study the relationship between environmental factors and benthic communities free from anthropogenic stressors such as overfishing, seabed dredging, sound/chemical pollution, or coastal development, which have been shown to fundamentally alter the relationship between biological and physical factors on reefs (Williams et al., 2015). The Chagos Archipelago is a remote system of atolls located at the heart of the Indian Ocean, which has been uninhabited since the 1970s following the forced removal of local inhabitants. The archipelago is now part of a large no-take marine-protected area (MPA), and whilst the protection of these islands has been shown to benefit current populations of fish, turtles, and seabirds (Hays et al., 2020), shallow coral reefs across atolls have experienced bleaching events driven by climate change (Sheppard et al., 2017; Head et al., 2019; Lange and Perry, 2019). A recent review of climate change impacts on the Chagos Archipelago MPA highlights the urgent need for continuous monitoring of coral reef communities and local environmental variables across atolls (Koldewey et al., 2021). To our knowledge, no studies have investigated whole cryptobenthic communities from the reefs of the Central Indian Ocean, and few studies have investigated particular groups of cryptobenthic invertebrates from the Chagos Archipelago MPA (Head et al., 2018; Head et al., 2018; Hays et al., 2020).

Here, we present the first analysis of sessile cryptobenthic diversity and *in situ* environmental parameters for three shallow reef sites across the Chagos Archipelago MPA. We (1) use *in situ* measurements of abiotic factors including temperature, oxygen, light, pH, salinity, wave heights, and flow velocity to explore differences in environmental profiles between sites; (2) compare the percentage cover and composition of invertebrate communities using ARMS devices; and (3) investigate how environmental factors correlate with observed abundances of cryptobenthic taxa across reefs. Additionally, we (4) compare *in situ* measurements of temperature and wave exposure to remote sensing data, to evaluate how representative these products are of local conditions. Overall, this study

aims to advance our knowledge of cryptobenthic reef ecology in this understudied region by co-presenting and integrating analyses across fields of reef ecology, biogeochemistry, and physics.

3.3. Materials and Methods

3.3.1 Study sites

Sampling sites (*n*=3) were distributed across two atolls of the Chagos Archipelago marine-protected area (MPA): one on the ocean-facing side of Moresby Island (Peros Banhos atoll), one on the ocean-facing side of Ile Anglaise (Salomon atoll), and another on the lagoonal side of Ile du Coin (Peros Banhos atoll) (Figure 3.1; Appendix Table B.1). For each site, benthic communities were sampled using triplicate autonomous reef monitoring structures (ARMS) and environmental parameters including temperature, salinity, dissolved oxygen, wave heights, depth, flow velocity, and photosynthetically active radiation (PAR) were recorded using *in situ* instrumentation (Figure 3.1).

3.3.2. Deployment, recovery, and processing of environmental data

Long-term environmental parameters were recorded at each site between 2018 and 2020, although recordings were asynchronous at times (Table B.3). The temperature was measured using an SBE56 temperature sensor (Sea-Bird Scientific, 30-s resolution) and an SBE37-SM/SMP MicroCAT (Sea-Bird Scientific, 10-min resolution). Flow velocity was measured using an Acoustic Doppler Profiler (1-MHz ADP; Nortek, 30-min resolution) in Ile Anglaise and an Acoustic Doppler Current P—filer (1200-KHz ADCP; RD Instruments, 20-min resolution) in Ile du Coin and Moresby. Dissolved oxygen (DO) was measured by miniDOT [PrecisionMeasurement Engineering (PME), 5–10–min resolution]. Salinity was measured by SBE37-SM/SMP MicroCAT (Sea-Bird Scientific, 10-min resolution), and pressure (waves) was measured by RBR Virtuoso (Ruskin, 1-Hz resolution) in Ile Anglaise and an RBR solo (Ruskin, 1 Hz) in Ile du Coin and Moresby. Long-term temperature, salinity, and dissolved oxygen measurements were taken directly adjacent to ARMS across all three sites (Figure 3.1). Flow velocity and wave heights were taken adjacent to ARMS at Ile Anglaise but were measured 500 to 700 m away from ARMS in Ile du Coin and Moresby (Figure 3.1). Additional details of individual instruments, deployment timelines, and calibration parameters recording these long-term variables can be found in Appendix Table B.4.

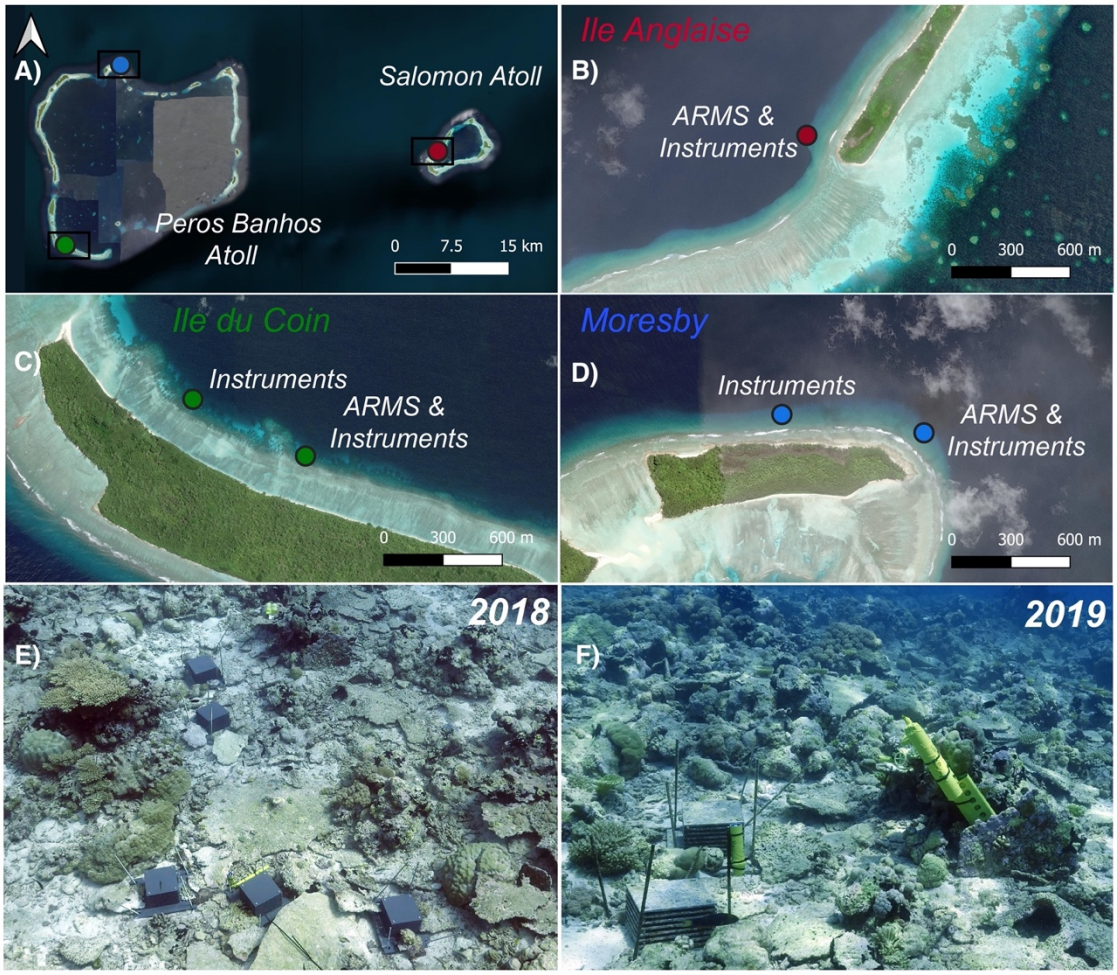

Figure 3.1. Maps displaying the location of (A) sampling sites across Peros Banhos and Salomon atolls in the Chagos Archipelago marine-protected area (MPA), (B) autonomous reef monitoring structures (ARMS) and environmental instruments at Ile Anglaise, (C) ARMS and environmental instruments at Ile du Coin, and (D) ARMS and environmental instruments at Moresby Island. (E) ARMS devices and environmental instruments at Ile Anglaise in 2018 following deployment and (F) ARMS devices and instruments at the same site in 2019.

Leading up to the retrieval of ARMS in March 2019, short-term deployments (2 to 3 weeks) of the aforementioned parameters, along with pH and photosynthetic active radiation (PAR), were also conducted at each site. pH was recorded by SeaFET V2 pH logger (Sea-Bird Scientific, 10-s resolution) in Ile Anglaise and by SeapHOx V2 CTD-pH logger (Sea-Bird Scientific, 30-s resolution) at Ile du Coin and Moresby (Appendix Table B5). Both instruments have an accuracy of 0.05 pH units and a precision of 0.004 units and were calibrated using collected discrete water samples at each site. PAR was measured by miniPAR [Precision Measurement Engineering (PME), 1-min resolution]. Short-term measurements were taken adjacent to ARMS at Ile Anglaise but were taken 500 to 700 m from ARMS for Ile du Coin and Moresby (Figure 3.1). Additional details of individual instruments, deployment timelines, and calibration parameters recording these short-term variables can be found in Appendix Table B.5.

Following Wyatt et al. (2020), the temperature time series was separated into high- and low-frequency signals, using the inertial frequency at −5.5° south as the cutoff, and temperature perturbations at higher frequencies are attributed to internal waves (IW). To determine the contribution of internal waves to overall temperature profiles, a time series was created where the internal wave signal is removed for Ile Anglaise and Moresby, labelled “Internal waves removed.”

3.3.3. Satellite-derived sea surface temperature and modelled wave data

In situ data for wave heights and temperature were compared to NOAA’s (National Oceanic and Atmospheric Administration) WaveWatch III wave model (WAVEWATCH III Development Group, 2016) and NOAA’s (National Oceanic and Atmospheric Administration) Coral Reef Watch (CRW) (Liu et al., 2008) temperature observations for our three study sites. WaveWatch III (WWIII) simulates global wave characteristics at varying scales, and the available resolution around the Chagos Archipelago is to a 0.5°, equivalent to approximately 55 km. CRW provides daily sSST on a 5-km grid. *In situ* observations were compared to the WWIII output of significant wave height combining wind and swell, produced every 3 h. WWIII model output and daily sSST were available for the duration of *in situ* deployments of wave height and temperature loggers.

3.3.4. Deployment, recovery, and processing of Autonomous Reef Monitoring Structures

A total of nine ARMS were deployed across the three sampling sites in March 2018 at depths ranging from 5.9 to 9.3 m. Triplicate ARMS were collected from each site in March 2019 (n = 9). The use of triplicate units per sampling site, instead of duplicates, has been previously recommended in a study of ARMS communities from the Red Sea, as it was shown to significantly improve statistical power in the analysis of recruitment plate images (David et al., 2019). Each ARMS device is composed of nine square PVC plates (22.5 cm × 22.5 cm) stacked atop each other and attached to one larger base plate (35 cm × 45 cm). Between each plate are a series of alternating “open” and “closed” gaps created using round nylon spacers or long and short PVC cross spacers, thus creating multiple microhabitats. Each ARMS has a total of 17 colonisable plate “faces,” referring to either the top (T) or bottom (B) side of each square plate (Appendix Figure B.1).

ARMS were retrieved on scuba and immediately submerged in a bin filled with filtered seawater and aquatic bubblers to maintain sessile communities. Each plate was carefully taken apart from the ARMS units by removing steel bolts, washers, and PVC crossbars, and each top and bottom plate face was photographed. For each face, a series of six close-up photographs were captured using a Nikon D810 camera (105-mm macro lens), then stitched together in Adobe Photoshop Lightroom Classic (version 9.2.1) to produce a single high-resolution image. Following photography, sessile communities were immediately subsampled and homogenised for downstream genetic analysis, the results from which are not presented in this study. All ARMS were processed and photographed on board an expedition vessel.

All final high-resolution plate images were exported in JPEG format with an image size of 6,000 × 6,000 pixels (240 pixels/in.). Labels of images contain the ARMS number, followed by the plate number (1 to 9 from top to lower plate) and the plate face (T or B). For instance, ARMS3_1B refers to the bottom side (B) of the uppermost plate (1) of the third ARMS device. Plate 9B lies flush with the base attachment plate and therefore, is not available for benthic recruitment.

3.3.5. Photo analyses of Autonomous Reef Monitoring Structures

The benthic composition of 139 ARMS plate images was analysed using CoralNet, an open-source cloud-based image-analysis website (coralnet.ucsd.edu). Five plate images from Ile Anglaise were missing from our dataset, and to focus our analysis on communities within cryptic reef spaces, we did not analyse the top plate (plate 1T) on each of the nine ARMS, as it is the only plate face that is fully exposed and has been shown to harbour significantly different communities than other ARMS microhabitats (David et al., 2019). A list of identification groups based on NOAA's Coral Reef Ecosystem Program's (CREP) protocol was created to reflect the major taxonomic groups found in sessile tropical reef communities (Appendix Table B.2). A total of 225 annotation points were randomly generated on each ARMS plate image within a 15-row × 15-column grid format (one point randomly placed per cell). Identifications were made manually, and images were analysed in a randomised order across ARMS and sites.

3.3.6. Statistical analyses

One-way analysis of variance (ANOVA) tests were performed on individual long-term (*in situ* temperature, DO, flow velocity, and wave heights) and short-term (pH, salinity) environmental parameters between sampling sites, using the "rstatix" package (Kassambra, 2021). For each environmental parameter, 1,000 data points were randomly chosen for each site across overlapping instrument deployment periods. For each subset dataset, assumptions of data normality across sampling sites were checked by plotting model residuals and computing a Shapiro–Wilk test, and assumptions of homogeneity of variances were checked by plotting residual versus fitted plots. Only daytime values of PAR were retained and compared between sites. *Post-hoc* Tukey's tests were then used to perform pairwise comparison between sites. Plots summarising average diel cycles were then created for each parameter found to have significant differences in mean values across sites. The correlation between flow velocity and wave heights, as well as pH and DO, were investigated separately using Pearson's correlation analysis.

Live percentage cover was calculated as the percentage of counts assigned to live sessile taxonomic groups out of all counts observed on available space (i.e., excluding "unavailable" counts, which are characterised by any point falling outside of an ARMS plate or onto portions of plates obstructed by

washers or crossbars). This was done to standardise the abundance of individual taxa between "open" and "closed" plate faces, as the latter has fewer counts on available space due to the presence of PVC crossbars during deployment. The mean values of the percentage cover of live sessile organisms were calculated for each site and across top/bottom plate faces. All plots of ARMS data were created using either the package "ggplot2" v3.3.5 (Wickham, 2016) or basic R plotting tools (R Core Team, 2022).

A series of univariate generalised linear models (GLMs) were used to investigate the relationship between live sessile percentage cover (%) with sites and plate faces, using the R package "MASS" v7.7.3.54 (Venables and Ripley, 2002). Percentage cover was transformed to proportional values (between 0 and 1) prior to running GLMs, and a quasi-binomial distribution was chosen to account for observed underdispersion (Gelman and Hill, 2006). *Post-hoc* Tukey's tests were used to determine significant patterns amongst explanatory variables.

Overall, community similarity between sites and plate faces was visualised using a non-metric multidimensional scaling (NMDS) approach using the R package "vegan" v2.5.7 (Oksanen et al., 2013), using Bray–Curtis distances. The distance matrix was created using the counts of sessile groups, except for groups "Hydrocorals" and "Corallimorphs," which were removed due to either low (n = 2 for hydrocorals) or no counts (n = 0 for corallimorphs). Top plate counts and bottom plate counts were merged for each ARMS device. Multivariate generalised linear modelling (GLM) was then used to determine the relationship between benthic group abundances and explanatory variables (plate face and site), using the *manyglm* function in the "mvabund" package (Wang et al., 2012), which uses row resampling to ensure correlations between taxa groups are taken into account when making community-wide and group-specific inferences. This method was used as a strong mean–variance relationship was observed across this study's benthic dataset (see Warton et al., 2012). Multivariate models with and without an interaction between the plate face and sites were computed, and the former was found to provide a better fit based on AIC Akaike Information Criterion values. A negative binomial distribution also provided a good model fit in a residual analysis and was therefore used to account for the overdispersion observed in our count dataset. Analyses of deviance were undertaken on multivariate and univariate model outputs using the *anova.manyglm* function, with a default PIT Probability Integral Transform-trap resampling parameter.

A distance-based redundancy ordination analysis (dbRDA) was used to determine the contribution of environmental parameters to the structure of ARMS cryptobenthic communities observed across sites, using Bray–Curtis distances with the *capscale* function in the "vegan" package v2.5.7 (Oksanen et al., 2013). The number of site replicates in this study limited our ability to simultaneously model the effect of all environmental variables with diversity patterns observed in our ARMS dataset, and therefore, we conducted individual dbRDAs on mean (i) *in situ* and *ex situ* temperature, (ii) pH and oxygen, and (iii) velocity and wave height. *Ex situ* wave values were not included in this analysis as the WaveWatch III model was unable to determine wave profiles between the Ile du Coin and Moresby sites. PAR and salinity were also not included in this analysis, as no difference was observed in the PAR profiles across sites and the significant profiles in salinity observed between sites were determined not to be biologically significant. ANOVA-like permutation-based tests were carried out to test the significance of each full model using the *permutest* function. The significance of individual explanatory variables within each model was also tested using the *anova.cca* function. Ordination plots were then used to visualise modelled relationships between environmental factors and benthic communities for each model.

The *multipatt* function in the package "indicspecies" v1.7.9 (Cáceres and Legendre, 2009) was then used to determine the extent of correlation between sessile taxonomic groups and environmental parameters. Following our findings from the analysis of our environmental dataset (one-way ANOVAs and average diel plots), we categorised each site, or groups of sites, into regimes based on relatively significant differences observed between sites (Figure 3.2, see Sec. 2. Materials and methods). For flow velocity, we categorised Moresby as having a "high" regime, Ile Anglaise as "medium," and Coin as a "low" regime. For wave heights, Moresby was categorised as a high regime, Ile Anglaise as medium, and Ile du Coin as low. For *in situ* temperature, Ile du Coin was categorised as a high regime, and both Ile Anglaise and Moresby as low. For DO, Ile du Coin was categorised as low whilst both Ile Anglaise and Moresby were categorised as high. For pH, Ile du Coin was categorised as low, Moresby as medium, and Ile Anglaise as high. Finally, for PAR, we grouped Ile du Coin and Ile Anglaise sites together and categorised them as low, and categorised Moresby as high. This analysis was run on top and bottom plate face communities separately, and only results from taxa whose abundance was previously found to be significantly affected by plate face and site choice by multivariate GLMs were

retained. The function parameter “r.g” was chosen to account for unequal group size (for the site) and to determine point biserial correlation coefficients.

3.4. Results

3.4.1. Tides, wave heights, and flow velocities

Tides were semidiurnal, and all sites had a similar tidal range of approximately 1 m (Appendix Figures B.2 & B.3). Limited wave forcing was observed in Ile du Coin, with root-mean-square wave heights (H_{rms}) varying between 0.07 and 0.57 m, and average (± sd) values of 0.23 (± 0.09) m across March–November 2019 (Figure 3.2; Appendix Figure B.2). In contrast, Ile Anglaise and Moresby reefs consistently experienced larger waves with root-mean-square wave heights of up to 1.40 and 1.33 m, respectively. On average, Moresby showed the highest average wave heights (0.35 ± 0.15 m), followed by Ile Anglaise (0.27 ± 0.16 m). Overall, average root-mean-square wave height values were significantly different between sites (ANOVA, F = 142.81, p-value < 0.001), but site choice accounted for only ~10% of the variance observed across this dataset (n_g^2 = 0.09).

Flow velocities were lower and less variable in the lagoonal reef (1.9 ± 1.0 cm/s; mean ± SD) compared to Moresby (10.1 ± 7.2 cm/s) and Ile Anglaise (11.6 ± 6.9 cm/s), over an annual period (Appendix Figure B.2). The mean flow velocities were also found to significantly differ between all three sites (ANOVA, F = 78.14, p-value < 0.001), and the site accounted for over a third of the variance observed (n_g^2 = 0.34) (Figure 3.2). A low positive correlation between flow and velocity was found in Ile du Coin (Pearson’s coefficient = 0.215, p-value < 0.05) and Moresby (0.059, p-value < 0.05), whilst no correlation was observed between parameters in Ile Anglaise (0.003, p-value > 0.05) over overlapping instrument deployments.

3.4.2. Temperature

The *in situ* temperature profiles of the three sites were successfully recovered across April 2018 to January 2019 and March to April 2019 (Appendix Figure B.2). For all three sites, the maximum monthly mean (MMM) was 29.3°C. The average temperature (mean ± SD) in both ocean-facing reefs was similar (28.51°C ± 0.60 for Ile Anglaise, 28.57°C ± 0.58 for Moresby), with the lowest temperature recorded in Ile Anglaise (24.74°C on 15 October 2018). On average, the temperature was significantly higher in the lagoon-facing reef than in other sites (29.40°C ± 0.94) (ANOVA, F = 9.72, p-value < 0.001) (Figure 3.2), and the maximum temperature (30.98°C) was recorded there on 1 April 2019. Whilst a clear daily cycle was observed in Ile du Coin, a 24-h cycle of temperature variability was less clear in the two outer reefs (Figure 3.2; Appendix Figure B.3).

It was estimated that the site alone accounted for less than 1% of the variance observed in the subset temperature dataset (n_g^2 = 0.007). Events of cold intrusions, most likely caused by internal waves, were frequently detected in both outer-reef sites, during which significant drops in temperatures were observed, characterised by changes in hourly standard deviation temperature values (Figure 3.3). No internal waves were detected in Ile du Coin (Figure 3.3).

We determined that temperature values below 26.96°C and 27.22°C were attributable to internal wave events for the Ile Anglaise and Moresby sites, respectively. Overall, 0.20% of Moresby *in situ* temperature data was identified as potential internal wave events, compared to 0.42% of data points for Ile Anglaise, over the same period. Following the removal of internal wave signal from *in situ* data across these two sites, we find that whilst significant differences were still detected between reefs (ANOVA, *F* = 247.17, p-value < 0.001), the site was estimated to account for 14% of the variance observed (n_g^2 = 0.14), which is 20 times greater than what is estimated for the original *in situ* temperature dataset.

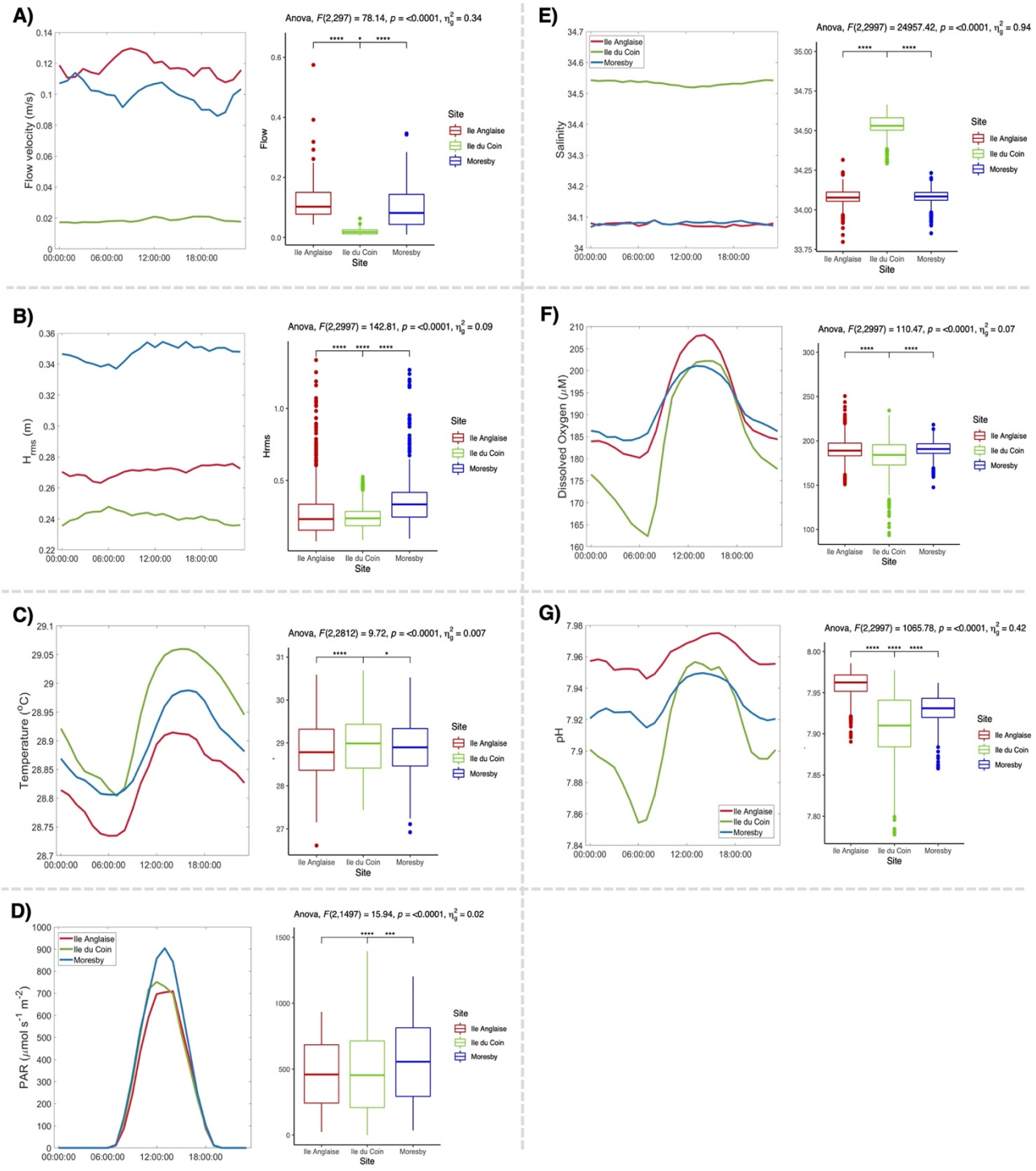

Figure 3.2. Average diel cycle plots for (A) flow velocity, (B) root-mean-square wave height, (C) *in situ* temperature, (D) photosynthetically active radiation (PAR), (E) salinity, (F) dissolved oxygen (DO), (G) pH, and, and boxplots displaying values across subset datasets for each parameter, along with corresponding one-way ANOVA test results [including *F*-statistic with degrees of freedom, p-value, and effect size (generalised eta squared (n_g^2)].

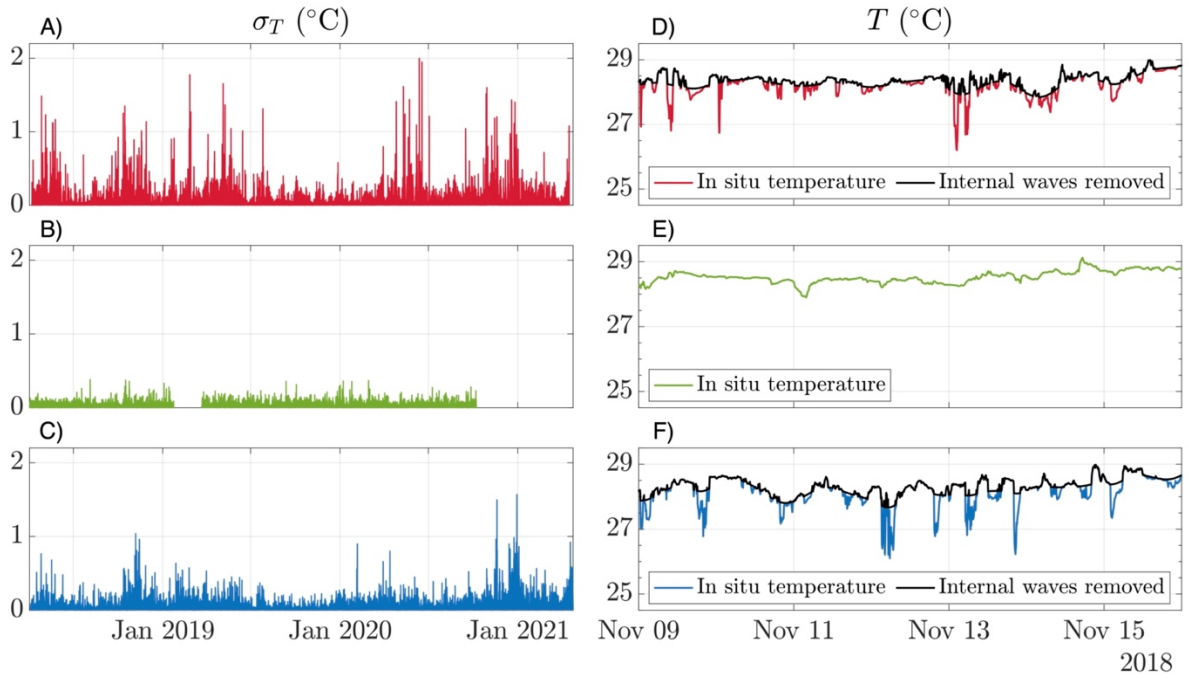

Figure 3.3. The hourly standard deviation of temperature across (A) Ile Anglaise (red), (B) Ile du Coin (green), and (C) Moresby (blue) between April 2018 and April 2021, as well as *in situ* temperature profiles, alongside modelled temperature profiles with internal waves removed, over the same 2-week period, across (D) Ile Anglaise, (E) Ile du Coin, and (F) Moresby. Note that no internal waves were detected in Ile du Coin, and therefore no model removing internal waves was run.

3.4.3. Photosynthetically active radiation, salinity, oxygen, and pH

The highest value of PAR (mean and daily max mean ± SD) was recorded in Moresby, with a total mean of 235.4 µmol photons/m^{-2} s^{-1} and a daily max mean of 1,579.5 µmol photons/m^{-2} s^{-1} (± 333.74). The lowest PAR was recorded in Ile Anglaise (total mean 189.3, daily max mean 1,089.1 µmol photons/m^{-2} s^{-1} ± 280.36), with an intermediate mean value in Ile du Coin (total mean 214.7, daily max mean 1,354.2 µmol photons/m^{-2} s^{-1} ± 313.33) (Appendix Figure B.3). Significant differences were observed between mean daytime PAR values across sites (ANOVA, F = 15.94, $p < 0.001$), but site choice was estimated to account for only 2% of the variance observed (n_g^2 = 0.02).

Higher salinity values (mean ± SD) were observed on average in Ile du Coin (34.53 ± 0.06 psu) than in Moresby (34.08 ± 0.04 psu) and Ile Anglaise (34.08 ± 0.04 psu), where values were identical. Overall, similar seasonal patterns were observed across all three sites, with a steady rise in salinity over the months of April to July (Appendix Figure B.2). Whilst statistically significant differences in mean values were observed across a subset of salinity data between ocean-facing sites and the lagoon-facing reef (ANOVA, F = 24,957.42, $p < 0.001$) (Figure 3.2), differences in these profiles are likely not biologically significant.

Dissolved oxygen (DO) concentration was lower in Ile du Coin on average (183.40 ± 18.71 µM) compared to Moresby (191.39 ± 8.57 µM) and Ile Anglaise (191.48 ± 12.88 µM) (Appendix Figure B.2). These differences in mean values were also found to be significantly different (ANOVA, F = 110.47, $p < 0.001$), and the site was estimated to account for only 7% of the variance observed ($n_g^2 = 0.07$). The highest oxygen concentration was recorded in Ile Anglaise (277.06 µM on 30 September 2018). Daily DO cycles are observed across all three sites, but on average, the cycle in Ile du Coin was more pronounced, with values dipping below 165 µM around 6:00 a.m., compared to 180 and 185 µM in Ile Anglaise and Moresby, respectively (Figure 3.2).

Similarly, Ile du Coin also displayed the lowest pH values on average (7.91 ± 0.04), compared to Moresby (7.93 ± 0.02) and Ile Anglaise (7.96 ± 0.01) (Appendix Figure B.3). The lowest pH was also recorded in Ile du Coin, with a value of 7.78, compared to minimums of 7.92 and 7.86 in Ile Anglaise and Moresby, respectively. On average, pH was found to be significantly different across all three sites (ANOVA, F = 1,065.78, $p < 0.001$), and the site accounted for over 40% of the variance observed ($n_g^2 = 0.42$). Daily pH cycles were also, on average, more pronounced in the lagoon-facing reef (Figure 3.2). DO and pH were found to strongly correlate across all three sites throughout overlapping instrument deployments (Pearson's correlation; Ile Anglaise = 0.754, Moresby = 0.944, and Ile du Coin = 0.821, $p < 0.001$ for all three sites).

3.4.4. Comparison of in situ and ex situ measurements of temperature and wave heights

On average, sea surface temperatures retrieved using NOAA's CRW model were highly similar across all sites, with 28.75°C in Moresby and 28.72°C for both Ile du Coin and Ile Anglaise. The highest temperature was estimated to be in Ile du Coin (30.71°C), followed by Moresby, and then Ile Anglaise. Unlike *in situ* data, the lowest temperature was also estimated to occur in Ile du Coin (27.58°C). Comparing CRW SST values and *in situ* measurements shows that sSST does not capture internal wave events (Figure 3.4). Wave heights measured using WaveWatch III (WWIII) were also found to be overestimated when compared to *in situ* using fast-sampling pressure sensors (Figure 3.4). From WWIII results, Ile du Coin and Moresby are located in the same grid cell; hence, the model gives no distinction of the wave height profiles at the two sites.

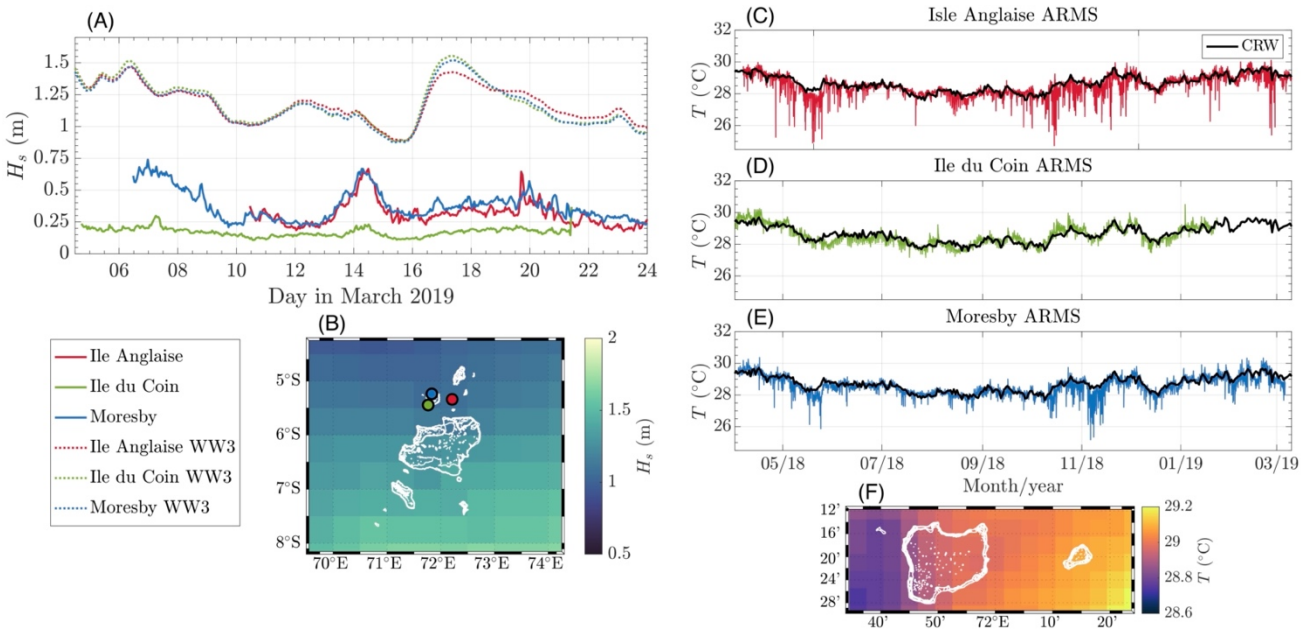

Figure 3.4. Comparison of *in situ* and *ex situ* data for wave heights (WaveWatch III model) and sea surface temperature (Coral Reef Watch (CRW) model) at each reef site. (A) Observed and estimated significant wave heights from the nearest WWIII cell during March 2019. (B) Visualisation of the WWIII resolution across the Chagos Archipelago marine-protected area (MPA), where one-coloured pixel represents a single value for the estimated wave height. (C–E) significant temperature values for individual reef sites (the black line represents CRW data, coloured lines represent *in situ* data). (F) Visualisation of the CRW resolution across the Peros Banos and Salomon atolls of the MPA, where one coloured pixel represents a single value for estimated temperature.

3.4.5. Total percentage cover and composition of sessile communities across Autonomous Reef Monitoring Structures and sampling sites

A total of 27,144 identifications were made across the nine ARMS, of which 62.3% were assigned to sessile organisms across 22 benthic taxonomic groups, 6.2% were sediment, and 30.3% to noncolonised surfaces (no recruitment) (Appendix Table B.6). Some predation of sessile communities was observed, with 0.5% of counts identified as fish bite scars. Very few sessile organisms were unidentifiable, with an average of 1% of counts assigned as "unknown" across the three sites.

On average, the total percentage cover of live sessile organisms was the lowest in Ile du Coin (mean ± standard deviation, 61.12 ± 18.2%), compared to Ile Anglaise (73.34 ± 11.7%) or Moresby (73.16 ± 14.9%) reef sites. A quasibinomial GLM regression showed that both sites ($F = 14.26$, $p < 0.001$) and plate face ($F = 64.6$, $p < 0.001$) had a significant effect on overall live percentage cover across ARMS plates (full model output in Appendix Table B.8). *Post-hoc* Tukey's tests indicate that live percentage cover of sessile taxa was significantly higher on ARMS in Ile Anglaise ($p < 0.001$) and Moresby ($p < 0.001$) than at Ile du Coin. Live sessile percentage cover was also significantly higher on bottom plate faces (77% ± 1.23, $p < 0.001$) than on top plate faces (61% ± 2.02) across all sites. Sediment attached to or covering sessile organisms and plate surfaces were observed across all sampling sites despite efforts to shake these off (see Materials and methods, section 3.3), with 9.4% of sessile counts in Ile du Coin assigned to this category compared to 4.5% in Moresby and 3.8% in Ile Anglaise.

Overall, sponges, soft-tube worms, and red macroalgae were the most abundant taxa groups in the lagoon-facing reef (Figure 3.5). On exposed reefs, bryozoans, sponges, and red and fleshy macroalgae were the most abundant, with red macroalgae in the highest abundance in Moresby and brown macroalgae in the highest abundance in Ile Anglaise (Figure 3.5).

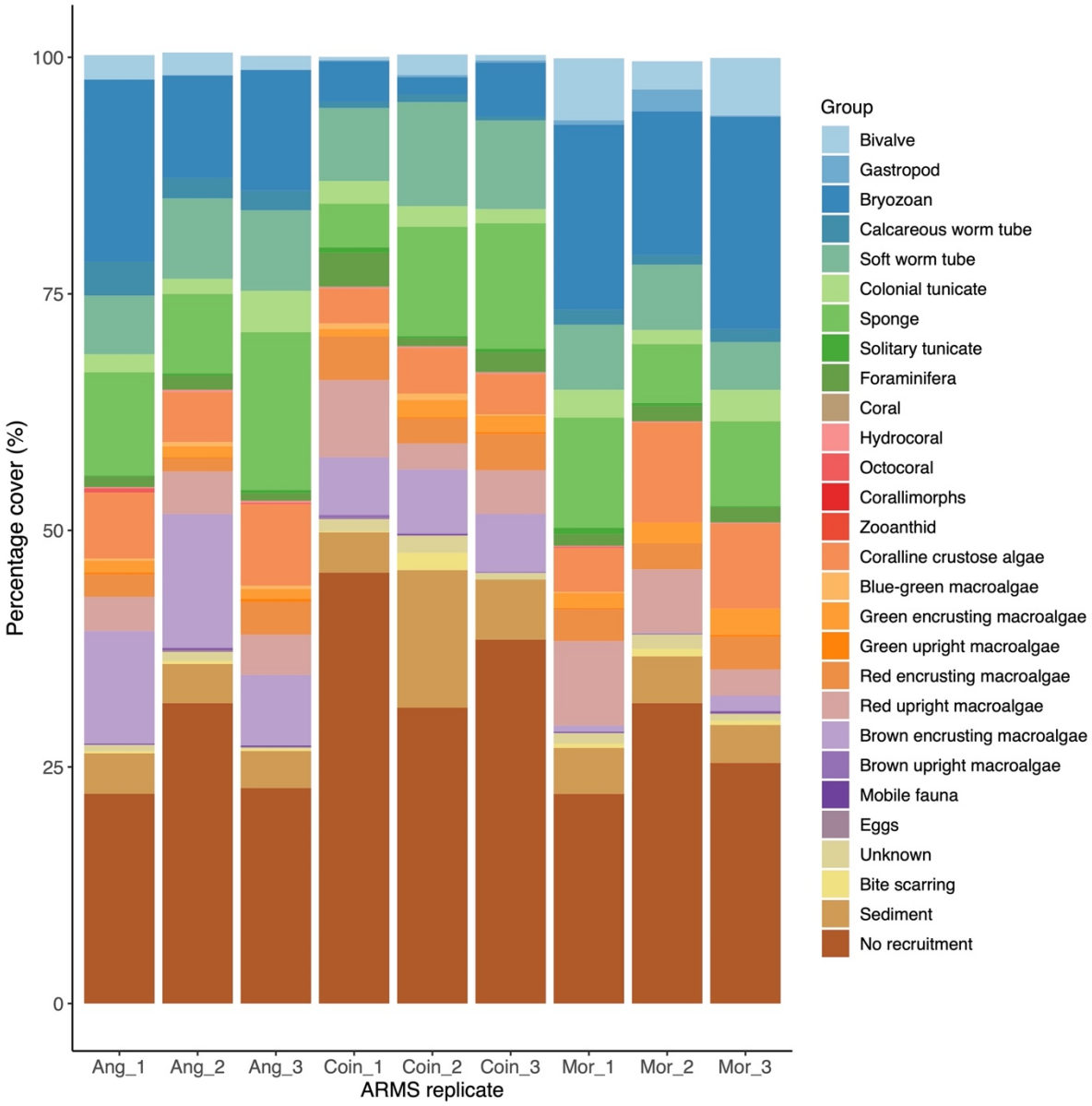

Figure 3.5. Stacked barplot displaying the percentage cover of sessile taxonomic groups, the percentage of counts assigned to non-sessile taxa as well as other identification groups, across replicates of autonomous reef monitoring structures (ARMS) from each sampling site (Ang, Ile Anglaise; Coin, Ile du Coin; Mor, Moresby).

The NMDS analysis showed the extent of dissimilarity between the top and bottom plate faces across sampling sites (Figure 3.6). Whilst the dispersion of data between the top and bottom plate face communities amongst triplicate ARMS was similar within Moresby and Ile Anglaise sites, a large difference was observed within Ile du Coin, with top plate face communities displaying a higher variability than bottom face communities (Figure 3.6).

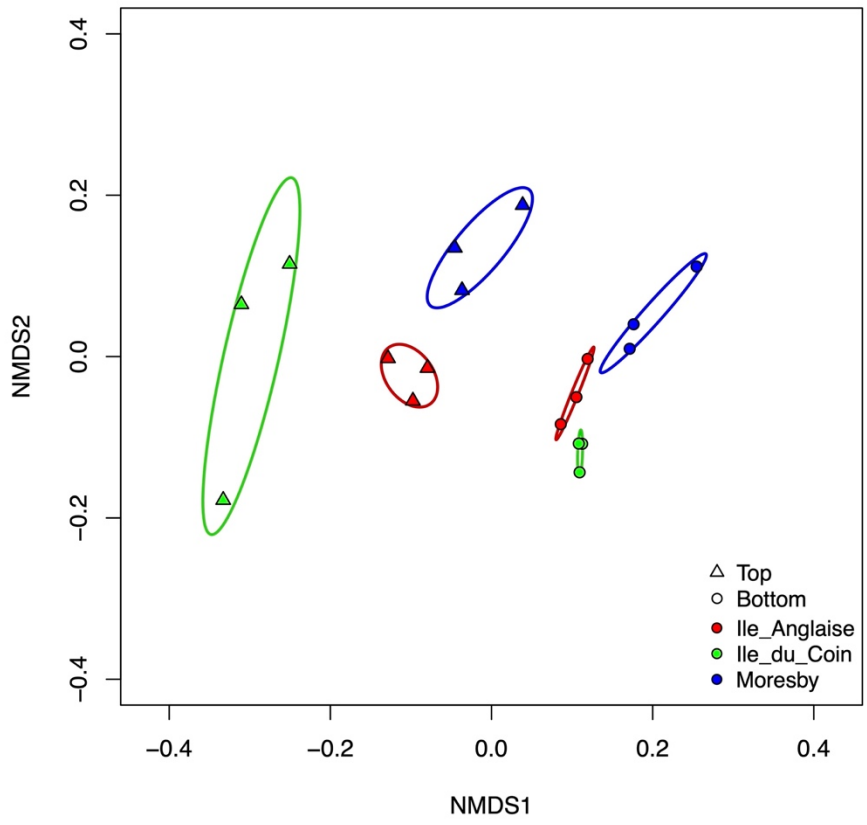

Figure 3.6. Non-metric multidimensional scaling (NMDS) ordination plots of autonomous reef monitoring structures (ARMS) communities on top or bottom plate faces across sampling sites, based on Bray–Curtis distances using fourth-root transformed count data and over two reduced dimensions (k = 2) (stress value = 0.106). Ellipses represent 95% confidence intervals fitted to the spatial ordination.

The multivariate model indicated that site, plate face, and the interaction between both factors had a significant impact on the abundance of sessile taxonomic groups across ARMS (Table 3.1). Univariate regressions across groups showed that site choice has a significant impact on bryozoan, gastropod, and brown encrusting macroalgae abundances, whilst plate face had a significant effect on the abundance of calcified tube worms, soft tube worms, and colonial tunicates (Table 3.2). CCA, green encrusting, and red encrusting macroalgae abundance were also shown to be most abundant different across sites, but only when plate face is taken into account. Boxplots of the nine most abundance taxonomic groups highlight these significant patterns, such as the contrast in red encrusting macroalgae abundance across the top and bottom plates in Ile du Coin in comparison to Ile Anglaise and Moresby, as well as the dominance of brown encrusting macroalgae in Moresby (Figure 3.7).

Table 3.1. Summary of statistical significance of a multivariate GLM assessing the effect of site and plate face on the abundance of sessile groups. Res.D.f = residual degrees of freedom, Df.diff = difference in degrees of freedom, Dev. = deviance, Pr(>Dev) = p-value. Full model output coefficients can be found in Appendix Table B.9.

Factors	**Res.Df**	**Df.diff**	**Dev.**	**Pr(>Dev)**
(Intercept)	17			
Site	15	2	133.4	**0.001*** **
Plate face	14	1	229.4	**0.001*** **
Site : Plate face	12	2	149.4	**0.002** **

Table 3.2. Summary of statistical significance of resampling based univariate GLMs assessing the effect of site and plate face on the abundance of individual sessile groups. Only taxa with significant values are listed. Dev = deviance, Pr(>Dev) = p-value. Significant p-values are highlighted in bold (p<0.001***, p<0.01**, p<0.05*).

Predictors	**Bryozoan**		**Gastropods**		**Brown encrusting macroalgae**	
	Dev.	Pr(>Dev)	Dev.	Pr(>Dev)	Dev.	Pr(>Dev)
Site	17.62	**0.016***	17.95	**0.014***	19.66	**0.008****
Plate face	9.78	0.10	0.73	0.89	1.07	0.89
Site : plate face	2.40	0.96	2.25	0.96	7.14	0.56
	Colonial ascidians		**Soft-tube worms**		**Calcified tube worms**	
	Dev.	Pr(>Dev)	Dev.	Pr(>Dev)	Dev.	Pr(>Dev)
Site	0.14	1.00	0.25	0.99	12.1	0.12
Plate face	31.14	**0.001*****	62.38	**0.001*****	23.9	**0.001*****
Site : plate face	15.49	0.06	5.22	0.73	0.7	1.00
	Green encrusting macroalgae		**Red encrusting macroalgae**		**CCA**	
	Dev.	Pr(>Dev)	Dev.	Pr(>Dev)	Dev.	Pr(>Dev)
Site	1.99	0.91	2.59	0.85	1.79	0.92
Plate face	21.92	**0.002****	16.88	**0.003****	22.01	**0.002****
Site : plate face	17.18	**0.04***	20.30	**0.014***	20.86	**0.014***

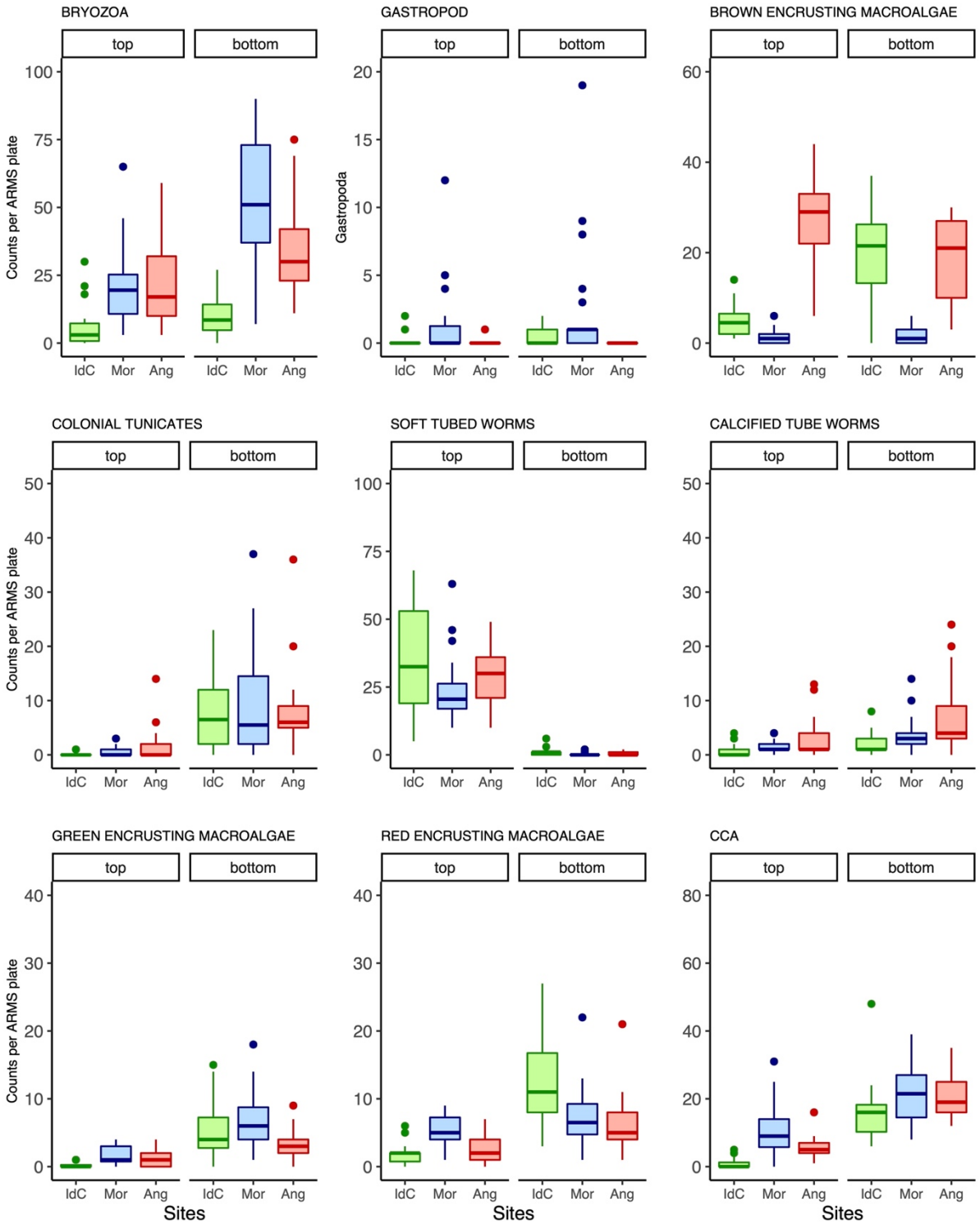

Figure 3.7. Boxplots comparing the counts of nine taxonomic groups were found to have significantly different abundances across autonomous reef monitoring structures (ARMS) plate face and/or across sampling sites (IdC, Ile du Coin; Mor, Moresby; and Ang, Ile Anglaise).

3.4.6. Associations between environmental factors, habitat type, and benthic communities

The dbRDA of *in situ* and *ex situ* temperature, pH, and DO, as well as flow velocity and wave heights, were all significant in explaining the same amount of variation observed in benthic communities across sites: *in situ* and *ex situ* temperature (permutation-based ANOVA, $F = 3.14$, p-value = 0.008, $R_2 = 0.31$, permutations = 999), pH, and DO ($F = 3.13$, p-value = 0.02, $R_2 = 0.31$), and flow velocity and wave heights ($F = 3.13$, p-value = 0.02, $R_2 = 0.31$) (Figure 3.8). Contrasting patterns of association were observed across the temperature model, with higher mean *ex situ* temperature associated with ARMS communities on ocean-facing reef Moresby ($F = 2.98$, p-value = 0.025) but higher *in situ* values associated with sheltered Ile du Coin ARMS communities ($F = 3.3$, p-value = 0.017). Both mean pH values ($F = 2.74$, p-value = 0.035) and mean DO values ($F = 3.54$, p-value = 0.018) were negatively associated with ARMS communities in the lagoon-facing reef. Mean flow velocity values were also negatively associated with Ile du Coin communities ($F = 3.28$, p-value = 0.025), whilst mean wave heights were positively associated with Moresby ARMS communities ($F = 3.00$, p-value = 0.023).

Our “indicspecies” analysis highlights correlations between average values of environmental parameters and taxa groups previously found to drive community dissimilarity between sampling sites and ARMS (Table 3.3). The percentage cover of CCA, colonial tunicates, green encrusting macroalgae, and bryozoans were observed to significantly correlate with sites presenting significantly higher DO values and lower temperature values. Bryozoan abundance also correlated significantly with higher PAR regimes observed across sites. The abundance of calcified tube worms found on both top and bottom plate face communities also significantly correlated with a lower *in situ* temperature regime and a higher DO regime. Brown encrusting macroalgae abundance on top plate face communities was observed to correlate with high pH and wave height regimes, as well as medium-flow velocities. Furthermore, the abundance of brown encrusting macroalgae across both plate faces correlated positively with lower PAR regimes. The abundance of red encrusting macroalgae on top and bottom plate face communities showed contrasting patterns of correlation with environmental parameters, with top plate abundances significantly correlating with medium wave and pH values and high flow velocities, whilst bottom plate abundances correlating with low DO and higher temperature profiles.

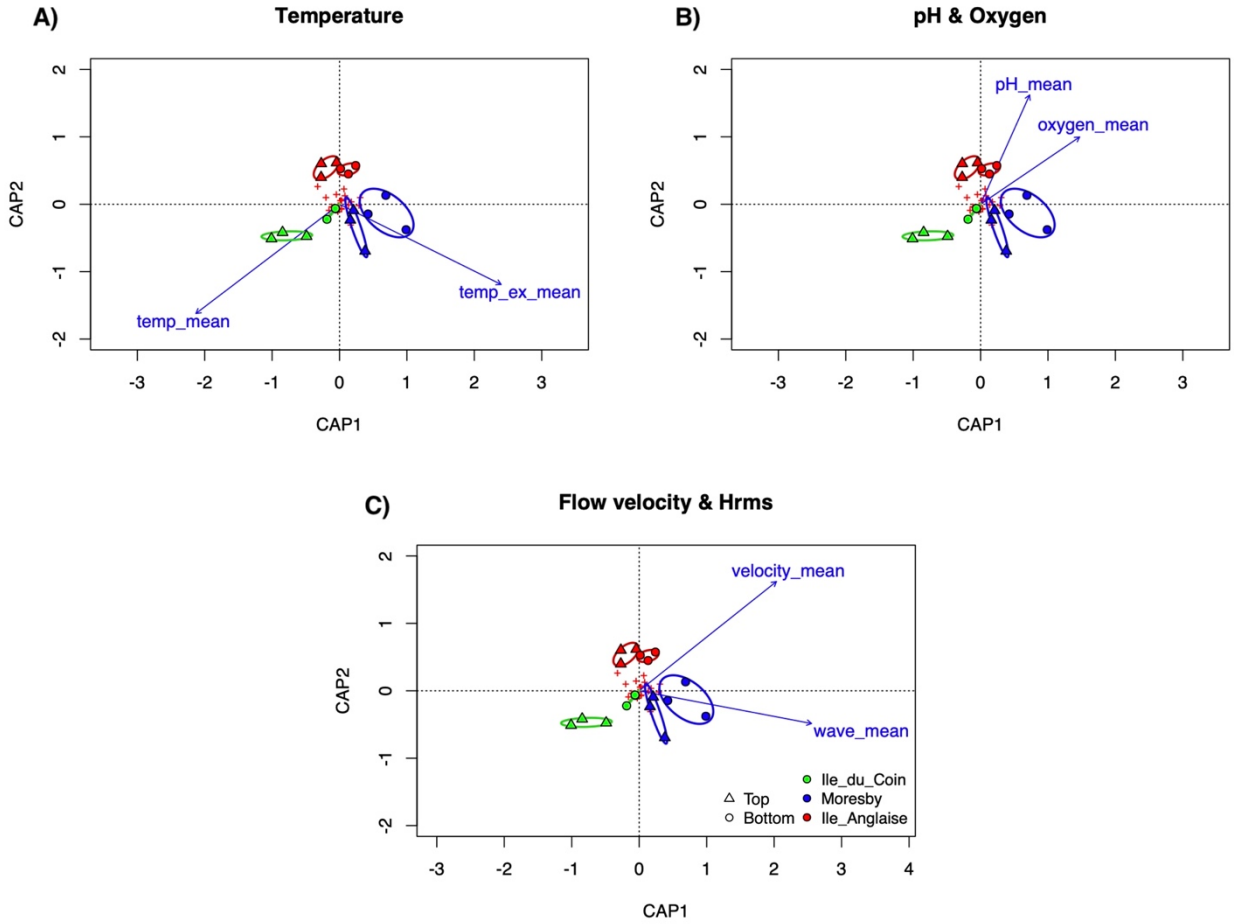

Figure 3.8. Distance-based redundancy analysis (db-RDA) ordinations of top or bottom plate face benthic communities across sites, based on Bray–Curtis distances using fourth-root transformed count data, factored with mean (A) *in situ* (temp_mean) and *ex situ* temperatures (temp_ex_mean), (B) pH and oxygen, and (C) flow velocity and wave heights. Ellipses represent 95% confidence intervals fitted to the spatial ordination. Red crosses highlight the positioning of benthic groups amongst the ordination.

Table 3.3. Results of point biserial correlation analyses of benthic taxonomic groups with mean environmental parameter values, across either top (T) or bottom (B) plate communities. Only taxa with significant correlations ($p<0.05$) are displayed, along with their correlation coefficient (*r*). Furthermore, only taxa whose abundance was previously found to be significantly impacted by site and plate face with multivariate GLM are presented in this table (see Methods).

Environmental parameter	**State**	**Taxonomic group**	***r***	**p-value**
Flow/Wave height	High	Red encrusting macroalgae (T)	0.936	0.377*
	Medium	Brown encrusting macroalgae (T)	0.87	0.035*
In situ temperature	High	Soft worm tube (T)	0.765	0.045*
		Red encrusting macroalgae (B)	0.778	0.025*
	Low	CCA (T)	0.901	0.012*
		Calcified worm tube (T + B)	0.879 (T) 0.811 (B)	0.012* (T) 0.012* (B)
		Green encrusting macroalgae (T)	0.722	0.012*
		Tunicate colonial (T)	0.715	0.025*
		Bryozoan (B)	0.878	0.012*
pH	Medium	Red encrusting macroalgae (T)	0.936	0.036*
	High	Brown encrusting macroalgae (T)	0.87	0.036*
DO	High	CCA (T)	0.901	0.014*
		Calcified worm tube (T + B)	0.879 (T) 0.811 (B)	0.014* (T) 0.013* (B)
		Bryozoan (T + B)	0.837 (T) 0.878 (B)	0.014* (T) 0.013* (B)
		Green encrusting macroalgae (T)	0.722	0.014*
		Tunicate colonial (T)	0.715	0.026*
	Low	Red encrusting macroalgae (B)	0.778	0.025*
PAR	High	CCA (T)	0.755	0.033*
		Red encrusting macroalgae (T)	0.953	0.011*
		Bryozoan (B)	0.832	0.022*
	Low	Brown encrusting macroalgae (T + B)	0.903 (T) 0.870 (B)	0.036* (T) 0.012* (B)

3.5. Discussion

3.5.1. In situ environmental profiles of sampling sites

By measuring *in situ* physicochemical factors, we recover the environmental profile of three reefs over yearly, monthly, and daily time periods. Ocean-facing reefs (Moresby and Ile Anglaise) are characterised by higher and more variable flow regimes as well as higher wave heights compared to a lagoon-facing reef site. Flow regimes impact the accumulation of DO and particulate CO2 in reef systems by interacting with sessile organisms' diffusive boundary layers (Finelli et al., 2006), and in part, can therefore, shape benthic metabolic rates. In our study, we observe significantly lower mean pH and DO values in a low-flow site when compared to two sites with high-flow regimes, as well as more variable average daily cycles of both parameters (Figure 3.2). Further work could investigate flow velocities across ARMS surfaces, as well as DO/pCO2 fluxes, for example, using *in situ* incubation methods, as done by (Roth et al., 2019).

Internal wave events can reduce thermal stress on shallow reefs (Wyatt et al., 2020), but they also increase concentrations of nutrients (Reid et al., 2019) and fluxes of organic matter (Leichter et al., 1998) and decrease the risk of reef bleaching and mortality (Safaie et al., 2018). Within the Chagos Archipelago MPA, Sheppard (2008) previously recorded *in situ* temperature measurements across reef sites and found that internal wave events temporarily caused temperature drops of up to 7°C and that the effect increased with depth. We see similar dips in temperature across ocean-facing reefs in our study, with temperatures dropping up to ~5°C for short periods of time (Appendix Figure B.2). We see that sites where frequent internal waves occur (Ile Anglaise and Moresby) have significantly lower mean temperature values than a site where no internal waves are detected (Ile du Coin) (Figure 3.5). Indeed, internal waves contribute to the variability of temperature observed across our sites, even if they occur only 0.2%–0.42% of the time. Removing internal wave signals from our dataset and comparing edited temperature values across our sampling sites, result in an estimate that site choice alone accounts for 20 times more variance observed across temperature profiles than the same analysis of our dataset that does include internal waves. Our results suggest that measuring the temperature at short intervals is key for recovering accurate *in situ* benthic temperature profiles. Although not presented in the main body of this article, we also calculated degree-heating-days (DHD) across all three sites and show how

internal waves reduce DHD by 8%–12% (Appendix Section B.i.). Whilst we did not investigate bleaching across local reef or ARMS communities in this study, we present methods and results of this additional analysis in the Appendix, as additional environmental context for future studies in this region (Appendix Section B.i.).

Satellite-derived SST is a popular metric for ecological studies of reef benthos (Carvalho et al., 2019; Floyd et al., 2020; Bosch et al., 2021), and with climate predictions indicating an increase in water temperatures globally (IPCC, 2022), it is important we obtain accurate temperature measurements when assessing or modelling the impact of heating on shallow reef cryptobenthic communities. Recent large-scale ARMS-based studies co-analysing benthic community diversity patterns and environmental parameters have used remote sensing data, including sSST and PAR (Carvalho et al., 2019; Pearman et al., 2020). Here, we show that *in situ* instrumentation is crucial for resolving patterns of local temperature and wave heights that cannot be detected using remote-sensing products. We find that NOAA's remote-sensing CRW model can overestimate and/or underestimate local temperatures across sites. For Ile du Coin, the sSST may underestimate actual sea surface conditions, and vice versa for the outer reef sites. This is because the mean SST provided by the CRW grid cell is 5 km × 5 km, covering both outer and inner reefs within the same grid, and hence does not offer data at the required resolution. Not detecting internal waves on reefs that experience them runs the risk of overestimating average temperature values and skewing estimates of heat stress on local communities. Temperature loggers are not expensive in comparison to other oceanographic instruments, and thus, we recommend that if budgets allow, temperature loggers should be deployed alongside ARMS. For wave heights, due to the coarse grid at the island scale, the WWIII model does not consider the sheltering effect of the archipelago (Pawka, 1983), and values were approximately five times larger than observed *in situ* wave heights. Our results show that the WWIII model is unable to recover individual wave profiles for each site, and therefore, we recommend that if resources allow, this model should not be used as a substitute for local, *in situ* measurements of wave exposure in the Chagos Archipelago MPA.

3.5.2. Percentage cover and diversity of ARMS sessile communities

Our image analysis recovers a diverse community of benthic invertebrate and algal groups after 1 year. Other studies have investigated the sessile benthic community composition and condition of exposed

reef surfaces across the Chagos Archipelago MPA (Head et al., 2019; Lange et al., 2021; Pilly et al., 2022), but none have previously investigated sessile cryptobenthic communities in this region. We find that sponges, fleshy and calcareous macroalgae, bryozoans, and annelid worms dominated recruitment surfaces, whilst colonial ascidians, molluscs, colonial ascidians, tunicates, and large foraminifera were less frequently observed.

Our findings show that site choice also had a significant effect on ARMS community composition. Whilst almost all taxonomic groups are observed across all three sites (except for octocorals), and triplicate ARMS devices harbour highly similar communities within sites, overall community composition between reefs significantly differs. Image analysis has been shown to effectively recover the benthic profile of different sites using triplicate ARMS devices (David et al., 2019), and previous genetic analyses found that differences in sampling site and region shape the cryptobenthic composition and diversity on ARMS (Pearman et al., 2020). Here, by analysing 15 plate faces per device and following NOAA's CREP program's identification groupings, we demonstrate that ARMS photoanalysis alone can discriminate amongst reef sites within the same region, as well as between sites with similar local environmental conditions. The analysis of 225 points across 15 images per ARMS was feasible here due to the restricted number of sampling sites, but future studies could employ automated annotation tools, such as CoralNet's latest deep-learning engine, to increase coverage and decrease analysis time (Beijbom et al., 2015; Chen et al., 2021).

We also see a strong and significant effect of plate face on the composition of ARMS benthic communities. Indeed, we observe a significantly lower percentage cover and significantly different assemblages of taxonomic groups on the top faces of ARMS plates than on the bottom faces, across all three sites. Our results show that several filter-feeding invertebrates and macroalgal taxa are significantly more abundant on the underside of ARMS plates, whilst only soft-tube annelids are found in higher abundance on top plate faces (Table 3.2). Similar patterns of community composition have been observed under sheeting coral colonies (Jackson and Winston, 1982), within reef cavities (Scheffers et al., 2010; Kornder et al., 2021), on artificial recruitment tiles (Higgins et al., 2019; Mallela et al., 2017), as well as by David et al. (2019) on the underside of ARMS plates from the Red Sea. We find that together, plate face and site choice significantly contribute to differences observed in the

abundance of CCA, fleshy red encrusting algae and green encrusting algae across sampled reefs. Whilst the percentage cover of fleshy macroalgae has been estimated to be between 1% and 4% across shallow reefs of the Chagos Archipelago (Head et al., 2019; Lange et al., 2021), they represent around a third of benthic communities across ARMS devices in this study. Unlike some cryptobenthic invertebrates (e.g., bryozoan, ascidian, and encrusting sponges), macroalgae are often included in reef biomonitoring protocols and surveys. Encrusting macroalgae are commonly found within cryptic reef cavities but often form a minor part of organism biomass within cryptobenthic communities (Kornder et al., 2021). Our findings highlight how traditional benthic surveys, where only exposed surfaces are analysed, could underestimate the true percentage cover of key phototrophic groups. However, further comparisons between the cryptobenthic communities found on ARMS and those on nearby cryptic surfaces and cavities are now needed to determine if ARMS plates overestimate the percentage cover of any taxa. Nevertheless, based on our findings, we recommend that future image-based studies of ARMS from tropical coral reefs investigate top and bottom plate communities independently.

The presence of sand and sediment likely impacts the percentage cover and community composition across the top surfaces of ARMS plates. Sediment loading on reef surfaces has been shown to negatively affect the recruitment of stony coral, sponges, tunicates, and CCA (Fabricius and De'ath, 2001; Babcock and Smith, 2002; Maldonado et al., 2008) and can have mixed impacts on fleshy macroalgae recruitment by either inhibiting or abrading zygote attachment (Gao et al., 2019) or conversely by reducing fish and urchin herbivory (Tebbett et al., 2018; Kriegisch et al., 2019). We did not record actual sedimentation rates in this study but recommend pilot studies now be conducted on the extent of sedimentation on ARMS, for example, by using traps (Storlazzi et al., 2011) to record accumulation rates throughout unit deployments.

3.5.3. Associations between sessile communities and environmental parameters

We find that some of the variations in ARMS cryptobenthic communities observed across our three study sites can be explained by differences in mean *in situ* or *ex situ* temperature, pH, DO, flow velocities, and wave heights. Previous ARMS-based studies found that SST, PAR, pH, and surrounding coral cover are important variables in shaping the taxonomic diversity of sessile, mobile, or microbial communities across geographic regions (Pearman et al., 2019; Pearman et al., 2020). We recognise

that benthic assemblages can show non-linear responses to changes in abiotic factors in reef ecosystems (Gove et al., 2015) and that our dbRDA analysis only represents a facet of biophysical interactions between benthic communities and environmental parameters. In part, this is due to our small number of site replicates and the fact that mean values offer limited information on long-term datasets. Nevertheless, our results support the need for *in situ* physicochemical measurements rather than remote sensing. For example, the temperature dbRDA displays contrasting trends, with increasing mean *in situ* temperature values associated only with Ile du Coin communities but *ex situ* values significantly associated only with Moresby communities (Figure 3.8). This finding highlights the risk that *in situ* biophysical relationships could be misinterpreted when using satellite-derived SST for the study of cryptobenthic communities across reefs in close geographical proximity.

The abundance of some cryptobenthic taxa on ARMS devices significantly correlates with different regimes of temperature, pH, PAR, oxygen, flow velocity, and wave heights observed across our sampling sites (Table 3.3). For some groups (e.g., red fleshy macroalgae), we find that abundances on top and bottom plate face communities significantly correlate with a different set of environmental drivers, whilst for others (e.g., calcareous worms and bryozoans), both top and bottom plate face abundances correlate with the same environmental regimes.

We find that encrusting macroalgal groups correlate differently with *in situ* environmental regimes identified across our sampling sites. Top-plate CCA abundance correlates with lower *in situ* temperature profiles, but the opposite is observed for fleshy red encrusting macroalgae abundance on the underside of ARMS plates (Table 3.3). On top plate communities, we see that red and brown macroalgal abundance correlates with medium/high flow (10–12 cm/s) and wave height regimes (0.27–0.34 m), as well as medium/high pH profiles (7.93–7.96). Growth responses of fleshy marine macroalgae to water flow rates can be based on species-specific physiological adaptations (Ho and Carpenter, 2017), and water flow can increase photosynthetic rates, and therefore growth, up to a point (Stewart and Carpenter, 2003). Macroalgae of different forms can interact both positively or negatively, through competition for resources (Fong and Paul, 2011) or by protecting one another from herbivory and sediment loading (Bittick et al., 2010; Sura et al., 2019), and competition may play a role in shaping macroalgal abundances observed between reef sites in this study.

CCA form a major component of benthic calcifiers on reefs but have shown to fare worse than their non-calcifying counterparts under higher temperatures and lower pH conditions (Porzio et al., 2011; Zweng et al., 2018; Diaz-Pulido and Barrón, 2020), a worrying trend for the future of accreting reefs as oceans continue to warm and acidify. Our environmental analysis shows that average pH values differ significantly between sites, and whilst the pH at the sheltered site (Ile du Coin) was found to be at 7.91 on average; the large diel variations observed *in situ* resulted in minimum values at or below 7.85 (Figure 3.2; Appendix Figure B.3). These minimum pH values, alongside higher temperatures, may not be more conducive for the growth of CCA at this site, as co-occurring low pH and high-temperature conditions can reduce calcification and productivity rates (Anthony et al., 2008; Diaz-Pulido et al., 2012). To further investigate the relationship between *in situ* temperature, DO, and pH and the abundance of both calcifying and encrusting macroalgae, net community calcification (NCC) and net community productivity (NCP) could be calculated. Longer deployments of SeapHOx/SeaFET loggers, matching those of temperature loggers, would also be needed to identify the extent of time during which ARMS communities experience acidifying conditions.

We find that increases in the abundance of other calcifying groups, bryozoans, and calcareous tube worms, also significantly correlate with lower *in situ* temperature and higher DO regimes (Table 3.3). Differences in thermal tolerance have been shown in bryozoans across marine habitats (see review by Lombardi et al., 2020), but co-occurring low pH and high temperatures can negatively affect bryozoan cover by reducing growth and calcification rates as well as increasing the dissolution of dead colonies (Rodolfo-Metalpa et al., 2010). Calcareous serpulids have been shown to thrive on reefs experiencing regular cooling (Leichter et al., 1998). However, co-occurring low-oxygen and high-temperature conditions can be unfavourable for the growth rate of calcifying reef organisms in general (Nelson and Altieri, 2019). Whilst frequent internal waves at Ile Anglaise and Moresby likely provide a conducive environment for calcareous worms and bryozoan growth through regular cooling, these events may also benefit these groups through the regular upwelling of prey plankton and nutrients (Leichter et al., 1998), as well as a mechanism for increased larval dispersal (Fernández-Aldecoa et al., 2019).

3.5.4. Study limitations

We recognise there are several potential limitations to our study's methodologies. Firstly, we made observations of cryptobenthic groups at a high taxonomic level, limiting our ability to look at diversity patterns across ARMS and sites. Restricted time in the field and limited resources for the identification of sessile cryptobenthic species available for this region meant we were unable to classify organisms to lower levels. Furthermore, our 2D photography of ARMS surface cover likely neglects the 3D structure of cryptobenthic reef communities (Kornder et al., 2021), and since photographs were taken from a top-down perspective, organisms with the ability to grow over others are more likely to have been visible and therefore recorded. Whilst we find that not all available ARMS recruitment surface was covered by live sessile organisms, we observed that recruitment cover was denser on the outer edges of ARMS plates, which are usually composed of both overlapping encrusting and upright macroalgae. Future ARMS studies could employ fluorescence photography, as shown in Steyaert et al. (2022), to improve estimates of the percentage cover of encrusting organisms, such as CCA and juvenile hard corals, using group-specific wavelengths.

Secondly, the number of site replicates (n = 3) in our study limits our ability to simultaneously model the relationship between multiple environmental parameters and community composition. We explore correlations between taxa abundances and *in situ* environmental profiles but cannot perform regression-based models integrating all parameters simultaneously. Increasing the number of sites and merging this dataset with other ARMS studies across the Indian Ocean could provide enough sampling replicates, as done by Pearman et al. (2020).

Thirdly, whilst we have long-term data on environmental parameters over a full year, we analyse cryptobenthic communities only at the end of these 12 months. Such is the nature of current ARMS studies that once collected, sessile communities on each unit are subsampled and scraped off. However, pilot studies could explore the potential of ARMS to act as long-term biomonitoring stations, where plates could be photographed and then re-assembled and re-deployed.

3.5.5. Conclusion

The need for continuous and comprehensive monitoring of both benthic communities and environmental parameters on coral reefs is crucial in the face of increasing climate change impacts (Koldewey et al., 2021). Whilst the degradation of coral reef habitats is set to reduce (Brandl et al., 2020) or alter (Kubicek et al., 2019) diversity over the coming decades, relatively few studies have been conducted on the functional or taxonomic diversity of sessile invertebrates or macroalgae on tropical reefs in comparison with hard corals and fish (Brandl et al., 2019). Fewer studies have co-analysed *in situ* environmental parameters and the biodiversity of cryptic reef spaces (but see Scheffers et al., 2010; Kornder et al., 2021). By analysing large and detailed datasets of benthic communities and environmental parameters from three tropical reef sites, we identify subtle but significant differences in the abundance and composition of cryptobenthic taxa and the environmental profile that they experience, after just 1 year. Our study provides an example of how *in situ* environmental parameters can be integrated with image-analysis data for future ARMS-based monitoring efforts and is the first step in this endeavour for the reefs of the Chagos Archipelago.

3.6. Author contributions

MS, AK, ML, CH, RB, and DM collected the data. MS, AK, ML, and PW analysed the data. All authors made substantial contributions to the discussion of the content, the writing, and the editing of the manuscript. All authors contributed to the article and approved the submitted version.

Data availability statement

Benthic abundance data from the analysis of Autonomous Reef Monitoring Structure (ARMS) images presented in this study is included in the published article's Supplementary Material (https://www.frontiersin.org/articles/10.3389/fmars.2022.932375/full#supplementary-material). Further inquiries regarding this dataset, and any enquiries regarding environmental/physical data presented in this study, can be directed to the corresponding author.

Conflict of interest

The authors declare that the research was conducted in the absence of any commercial or financial relationships that could be construed as a potential conflict of interest.

CHAPTER 4

Linking ARMS: investigating the similarity between cryptobenthic communities on Autonomous Reef Monitoring Structures (ARMS) and surrounding natural reef using image-analysis and environmental DNA

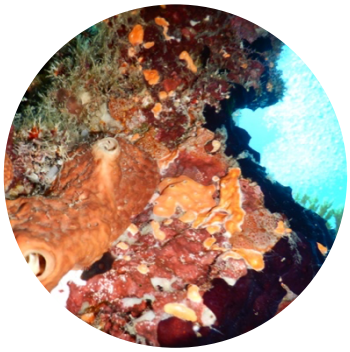

Margaux Steyaert[1,2], Emma Ransome[3], Michael Bonsall[2], Nicholas Dunn[2,3], Rosalie Dowell[2,3], Kevin Hopkins[2] and Catherine Head[1,2]

[1] Department of Biology, University of Oxford, Oxford, OX1 3SZ, United Kingdom

[2] Institute of Zoology, Zoological Society of London, London, NW1 4RY, United Kingdom

[3] Department of Life Sciences, Imperial College of London, London, SL5 7PY, United Kingdom

This chapter is not submitted to any academic journals

4.1. Abstract

Coral reef cryptobenthic communities are intrinsically linked to complex but fragile reef matrix. To limit the impact of scientific exploration of such communities, non-destructive sampling methods are therefore important. Benthic image analysis, Autonomous Reef Monitoring Structures (ARMS) and environmental DNA (eDNA) are three ways to non-destructively sample the cryptic coral reef, but the communities retrieved from each method have yet to be critically compared. Here, we investigated how sessile recruitment and diversity patterns on ARMS compare with those on in-situ dead *Acropora* sp. tabular coral using image-analysis and determined the extent of genetic overlap between ARMS and ambient seawater using community and eDNA multi-marker metabarcoding, across two reefs of the Chagos Archipelago Marine Protected Area (MPA) (Central Indian Ocean). Firstly, we found the percentage cover of bryozoans, calcified tube worms and bivalves to be significantly higher on ARMS, whilst the percentage cover of hard corals, as well as turf, red fleshy and crustose coralline algae was higher on dead coral. On the other hand, sponges, brown encrusting macroalgae, soft-tube worms and ascidians were found in similar abundances across dead *Acropora* sp. coral and ARMS. Whilst the age of communities likely plays a key role in determining overall sessile percentage cover, we highlight how ARMS may bias or under-report the recruitment of certain groups. As expected, we find that communities across ARMS and eDNA samples recovered using metabarcoding are different, and that more cryptobenthic taxa are detected within ARMS communities. More importantly, we show how eDNA can increase the number of cryptobenthic taxa detected from in-situ reef communities, and when integrated with ARMS, provide a valuable tool for the detection of sessile groups such as sponges. Our findings show that non-destructive methods can be powerful analysis tools for recovering patterns of cryptobenthic abundance and diversity across reef ecosystems and highlight the importance of combining image and DNA-based approaches for studying cryptobenthos.

4.2. Introduction

Man-made materials have long been used to study the ecological processes and biodiversity of tropical coral reefs (Mundy, 2000). Tropical coral reefs are highly biodiverse ecosystems, and much of this diversity resides within the hidden cavities and surfaces of the reef matrix and can be referred to as the cryptobenthos or cryptofauna (Kornder et al., 2021; Enochs & Manzello, 2012; Klump et al., 1988). Artificial materials such as polyvinyl chloride (PVC), ceramics, terracotta and fibreglass allow for a standardised collection of data from cryptobenthic communities (Monroy-Velázquez et al., 2020; Myers & Southgate, 1980). Whilst each type of material, along with differences in rugosity, orientation, or colour, can have their own inherent bias (Randall et al., 2021; Mallela et al., 2018; Salinas de León, 2011; Harriot & Fisk, 1987), they are an ecologically more sensitive option than destructive sampling of the natural reef matrix.

Autonomous Reef Monitoring Structures (ARMS) are highly standardised 3D recruitment devices used for the collection and study of marine cryptobenthic fauna (Zimmerman & Martin, 2004). Each ARMS unit is composed of a stack of nine 22.5cm x 22.5cm square PVC plates, between which small gaps left either open or closed (with the addition of PVC cross bars) provide the structural complexity otherwise lacking from traditional single unit recruitment tiles. Attached to the benthos for a prolonged duration (on average 12-36 months), ARMS act as passive collectors of both sessile and motile organisms. A highly standardised set of protocols guide researchers to collect both genetic (barcoding, metabarcoding) and image-based data from each unit, with the aim to produce comparable datasets of cryptobenthic diversity (Knowlton et al., 2010; Ransome et al., 2017). ARMS are now being employed globally to assess and monitor biodiversity (Palomino-Alvarez et al., 2021), in programs such as the European ARMS programme (ARMS-MBON) and the Global ARMS Program (Smithsonian) (Obst et al., 2020).

In recent years, the use of ARMS to study marine systems has gained recognition and furthered our knowledge of cryptobenthic diversity across the globe. Several studies have shone a light on the diversity of tropical reef cryptobiomes using metabarcoding and barcoding (Pearman et al., 2020; Carvalho et al., 2019; Pearman et al., 2019; Al-Rshaidat et al., 2016; Ransome et al., 2017). A few

genetic studies have investigated the relationship between physical and chemical environmental drivers with diversity (Ip et al., 2022; Plaisance et al., 2021; Pearman et al., 2019), whilst others have focused on presenting novel taxonomic records for local regions (Palomino-Alvarez et al., 2021; Moews-Asher, 2018) or for specific taxa groups, such as sponges (Vicente et al., 2022; Timmers et al., 2020) or crustaceans (Hazeri et al., 2019). A handful of studies have presented image-based analyses of the percentage cover and diversity of ARMS sessile communities and have shown community composition can be strongly determined by surface orientation, locality, and environmental drivers (Steyaert et al., 2022b; David et al., 2019). Methods-based studies such as Ransome et al. (2017) and Leray et al. (2015) have been instrumental in refining standardised protocols, whilst others have shown the promise of novel sequencing technology (Chang et al., 2020) and fluorescence imaging (Steyaert et al., 2022a) for furthering ARMS analyses.

PVC provides an adequate recruitment surface for coral larvae (Leonard et al., 2021), and some studies have compared sessile communities on PVC surfaces against those on natural reef surfaces (Mallela et al., 2017; Mallela, 2007). To our knowledge, only four studies have so far directly compared communities on ARMS with in-situ communities from natural surfaces or surrounding water column. Plaisance et al. (2011) compared crustacean diversity and abundance between ARMS and dead coral heads and did not find any within-site differences in diversity patterns between both. Pennesi & Danovaro (2017) showed that microphytobenthic communities were also similar between ARMS and natural surfaces, and that ARMS were able to recreate heterogeneous light conditions required for the presence of highly diverse plankton communities. Nichols et al. (2021) used metabarcoding of one broad eukaryotic marker to compare diversity estimates from ARMS communities against those recovered using environmental DNA from water collected from in-situ reef crevices and from water in which ARMS had been soaking and found that neither ARMS nor eDNA approaches recovered the same set of organisms. Finally, Ip et al. (2022) compared ARMS community diversity estimates from metabarcoding against in-situ coral cover. However, no studies to date have directly compared image-based analyses of the cover and abundance of sessile cryptbenthic groups between ARMS and local reef surfaces.

The sampling of environmental DNA (eDNA) for the study and monitoring of coral reef ecosystems has rapidly grown in popularity over the last decade (Dunn et al., 2022; Polanco-Fernandez et al., 2021; Shinzato et al., 2018; Stat et al., 2017), and recently, has been used to study benthic reef communities (Nguyen et al., 2020; Nichols & Marko, 2019). eDNA sampling offers a rapid and non-destructive approach for picking up diversity, but it's application for benthic monitoring remains, for the most part, uncertain (Antich et al., 2021; but see West et al., 2022; Alexander et al., 2020). Some known limitations of eDNA methods include the lack of knowledge of DNA shedding, degradation and degradation rates from specific taxa groups (Thomsen et al., 2015). Furthermore, many studies collect different volumes of water, and use filters of different materials and pore sizes, all of which are known to significantly impact recovered communities (Bessey et al., 2020; Spens et al., 2017). More studies ground-truthing eDNA samples with in-situ reef community tissue are needed to assess the benefits and limitations of this approach for long term benthic biomonitoring.

Overall, our main aim with this study was to establish how well ARMS represent cryptic communities found on dead colonies of an abundant coral in the Chagos Archipelago MPA and whether, or how, eDNA sampling could supplement the ARMS method. Firstly, using image analysis, we investigated similarities between the recruitment cover and composition of sessile communities on ARMS to that of nearby dead tabular *Acropora sp.* coral colonies. We used image-analysis here to avoid the destructive sampling of communities from natural reef substrate. We hypothesised that i) both surface orientation (top or undersides of ARMS plates and dead coral) and site would have a strong effect on community composition, and that whilst ii) total recruitment cover would be similar on ARMS and natural surfaces, iii) community composition would also significantly differ between artificial and natural substrates. Secondly, using metabarcoding, we compared communities recovered from ARMS to those recovered using environmental DNA sampling of the surrounding water column, using two genetic markers (COI, 18S v4). We hypothesised that whilst i) overall communities recovered using both approaches would significantly differ, ii) a significant overlap of genetic material between sample types (eDNA, ARMS) would be observed. Objectives for this part of the study included determining the extent of genetic overlap between ARMS and the surrounding water column, establishing which cryptobenthic taxa present on ARMS devices were detectable using eDNA sampling and inversely how many, if any, sessile cryptobenthic groups detected using eDNA were not found on ARMS.

4.3. Methods

4.3.1. Study sites and ARMS retrieval

This study was conducted across the Peros Banhos atoll of the Chagos Archipelago Marine Protected Area (MPA), Central Indian Ocean. Two shallow sites (7-12m depth), one exposed reef outside Moresby Island and one sheltered reef inside Ile du Coin Island, were surveyed and sampled in April 2021 (for GPS coordinates, see Appendix Table A.1).

Triplicate Autonomous Reef Monitoring Structures (ARMS) were retrieved on SCUBA from each site following a 36-month deployment. During each retrieval, a clear plastic bin was placed over the ARMS and secured flush against the base plate to minimise the loss of motile organisms. ARMS units were placed in blacked out 96L bins and covered with seawater filtered through 40 µm mesh and aerated using aquarium bubblers. Each unit was then disassembled, and mobile and sessile communities were then separated and fractioned off using standardised protocols (Leray et al., 2015).

4.3.2. ARMS image analysis

Following the disassembly of ARMS units, photographs were taken of both top and bottom faces of each ARMS plate using a Nikon D810 camera and 105mm macro lens (Figure 4.1). Images were uploaded to CoralNet (version 1.0) and individually analysed using 225 random points in a 15 x 15 grid and a label set reflecting the major invertebrate and macroalgal groups of cryptobenthic reef communities (see Appendix Table B.2) (Chen et al., 2021). All identifications were performed manually without using CoralNet's machine learning engine. Any point fallen on surfaces previously covered by PVC cross bars or bolts, or off the ARMS plate, was listed as 'Unavailable'.

Photographs were also taken of the topside and undersides of dead tabulate *Acropora sp.* coral colonies (Figure 4.1) at both sampling sites where ARMS units were recovered, with a Nikon Coolpix camera, using the flash option. Coral colonies that were dead but i) still attached to the coral matrix, ii) parallel to the reef benthos, and iii), where possible, within a 10-meter radius to the ARMS units, were chosen. The top and bottom sides of 9 *Acropora sp.* colonies were analysed for each site, using the same 225-point per image approach and label set mentioned above. Any point fallen on surfaces other than the dead coral colony was listed as 'Unavailable'.

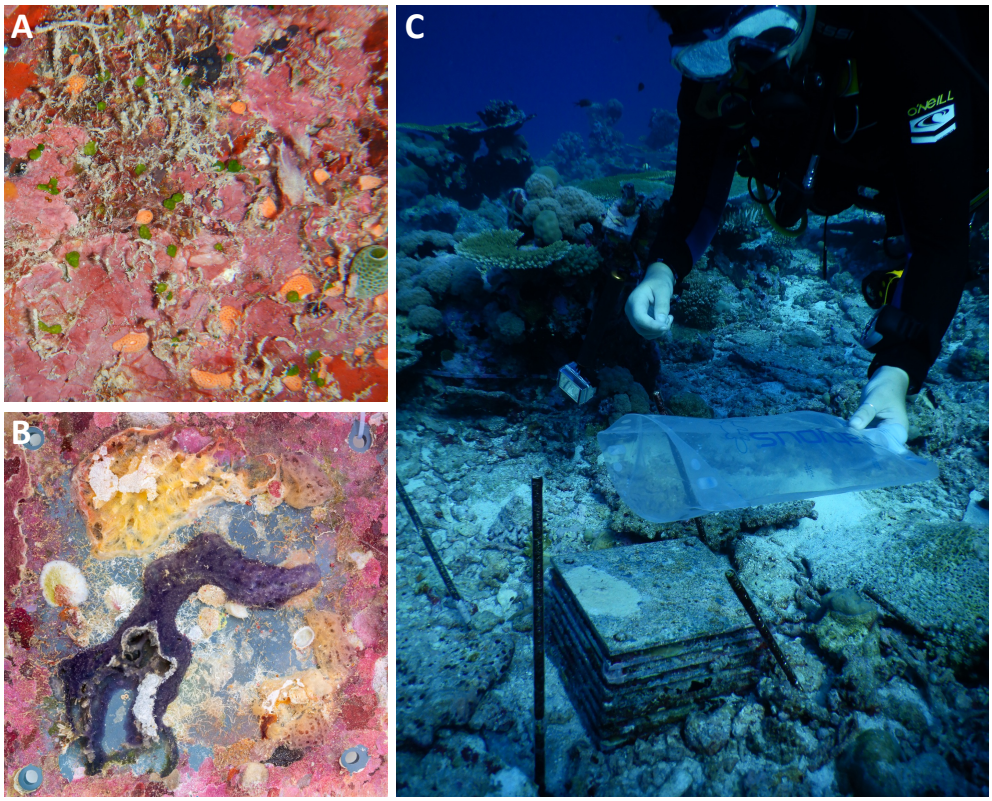

Figure 4.1. Photographs of sessile communities on (A) the underside of a dead *Acropora* tabular coral colony and (B) the underside of an ARMS plate, alongside (C) the collection of a water sample for eDNA analysis above an ARMS unit *in-situ*.

4.3.3. ARMS community and eDNA sample collection

Prior to the retrieval of each ARMS unit from the reef floor, triplicate water samples (2L each) were collected on SCUBA using sterile platypus bottles, within 1 meter of each device (Figure 4.1). Each sample was then individually filtered through a Sterivex capsule unit (Millipore; 0.22 µm pore size), and briefly filtered dry to remove excess seawater. A filtration negative was taken between both sampling sites by filtering clean fresh water (2L) through the eDNA filtration system, also using a Sterivex filter. Sterivex filter capsules were then sealed using sterile Luer caps and Parafilm, and immediately stored dry at -20°C.

For this study, the 500 µm - 2mm motile fraction, 100 µm - 500 µm motile fractions and sessile communities of ARMS were processed in the same manner described in Chapter 1 of this doctoral thesis.

4.3.4. DNA extraction, library prep and sequencing

DNA extracted from Sterivex capsules using the DNEasy Blood & Tissue kits following the manufacturer's protocols, except for an extended overnight lysis step following modifications from Spens et al. (2017) The final elution step was carried out using 2 x 100ul of water at 70°C. DNA from each sample was then quantified on a QuBit fluorometer using the QuBit dsDNA Broad-Range assay. DNA from bulk ARMS motile (500µm-2mm, 100-500µm) and sessile samples was extracted following the same protocol presented in Chapter 1 of this doctoral thesis.

A short region of cytochrome oxidase I (COI) gene (313bp) and V4 region of the 18S gene (270-387bp) were amplified in both eDNA and ARMS samples using universal primers (for COI, mlCOIintF/jgHCO2198, Leray et al., 2013; for 18S, TAReuk454FWD1/TAReukREV3, Stoeck et al., 2010), with attached Illumina adapters on the 5' end, following recommendations made in Illumina's 16S Metagenomics Sequencing protocol (Illumina). Amplification by polymerase chain reaction (PCR) of both markers was carried out in the same manner as presented in Chapter 1 of this doctoral thesis.

Gel electrophoresis, library preparation and sequencing were also carried out for both eDNA and ARMS samples using the same methods presented in Chapter 1 of this thesis. All eDNA and ARMS samples presented in this chapter were run on the same sequencing reactions, with one for all COI samples and another for all 18S also.

4.3.5. Bioinformatics

As in Chapter 1 of this doctoral thesis, a custom bioinformatics pipeline was used to run merging, error-filtering (DADA2, Callahan et al., 2016), clustering (VSEARCH, Rognes et al., 2016), curation (LULU, Frøslev et al., 2017) and taxonomy assignment of COI and 18S sequence datasets (Williams et al., *manuscript in preparation*). For both datasets, the *filterAndTrim* function's truncLen parameter was set to 240 bp for both forward and reverse reads, maxN was set to 0, maxEE was set to (2,2) and truncQ

was set to 2. For the core sample inference function *dada*, the pooling parameter was set to 'pseudo-pool' for both amplicon datasets. For 18S, Exact Sequence Variants (ESVs) obtained from the DADA2 step were curated directly using LULU (match rate set to 0.90, all other parameters left as default), with no clustering performed beforehand, into curated ESVs (cESVs). For COI, ESVs were first clustered into Operational Taxonomic Units (OTUs) using VSEARCH (Rognes et al., 2016), and then curated using LULU (all parameters left as default, including match rate at 0.84).

IDTAXA (Murali et al., 2018) was used to assign taxonomy to sequence variants, using the SILVA r138 dataset for 18S data (Quast et al., 2013), and a custom COI reference dataset composed of MIDORI (Leray et al., 2018) and BIOCODE (Meyer et al., 2006) sequences (Williams et al., *manuscript in preparation*). Both datasets were formatted for the IDTAXA algorithm prior to taxonomy assignment, and the assignment threshold minimum was set to 30.

The eDNA field negative was then examined to check for possible contamination across eDNA samples. For COI, whilst 52 cOTUs found in the field negative sample accounted for <1% of the number of cOTUs in the eDNA samples, they contributed to 10% of the total read count. Of these, 15 cOTUs contributed more than 1% individually to eDNA sample read counts and were deemed potential contaminants. Since these potential contaminants contributed to <1% across ARMS samples, it was deemed appropriate to remove these sequence variants entirely from both the eDNA and ARMS dataset. The process was also carried out for 18S, where 66 cESVs were found shared between the field and eDNA sample but accounted for 1.31% of all eDNA cOTU sequences and 3.7% of reads. A total of 6 cESVs were deemed 'potential contaminants' and were removed from all eDNA and ARMS samples.

4.3.6. Statistical analysis

All statistical analyses were performed in R (R Core Team, 2022) via the RStudio interface version 2022.02.03 (RStudio Team, 2022). The percentage live cover and composition of sessile communities was visualised and plotted using the R packages 'vegan' v 2.6.2 (Oksanen et al., 2022) and 'ggplot2' v 3.3.6 (Wickham, 2016). In this study, the percentage of live recruitment cover was calculated as the number of points assigned to a live sessile group out of the number of points identified as available

space, which is determined as any surface on the ARMS plate that was not covered by a nut, steel washer or PVC cross bar. The difference in recruitment cover % across the top and bottom of ARMS and Acropora tables was tested using a set of independent generalised linear models (GLM), with a negative binomial family distribution, using the R package "MASS" v.7.3.57 (Venables & Ripley, 2002).

The composition of sessile communities across the topside or underside of sample type (ARMS vs Acropora) was then visualised with non-metric multidimensional scaling (NMDS) plots, using Bray-Curtis distances. For all plots, ellipses drawn around groups represent 95% confidence intervals fitted to the ordination.

The relationships between benthic composition and sample type, site and plate face were further investigated using multivariate generalised linear models with the R package "mvabund" v4.2.1 (Wang et al., 2012). The *manyglm* function was used to run multivariate GLMs using a negative binomial distribution on a matrix of count abundance, against explanatory variables. A model with an interaction between all three terms had the lowest AIC score and was therefore chosen. Analyses of deviance tests were then run on the optimal model, with the test statistic parameter set to 'score' and adjusted p-values were requested (adjusted for multiple testing using a step-down resampling approach).

As in Chapter 2, a custom function was used to format the pipeline output to be usable with R package "phyloseq" v 1.40.0 (McMurdie & Holmes, 2013). Estimates of total sequence variant richness, along with respective standard errors, and high/low confidence intervals, were then calculated across ARMS and eDNA samples using the "breakaway" package (version 4.7.6)(Willis & Bunge, 2015). Samples were then rarefied to account for uneven sequencing depth using the *rarefy_even_depth* function (phyloseq) after setting a seed, for subsequent analyses, unless stated otherwise. Sequence variants found in each sample type (ARMS vs eDNA) were extracted and the overlap between these groups was visualised using area-proportional Venn diagrams (web-based DeepVenn software)(Hulsen et al., 2008). The presence of COI or 18S sequence variants across ARMS, eDNA samples or both, was determined for each metazoan phyla. Community composition across sample types (ARMS vs eDNA) was then explored using NMDS plots, using Jaccard distances based on the presence-absence of COI

cOTUs or 18S cESVs, using the R package 'vegan'. The rate of taxonomy assignment across taxonomy ranks by IDTAXA was then explored across both un-rarefied 18S and COI datasets.

The package DESeq2 v1.36.0 (Love et al., 2014) was used to carry out differential abundance analyses on COI cOTUs and 18S cESVs found to be present in both eDNA and ARMS samples. DESeq2 performs internal normalization of read counts across each dataset by calculating the geometric mean of counts per sequence variants, following which a size factor is calculated per sample. For this analysis, un-rarefied samples were used. A Wald test statistic was used to determine significance, with log2 fold change values and p-values adjusted for multiple testing outputted for each sequence variant. COI cOTUs found to have differential abundances ($p<0.05$) between eDNA and ARMS samples were then grouped by genera, and the distribution of log2Fold values across these taxa was visualised using plots. The same was carried out for 18S cESVs but these were grouped by order. Sequence variants found in both eDNA and ARMS samples but not found to have differential abundances between sample type were also investigated.

4.4. Results

4.4.1 Percentage cover and community composition on ARMS and Acropora sp. coral using image analysis

A range of algal and metazoan groups were identified across ARMS and dead *Acropora sp.* coral tables (Figure 4.2), with sponges, CCA and soft-tube worms observed as the most abundant groups across both substrate type and both sites. Almost all groups were observed across both recruitment surfaces, except for hydroids and blue-green algae on ARMS, and empty bivalves and foraminifera on Acropora tables.

The proportion of live sessile recruitment was significantly higher on the underside of dead coral (average of 97.63%) than on the underside of ARMS plates (average of 84.47%) across both exposed (Moresby, $p<0.001$***) and sheltered (Coin, $p<0.001$***) sites (Table 4.1, Figure 4.2). No significant difference was found between the proportion of live sessile recruitment on the top of dead Acropora

tables (average of 68.53%) and ARMS (average of 61.43%) in either site. However, live sessile recruitment was significantly higher on the top of dead coral in the exposed site than on the top of dead coral in the sheltered site ($p<0.001^{***}$), with an average of 76.33% and 60.72% respectively. Overall, 6.3% of counts on coral tables fell on surfaces with no live recruitment (including 'No Recruitment', 'Bite scars' and 'Calcium carbonate'), compared to 30.3% on ARMS. In contrast, 11.7% of counts on Acropora tables were identified as covered in sediment, compared to 5.5% on ARMS.

Table 4.1. Output of Tukey tests on beta regression models on the effect of substrate type (ARMS vs dead coral) and site (Moresby, Ile du Coin) on the overall percentage cover (%) of live sessile communities observed using image analysis. Top and bottom communities are modelled separately, and only pairwise comparisons with significant outcomes are presented.

Plate face	Pairwise comparison	estimate	SE	Z	P
Top	ARMS Coin - ARMS Moresby	-0.1366	0.033	-4.139	<0.001***
	Acropora Coin - Acropora Moresby	-0.1233	0.0304	-4.058	<0.001***
	ARMS Coin - Acropora Moresby	-0.2049	0.0461	-4.447	<0.001***
Bottom	Acropora Coin - ARMS Coin	0.11161	0.01549	7.206	<0.001***
	Acropora Moresby - ARMS Moresby	0.1149	0.01583	7.259	<0.001***
	ARMS Coin - Acropora Moresby	-0.11016	0.01939	-5.68	<0.001***
	Acropora Coin - ARMS Moresby	0.11635	0.01944	5.985	<0.001***

In NMDS plots of sessile community composition across either top or bottom plate faces, communities of individual images are seen to cluster strongly by sample type (ARMS, Acropora) (Figure 4.3). The community composition of ARMS 1T plates, the upmost and only exposed plate on ARMS units (visible on the top of the ARMS device pictured in Figure 4.1), was found to be more like communities on top of *Acropora* tables than other ARMS plates. When 1T plates were removed from the ARMS dataset, this resulted in non-overlapping 95% ellipses for sample types (Figure 4.3). There was no discernible clustering around individual sites across the bottom side of ARMS plates or dead Acropora tables. However, for topside communities, clustering was observed between sites for communities found on Acropora tables, but not for those found on ARMS plates, suggesting that whilst communities across the topside of natural substrates are different across the two sites, communities on the topside of ARMS plates are not.

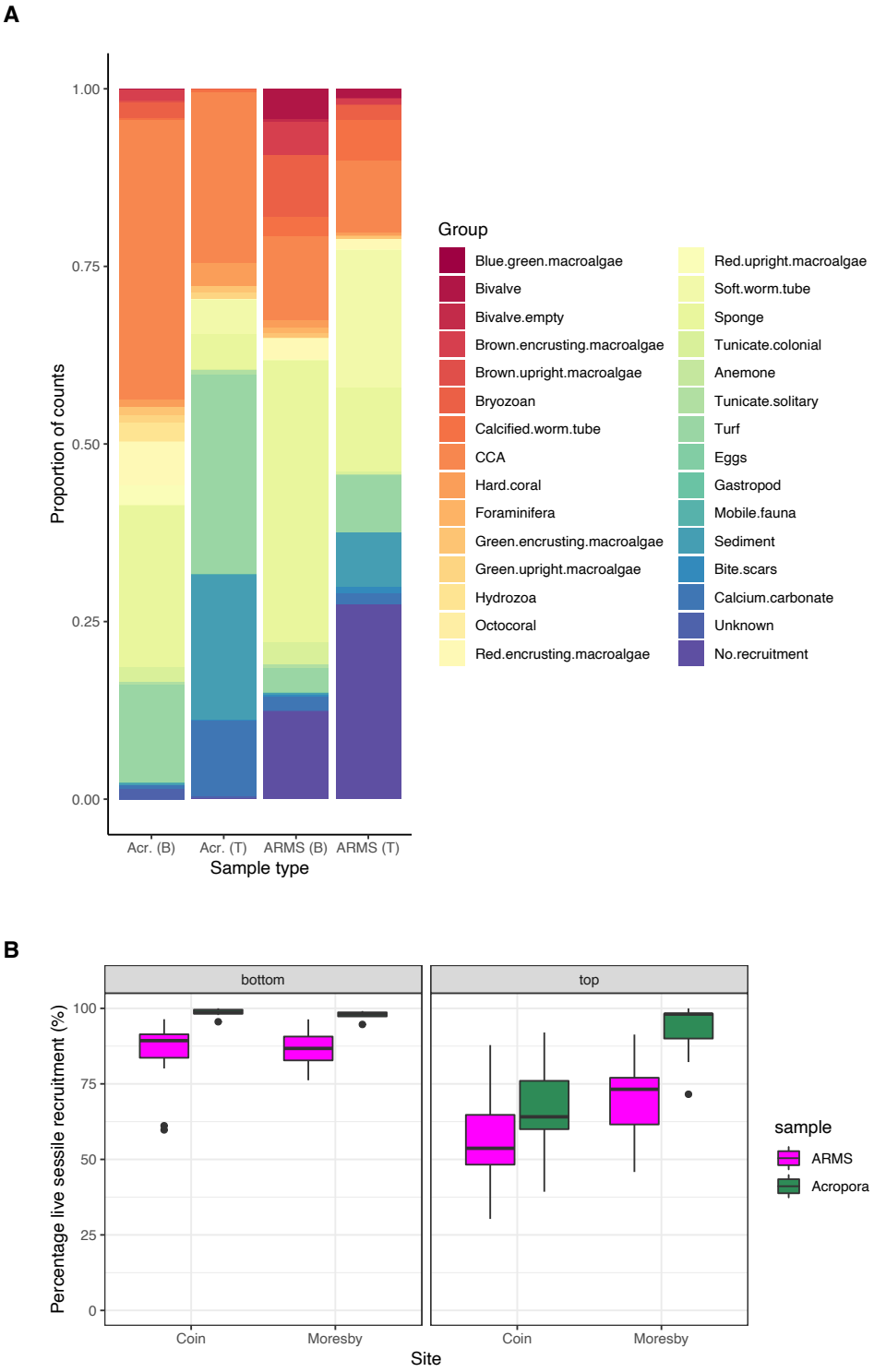

Figure 4.2. Patterns of the percentage cover of sessile taxa across substrate type (ARMS, dead Acropora (Acr.)), sites (Moresby, Coin) and substrate orientation (top (T), bottom (B)) with **A**) a stacked barplots displaying proportion of counts assigned to sessile and non-sessile groups, and **B**) boxplots of live percentage cover (%) of sessile fauna on available space.

Sample type, site, and face, as well as their interactions, were found to have a significant effect on sessile community composition observed across samples (Table 4.2). These predictor variables were then found to significantly impact the abundances of 15 individual sessile groups, using resampling-based univariate tests (Table 4.3). Overall, site choice best explains the variation observed across the image analysis dataset (R^2 = 0.218), followed by sample type (R^2 = 0.191) and face (R^2 = 0.09).

Table 4.2. Output from an analysis of deviance testing for multivariate effects of sample type (ARMS, Acropora), site and face (top, bottom) on the overall composition of sessile communities from image analysis. P-values (P) are calculated using 999 iterations, via PIT-trap resampling. Maximum-likelihood 'Score' statistic (T) and deviance (Dev) values are also presented for all predictors and their interactions.

	Residual degrees of freedom	Dev	P	T
(Intercept)	137			
sample	136	465.8	0.001 ***	135.71
site	135	102.5	0.001 ***	54.67
face	134	503.7	0.001 ***	121.45
sample: site	133	44.9	0.019*	29.87
sample: face	132	122.6	0.001 ***	63.08
site: face	131	104.2	0.001 ***	71.44
sample: site: face	130	76	0.001 ***	77.12

Sponges and ascidians were significantly more abundant on the undersides of either ARMS or dead coral substrates (p<0.001*** for both), whilst hard coral abundance was significantly lower on ARMS than on dead coral (Table 4.3). The abundances of calcified tube worms, algal turf, hydrozoans, empty bivalves, and foraminifera individually were all found to be significantly affected by face and sample type independently (all p<0.01**). On the other hand, the abundance of red upright (p = 0.013*) and encrusting macroalgae (p<0.001***) were significantly higher on the undersides of dead Acropora. A significant effect of the interaction between sample type and site on soft tubed worm abundance was found (p=0.012*), whilst a significant interaction between site and plate face significantly affected bivalve abundance (p<0.01**). Finally, the abundances of CCA (p<0.01**) and bryozoans (p= 0.034*) were determined to be significantly affected by an interaction between all three predictor variables, with the highest abundances of bryozoans observed on the undersides of ARMS plates in the exposed reef (Moresby), and the highest abundance of CCA observed on the top of dead Acropora also at this site (Table 4.3).

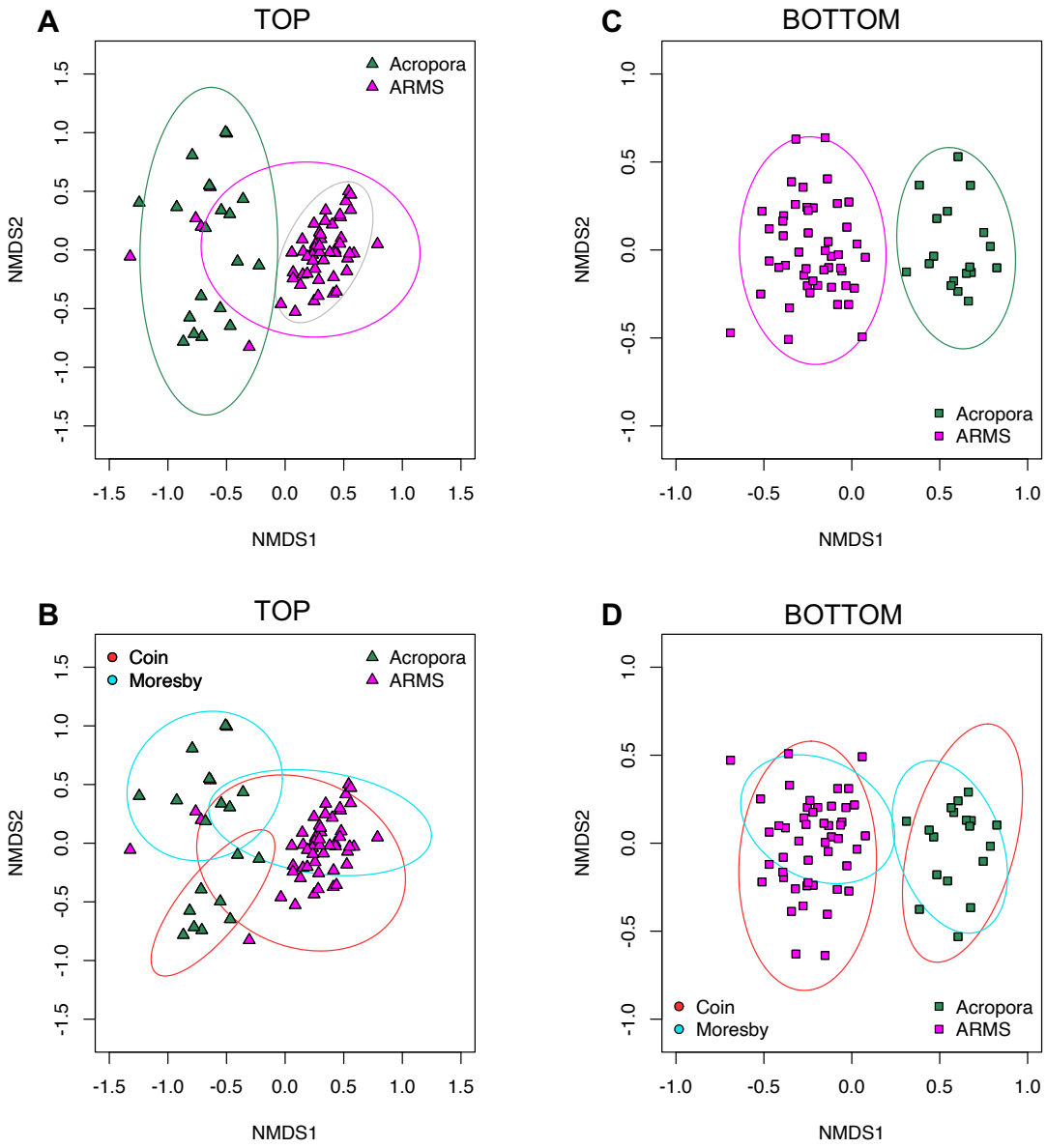

Figure 4.3. NMDS plots of sessile communities across the (A)(B) topsides or (C)(D) undersides of ARMS and dead *Acropora sp*. coral substrates. All ellipses represent 95% confidence intervals around group centroids, and are projected for each substrate type (A, B) and for each sample site across individual substrate type (C, D). The grey ellipse in (A) is projected around the centroid of topside ARMS plate communities if sessile communities from plate 1T, the exposed and upmost plate on each ARMS unit, were to be removed from the ordination. K =3 for both ordinations, and Bray Curtis distances are used throughout.

Table 4.3. Output from an analysis of deviance comparing the univariate effects of sample type (ARMS, Acropora), site and face (top, bottom) on the abundance of individual sessile groups from image analysis. Score test statistics (T) and P-values (P) are presented for each group, the latter having been calculated using PIT-trap resampling (999 iterations) and adjusted for multiple testing. Only groups found to have a significant relationship with predictor variables are shown, and the most significant p-value for each group is highlighted in green. The direction of single-term effects (sample, site or face individually) is displayed using arrows, where 'A' = ARMS, 'Acr.' = Acropora, 'B' = bottom plate face, 'T' = top plate face, 'M' = site Moresby, 'C' = site Ile du Coin. For example, '↑ A+M+B' indicates that abundance was significantly higher on the bottom face (B) of ARMS (A) found in site Moresby (M).

species	Sponge		Bryozoan		Calcified worm tube		Soft worm tube		Colonial ascidians	
	P	T	P	T	P	T	P	T	P	T
sample	0.164	3.18	**0.017***	8.72	**0.001*** (↑A)**	26.86	0.146	3.33	0.741	0.37
site	0.939	1.45	**0.001*****	21.00	0.999	0.35	0.415	3.56	0.233	5.27
face	**0.001*** (↑B)**	35.22	**0.001*****	36.12	**0.001*** (↑B)**	16.19	**0.001*****	20.77	**0.001*** (↑B)**	28.21
sample: site	0.987	0.12	0.978	0.29	0.987	0.11	**0.012* (↑C+B)**	11.62	0.963	1.00
sample: face	0.977	0.56	0.221	5.71	0.977	0.79	0.257	5.12	0.977	0.02
site: face	0.107	7.74	0.978	0.68	0.272	5.84	0.482	4.49	0.506	4.10
sample: site: face	0.828	1.06	**0.034* (↑A+M+B)**	9.75	0.984	0.13	0.997	0	0.545	2.41
	Brown encrusting macroalgae		Red encrusting macroalgae		Red upright macroalgae		Turf		CCA	
	P	T	P	T	P	T	P	T	P	T
sample	0.188	2.92	0.138	4.01	**0.001*****	24.45	**0.001*** (↑Acr.)**	49.99	**0.001*****	44.75
site	**0.002** (↑C)**	14.89	0.955	1.35	1.000	0.09	0.318	4.61	0.059	7.86
face	**0.001*** (↑B)**	12.70	**0.001*****	20.07	0.336	3.09	**0.001*** (↑T)**	16.67	0.132	4.81
sample: site	0.963	1.19	0.649	3.30	0.891	1.92	0.649	3.42	0.891	2.03
sample: face	0.977	0.65	**0.001*** (↑Acr.+ B)**	22.50	**0.013* (↑Acr.+B)**	13.13	0.977	0.47	0.215	6.09
site: face	0.272	5.94	0.955	1.56	0.955	1.24	0.955	1.55	**0.001*****	21.39
sample: site: face	0.053	8.18	0.997	0	0.828	0.97	0.984	0.12	**0.002** (↑Acr.+M+T)**	30.10
	Hard coral		Hydrozoa		Bivalve		Bivalve (empty)		Foraminifera	
	P	T	P	T	P	T	P	T	P	T
sample	**0.008** (↑Acr.)**	14.40	**0.006** (↑Acr.)**	16.66	**0.008****	12.51	**0.036* (↑A)**	7.01	**0.008** (↑A)**	13.18
site	1.000	0.17	1.000	0.07	0.999	0.43	1.000	0	0.955	1.35
face	0.561	1.84	**0.022* (↑B)**	7.27	**0.001*****	13.93	**0.022* (↑B)**	7.24	**0.001*** (↑B)**	27.43
sample: site	0.978	0.38	0.987	0	0.569	3.80	0.987	0	0.987	0
sample: face	0.151	6.92	0.977	0	0.977	0.66	0.986	0	0.977	0
site: face	0.978	0.63	0.978	0.13	**0.002** (↑M+B)**	12.29	0.193	6.69	0.978	0.09
sample: site: face	0.984	0.04	0.994	0	0.984	0	0.997	0	0.997	0

4.4.2. Overlap and community composition of metabarcoding sequence variants between ARMS and eDNA samples

A DADA2 error-filtering and chimera-removal pipeline resulted in 7,302,279 COI reads and 4,415,184 18S reads across all 2021 ARMS and eDNA samples, with an average sampling depth of 304,261 COI reads and 183,966 18S reads per sample (Appendix Table A.2 & A.3). After the removal of potential contaminant sequences across eDNA samples, a total of 9476 18S curated ESVs (cESVs) were identified (following LULU-curation), and 14,644 COI curated OTUs (cOTUs)(after a VSEARCH clustering step, followed by LULU-curation) across both ARMS and eDNA samples. Separately, a total of 6923 18S cESVs were identified across ARMS and 4029 across eDNA samples, whilst 11,488 COI cOTUs were identified across ARMS samples and 5687 across eDNA samples. Breakaway estimated richness was 5691 (standard error = 2.12, high confidence interval threshold (HCI) = 5709, low confidence interval threshold (LCI) = 5688) across eDNA samples and 11,580 (standard error = 24.8, HCI = 13,000, LCI= 11,494) in ARMS samples in the COI dataset. Breakaway estimated richness was 4088 (standard error = 16.26, HCI = 4788, LCI = 4034) in eDNA samples and 6931 (standard error = 2.94, HCI = 6965, LCI = 6924) in ARMS samples in the 18S dataset.

Highly similar patterns of genetic overlap between ARMS and eDNA samples are observed across both rarefied 18S and COI datasets (Figure 4.4). More COI cOTUs and 18S cESVs were found uniquely in ARMS samples than in eDNA samples. Overall, a total of 1989 COI cOTUs (15.4% of all COI cOTUs) and 1334 18S cESVs (15% of all 18S cESVs) were detected in both ARMS and eDNA samples. Most sequence reads in COI and 18S datasets belonged to sequence variants detected in both sample types (70.3% of all COI reads, 65.1% of all 18S reads), whilst only 3.8-4.1% of sequence reads belonged to sequence variants uniquely found in eDNA samples (Figure 4.4).

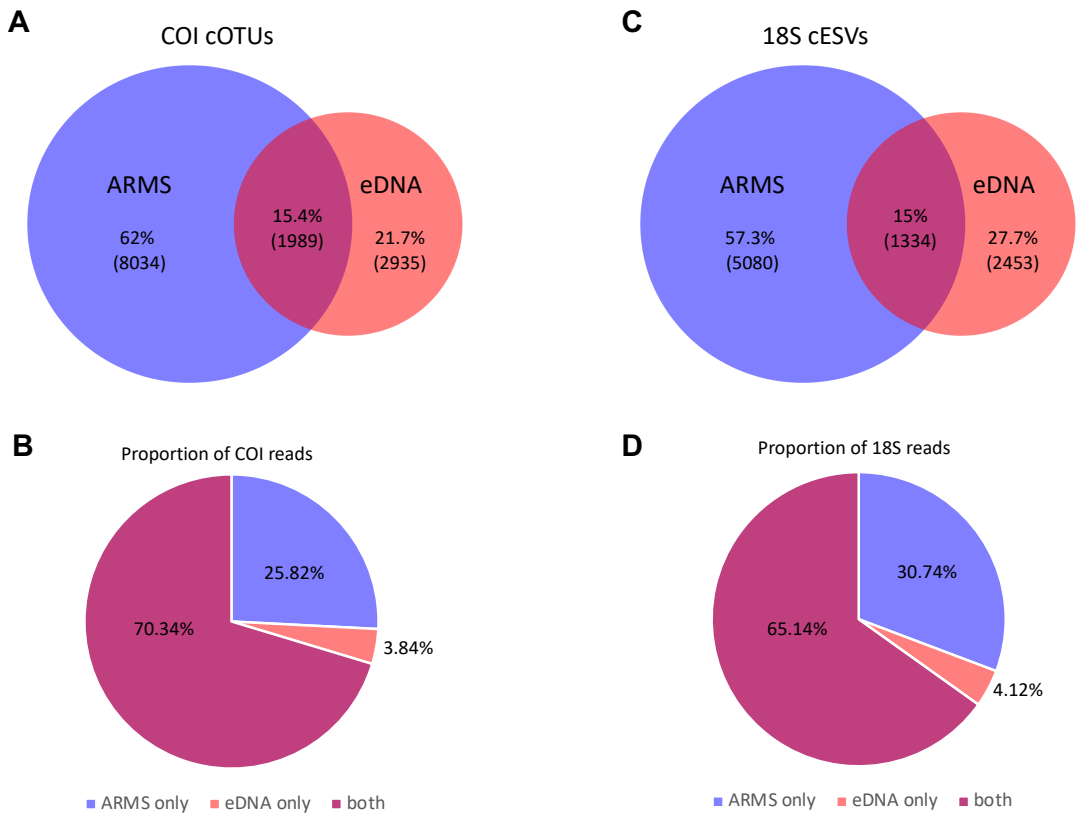

Figure 4.4. Area-proportional Venn diagrams and pie charts displaying the extent of overlap between rarefied ARMS and eDNA samples of (A) COI cOTUs and (B) the proportion of rarefied reads assigned to those cOTUs found either uniquely in ARMS, uniquely in eDNA, or across both sample types, and of (C) 18S cESVs and (D) the proportion of those cESVs found uniquely in ARMS, uniquely in eDNA, or both sample types.

Strong clustering is observed within ARMS and eDNA samples separately, with no observed overlap between 95% confidence ellipses of each sample type, suggesting a difference in composition patterns across sample types (Figure 4.5). Clustering was also observed across samples from both sampling sites, with little to no overlap between ellipses. On average, eDNA samples were more similar within sites (mean Jaccard distance = 0.68) than between sites (mean Jaccard distance 0.79). Environmental DNA samples were slightly more like ARMS communities from the same sampling site (mean total Jaccard distance between eDNA, sessile and motile ARMS fractions = 0.93) than from the other site (mean total Jaccard distance = 0.96).

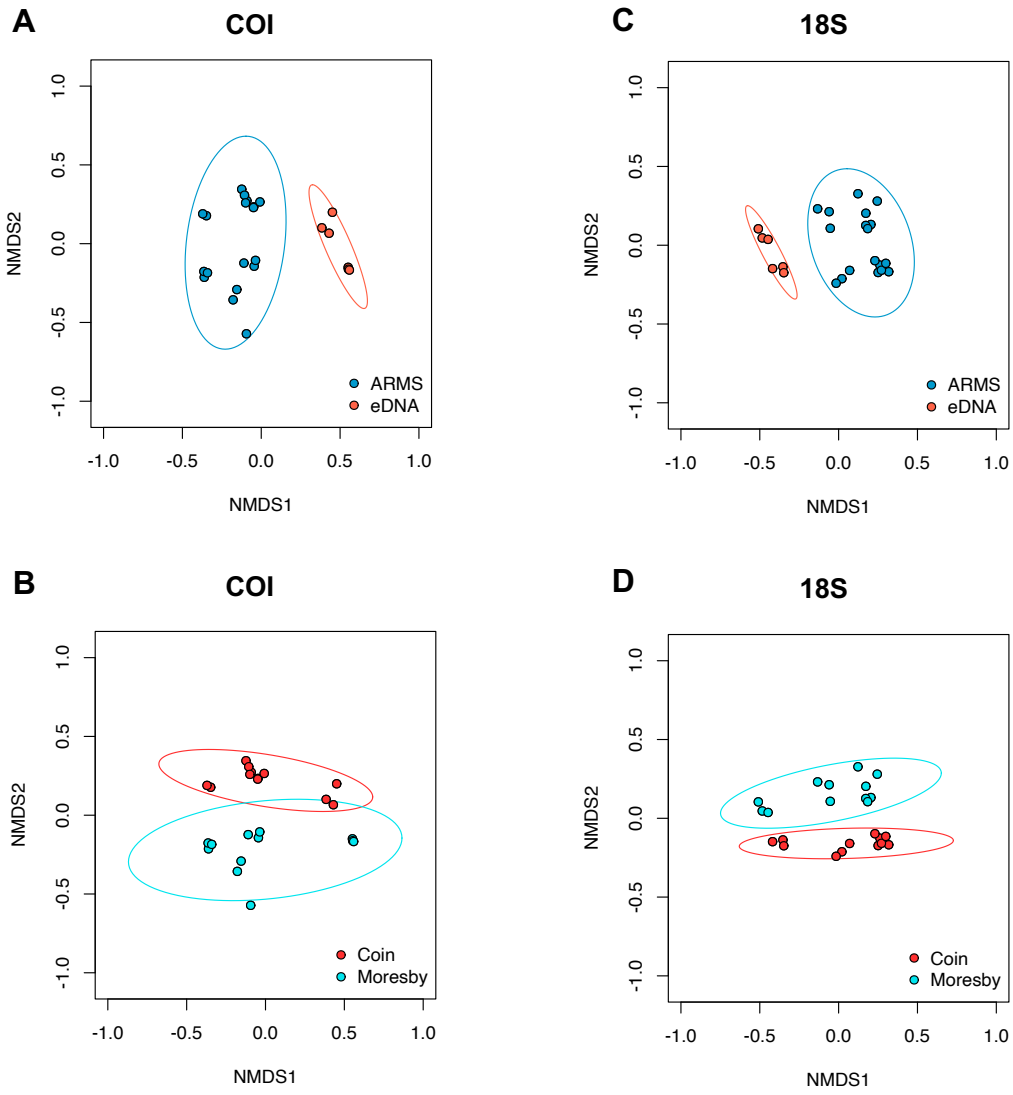

Figure 4.5. Non-metric multi-dimensional (NMDS) scaling plots of community composition based on the presence-absence of COI cOTUs and 18S cESVs across rarefied samples with 95% confidence interval ellipses drawn for centroids around (A) sample type (ARMS, eDNA) across for COI cOTUs, (B) sampling site for COI cOTUs, (C) sample type across 18S cESVs, and (D) sampling site for 18S cESVs. K = 2 for all ordinations, and Jaccard distances were used.

4.4.3. Taxonomic assignment success and patterns of taxa presence-absence and abundance across sample type and sites

A total of 8,810 (92.97% of all cESVs) 18S cESVs and 13,841 (94.52%) COI cOTUs were identified to kingdom level (Table 4.4). The success rate of taxonomic assignment of cESVs across all 18S samples then gradually drop across taxa ranks. For COI samples, the rate of assignment significantly drops at phyla level, with a total of 2031 cOTUs (13.87%) identified across all samples for this taxonomic rank.

Table 4.4. Percentages of COI and 18S sequence variants assigned per taxa rank across all samples, or ARMS and eDNA samples individually. No genus or species-level assignments were obtained for 18S sequences as this region is not recommended for assigning taxonomy below family level.

Amplicon	**Sample**	**Percentage of sequence variants assigned per taxa rank (%)**						
		Kingdom	Phylum	Class	Order	Family	Genus	Species
COI	all samples	94.52	13.87	10.45	4.35	3.56	3.00	2.27
	ARMS only	94.79	14.83	10.84	6.40	5.04	4.13	3.02
	eDNA only	95.04	17.00	15.17	10.08	8.37	7.02	5.35
18S	all samples	92.97	65.42	59.77	40.72	13.14	na	na
	ARMS only	95.54	70.81	64.29	45.59	11.08	na	na
	eDNA only	90.32	61.26	57.83	35.62	17.35	na	na

A total of 50 recognised phyla were identified using 18S metabarcoding, and 29 phyla using COI metabarcoding. A total of 503 species (COI) and 84 orders (18S) were identified across both eDNA and ARMS datasets. For COI, 169 species were identified in both eDNA and ARMS samples. Conversely, 223 species were found uniquely in ARMS samples, whilst 153 species were found uniquely in eDNA.

We know from image analysis that the percentage cover of some sessile invertebrates such as sponges are found in equal abundances across ARMS plates and dead tabular *Acropora sp.* coral (Table 4.3). In the metabarcoding dataset, a total of 31 sponge COI cOTUs are only detected in eDNA samples, 9

of which are identified to species level (Figure 4.6). Species such as *Halichondria bowerbanki*, *Cliona yorkin* and *Paracornulum dubium* are detected in more than one eDNA sample but are absent from ARMS metabarcoding samples. Conversely, eDNA was not able to pick up the presence of 60 sponge COI cOTUs, including 14 species, of which several were found across multiple ARMS devices (Figure 4.6). However, eDNA sampling was able to recover the presence of 17 of the 20 most abundant sponge cOTUs found across ARMS.

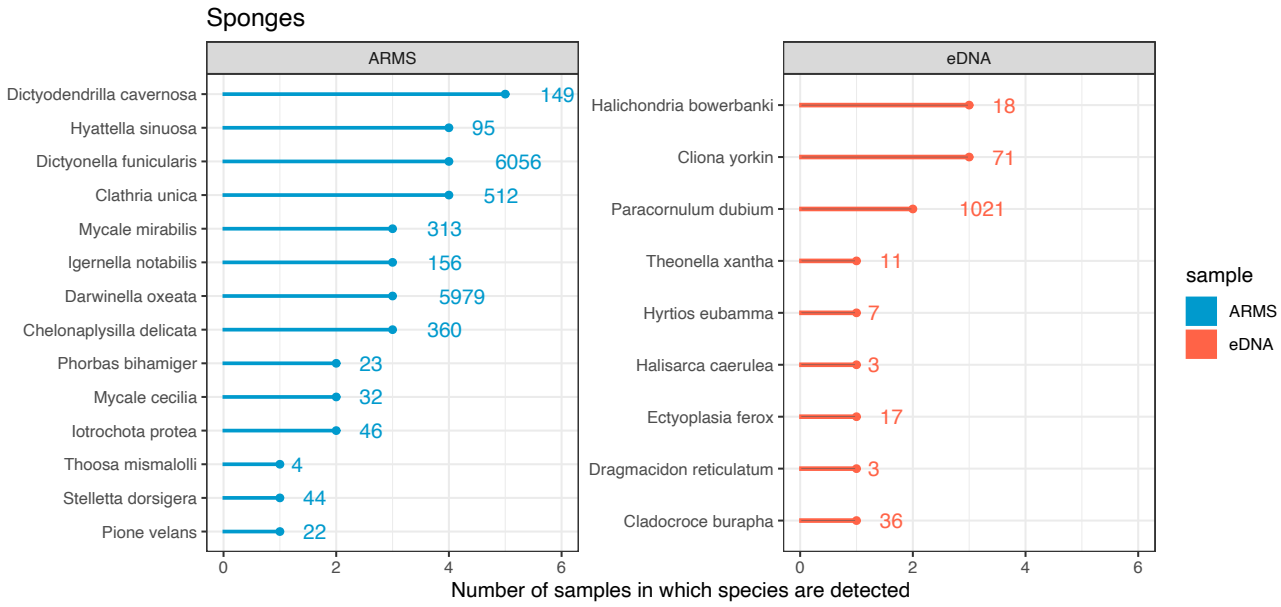

Figure 4.6. Plot displaying the number of species found uniquely in either ARMS (left-hand plot) or eDNA (right-hand plot) samples, along with the number of samples in which these are found, and their total read abundances.

Varying patterns of genetic overlap between eDNA and ARMS are observed across metazoan phyla groups (Appendix Figure C.1, C.2). A large portion of COI cOTUs and 18S cESVs identified as arthropods, molluscs, annelids, platyhelminthes, nematozoans and nemerteans were found uniquely in ARMS samples. In comparison, a large portion of cOTUs and cESVs identified as sponges, tunicates and cnidarians were found in both eDNA and ARMS samples. Chordates, identified using the COI amplicon, are the only group where more cOTUs are observed uniquely in eDNA samples than in either ARMS or both samples. The same patterns were observed across both rarefied and unrarefied samples.

4.4.4. Differential abundance analysis for sequence variants found across both ARMS and eDNA samples

For sequence variants found in both ARMS and eDNA samples, the DESeq2 analysis revealed those with significantly different read abundances between both sample types across reef sites (Figure 4.7; Figure 4.8; Supplementary Tables C.1 & C.2). A total of 181 COI cOTUs and 839 18S cESVs were detected in both ARMS and eDNA samples and found to have significantly different abundances between sample types.

A total of 54 18S and 19 COI sponge sequence variants were found to be significantly more abundant on ARMS units across both sampling sites. On the other hand, five COI cOTUs, from genera including Spirastrella and Halisarca, and ten 18S cESV belonging to orders Suberitida and Hadromerida, were found to be significantly more abundant in eDNA samples than ARMS. For cnidarians, several sequence variants identified as corallimorphs (Corynactis), scleractinian corals, thecate and athecate hydroids (Leptothecata, Anthothecata) and other hydrozoans (Pandeopsis, Clytia) were significantly more abundant on ARMS than in eDNA samples. On the other hand, sequence variants from soft coral order Ovabunda, hard coral genus Galaxea and anemone order Actinaria were found to be more abundant in eDNA samples than on ARMS.

Many arthropod sequence variants were found to be significantly more abundant in ARMS samples across both amplicon datasets and across sampling sites, belonging to groups such as decapods (e.g., Periclimenella, Caridea, Cuapetes, Xanthidae, Porcellanidae), benthic copepods (Harpacticoidea) and ostracods (Podocopida). Only a few arthropod sequence variants were found to be more abundant in eDNA samples, and were all identified as pelagic copepods (e.g., Bestiolina, Calocalanus, Copilia). Almost all bryozoan, annelid and mollusc sequence variants found to have significantly different abundances between sample types were more abundant on ARMS, except for the Octopus genus and a Veneroida bivalve, which were more abundant in eDNA samples.

A total of 60 dinoflagellate sequence variants (6 COI cOTUs, 54 18S cESVs) had significantly higher abundances in eDNA samples than on ARMS across both reef sites. On the other hand, 5 sequences variants belonging to the genus Symbiodinium were found to be significantly more abundant in ARMS

than eDNA samples. For plants, many bacillariophytes, haptophytes and chlorophytes were more abundant in eDNA samples across both sites, whilst more ochrophyte and rhodophyte genera were found to have a higher abundance on ARMS. Sequence variants identified to the genus Ramicrusta, a crustose calcareous algae known to overgrow scleratinian corals, was found to be significantly more abundant on ARMS samples.

Finally, a total of 264 cOTUs (COI) and 1058 cESVs (18S) detected in both ARMS and eDNA samples were found in similar abundances (adjusted p-value>0.05) between sample types. These included 80 COI cOTUs and 140 18S cESVs were identified as sponges, belonging to 17 orders (18S) and 29 genera (COI), including Oscarella, Clathria, Tedania, Petrosia, Crella and Hexadella. A total of 35 rhodophyte cOTUs were also found in equal amounts between ARMS and eDNA samples, from a range of genera including Peyssonnelia, Palisada, Laurencia, Polysyphonia and Chondria. Fewer cOTUs and cESVs from other important cryptofauna sessile groups such as cnidarians, tunicates and bryozoans were detected equally by both methods. Few cOTUs and/or cESVs from motile cryptofauna groups such as echinoderms 10 COI cOTUs), gastropods (10 COI cOTUs, 25 18S cESVs) and decapods (10 COI cOTUs) were also picked up in equal measure by both methods

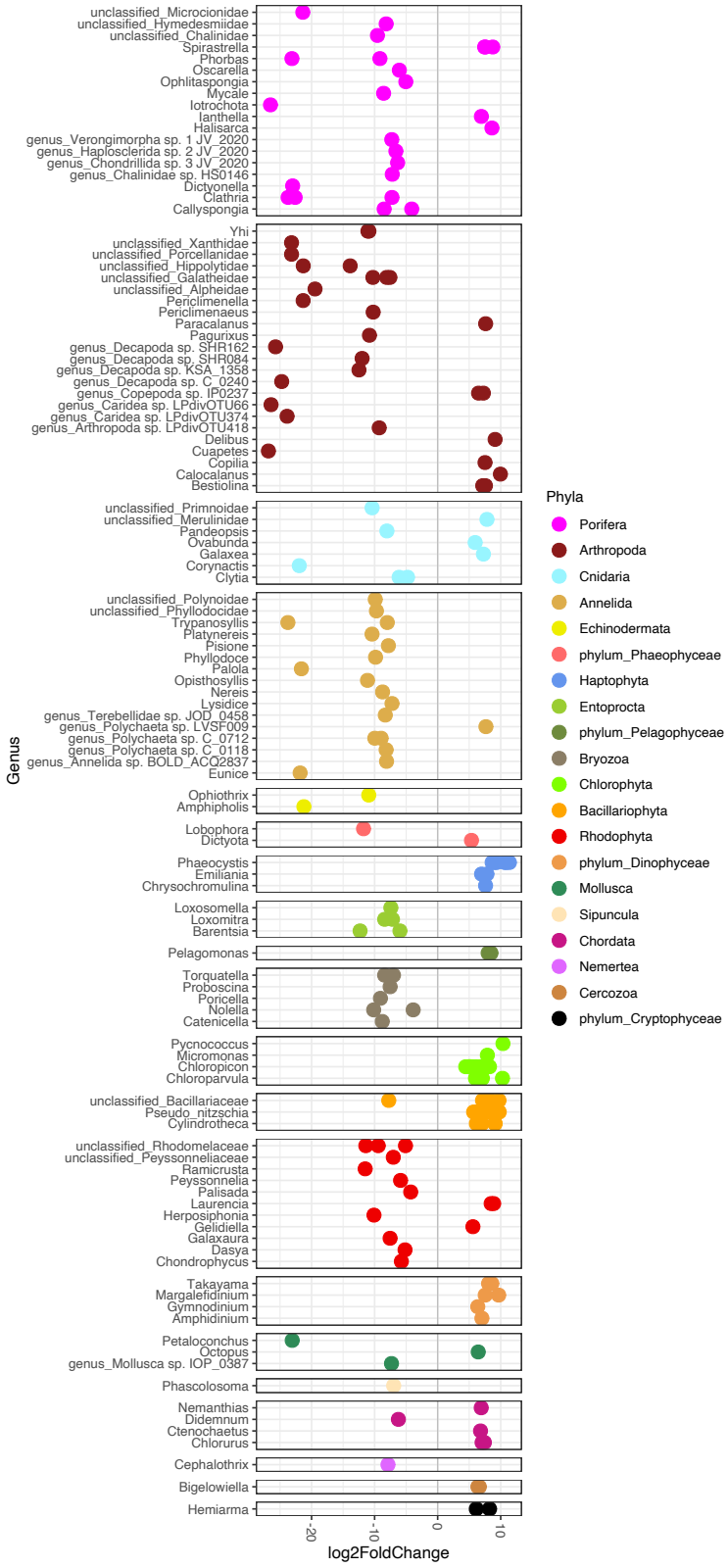

Figure 4.7. Genera identified in the COI cOTU dataset with significantly ($p<0.05$) differential abundances between sample type. Each data point represents a unique cOTU, coloured by phyla. A positive log2FoldChange value indicates when a cOTU has a significantly higher abundance in eDNA samples, and a negative value a significantly higher abundance in ARMS samples.

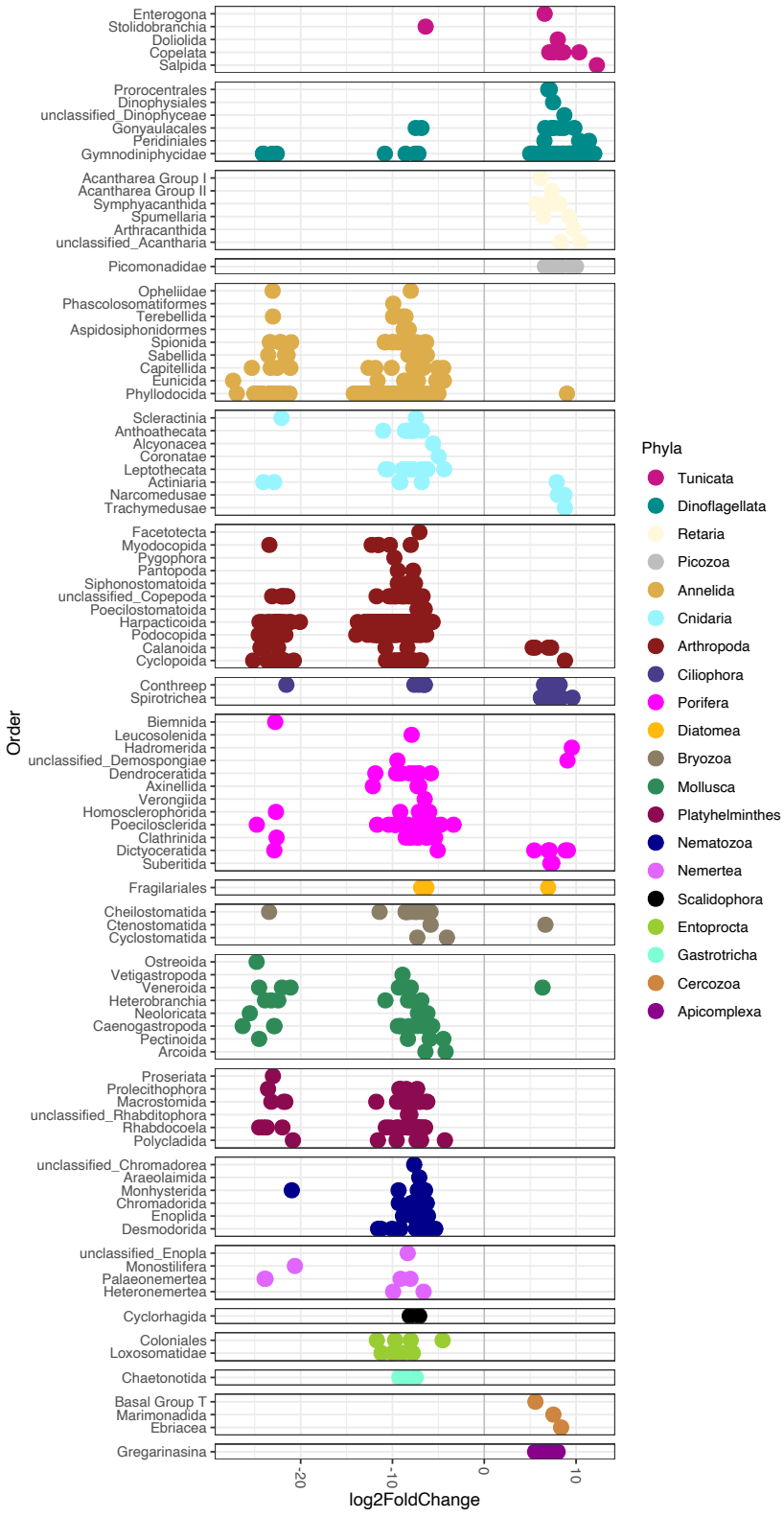

Figure 4.8. Orders identified in the 18S cESV dataset with significantly ($p<0.05$) differential abundances between sample type. Each data point represents a unique cESV, coloured by phyla. A positive log2FoldChange value indicates when a cESV has a significantly higher abundance in eDNA samples, and a negative value a significantly higher abundance in ARMS samples.

4.5. Discussion

Cryptobenthic communities inhabiting tropical coral reefs are understudied and under-represented in genetic reference databases, as the structural complexity of coral reefs renders them difficult to study or monitor in non-destructive ways. Here, we use image analysis to directly compare and ground truth patterns of cryptobenthic sessile recruitment and diversity on ARMS with those on *in situ* dead tabular coral (*Acropora* sp.). We present novel data on the composition of cryptobenthic groups within the Chagos Archipelago on both natural and artificial reef substrate and show that the ARMS method results in the collection and detection of highly biodiverse cryptobenthic assemblages, and that for some (but not all) taxa groups, can be representative of recruitment patterns observed on local natural reef surfaces. We also investigate the usability of water-borne environmental DNA (eDNA) for capturing cryptobenthic communities, in comparison to ARMS. We find eDNA to be a useful complimentary tool for the study of cryptobenthic assemblages, which detects the presence of abundant taxa found on ARMS, and increases the detection of sessile cryptobenthic organisms which not found on ARMS but are present within the reef ecosystem.

4.5.1. Cryptobenthic percentage cover and composition across ARMS and natural reef using image analysis

Using image analysis, we uncover a diverse and complex assemblage of sessile organisms on artificial and natural reef surfaces across two shallow tropical reefs. Our results suggest that both percentage cover and composition of sessile communities found on Autonomous Reef Monitoring Structures (ARMS) can significantly differ from dead coral, but are also influenced by recruitment surface orientation and sampling site choice. Overall, we find that less space is unoccupied by live organisms on natural surfaces (~17%) compared to ARMS, where even after 3 years, over a quarter of available recruitment surface remains bare (~27%). Whilst we know the maximum age of communities on ARMS devices in this study (3 years), we do not know the exact age since death for tabular coral colonies inspected. *Acropora sp.* coral colonies in the Chagos Archipelago MPA were severely impact by bleaching events in 1998 (Sheppard et al., 2002) and again in 2015-16 where populations declined by 86% (Head et al., 2019). Whilst we cannot be certain, it is a possibility that tabular *Acropora* sp. coral investigated in this study died following the 2015/16 mass bleaching event. If this is indeed the case, a

possible explanation for the higher percentage cover of sessile cryptobenthic communities observed on dead *Acropora* sp. tables could be that they are a few years older than those observed on ARMS, which were first deployed in 2018. Nevertheless, our image analysis provides insights into naturally occurring understorey cryptobenthic assemblages across two remote and highlights the key role of *Acropora sp.* tabular coral plays in supporting cryptobenthic sessile organisms beyond the death of the colony.

Many studies have demonstrated how different artificial materials, with varying rugosity, durability, or colour, can impact the larval recruitment patterns of benthic groups such as corals (Leonard et al., 2021; Burt et al., 2009), bryozoans (Siddik et al., 2021) and algae (Kennedy et al., 2017), as well as whole invertebrate communities (Siddik et al., 2019; Vaz-Pinto et al., 2014). In this study, almost all sessile phyla found on natural surfaces were also identified on ARMS, except for hydroids. Hydroids are benthic heterotrophic animals which filter- and suspension-feed on plankton in the water column, and in this study are only observed on the underside of dead *Acropora* sp. tables. The lack of hydroids observed on ARMS may be due to the restricted space between ARMS plates (~2.5cm gap), which could be a limiting factor for their feeding and/or growth.

As in Higgins et al (2019), we find that by providing a new surface on a coral reef, we obtain a different composition of some of the sessile groups also present on natural surfaces. For example, we find that hard coral abundance is significantly impacted by substrate type, and that hard coral cover was higher on natural reef surfaces than on ARMS. In another study, we found that juvenile coral recruits were in fact abundant on the same ARMS units investigated here (Chapter 5, Steyaert et al., 2022a), but that most adult coral colonies grew off the side of the device. PVC is a suitable surface for the recruitment and growth of hard coral colonies (Leonard et al., 2021), and we suggest that the difference in adult coral abundance observed between surface type in this study is at least partly dependent on the limited space available between plates, as well as the age of dead *Acropora* sp. coral colonies in comparison to that of the ARMS.

For groups such as sponges, colonial ascidians, soft tube worms and brown encrusting macroalgae, percentage cover was similar between ARMS and dead *Acropora sp*. coral tables but significantly differed between topsides and undersides of artificial and natural surfaces. Recruitment face orientation

is known to be a strong predictor of reef cryptobenthic community composition (Higgins et al., 2019, David et al., 2019), and our study recovers similar findings of significantly increased live percentage cover on undersides of both artificial and natural surfaces (Figure 4.2). Here, the difference in community composition between ARMS and dead coral becomes evident when looking at topside and bottom communities individually. As in Higgins et al. (2019), David et al. (2019) and Steyaert et al. (2022b) (Chapter 3), we also find that filter feeding organisms such as sponges, and colonial ascidians, are more common on the underside of ARMS surfaces. Here we show these patterns also occur on dead *Acropora* sp. coral, and that substrate orientation is the only significant predictor of percentage cover for both groups. Interestingly, the composition of sessile communities on the top of ARMS (plate 1T), which is exposed to the reef environment, is more like communities observed on dead coral than other, non-exposed, ARMS plates. The communities on the top of ARMS (plate 1T) have been shown to be significantly different to other ARMS plates (David et al., 2019), and our results highlight the need to carefully consider whether plate 1T should be included in image-based analyses of percentage cover and composition of cryptobenthic organisms on ARMS.

We show that differences between ARMS and natural reef surfaces, when interacting with site choice and face orientation, has a significant impact on the recruitment cover of bryozoans and CCA, where the former were found to be more abundant on ARMS devices, and the latter more abundant on dead *Acropora* sp. coral. Both groups are calcifying organisms and differences between environmental conditions across this study's sites may have impacted their percentage cover, as has been suggested in Steyaert et al. (2022b) (Chapter 3). Here, our findings highlight how only using ARMS-based image analysis to study reef cryptobenthos may under-record actual *in-situ* CCA abundance. This is especially important as CCA is a key group in tropical coral reef ecosystems, with functional roles including reef-binding (Weiss & Martindale, 2017), reef accretion (Lange et al., 2022; Chisholm, 2000), coral larval recruitment (Tebben et al., 2005) as well as providing a food-source to key reef fish groups such as parrotfish (Littler & Littler, 2013). On the other hand, our findings suggest that analysing ARMS images may over-estimate the percentage cover of bryozoans across reefs. There may be several reasons as to why different patterns of abundance of these two groups are observed between ARMS and dead *Acropora* sp. coral, including differences in community age, light availability across substrate type and accumulation of sediments.

4.5.2. Genetic overlap and community similarity between ARMS and surrounding water column

We show that when combined, multi-marker metabarcoding of both ARMS communities and *in-situ* eDNA samples recovers the presence of over 14,500 individual eukaryotic taxonomic units, including 503 species, across just 2.7m^2 of artificial reef surface and 36 litres of water. We observe greater COI and 18S sequence variant estimated richness in ARMS bulk community samples than in eDNA samples and find that eDNA and ARMS approaches recover different patterns of community composition. These results are consistent with findings from similar studies in other locations (Nichols et al., 2022; Antich et al., 2021), and are to be expected due to inherent differences in sampling methods between eDNA and ARMS approaches.

One of the aims of this study was to assess how complimentary the collection of eDNA can be to the ARMS method, and ground truth eDNA sampling for benthic monitoring. Whilst only 15-17% of all sequence variants are found in both eDNA and ARMS samples, these make up ~62% (COI) and ~ 65% (18S) of total sequence reads. This suggests that both methods can detect the presence of abundant taxa, and that either i) a large majority of genetic material in the water column near ARMS originates from organisms inhabiting the artificial structures, and/or ii) that a significant portion of DNA signal detected in ARMS samples originates from sources on the natural reef matrix, and that DNA signal from these communities is present in the water column.

We find that not only does eDNA sampling pick up a significant portion of sessile cryptobenthic richness also present on ARMS, but it also detects the presence of sessile reef cryptobenthic taxa not found within ARMS samples. We focus on sponges in our analysis and show that eDNA sampling recovers the presence of almost all the most abundant sponge sequence variants found on ARMS, as well as several species not identified within ARMS communities. Sponges are ubiquitous on coral reefs and can filter large quantities of water per day (Kahn et al., 2015; Turon et al., 1997). Recent research shows that sponges regularly expel mucus as a way of removing sediment and particulate waste (Kornder et al., 2021), which could result in quantities of sponge DNA in the water column detectable using eDNA sampling. Overall, we identify 24% of all COI reads with phyla-level assignment, and 14%

of all 18S reads with phyla-level assignment as sponges. This confirms the dominance of sponges on reefs as found in the image analysis (Figure 4.2) and suggests that eDNA sampling, alongside ARMS collection, is an advantageous tool in exploring sponge diversity across diverse reef cryptobenthic communities.

On the other hand, we find more unique sequence variants in ARMS samples than in eDNA samples are identified as mobile cryptobenthic invertebrates (incl. arthropods, molluscs, annelids, echinoderms, and nematodes). Sampling eDNA from the water column is less sensitive for the detection of mobile benthic invertebrates than for vertebrates such as fish (West et al., 2020; Forsström & Vasemägi, 2016), and can be highly dependent on whether organisms have meroplanktonic life stages (Crane et al., 2021; Leduc et al., 2019). However, recent studies have shown the promise of eDNA sampling for the detection of invasive or rare species (Danziger & Frederich, 2022; Komai et al., 2019; Cowart et al., 2018). In our study, a total of 288 mobile cryptofauna cOTUs, including 133 species of echinoderms, gastropods, decapods, and polychaete worms, are uniquely found in ARMS samples and not detected through eDNA sampling. Previous studies have shown that a high diversity of coral-associated decapods (species richness 164) and molluscs (species richness 72) can be found in the Chagos Archipelago (Head et al., 2018; Head et al., 2015). Here we find that combining both ARMS and eDNA approaches recovers the presence of 180 mollusc and 102 decapod cOTUs, and that whilst eDNA sampling alone should not replace ARMS for the study of motile cryptofauna, it certainly could provide a valuable addition when the aim of an ARMS-based study is to assess baseline cryptofauna richness and diversity from the local natural reef system.

Our findings also suggest half of the richness observed across both ARMS and eDNA datasets may come from less abundant taxa, or from trace/extra-cellular DNA. Indeed, we find that 46-49% of sequence variants found in eDNA samples, and 49-50% of ARMS sequence variants, have read abundances equal or less than 10. A high number of rare species is often a characteristic of highly biodiverse ecosystem such as coral reefs (Head et al., 2018; Mouillot et al., 2013), and can be important for maintaining functional diversity and redundancy (Guillemot et al., 2011; Lyons et al., 2005). The ability of metabarcoding to detect the presence of rare species is well documented, and in structurally complex marine systems such as coral reefs, can be preferable to traditional visual census methods

(McElroy et al., 2020). However, false-positives, low sequencing depth and PCR bias can lead to over or under-estimates of DNA signal from species in both metabarcoding samples (Nichols et al., 2018; Alberdi et al., 2019). Here, by i) employing conservative error-filtering and sequence variant curation steps, ii) ensuring high sequencing depth per sample, iii) amplifying two marker genes using PCR technical replicates, and iv) and sequencing both ARMS and eDNA samples on the same sequencing cartridge, we have strived to reduce the rate of false positives.

Differential abundance testing between eDNA and ARMS samples reveals which taxa group are more likely to be found in higher abundance using each method. As expected, we find that most mobile cryptofauna taxa (decapods, molluscs) found in both samples are found in higher abundance on ARMS, whilst pelagic copepods, dinoflagellates and diatoms, which inhabit the water column, are in higher abundance in eDNA samples. We find that eDNA samples are more likely to pick up the presence of soft coral and anemones, and since these were rarely observed on ARMS plates using image analysis, this finding suggests ARMS may not be an ideal tool for studying these taxa groups. Interestingly, many shared sequence variants identified as sponges and rhodophytes were not found to have significantly different abundances between sample types, suggesting that both eDNA and ARMS metabarcoding perform equally well in detecting their presence on the reef. Whist we do not equate read abundance to individual or population abundance in this study, we are able to show which taxa groups can be equally detected using eDNA sampling than by using ARMS. For example, many shared sequence variants identified as sponges and rhodophytes were not found to have significantly different abundances between sample types, suggesting that both eDNA and ARMS metabarcoding perform equally well in detecting their presence on the reef. Previous studies have shown that collecting larger volumes of water can help to increase the detection of rare or invasive species (Stauffer et al., 2021; Sepulveda et al., 2019), and further extension to this work could include the collection of larger volumes of water, as well as increasing sequencing depth, to determine if eDNA sampling can recover even more reef cryptobenthic taxa.

4.5.3. Study limitations and future work

Our image analysis provides insights into naturally occurring understorey cryptobenthic assemblages in remote and protected, but vulnerable, coral reefs, and highlights the key role of *Acropora sp.* tabular coral plays in supporting cryptobenthic sessile organisms beyond the death of the colony. However, the diversity and recruitment patterns of cryptobenthic communities on other coral morphotypes was not explored in this study. Whilst *Acropora* sp. coral analysed in this study were dead, they remained upright and attached to the overall reef matrix. Coral rubble has been shown to harbour high cryptobenthic richness and density (Stella et al., 2022; Enochs & Manzello, 2012), and further work comparing ARMS sessile communities with those found across rubble communities is now needed to understand if, and how, ARMS could be used to monitor degrading reef ecosystems in other parts of the world.

Site choice, even within the same geographical region, can be a strong predictor of ARMS communities (David et al., 2019), and in this study has a significant effect on overall community composition detected using metabarcoding, as well as the percentage cover of sessile groups across image-based analysis. We find little to no overlap in the beta diversity of sampling sites when metabarcoding ARMS and eDNA samples, suggesting that both methods can recover site-based differences, as observed in other studies (West et al., 2022). On the other hand, our NMDS analysis of sessile communities from image-analysis shows that overall communities on the topside of ARMS are less dissimilar than those observed on the top of dead *Acropora* sp. coral across sampling sites, suggesting that ARMS image analysis alone may be less able to pick up differences in communities between different reef sites. However, our site replication in this study is low, and further work could include the addition of more sites across the Archipelago.

Finally, despite using a reference database composed of curated sequences from the Moorea Biocode and Midori datasets, we are still unable to assign most of the diversity in our ARMS and eDNA metabarcoding samples. We find that less than ~20% of all COI cOTUs are assigned at phyla level, compared to ~60% for 18S cESVs. Interestingly, a higher proportion of eDNA cOTUs are assigned across taxonomic ranks than ARMS cOTUs, whilst the opposite is observed in the 18S dataset, which suggest larger gaps in COI representation for sessile cryptobenthic organisms, and 18S representation for water-column based organisms, in our reference dataset. The incompleteness of genetic reference

databases is well recognised (van der Loos & Nijland, 2021), and its impact on metabarcoding studies is profound and limits our ability to describe and study coral reefs using a metabarcoding approach.

4.5.4. Conclusion

With ARMS increasingly being used to monitor marine benthic ecosystems across the globe, further studies comparing and ground truthing ARMS methods are warranted. To our knowledge, our study provides the first comparison of sessile communities on ARMS versus that of coral understoreys and provides further support for the integration of eDNA sampling for cryptobenthic monitoring. Few ARMS studies have presented both image and metabarcoding data from the same devices (Pearman et al., 2016; Ransome et al., 2017). Here, we find that analysing images from exposed and cryptic reef surfaces helps to ground-truth recruitment patterns observed on ARMS, and that collecting eDNA helps to increase the number of recovered cryptobenthic taxa. Both are cost-effective ways to increase the analysis power of ARMS-based studies and should be considered as valuable non-destructive tools for the study of reef cryptobenthos.

4.6. Author contributions

CH deployed ARMS in 2018 and MS/RD/ND retrieved them in 2021. ARMS and eDNA samples were processed by MS/RD/ND, and ARMS and coral photographs were taken by MS. MS carried out all laboratory work and image analysis and wrote this manuscript. KH assisted in laboratory work including library prep and sequencing steps. ER/MB/CH contributed to the revision of this manuscript.

CHAPTER 5

Observations of coral and cryptobenthic sponge fluorescence and recruitment on Autonomous Reef Monitoring Structures (ARMS)

Margaux Steyaert[1,2], Andrew Mogg[3], Nicholas Dunn[2,4], Rosalie Dowell[2,4], Catherine Head[1,2]

[1] Department of Biology, University of Oxford, Oxford, OX1 3SZ, United Kingdom

[2] Institute of Zoology, Zoological Society of London, London, NW1 4RY, United Kingdom

[3] Tritonia Scientific Ltd, Oban, Argyll PA37 1QA, United Kingdom

[4] Department of Life Sciences, Imperial College of London, London, SL5 7PY, United Kingdom

This chapter has been published as a short paper in the journal *Coral Reefs*

Steyaert, M., Mogg, A., Dunn, N., Dowell, R., Head, C.E.I. (2022) Observations of coral and cryptobenthic sponge fluorescence and recruitment on autonomous reef monitoring structures (ARMS). *Coral Reefs* **41**, 877–883. https://doi.org/10.1007/s00338-022-02283-2

5.1. Abstract

Fluorescence imaging of benthic communities is a widely used tool for determining the rate of hard coral recruitment in tropical reefs. Whilst fluorescent proteins are well-studied in scleractinian corals, less is understood about their distribution and function in other sessile reef invertebrates. This short study examines fluorescence images of benthic communities on Autonomous Reef Monitoring Structures (ARMS) from a remote and protected Indian Ocean reef system. We compare the abundance of adult and juvenile hard corals across three sites and between the topside and underside of ARMS recruitment plates. We also discuss observations of skeletal fluorescence in sponges, as well as uneven green fluorescent protein (GFP) concentrations across adult coral colonies. Our findings provide an insight into the recovery of shallow reefs previously hit by severe bleaching events and highlight the potential of ARMS fluorescence imaging for the analysis of cryptobenthic communities.

5.2. Introduction

Recording the success and rate of the recruitment of reef benthic organisms can give us vital insights into coral reef health, recovery, and diversity. With high mortality bleaching events increasing in frequency across tropical reefs, and in the face of bleak climate predictions (IPCC 2021), it is necessary to monitor recruitment patterns if we are to predict and understand the state of future reefs and implement useful management plans. This is especially true of reefs which have experienced severe bleaching events in the past and can now be said to be at high risk from further large-scale climate-induced mortality events (Sheppard et al. 2020).

Reef sessile invertebrates, such as hard corals, soft corals, sponges, ascidians, tube-forming worms and bivalve molluscs, shape or are anchored to the reef matrix. Cryptic surfaces and crevices within the reef matrix often harbour highly diverse communities of non-hard coral invertebrates and provide shelter for young coral recruits (Kornder et al. 2021). Studying the recruitment of both hard corals and non-coral invertebrate recruitment in-situ can be complicated, as cryptic spaces are often inaccessible for sampling or photography. Autonomous Reef Monitoring Structures (ARMS) are artificial recruitment devices used for the collection and study of diversity usually found in cryptic reef spaces (Carvalho et al. 2019; Pearman et al. 2020). Composed of 9 stacked PVC plates, with alternating gaps between each layer, each ARMS provides recruitment surfaces and varied microhabitats for cryptobenthic fauna.

These devices are now employed around the world to study these communities using a mix of standardised genetic and image analyses.

Fluorescence imaging is a popular census technique for identifying coral recruits on artificial tiles or in-situ reef surfaces (Baird et al. 2006; Zweifler et al. 2017). This method allows the capture of fluorescent pigments within organisms such as green fluorescent proteins (GFPs), other fluorescent proteins (FPs) and photosynthetic pigments such as chlorophyll. Fluorescence imaging of hard coral recruits on artificial recruitment tiles has been widely used, but no study has yet used it to look at sessile communities on ARMS devices. In this study, we present results from high-resolution fluorescence images of ARMS devices deployed across the Chagos Archipelago, a remote and protected Indian Ocean reef system. We record abundances of hard coral adult colonies and juvenile recruits from sites previously impacted by severe bleaching events (Head et al. 2019) and present observations of the distribution of coral fluorescent pigments across ARMS. Observations of fluorescence from the skeletal elements of several sponge specimens are also presented and discussed.

5.3. Materials and methods

Fluorescence images were taken of Autonomous Reef Monitoring Structures (ARMS) in April 2021 in the Chagos Archipelago Marine Protected Area (MPA) as part of a wider research project on shallow reef benthic communities. Triplicate ARMS devices were retrieved from a depth of approximately 5–12 m across three sites across the northern atolls, including two exposed ocean-facing reefs (Ile Anglaise, 5°20′04.7"S 72°12′48.5"E, and Moresby, 5°14′00.3"S 71°49′50.3"E) and one sheltered lagoonal reef (Ile du Coin, 5º27′04.5"S 71º46′30.8"E). ARMS plates photographed for this article were retrieved and processed following standardised Global ARMS NOAA protocols after a 36-month deployment (Leray et al. 2015).

A Sony RX100 MkII camera with a Nightsea 450 nm barrier filter and two Inon Z240 UV strobe lights with Nightsea fluorescence excitation filters were used to capture sessile fluorescence on 153 plate faces across 9 ARMS devices (17 plate faces per device), from three shallow reef sites (Fig. 5.1). Photographs were taken at night inside a shaded bin with filtered seawater. Some plates were photographed multiple times to enhance resolution.

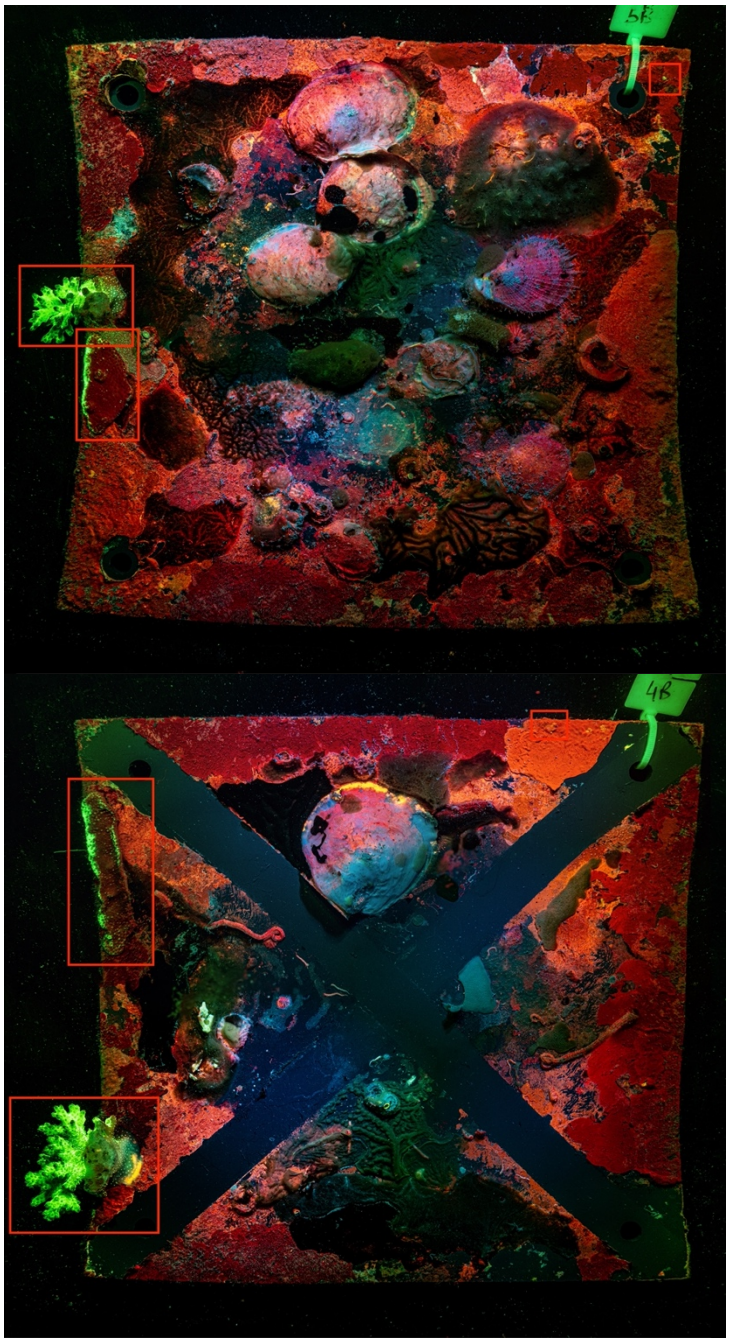

Figure 5.1. Fluorescence images of two Autonomous Reef Monitoring Structure (ARMS) recruitment plates (23 cm × 23 cm). Red boxes highlight scleractinian coral adult colonies and juvenile recruits. The bottom image is of a 'closed' surface, where PVC bars were placed across this plate and its adjoining neighbour to create four distinct recruitment surfaces, and the right-hand image is the equivalent with no PVC bars.

Images were processed using Adobe Lightroom Classic (for cropping, merging and enhancing brightness and contrast). The number of hard corals was counted in each image; individuals smaller than 15 mm were recorded as juveniles, whilst larger individuals were recorded as adults (Sheppard et al. 2017).

Counts of corals were then plotted using the 'ggplot2' package in R (v3.3.5) and negative binomial generalised linear models were used to test for differences in abundance between sites and ARMS (as the data is count-based and does not follow a normal distribution), using the 'MASS' and 'vegan' packages (v7.3.54 and v2.5.7, respectively)(Venables & Ripley, 2002; Wickham, 2016; Oksanen et al. 2013).

5.4. Results and discussion

5.4.1. Hard coral recruitment across sampling sites and ARMS

A total of 268 hard corals were counted on ARMS devices across the three sampling sites, with an average of 35 individuals per m2. Juvenile recruits (< 15 mm) were consistently more abundant than adult colonies, with 57 juveniles and 34 adults found on average on each ARMS unit, and a density of 22 juvenile and 13 adult individuals per m^2 (Fig. 5.2). No significant differences in the abundance of adult or juvenile corals were observed between sampling sites, suggesting uniform recruitment patterns across sampled reefs.

The abundance of juvenile corals was found to be equal between the underside and topside of ARMS plates across all sites. Adult coral abundance was also equal between plate faces in Ile Anglaise and Moresby but was significantly higher on plate undersides in Ile du Coin ($p < 0.001$***). This reef site is sheltered from prevailing currents and higher sedimentation has been observed in-situ compared to the two exposed reef sites. Juvenile recruit survival may be lower on the topside of ARMS plates at this site due to sediment loading.

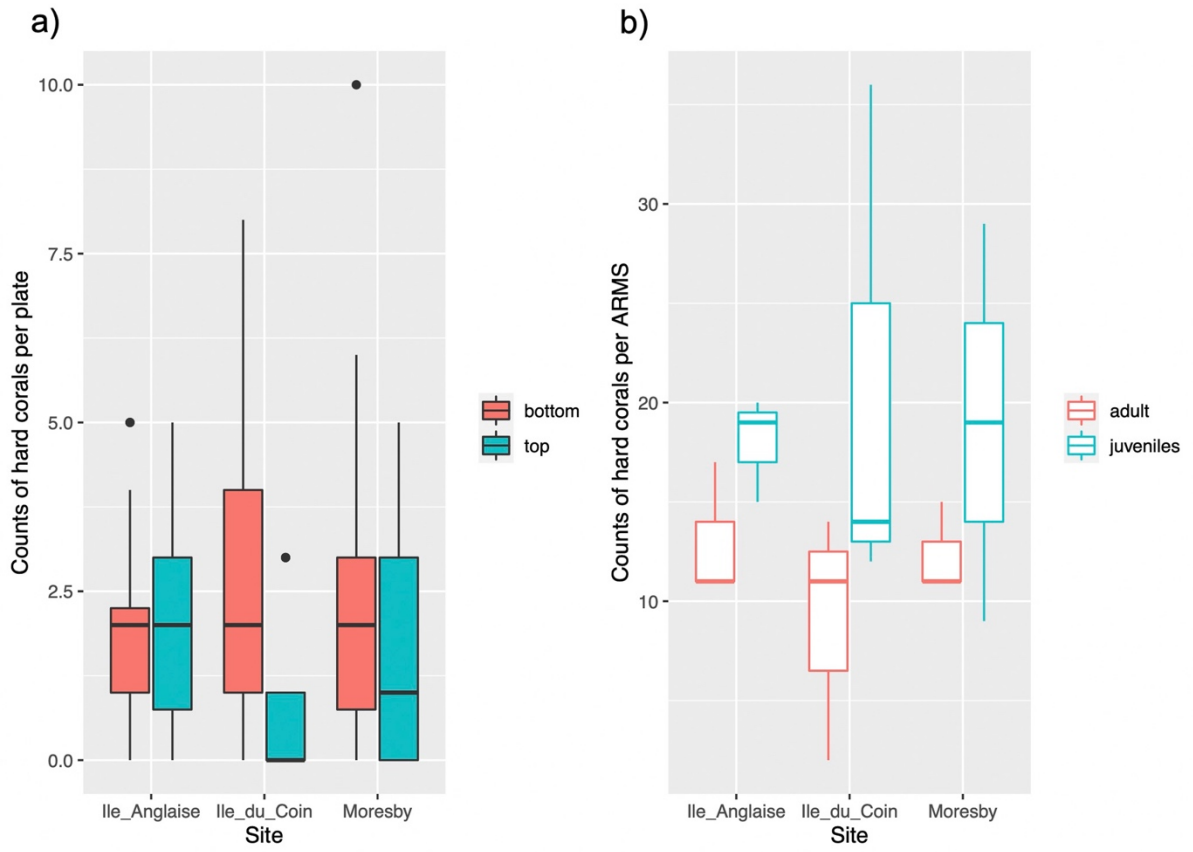

Figure 5.2. Boxplots displaying count abundances of (a) all hard corals across top and bottom ARMS plate face images and of (b) juvenile recruits and adult coral colonies on ARMS devices across sampling sites.

The surface area of cryptic reef cavities has been shown to exceed that of exposed benthos by up to a factor of eight (Scheffers et al. 2010), meaning exposed surfaces represent only a portion of available recruitment space on the reef matrix. ARMS provide ideal refugia for non-photosynthesising cryptobenthic invertebrates but inadvertently also provide a desirable settlement surface for hard corals. Similar patterns of coral recruitment have been observed in other studies using artificial settlement tiles, with higher juvenile coral recruitment recorded in cryptic and grooved ridges than on flat exposed surfaces (Mallela 2018). Tight gaps between ARMS plates likely provide protection from grazers and physical damage (e.g., from loose rubble), resulting in coral colonies growing across sampling sites. Our results provide new insights into coral recruitment across reefs which are still recovering from back-to-back high mortality bleaching events (Sheppard et al. 2020) and highlight the importance of investigating both exposed and hidden surfaces when assessing coral recruitment rates.

The highly standardised format of ARMS makes them an advantageous tool for studying coral recruitment with minimal disturbance to the natural matrix, as well as monitoring in-situ coral density of cryptic surfaces. However, whilst previous work has shown ARMS-based communities are comparable to those found across dead coral heads (Plaisance et al. 2011), further work is now required to determine whether ARMS's PVC plates bias the attachment and survival of hard coral juveniles compared to exposed natural reef surfaces. Fluorescence imaging allows for a quick scan of adult and juvenile recruits across ARMS plates but may overestimate counts due to increased signal to noise ratio or underestimate them due to genetic variability or the fact that shaded ARMS surfaces may lead to minimal or absent recruit fluorescence. Further work investigating coral recruitment on ARMS could include both daylight and fluorescence counts to allow for meaningful comparisons with similar studies.

5.4.2. Observations of fluorescence concentration across colonies

Fluorescent proteins are ubiquitous in scleractinian corals, but their functional role has often been a highly debated topic. Green fluorescent proteins (GFP) have been suggested to play multiple roles including photoprotection (Smith et al. 2013), internal light regulation in mesophotic corals (Smith et al. 2017), immune response regulation (Palmer et al. 2009), and to attract symbionts (Field et al. 2006; Aihara et al. 2019).

Several adult hard coral colonies displayed uneven concentrations of green fluorescence across ARMS plates (Fig. 5.3). Encrusting colonies were observed to emit the brightest fluorescence closer to and along the exposed edges of ARMS recruitment plates (Fig. 5.3a, b and c). Furthermore, polyps along the topside of an adult Pocillopora sp. colony growing off the side of an ARMS plate (i.e., facing towards surface light) were shown to emit brighter fluorescence than polyps found on the underside of this colony (i.e., facing reef benthos) (Fig. 5.3d).

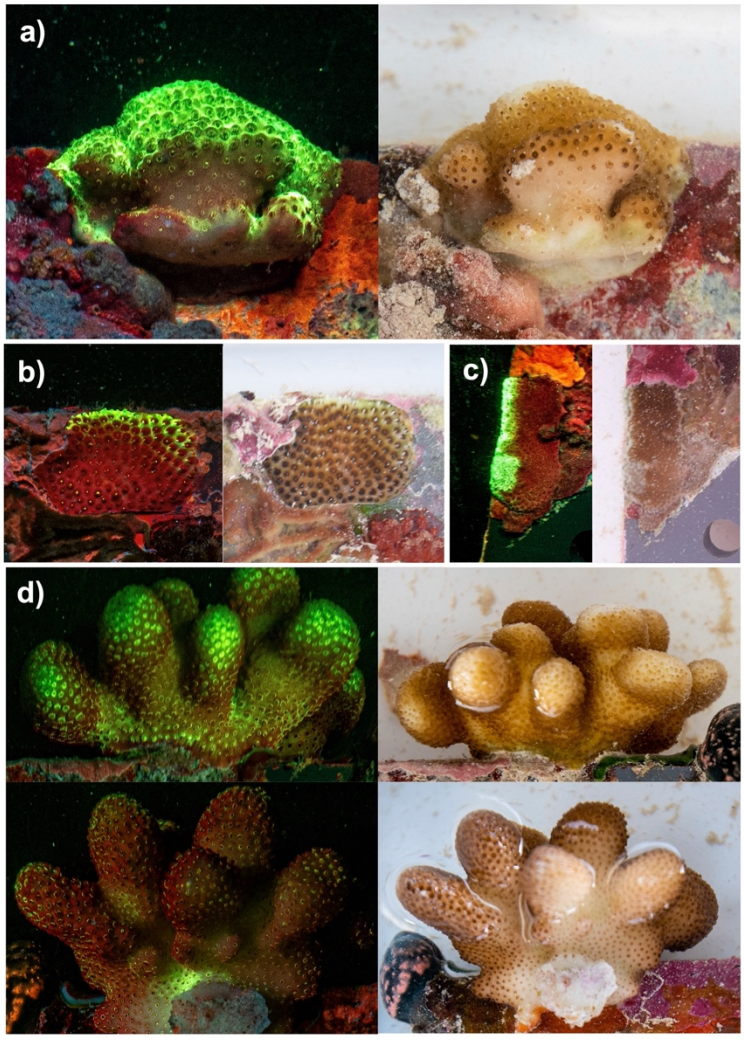

Figure 5.3. Images of the same scleractinian coral colonies under UV light and daylight, where differences in GFP concentration can be observed across colonies close to ARMS plate edges (a, b and c) and between the topside (top left and right-hand images) and underside (bottom left and right-hand images) of the same Pocillopora spp. colony (d).

ARMS plates are stacked closely together with only 1-2 cm gaps between each plate face; this likely blocks a large amount of daylight from reaching the centre of each device. Patterns of fluorescence concentration across hard coral colonies were consistent with areas of ARMS plates most exposed to direct sunlight (i.e., the outer edge of plates). Our results support similar findings from other studies analysing coral fluorescence patterns in response to controlled (D'Angelo et al. 2008; Smith et al. 2013) or in-situ (Bollati et al., 2020) light conditions.

5.4.3. Fluorescence patterns in sponges and other cryptobenthic taxa

Green and orange fluorescence was also observed across the skeletal elements of a few sponge specimens, from ARMS in the exposed Ile Anglaise site (Fig. 5.4). Deep-sea glass sponge spicules have been shown to have fibre-optical features (Sundar et al. 2003), and the close association between green algae and the siliceous spicules of demosponge *Tethya seychellensis* has been hypothesised, and since confirmed, to serve as a natural pipeline for light (Gaino and Sara 1994). This in turn likely benefits the metabolic activity of phototrophic organisms and their associated sponge host. We hypothesise that fluorescence observed here likely originates from algae which developed in close association with sponge skeletal elements, and ongoing genetic and microscopy work will determine specimen taxonomy. Sponge fluorescence on coral reefs is poorly documented or understood and has not previously been reported from sponge specimens in the Chagos Archipelago. Furthermore, to our knowledge, in-situ images of fluorescing tropical reef sponges of this kind have not previously been published.

Fluorescence was also observed from other sessile invertebrates across ARMS plates, such as solitary ascidians (yellow-green fluorescence), limpets (red fluorescence), and from the opercula of serpulid calcareous worms (green fluorescence). Almost all research on fluorescence from coral reef benthic communities focuses on hard corals, and little is known about the presence and role of fluorescent proteins in non-coral sessile reef invertebrates (Zawada and Mazel 2014). Multicolour fluorescence is observed across ARMS plates (Fig. 5.1), and we recommend that future ARMS studies could use fluorescence imaging to extract quantitative information from cryptobenthic communities.

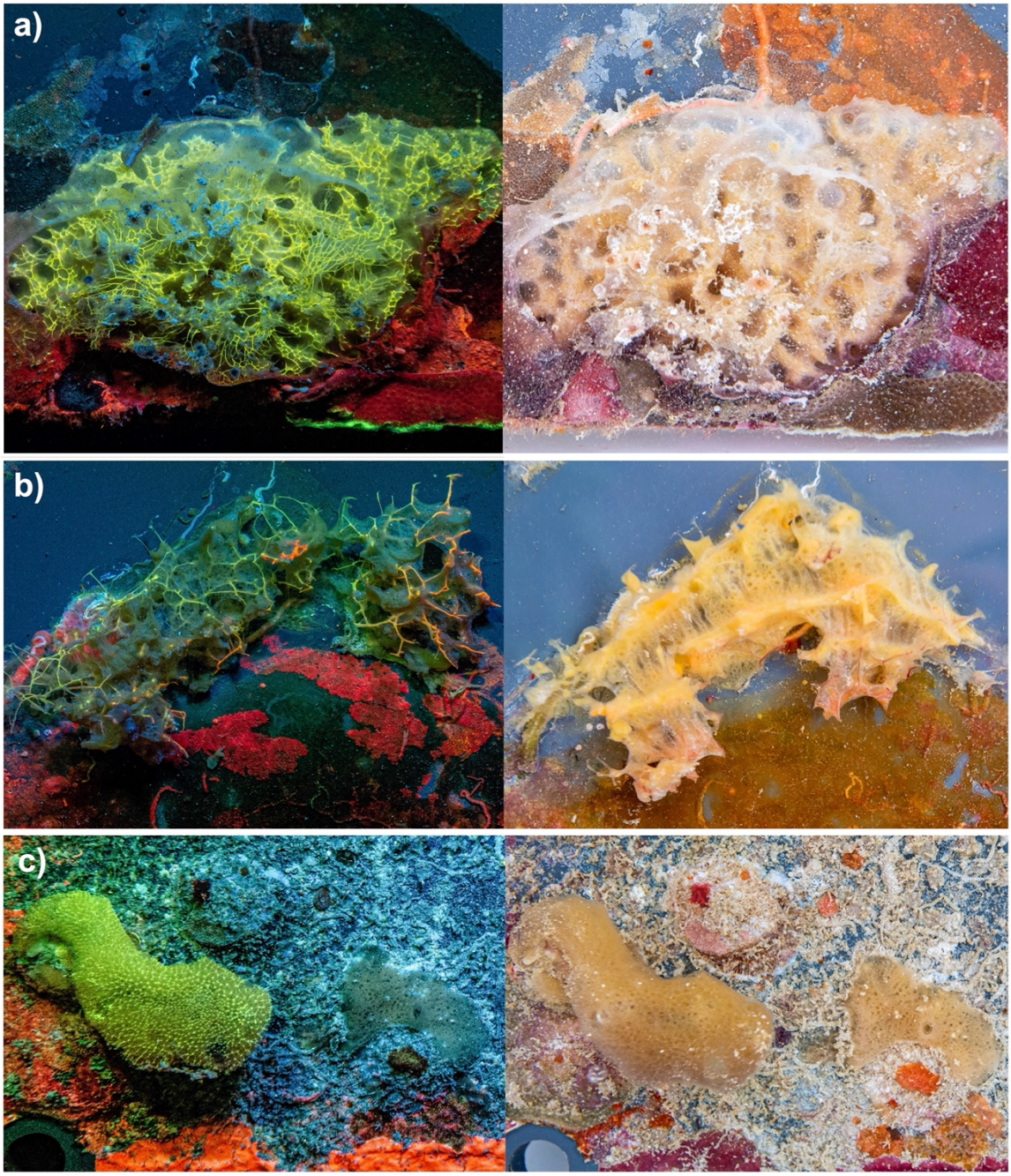

Figure 5.4. Images of the same sponge specimen on ARMS recruitment plates under both UV light (left-hand side) and daylight (right-hand side).

Benthic communities found on ARMS devices have been shown to be highly diverse (Carvalho et al. 2019; Pearman et al. 2020), with both genetic and image analysis methods required to determine community composition and diversity patterns (Pearman et al. 2016). Analysis of ARMS plate images has so far been conducted under white light, followed by a random point count approach to determine the recruitment cover and composition of sessile communities (David et al. 2019). This approach is ideal for determining overall functional composition but is likely inaccurate for recording coral recruit abundance. Our study of ARMS demonstrates how fluorescence imaging of these devices could be an ideal standardised tool for studying the in-situ recruitment of hard corals as well as the presence and patterns of fluorescent proteins in cryptobenthic invertebrates.

5.5. Author contributions

CH deployed ARMS in the Chagos Archipelago MPA in 2018. MS, RD, ND recovered ARMS and MS, RD, ND, AM photographed ARMS plates in 2021. MS analysed data and wrote the manuscript. All co-authors contributed to manuscript revisions.

Acknowledgments

This work was funded by the Bertarelli Foundation as part of the Bertarelli Marine Science Programme.

Conflict of interest

On behalf of all authors, the corresponding author states that there is no conflict of interest.

CHAPTER 6

General Discussion

Conserving global biodiversity must become a priority in order to safeguard ecosystems from further damage and degradation in the coming decades (IPCC, 2022). Doing so requires a solid and up-to-date understanding of what diversity looks like across natural habitats, and what factors most readily shape it across ecological scales. However, our understanding of the diversity of tropical coral reefs lags behind our need to monitor these ecosystems, as they face increasing harm from climate change and other human-led impacts.

This thesis aimed to explore the diversity and drivers of coral reef cryptobenthic communities in the Chagos Archipelago Marine Protected Area (MPA), a remote and relatively un-impacted region of the Central Indian Ocean. I studied spatiotemporal patterns of cryptobenthic community composition and diversity (Chapter 2) and explored potential relationships between sessile organisms and the environmental conditions they experience on the reef (Chapter 3). I published the findings of the latter

in an open-access research article which integrated analyses of both biological and physicochemical components of shallow reef ecosystems (in *Frontiers in Marine Sciences*). I also compared benthic communities recovered using artificial devices (Autonomous Reef Monitoring Structures) with those found on local natural reef substrates and used ARMS to ground truth the use of environmental DNA sampling from water samples for the study of coral reef benthic organisms (Chapter 4). Finally, I explored the use of fluorescence imaging to study cryptobenthic communities, a potential novel method for the ARMS toolkit, and published data on hard coral recruitment and observations of sponge fluorescence in a short note article (in *Coral Reefs*) (Chapter 5). Utilising ARMS as the collection tool throughout this project has meant that image and metabarcoding data presented in this thesis can be comparable and therefore useable for future similar studies. Over the course of this project, I performed 58,275 visual identifications of sessile organisms and obtained over 25,000,000 new genetic sequences for eukaryotes inhabiting shallow tropical coral reefs, which I intend on depositing to open access repositories following the submission of this thesis. Below I discuss key findings across data chapters and their implications within the wider academic field, as well as study limitations and future avenues for researchers employing the ARMS toolkit to assess coral reefs.

6.1. Biodiversity of cryptofauna across the Chagos Archipelago Marine Protected Area

Chapter 2 significantly advances our knowledge of the distribution and composition of cryptobenthic communities throughout the archipelago. The metabarcoding analysis of this chapter highlighted how cryptobenthic communities were both highly biodiverse and heterogeneous across small spatial scales. Whilst most metabarcoding studies average a sequencing depth of 60,000 reads per samples using a MiSeq sequencing platform (Singer et al., 2019), I averaged a total of 249,301 reads across amplicon datasets, which was enough to recover the diversity expected within ARMS samples based on rarefaction analysis. By targeting two genetic regions (COI, 18S v4), I recovered the presence of 32 eukaryotic phyla, including 21 belonging to metazoans. Using two genetic markers is widely recommended for metabarcoding studies (Casey et al., 2021; Marcelino & Verbruggen, 2016), and my findings support this notion. I find that both COI and 18S datasets recover a rich cohort of arthropods, with over a thousand curated Operational Taxonomic Units (cOTUs) detected by both amplicons, and similar numbers of cOTUs belonging to sponges (18S = 319, COI = 211) and molluscs (18S = 245, COI = 349). However, approximately 11 times fewer marine worms (nematozoans, platyhelminths,

nemerteans and annelids) were detected using COI compared to the 18S v4 genetic region. Overall, whilst both amplicons detect different sets of organisms, and do not provide information on individual cOTUs at the same taxonomic level, they do recover similar patterns of alpha and beta diversity across ARMS samples.

I observe that metazoan community composition is significantly shaped by both spatial and temporal factors, with significantly different communities observed between reef habitat types (lagoonal versus ocean-facing) and across sampling years (1 versus 3-year-old communities). Richness was high and similar across all three sampling sites, and the majority of community dissimilarity observed between samples of the same site collected either in 2019, or 2021, was found to be attributed to turnover (aka species replacement) rather than nestedness (species loss/gain). The same was observed for community dissimilarity between ARMS triplicates of individual sites (either in 2019 or 2021 collections). Overall, approximately a third of all cOTUs were found shared between i) all motile and sessile fractions, ii) 2019 and 2021 sampling collections including all three sites, and iii) between ARMS triplicates of each site and individual sampling collections, highlighting the extent of heterogeneity observed across collected samples. High heterogeneity and community dissimilarity has been observed in ARMS studies of the Red Sea too across short spatial scales and over two collection time points (Villalobos et al., 2022), and findings in this thesis also support the notion that ARMS can detect spatiotemporal variability in cryptobenthic diversity.

My findings in Chapter 2 also highlight how the study of cryptofauna species in the Chagos Archipelago MPA is handicapped by the paucity of currently available genetic reference datasets. Overall, with a confidence threshold set to average (IDTAXA, threshold 30), I only identified 3-4% of all COI cOTUs to species level. When using a highly conservative taxonomy assignment approach (100% query cover and 100% id match using BLAST), I identify 242 individual species, of which 168 are metazoan and fully described. This number increases as we relax our taxonomy assignment criteria, but since our metabarcoding amplicon size is only 313 base pair long, it is preferrable to remain conservative where possible. I find that few of the species I identify using metabarcoding are represented in the online archives of the Natural History Museum (London), Florida's Natural History Museum or the Smithsonian National Museum of Natural History, which all have historical collections of reef specimen collected

from the Chagos Archipelago dating back to 1905. In turn, less than half of the species within these archives, or those of decapods previously identified in the MPA by Head et al., (2018a), have representative sequences within the COI classifier used to assign taxonomy in my metabarcoding analysis. The paucity of reference datasets is a well-recognised problem for metabarcoding studies, which I discuss in the introduction of this thesis, and my findings in Chapter 2 highlight the extent of this knowledge gap.

My analysis of the diversity of cryptofauna across the Chagos Archipelago MPA stands incomplete as I was unable to explore the abundance and composition of larger mobile cryptofauna within the timeframe of this thesis. An important component of the ARMS toolkit is the collection, photography and barcoding of large voucher motile (>2mm) cryptofauna and sessile invertebrates. ARMS-based studies have demonstrated that large mobile invertebrates have varied and complex responses to difference in pH conditions (Plaisance et al., 2021), and can drive spatial patterns of overall cryptobenthic communities found on ARMS (Ip et al., 2022). Although important, the barcoding and/or morphological identification of such specimens from ARMS can often be both time-consuming and expensive (Danovaro et al., 2016). Collection and photography of large mobile motile and sessile voucher specimen was carried out in both 2019 and 2021 field collections, with 1784 motile individuals and 265 sessile tissue samples collected and photographed (Appendix section A.i) (Figure 6.1). I was able to obtain successful barcode sequences from a total of 123 motile specimen collected in 2019, by targeting the full Folmer region of the COI gene (see Appendix section A.i), but due to time constraints and delays relating to the 2020 global pandemic (detailed in the Covid-19 impact statement, page viii), I was unable to integrate these results within chapters of this thesis. The barcoding and morphological analysis of all mobile cryptofauna and sessile specimen collected from ARMS in the Chagos Archipelago MPA would be a valuable addition to the field and would undoubtedly improve genetic reference databases for future metabarcoding work. The use of Nanopore sequencing (e.g., MinION platform) may be a way to expedite this work and reduce financial costs, as shown by Chang et al., (2020). Efforts are now ongoing to secure funding to carry out this work and eventually contribute to ongoing efforts to describe and provide guides for the flora and fauna of the Chagos Archipelago MPA (iNaturalist).

In the meantime, and as shown in this thesis, the metabarcoding of ARMS samples enables researchers to take a snapshot of the range of cryptobenthic organisms inhabiting the reef matrix, but also of the whole reef ecosystem itself. We detect the presence of many species of fish in our metabarcoding analysis of Chapter 1, and even octopus. This can be useful when using metabarcoding as an exploratory tool but the detection of DNA signal from organisms expected on the reef, but not necessarily on ARMS, likely augments the community dissimilarity observed across ARMS samples. Delimiting DNA signal from organisms living on ARMS, and those living off of ARMS or from extra-organismal DNA sources, is impossible and makes the study of community succession difficult, especially within extremely diverse communities such as the ones explored in this thesis. A final set of ARMS triplicates were collected from each site in October 2022, delayed from the original intended fieldwork date in 2021, following the impact of the global pandemic on global travel. Analysing this remaining set of ARMS would help to better visualise trends in community succession and help to further characterise the similarity in community structure between sampling sites across the archipelago.

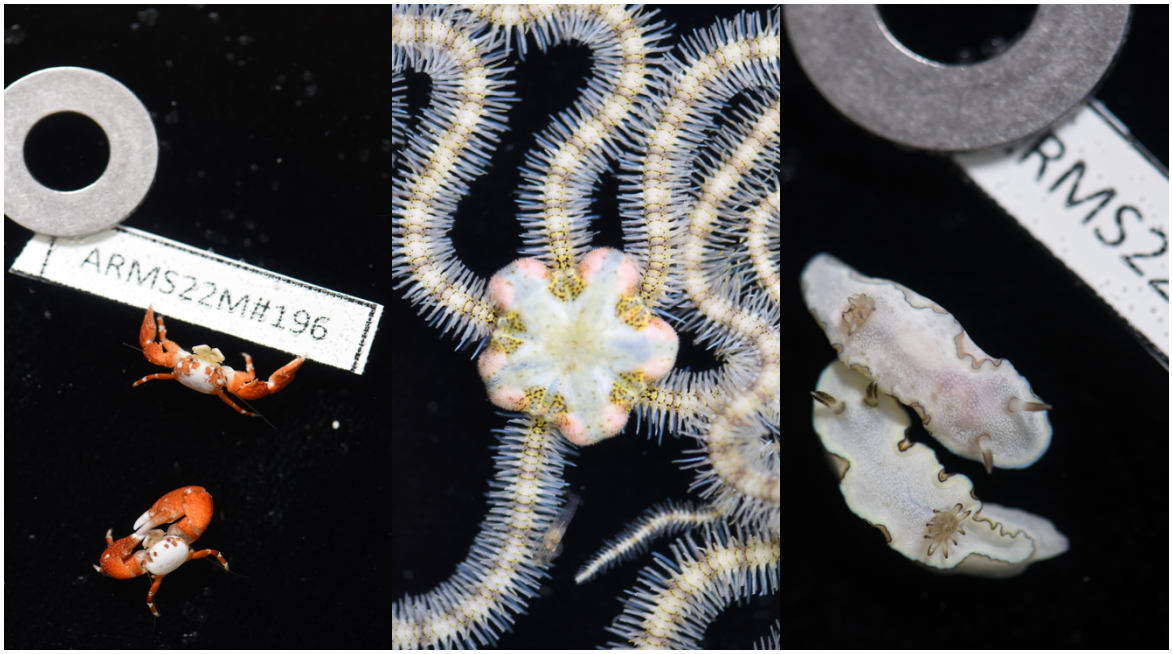

Figure 6.1. Images of large (>2mm) mobile invertebrates collected across ARMS in the Chagos Archipelago MPA, including crabs (left-hand image), brittlestars (centre image) and nudibranch molluscs (right-hand image).

6.2. Potential drivers of cryptobenthic communities

6.2.1. Physicochemical parameters across shallow ocean-facing and lagoonal reefs

Finding that site choice had a significant impact on the composition and distribution of ARMS communities in Chapter 2 led me to explore the abiotic conditions of each study site, and the possible relationship between local environmental parameters and cryptobenthic sessile communities, in Chapter 3. By using image analysis, I was able to obtain data on the total percentage of live cover of sessile organisms and on abundance patterns of individual groups, whilst project collaborators from Stanford University collected a suite of environmental parameters over both short (3 weeks) and long (12 months) time periods. Whilst other ARMS-based studies have investigated environmental drivers of cryptobenthic communities using remote sensing (Pearman et al., 2018; Pearman et al., 2019; Pearman et al., 2020), this study is the first to analyse ARMS communities alongside such a wide suite of parameters collected in-situ within coral reef habitats. Several key findings arose from this collaborative study, which was recently published in *Frontiers in Marine Sciences*' Research Topic 'Innovative Approaches to Coral Reef Science by Early Career Researchers' and gained over 600 views and an Altmetric score of 13 in the space of a month.

Firstly, we show that *ex-situ* satellite-based models for temperature and wave heights are unable to recover site-specific profiles for both variables across our three sampling sites. Unlike motile organisms, sessile communities are not able to translocate to other more favourable microhabitats if local conditions deteriorate. This means that if studying the impact of temperature change within benthic communities, accurate measurements are critical. We detect the presence of regular internal waves across two of our sites which cooled temperatures on the reef by ~5°C for short periods of time but find *ex-situ* remote sensing models cannot pick their presence or their impact on overall reef temperature profiles. The key takeaway message from these findings is that collecting in-situ data is preferrable than using remote sensing methods for remote regions such as the Chagos Archipelago MPA, as they can be over-generalised and inaccurate.

Indeed, wave exposure and temperature can have strong and significant effects on benthic community composition (Cecaralli et al., 2020; Lange et al., 2020), but other factors such as temperature, pH,

salinity, light availability (PAR) and dissolved oxygen are also important parameters which shape benthic composition and biodiversity (Diaz-Pulido & Barrón, 2020; Bell et al., 2018; Lopes et al., 2018; Gove et al., 2015; Scheffers et al., 2010). In Chapter 3, we also recover site-specific profiles of all of these conditions and find that both ocean-facing sites are more similar in their diurnal profiles of temperature, dissolved oxygen and pH, as well as their long-term regimes of flow velocities. Despite the number of site replicates (n = 3) limiting my ability to perform regression-based analyses of ARMS communities and environmental parameters in Chapter 3, we show how the abundance of individual groups correlate with different abiotic profiles identified across sites. For example, we observed the abundance of red and brown macroalgae correlate with high flow velocities as well as high pH and dissolved oxygen profiles, whilst bryozoans, CCA and colonial tunicates were associated with lower mean temperatures. I discuss these patterns in further detail within the discussion portion of Chapter 3, but it is important to remember that benthic communities are known to exhibit non-linear responses to changing conditions (Gove et al., 2015), and it is not possible to know within our analysis which environmental factors are most important for shaping the patterns of sessile communities observed across our sampling sites. Instead, we provide an integrated look at both biological and abiotic components of three reefs and present extensive data for both. Also, we collected data on environmental parameters over the course of a year, but only collect data on cryptobenthic sessile communities at one time point, after 12 months. Gathering images of early-successional communities (<6months) on ARMS (e.g., as done in Higgins et al., (2019) using single recruitment plates), or repeatedly at regular time intervals (e.g., every month), could help to map out the relationship between abiotic conditions and trends in sessile assemblages.

6.2.2. Surface orientation

In both Chapter 3 and 4, I find that surface orientation is a significant driver of community composition on artificial (ARMS) and natural (dead coral table) substrate. I find that the percentage cover of live sessile organisms is significantly higher under both dead tabular coral and ARMS recruitment plates than on top of them, and that the composition of organisms significantly differs between both substrate sides. For example, I observed that filter and suspension feeding groups like sponges, ascidians and bivalves, CCA and fleshy red macroalgae, as well calcified tube worms are consistently and significantly more abundant on the undersides of ARMS plates throughout sampling sites and across both 1- and

3-year-old cryptobenthic communities. I observed similar patterns on dead tabular *Acropora sp.* for sponges, ascidians, CCA, red fleshy encrusting and upright macroalgae and brown macroalgae. Similar patterns have been observed across artificial substrates and plates deployed on reefs, and so these findings are not surprising. However, finding similar patterns on natural dead coral does have important implications for studies on benthic reef composition and accretion. Several studies of the Chagos Archipelago MPA have also used image-analysis e.g., from transect and quadrat surveys, to quantify benthic composition and live percentage cover of corals and other sessile groups (Pilly et al., 2022, Lange et al., 2020. Head et al., 2018). These have focused on exposed surfaces, often from a view taken directly above the benthos. Live sessile cover under dead tabular coral in Chapter 4 was between 95-100%, with CCA covering 38% of available space on average, and sponges 23% of available space on average. CCA are important carbonate producers within tropical reef ecosystems which could eventually contribute more to overall reef accretion than corals themselves (Cornwall et al., preprint), and sponges are important habitat providers/shapers and nutrient cyclers across reef habitats (Maldonado et al., 2016; Bell, 2008; Diaz & Rützler, 2001). Previous estimates of percentage cover of sponges on shallow Chagos reefs range between 1-4% (Lange et al., 2020) and ~10% for CCA (Pilly et al., 2022). My findings highlight how solely investigating exposed surfaces could drastically under-estimate the true abundance of sessile groups which play key roles within reef ecosystems.

6.2.3. *Sedimentation*

Sedimentation can be a major factor shaping benthic communities on coral reefs (Tebbett & Bellwood, 2019), by affecting the recruitment or attachment success of sessile organisms such as corals, sponges and macroalgae (Maldonado et al., 2008; Fabricius and De'ath, 2001; Babcock & Smith, 2000) and likely influenced patterns observed across cryptobenthic sessile assemblages on ARMS and dead coral surfaces in Chapters 3, 4 and 5. Sediment deposits on the top of both artificial and natural surfaces were observed across all of our sampling sites and likely resulted in reduced live sessile recruitment on top surfaces (Figure 6.2). It is likely that sedimentation may also have played a role in differences observed between sites. High levels of benthic and water-column fine sediments were observed across the lagoonal site (Ile du Coin) during ARMS retrieval, in comparison to the exposed site (Moresby) where much less sediment and sand was observed across the reef matrix. In Chapter 3, we found that our estimates of water turbidity were higher in the lagoonal site (Ile du Coin), than on ocean-facing reefs

(Moresby, Ile Anglaise). In Chapter 3, significantly less recruitment was observed on the top of dead tabular *Acropora sp.* coral in the lagoonal site (60-75%) than on dead tabular *Acropora sp.* in the exposed site (90-100%)($p<0.001^{***}$).

I attempted to carry out a short experimental study in 2020 to explore the effect of sediment loading on ARMS communities. Coral recruitment studies which use artificial recruitment plates have shown that the orientation of individual plates (e.g., vertical, horizontal or at varied inclines) has an effect on the recruitment success of coral recruits, in part due to sediment retention (Mundy, 2000). I wanted to try a similar set up using ARMS and therefore deployed 4 ARMS across a reef site in the Diego Garcia atoll (south Chagos Archipelago), with two units laid flat on the reef benthos as per standardised deployment guidelines, and two laid on their side. I had the intention of collecting them a year later to study recruitment patterns and sessile community cover across the two treatments. However, when I returned in 2021 to this site, the 4 devices had been lost, likely due to a strong storm surge occurring in May-July 2020

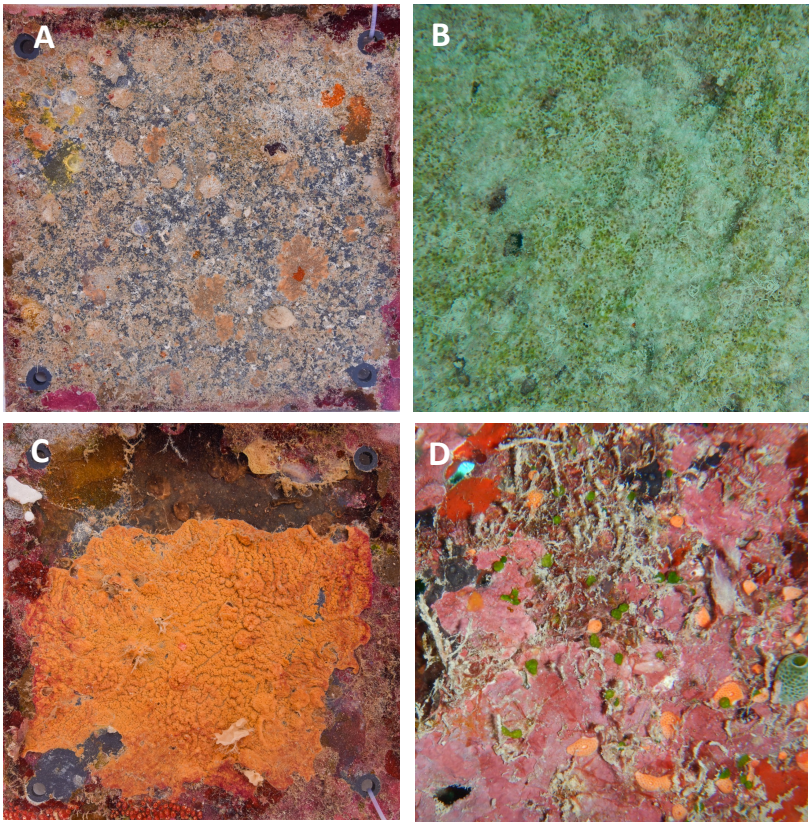

Figure 6.2. Images showing the different between sessile communities on the topside and undersides of artificial or natural reef substrates, with A) the topside of an ARMS plate, B) the topside of a dead tabular *Acropora sp.* coral, C) the underside of an ARMS plate and D) the underside of a dead tabular *Acropora sp.* coral.

6.3. Testing and furthering the ARMS method

As reviewed in the introduction of this thesis, the use of ARMS for the study of cryptobenthic communities across coral reefs and other marine ecosystems is gaining popularity. Their standardised design along with the range of protocols and methods recommended for the analysis of collected samples ensures that ARMS-collected data is comparable across time and locations. This makes them a valuable tool for monitoring purposes as data can be collected across multiple locations simultaneously by different teams or persons. However, there is a lack of comparisons between ARMS communities and natural references across recent ARMS studies and initiatives, which some have claimed is controversial (Carreira-Flores et al., 2021). Only a few ARMS-based studies have compared their findings to local natural communities (Plaisance et al., 2011).

In Chapter 4, I explored the similarity of image and genetic data collected using ARMS with those obtained from the natural reef matrix. Firstly, I investigated the complementarity of sessile communities on ARMS plates to those on nearby dead tabular *Acropora sp.* coral, using image analysis. Overall, both natural and artificial substrate communities displayed similar overall patterns of community dissimilarity across surface orientations (top and undersides of surfaces) and sampling sites. Some sessile groups were found in similar abundances on both substrate types, such as sponges, brown macroalgae, soft-tube worms and ascidians. However, I found that ARMS underestimated abundances of young coral colonies, red fleshy macroalgae and CCA observed on natural dead coral substrate, but overestimate the abundance of calcifiers such as bryozoans, bivalves and calcified tube worms. Whilst it commonly accepted that artificial substrates are not supposed to exactly mimic natural habitats, there is a need to understand the pitfalls and biases of the ARMS method in order to put into context the data collected using them, whether in experimental set-ups or when used to characterise community assemblages from individual locations. ARMS remain one of the best tools for collecting and studying cryptobenthic organisms, and my findings simply highlight which sessile groups may be under or oversampled. Further work could explore of community similarities between ARMS and natural substrates, for example by identifying taxa to lower taxonomic ranks (e.g., family, genus, species) or to morphospecies. This would help to determine if groups which are found in similar abundances (e.g., sponges, ascidians) between natural and artificial surfaces are also similar in species composition. Taking pictures of the underside of tabular corals was difficult with a handheld camera, and the use of

endoscopic cameras (Luong et al., 2019; Richter et al., 2001) or photogrammetry methods (Kornder et al., 2021) would be ways to improve the characterisation of natural communities within the reef matrix.

The use of environmental DNA sampling for the study of coral reef communities is rapidly increasing in popularity in recent years (DiBattista et al., 2020; Nguyen et al., 2020). Whilst most studies have focused on fish (e.g., Gelis et al., 2021), some are starting to look at whether water column eDNA sampling can be used to monitor or assess sessile benthic communities (Ip et al., 2022; West et al., 2022; Alexander et al., 2020). Such studies have compared their eDNA results with belt transect and photo quadrat surveys (West et al., 2022; Nichols & Marko, 2019). ARMS provide a unique opportunity for testing the ability of eDNA sampling for the study of cryptobenthic communities. I observed significantly different communities in Chapter 4, which is to be expected as many water-borne organisms are likely to be found in eDNA samples rather than ARMS benthic samples. I find that on average, 15-17% of COI/18S sequence variants are found in both sample types (eDNA, ARMS), but that in turn those sequence variants made up 65-70% of total DNA reads, suggesting that although each method picks up different organisms, they both pick up the presence of those most abundant. A similar study was published during the laboratory phase of this chapter (Nichols et al., 2021), which showed communities recovered from both methods were inherently different and that little overlap occurred between eDNA and ARMS communities.

In Chapter 4, I found that arthropods, molluscs, bryozoans and annelids, and the number of sequence reads belonging to these groups, were found in higher abundance within ARMS samples than eDNA. Many sponge sequence variants were found in the same abundance across both ARMS and eDNA samples, and whilst more sponge sequence variants were detected on ARMS overall, several species were only detected using eDNA sampling. Overall, I find that eDNA can detect certain sessile groups well (e.g., sponges, red macroalgae) but cannot replace the ARMS method for surveying whole cryptobenthic assemblages, and instead provides a useful additional tool when the aim of a study is to capture as much diversity as possible. The volume of water filtered can have a significant impact on the communities recovered using eDNA sampling (Tsuji et al., 2019; Goldberg et al., 2016) and increasing the volume of water collected, above 6L for the case of Chapter 4's analysis, would likely increase the amount of DNA signal from sessile groups.

Antich et al., (2020) tested the use of eDNA for surveying benthic communities and found it a poor proxy as they showed that the extent of overlap between water column and benthos was low, even at very close proximity. It is certain that for sessile organisms visible on exposed surfaces, traditional survey techniques using imaging (whether daylight or fluorescence) is likely more accurate. However, for cryptobenthic organisms that live deep and highly integrated within the complex reef matrix, the collection of eDNA may be valuable, even if taken within 50-100cm from the benthos, as was done in Chapter 4. Future work should further explore the use of eDNA for the study of cryptic reef sponges, for example by investigating shedding rates of different groups or by utilising sponge-specific primers to avoid the co-amplification of non-sponge organisms (Richards et al., 2022; Alexander et al., 2020).

My findings of Chapter 4 suggest that some cryptobenthic diversity from the natural reef matrix is not detected using the ARMS method. Whilst the whole reef cannot be represented on a single ARMS unit, it is possible that one way to amplify the detection power of ARMS for sessile diversity would be to increase the amount of bulk community extracted and sequenced. Currently, protocols recommend the extraction of DNA from ~8-10g of homogenised bulk sessile organisms from ARMS plates, as this is the maximum amount of weight that DNA can be extracted per sample tube of the widely available QIAGEN PowerMax Soil kit (Ransome et al., 2017). As observed during the fieldwork portion of this project, I estimate between 10-20 times as much weight is actually removed from ARMS plates, meaning most of the sessile community recovered is wasted. Whilst the cost of doubling the amount of tissue extracted may increase costs beyond the financial remit of many small projects, larger monitoring programs with additional funding could look to do this.

Finally, for Chapter 5, I carried out a short exploratory study on the use of fluorescence imaging for the study of ARMS sessile communities. In Chapter 3, I observed that hard corals were present across ARMS plates, and in Chapter 4 I saw that small and young hard coral colonies are found frequently on larger dead tabular coral substrate. I wanted to see if I could estimate the density of hard coral recruitment within cryptobenthic habitats using ARMS. In this short study, I counted 268 coral colonies across 153 plate images, and find that the density of adult or juvenile coral colonies are equal amongst sampling sites, suggesting equal recruitment patterns across ocean-facing and lagoonal reefs in the

Chagos Archipelago MPA. I observed similar patterns across dead *Acropora sp.* tabular coral. However, I found that significantly more hard coral recruits were found on the underside of ARMS plates, a pattern not observed on dead *Acropora sp.* coral, where instead the abundance of coral is similar on both surface orientations. In Chapter 5, I also presented images of interesting patterns of fluorescence across adult coral colonies and sponge specimen. Fluorescence imaging techniques are becoming increasingly used for surveying coral reefs, but almost all focus on collecting information from exposed reef surfaces (Zweifler et al., 2017; Beijbom et al., 2016 Treibitz et al., 2015). Our published study showed that fluorescence imaging and artificial reef substrates such as ARMS can easily be combined to look at cryptobenthic communities. This was a short study carried out over a couple of weeks using single wavelength UV light, but future work could look at the distribution of multi-colour fluorescing pigments across ARMS plates and extract quantitative information from cryptobenthic communities using this approach (Bollati et al., 2021).

6.4. Study limitations

A significant limitation to the work presented in this thesis was access to field sites and the limited time spent at each sampling location. This thesis presents data from a total of three sites and two field collections (April 2019 and March 2021) but was collected over a total span of only 8 weeks. The Chagos Archipelago MPA is a very remote part of the world and difficult to work in; no research station exists there, and month-long boat-based expeditions are the only way to access research sites in the northern atolls. The complex logistics of accessing and working within the MPA has meant that time in the field was limited and increasing the number of sites and ARMS was not possible. The number of sites was a limitation for the integrated image/environmental analysis of Chapter 3, as our comparison of lagoon-facing versus ocean-facing reefs was uneven (n = 1 for lagoonal reefs, n = 2 for ocean-facing reefs). The number of sites were limited due to both financial and logistical reasons, such as short field expeditions meaning that working across more than three site was not attainable. Due to the low number of site replicates, we were not able to perform regression-based modelling between environmental parameters and patterns of benthic community composition, and instead focused on using correlation-based analyses. An extra set of ARMS triplicates was deployed in the lagoon of the Salomon atoll on a coral knoll in 2018 and was originally supposed to be retrieved in 2021 as part of the last collection of ARMS from the archipelago, but due to the pandemic, this was pushed back to October 2022. The

integration of these ARMS would have balanced the lagoon versus ocean-facing reef experimental set-up.

The identification of sessile organisms to broad phyla groups in Chapter 3 and 4 limits my ability to explore patterns of community composition across sampling sites. Exploring patterns of sessile community composition at lower taxonomic categories (e.g., class/family level) or of morphospecies (e.g., as done for sponges by Timmers, 2021) could help to further the benthic image analyses of both chapters. This was not possible during the course of this thesis for several reasons. Firstly, the taxonomic skills required to do so takes time to acquire, and I am still learning to identify sessile taxa beyond phyla-level groupings. Secondly, the time to analyse all 58,275 points across ARMS/dead coral images to lower taxonomic ranks would have required time beyond what was available to complete this thesis. Finally, the CoralNet software has a semi-automated engine which learns from annotated images and improves it's identification capabilities over time; none of the six iterations of this machine learning engine were able to identify sessile groups such as sponges, soft-tube worms and octocorals with high confidence, and so it was decided best to avoid it's use.

6.5. Too small and too many, but within ARMS reach - future directions and concluding remarks

Meta-analyses across geographical regions and gradients of environmental conditions and human impacts will be needed in order to better understand the distribution and drivers of cryptofauna across coral reefs, and ultimately model the distribution and role of cryptobenthic groups across future climate scenarios. For non-cryptic reef benthic communities, monitoring programs such as ReefCheck, where quadrat and belt transect surveys are used to estimate coral cover and fish diversity, have reached 15,073 surveys to date since 1997 with the help of citizen scientists across the globe (https://www.reefcheck.org/tropical-program/). In turn, meta-analyses of such datasets have helped to monitor coral reef health and degradation across the world (Souter et al., 2020), assess spatial variability in coral resilience to bleaching (Sully et al., 2022), and presented new perspectives on what reefs may look like in the future (Reverter et al., 2022). Advances in sequencing and image processing technologies, the filling in of reference gaps, and the increased deployment and collection of ARMS around the globe, should ensure that meta-analyses of cryptobenthic assemblages across marine systems can soon be carried out. Some studies have already presented results from 50 ARMS or more

(Obst et al., 2020; Pearman et al., 2019), and no doubt there will soon be more studies reporting data from 100s of ARMS.

However, are we far from presenting meta-analyses on 1000's of ARMS and what are the current hurdles? Firstly, data publication and data sharing. Whilst over a thousand ARMS have been deployed across the world to date, data has only been shared or published on a fraction of these, as discussed in the introduction of this thesis. Most ARMS-based studies make their data readily available (e.g., most recently Reid et al., 2022), the sharing of ARMS image data is also important but seldom done. Secondly, computational space and variety of bioinformatic pipeline options for analysing large quantities of sequence reads. In this thesis, I present metabarcoding data across 18 ARMS, and found through rarefaction analysis that my sequencing depth was good enough to recover the majority of diversity within samples in the Chagos Archipelago MPA, a healthy and diverse reef system. It follows that when extrapolating the number of sequence reads obtained in this thesis to what would be needed to recover the diversity of 1000 ARMS, this could equate to over a billion reads (1,357,000,000). Several steps within a metabarcoding bioinformatics pipeline can take a long time, such as error-filtering and taxonomy assignment. Although some programs for these steps have been shown to be faster than others or more economical in terms of CPU and memory usage (Hleap et al., 2021), taxonomy assignment can take several days on an institutional high-power computer, as it did for this thesis' metabarcoding analysis. Ultra-deep flow cell technology is now available in new sequencing platforms such as NovaSeq, which has been shown to outperform the MiSeq platform for the study of marine seawater biodiversity using metabarcoding. In fact, NovaSeq outperforms MiSeq sequencing by recovering up to 7million reads per samples, but also at a depth-for-depth comparison (Singer et al., 2019). With the quantity of DNA data increasing from novel technologies, the performance and computational requirements of bioinformatic pipelines must be improved or made more readily accessible to coral reef researchers. Thirdly, a concise and clear set of guidelines for presenting results is needed. Metabarcoding datasets are large and complex; pulling out trends and patterns across taxonomically diverse datasets can be difficult and resulting analyses can be hard to interpret for those outside the field of metabarcoding. Reporting functional-species diversity (Guillemot et al., 2011) and productivity (Wolfe et al., 2020) from ARMS may be a way of improving the output and outreach of ARMS studies. Image-analysis data, as is presented in this thesis, is more straightforward to work with

and cheaper to obtain than metabarcoding data. Automated machine-learning based annotation of images is possible and already available via the use of Deep Learning Convulational Neural Networks, which is available in CoralNet or other similar programs (Gonzalez-Rivero et al., 2020; Beijbom et al., 2015). In this thesis, I found that after ~58,000 image identification points, the algorithm within CoralNet was able to identify some groups well (e.g., CCA, bryozoans) whilst others not well at all (e.g., sponges, soft corals and sediment covered organisms). However, once trained enough to identify sessile cryptobenthic groups correctly, this approach would make the analysis of image data from 1000 ARMS realisable.

Much further work needs to be carried out before we can say that coral reef cryptobenthic communities are well characterised across the globe. This thesis advances the knowledge for a very small portion of the world's coral reefs but provides a baseline for further studies across the Indian Ocean region. Priorities for this project beyond the work presented in this thesis include the publishing and sharing of data presented in Chapter 2 and 4, the completion of barcoding work on large mobile cryptofauna collected and the comparison and integration of metabarcoding data collected across the Chagos Archipelago MPA with other ARMS datasets from other hyperdiverse coral regions across the Indo-Pacific. The Chagos Archipelago MPA is a unique site for the scientific study of tropical coral reef biodiversity due to its geographic location and low direct human impacts, and as such research conducted there provides insight into the ecological workings of near-pristine coral reef ecosystems (Hays et al., 2020). The study of reference sites, which experience the absence of local anthropogenic pressure, and their comparison to sites which do experience local anthropogenic impacts (e.g., fishing, chemical and sound pollution, sediment run off from infra-structure, boat anchorage), can be used to understand how humans directly affect the trophic dynamics, diversity, resistance and resilience of coral reef ecosystems (Knowlton et al., 2008).

Human populations living near coral reefs around the Indian Ocean are rapidly increasing (Wong et al., 2022), and whilst the human pressure on these coral reefs will undoubtedly increase in the coming decades, the populations who depend on them will likely be negatively affected and disproportionally bear the burden of climate change (Schleussner et al., 2018). To our knowledge, this thesis and the studies published from its work, are the first to present ARMS data from the Central and Western Indian

Ocean. As such, it adds to a growing body of scientific work which can be used to determine how humans impact coral reefs across the Indian Ocean basin. ARMS are one tool which enable us to peer into the hidden diversity of coral reef ecosystems, and by testing potential biases associated with these devices, and by exploring other non-destructive sampling methods, part of this thesis has also furthered the ARMS toolkit. Importantly, the findings presented in this thesis show just how under-studied and under-represented cryptobenthic organisms are across genetic databases, as well as how hugely biodiverse and heterogeneous cryptic reef communities are within a remote protected reef system.

BIBLIOGRAPHY

Achlatis M, Pernice M, Green K, et al (2019) Single-cell visualization indicates direct role of sponge host in uptake of dissolved organic matter. *Proceedings of the Royal Society B,* **286**, 20192153.

Aerts L, Van Soest R (1997) Quantification of sponge/coral interactions in a physically stressed reef community, NE Colombia. *Marine Ecology Progress Series,* **148**, 125-134.

Ahmadia GN, Tornabene L, Smith DJ, Pezold FL (2018) The relative importance of regional, local, and evolutionary factors structuring cryptobenthic coral-reef assemblages. *Coral Reefs,* **37**, 279-293.

Aihara Y, Maruyama S, Baird AH, Iguchi A, Takahashi S, Minagawa J (2019) Green fluorescence from cnidarian hosts attracts symbiotic algae. *Proceedings of the National Academy of Sciences,* **116**, 2118-2123.

Alberdi A, Aizpurua O, Bohmann K, et al (2019) Promises and pitfalls of using high-throughput sequencing for diet analysis. *Molecular Ecology Resources,* **19**, 327-348.

Alexander JB, Bunce M, White N, et al (2020) Development of a multi-assay approach for monitoring coral diversity using eDNA metabarcoding. *Coral Reefs,* **39**, 159-171.

Al-Rshaidat MM, Snider A, Rosebraugh S, et al (2016) Deep COI sequencing of standardized benthic samples unveils overlooked diversity of Jordanian coral reefs in the northern Red Sea. *Genome,* **59**, 724-737.

Alvarado-Rodríguez JF, Nava H, Carballo JL (2019) Spatio-temporal variation in rate of carbonate deposition by encrusting organisms in different reef microhabitats from Eastern Pacific coral reefs. *Journal of the Marine Biological Association of the United Kingdom,* **99**, 1495-1505.

Anthony KR, Kline DI, Diaz-Pulido G, Dove S, Hoegh-Guldberg O (2008) Ocean acidification causes bleaching and productivity loss in coral reef builders. *Proceedings of the National Academy of Sciences,* **105**, 17442-17446.

Antich A, Palacín C, Cebrian E, Golo R, Wangensteen OS, Turon X (2021) Marine biomonitoring with eDNA: Can metabarcoding of water samples cut it as a tool for surveying benthic communities? *Molecular ecology,* **30**, 3175-3188.

Appeltans W, Ahyong ST, Anderson G, et al (2012) The Magnitude of Global Marine Species Diversity. *Current Biology,* **22**, 2189-2202.

Ayalon EBI, Einbinder S, Segev N, et al (2010) Grazing pressure on coral reefs decreases across a wide depth gradient in the Gulf of Aqaba, Red Sea. *Marine Ecology Progress Series,* **399**, 69-80.

Babcock R, Smith L (2002) Effects of sedimentation on coral settlement and survivorship. Proceedings 9th International Coral Reef Symposium, Bali, Indonesia, **1**, 245-248.

Baird AH, Salih A, Trevor-Jones A (2006) Fluorescence census techniques for the early detection of coral recruits. *Coral Reefs,* **25**, 73-76.

Baronio MdA, Bucher DJ (2008) Artificial crevice habitats to assess the biodiversity of vagile macro-cryptofauna of subtidal rocky reefs. *Marine and Freshwater Research,* **59**, 661-670.

Baselga A, Orme CDL (2012) betapart: an R package for the study of beta diversity. *Methods in ecology and evolution,* **3**, 808-812.

Bayer K, Schmitt S, Hentschel U (2008) Physiology, phylogeny and in situ evidence for bacterial and archaeal nitrifiers in the marine sponge *Aplysina aerophoba*. *Environmental Microbiology,* **10**, 2942-2955.

Beijbom O, Edmunds PJ, Roelfsema C, et al (2015) Towards automated annotation of benthic survey images: Variability of human experts and operational modes of automation. *PloS one,* **10**, e0130312.

Beijbom O, Treibitz T, Kline DI, et al (2016) Improving automated annotation of benthic survey images using wide-band fluorescence. *Scientific reports,* **6**, 1-11.

Bell JJ (2008) The functional roles of marine sponges. *Estuarine, Coastal and Shelf Science,* **79**, 341-353.

Bell JJ, Bennett HM, Rovellini A, Webster NS (2018) Sponges to be winners under near-future climate scenarios. *Bioscience,* **68**, 955-968.

Bell JJ, Davy SK, Jones T, Taylor MW, Webster NS (2013) Could some coral reefs become sponge reefs as our climate changes? *Global Change Biology,* **19**, 2613-2624.

Bell JJ, Rovellini A, Davy SK, et al (2018) Climate change alterations to ecosystem dominance: how might sponge-dominated reefs function? *Ecology,* **99**, 1920-1931.

Bellwood DR, Streit RP, Brandl SJ, Tebbett SB (2019) The meaning of the term 'function' in ecology: A coral reef perspective. *Functional Ecology,* **33**, 948-961.

Benkwitt CE, Wilson SK, Graham NA (2019) Seabird nutrient subsidies alter patterns of algal abundance and fish biomass on coral reefs following a bleaching event. *Global Change Biology,* **25**, 2619-2632.

Bennett HM, Altenrath C, Woods L, Davy SK, Webster NS, Bell JJ (2017) Interactive effects of temperature and pCO 2 on sponges: from the cradle to the grave. *Global Change Biology,* **23**, 2031-2046.

Bennett H, Bell JJ, Davy SK, Webster NS, Francis DS (2018) Elucidating the sponge stress response; lipids and fatty acids can facilitate survival under future climate scenarios. *Global Change Biology,* **24**, 3130-3144.

Bessey C, Jarman SN, Berry O, et al (2020) Maximizing fish detection with eDNA metabarcoding. *Environmental DNA,* **2**, 493-504.

Biggerstaff A, Smith DJ, Jompa J, Bell JJ (2017) Metabolic responses of a phototrophic sponge to sedimentation supports transitions to sponge-dominated reefs. *Scientific Reports,* **7**, 1-11.

Biggs BC (2013) Harnessing natural recovery processes to improve restoration outcomes: an experimental assessment of sponge-mediated coral reef restoration. *PloS one,* **8**, e64945.

Bittick SJ, Bilotti ND, Peterson HA, Stewart HL (2010) *Turbinaria ornata* as an herbivory refuge for associate algae. *Marine Biology,* **157**, 317-323.

Bollati E, D'Angelo C, Alderdice R, Pratchett M, Ziegler M, Wiedenmann J (2020) Optical feedback loop involving dinoflagellate symbiont and scleractinian host drives colorful coral bleaching. *Current Biology,* **30**, 2433-2445. e3.

Bosch NE, Wernberg T, Langlois TJ, et al (2021) Niche and neutral assembly mechanisms contribute to latitudinal diversity gradients in reef fishes. *Journal of Biogeography,* **48**, 2683-2698.

Bradshaw CJ, Sodhi NS, Brook BW (2009) Tropical turmoil: a biodiversity tragedy in progress. *Frontiers in Ecology and the Environment,* **7**, 79-87.

Brandl SJ, Goatley CH, Bellwood DR, Tornabene L (2018) The hidden half: ecology and evolution of cryptobenthic fishes on coral reefs. *Biological Reviews,* **93**, 1846-1873.

Brandl SJ, Johansen JL, Casey JM, Tornabene L, Morais RA, Burt JA (2020) Extreme environmental conditions reduce coral reef fish biodiversity and productivity. *Nature communications,* **11**, 1-14.

Brandl SJ, Rasher DB, Côté IM, et al (2019) Coral reef ecosystem functioning: eight core processes and the role of biodiversity. *Frontiers in Ecology and the Environment,* **17**, 445-454.

Brandt MI, Trouche B, Quintric L, Wincker P, Poulain J, Arnaud-Haond S (2020) A flexible pipeline combining clustering and correction tools for prokaryotic and eukaryotic metabarcoding. *BioRxiv,* , 717355.

Britayev TA, Spiridonov VA, Deart YV, El-Sherbiny M (2017) Biodiversity of the community associated with Pocillopora verrucosa (Scleractinia: Pocilloporidae) in the Red Sea. *Marine Biodiversity,* **47**, 1093-1109.

Burt J, Bartholomew A, Bauman A, Saif A, Sale PF (2009) Coral recruitment and early benthic community development on several materials used in the construction of artificial reefs and breakwaters. *Journal of experimental marine biology and ecology,* **373**, 72-78.

Cáceres MD, Legendre P (2009) Associations between species and groups of sites: indices and statistical inference. *Ecology,* **90**, 3566-3574.

Cahyani NKD (2021) Delineating macro and micro marine biodiversity in the coral triangle using autonomous reef monitoring structures and DNA metabarcoding (Thesis) University of California, Los Angeles.

Cai W, Harper LR, Neave EF, et al (2022) Environmental DNA persistence and fish detection in captive sponges. *Molecular Ecology Resources,* **22,** 2956-2966.

Caley MJ, Fisher R, Mengersen K (2014) Global species richness estimates have not converged. *Trends in Ecology & Evolution,* **29**, 187-188.

Cameron ES, Schmidt PJ, Tremblay BJ, Emelko MB, Müller KM (2021) Enhancing diversity analysis by repeatedly rarefying next generation sequencing data describing microbial communities. *Scientific reports,* **11**, 1-13.

Camp EF, Schoepf V, Mumby PJ, et al (2018) The future of coral reefs subject to rapid climate change: lessons from natural extreme environments. *Frontiers in Marine Science,* **5**, 4.

Cardinale BJ, Duffy JE, Gonzalez A, et al (2012) Biodiversity loss and its impact on humanity. *Nature,* **486**, 59-67.

Carr P, Votier S, Koldewey H, Godley B, Wood H, Nicoll MA (2021) Status and phenology of breeding seabirds and a review of Important Bird and Biodiversity Areas in the British Indian Ocean Territory. *Bird Conservation International,* **31**, 14-34.

Carreira-Flores D, Neto R, Ferreira H, Cabecinha E, Díaz-Agras G, Gomes PT (2021) Two better than one: The complementary of different types of artificial substrates on benthic marine macrofauna studies. *Marine environmental research,* **171**, 105449.

Carvalho S, Aylagas E, Villalobos R, Kattan Y, Berumen M, Pearman JK (2019) Beyond the visual: using metabarcoding to characterize the hidden reef cryptobiome. *Proceedings of the Royal Society B,* **286**, 20182697.

Casey JM, Ransome E, Collins AG, et al (2021) DNA metabarcoding marker choice skews perception of marine eukaryotic biodiversity. *Environmental DNA,* **3**, 1229-1246.

Ceccarelli DM, Evans RD, Logan M, et al (2020) Long-term dynamics and drivers of coral and macroalgal cover on inshore reefs of the Great Barrier Reef Marine Park. *Ecological Applications,* **30**, e02008.

Chang JJM, Ip YCA, Bauman AG, Huang D (2020) MinION-in-ARMS: nanopore sequencing to expedite barcoding of specimen-rich macrofaunal samples from autonomous reef monitoring structures. *Frontiers in Marine Science,* **7**, 448.

Chase AL, Dijkstra JA, Harris LG (2016) The influence of substrate material on ascidian larval settlement. *Marine pollution bulletin,* **106**, 35-42.

Chave J (2013) The problem of pattern and scale in ecology: what have we learned in 20 years? *Ecology Letters,* **16**, 4-16.

Chen Q, Beijbom O, Chan S, Bouwmeester J, Kriegman D (2021) A New Deep Learning Engine for CoralNet. 3693-3702.

Chisholm JR (2000) Calcification by crustose coralline algae on the northern Great Barrier Reef, Australia. *Limnology and Oceanography,* **45**, 1476-1484.

Clarke LJ, Beard JM, Swadling KM, Deagle BE (2017) Effect of marker choice and thermal cycling protocol on zooplankton DNA metabarcoding studies. *Ecology and evolution,* **7**, 873-883.

Coker DJ, DiBattista JD, Sinclair-Taylor TH, Berumen ML (2018) Spatial patterns of cryptobenthic coral-reef fishes in the Red Sea. *Coral Reefs,* **37**, 193-199.

Coleman CO (2015) Taxonomy in times of the taxonomic impediment–examples from the community of experts on amphipod crustaceans. *Journal of Crustacean Biology,* **35**, 729-740.

Coles SL, Bolick H (2007) Invasive introduced sponge Mycale grandis overgrows reef corals in Kāne ʻohe Bay, O ʻahu, Hawai ʻi. *Coral Reefs,* **26**, 911.

Colin PL, Johnston TM (2020) Measuring Temperature in Coral Reef Environments: Experience, Lessons, and Results from Palau. *Journal of Marine Science and Engineering,* **8**, 680.

Coneo S, Escrigas SS, Ramirez PD, Urueña RG (2022) Nuevos registros de anélidos del banco de las Ánimas, Caribe colombiano: New records of annelids from banco de las Ánimas, Colombian Caribbean. *Boletín de Investigaciones Marinas y Costeras,* **51**, 9-36.

Cornwall CE, Comeau S, DeCarlo TM, et al (2020) A coralline alga gains tolerance to ocean acidification over multiple generations of exposure. *Nature Climate Change,* **10**, 143-146.

Cornwall C, Carlot J, Branson O, et al (2022) Increasing importance of crustose coralline algae to coral reef carbonate production under ongoing climate change.

Costello MJ (2015) Biodiversity: the known, unknown, and rates of extinction. *Current Biology,* **25**, R368-R371.

Costello MJ, Vanhoorne B, Appeltans W (2015) Conservation of biodiversity through taxonomy, data publication, and collaborative infrastructures. *Conservation Biology,* **29**, 1094-1099.

Costello MJ, Coll M, Danovaro R, Halpin P, Ojaveer H, Miloslavich P (2010) A census of marine biodiversity knowledge, resources, and future challenges. *PloS one,* **5**, e12110.

Cowart DA, Breedveld KG, Ellis MJ, Hull JM, Larson ER (2018) Environmental DNA (eDNA) applications for the conservation of imperiled crayfish (Decapoda: Astacidea) through monitoring of invasive species barriers and relocated populations. *Journal of Crustacean Biology,* **38**, 257-266.

Cox KD, Woods MB, Reimchen TE (2021) Regional heterogeneity in coral species richness and hue reveals novel global predictors of reef fish intra-family diversity. *Scientific reports,* **11**, 1-12.

Crane LC, Goldstein JS, Thomas DW, Rexroth KS, Watts AW (2021) Effects of life stage on eDNA detection of the invasive European green crab (*Carcinus maenas*) in estuarine systems. *Ecological Indicators,* **124**, 107412.

Crossland CJ, Hatcher BG, Smith SV (1991) Role of coral reefs in global ocean production. *Coral Reefs,* **10**, 55-64.

Cummings VJ, Beaumont J, Mobilia V, et al (2020) Responses of a common New Zealand coastal sponge to elevated suspended sediments: Indications of resilience. *Marine environmental research,* **155**, 104886.

Curnick DJ, Collen B, Koldewey HJ, Jones KE, Kemp KM, Ferretti F (2020) Interactions between a large marine protected area, pelagic tuna and associated fisheries. *Frontiers in Marine Science,* , 318.

D'Aloia CC, Majoris JE, Buston PM (2011) Predictors of the distribution and abundance of a tube sponge and its resident goby. *Coral Reefs,* **30**, 777-786.

Danziger AM, Frederich M (2022) Challenges in eDNA detection of the invasive European green crab, Carcinus maenas. *Biological Invasions,* **24**, 1881-1894.

Darling ES, Graham NA, Januchowski-Hartley FA, Nash KL, Pratchett MS, Wilson SK (2017) Relationships between structural complexity, coral traits, and reef fish assemblages. *Coral Reefs,* **36**, 561-575.

David R, Uyarra MC, Carvalho S, et al (2019) Lessons from photo analyses of Autonomous Reef Monitoring Structures as tools to detect (bio-) geographical, spatial, and environmental effects. *Marine pollution bulletin,* **141**, 420-429.

Davis KL, Colefax AP, Tucker JP, Kelaher BP, Santos IR (2021) Global coral reef ecosystems exhibit declining calcification and increasing primary productivity. *Communications Earth & Environment,* **2**, 1-10.

de Goeij JM, Van Duyl FC (2007) Coral cavities are sinks of dissolved organic carbon (DOC). *Limnology and Oceanography,* **52**, 2608-2617.

De Goeij JM, Van Oevelen D, Vermeij MJ, et al (2013) Surviving in a marine desert: the sponge loop retains resources within coral reefs. *Science,* **342**, 108-110.

DeCarlo TM, Carvalho S, Gajdzik L, et al (2021) Patterns, drivers, and ecological implications of upwelling in coral reef habitats of the southern Red Sea. *Journal of Geophysical Research: Oceans,* **126**, e2020JC016493.

Depczynski M, Bellwood DR (2003) The role of cryptobenthic reef fishes in coral reef trophodynamics. *Marine Ecology Progress Series,* **256**, 183-191.

Love MI, Huber W, Anders S (2014) Moderated estimation of fold change and dispersion for RNA-seq data with DESeq2.*Genome Biology*, **15**, 550.

Diaz-Pulido G, Anthony KR, Kline DI, Dove S, Hoegh-Guldberg O (2012) Interactions between ocean acidification and warming on the mortality and dissolution of coralline algae. *Journal of Phycology,* **48**, 32-39.

Diaz-Pulido G, Barrón C (2020) CO 2 enrichment stimulates dissolved organic carbon release in coral reef macroalgae. *Journal of Phycology,* **56**, 1039-1052.

Diaz MC, Rützler K (2001) Sponges: an essential component of Caribbean coral reefs. *Bulletin of Marine Science,* **69**, 535-546.

Díaz S, Fargione J, Chapin III FS, Tilman D (2006) Biodiversity loss threatens human well-being. *PLoS biology,* **4**, e277.

Duffy JE (1996) Species boundaries, specialization, and the radiation of sponge-dwelling alpheid shrimp. *Biological Journal of the Linnean Society,* **58**, 307-324.

Duffy JE, Hay ME (2000) Strong impacts of grazing amphipods on the organization of a benthic community. *Ecological Monographs,* **70**, 237-263.

Dunn N, Curnick D (2019) Using historical fisheries data to predict tuna distribution within the British Indian Ocean Territory Marine Protected Area, and implications for its management. *Aquatic Conservation: Marine and Freshwater Ecosystems,* **29**, 2057-2070.

Dunstan PK, Johnson CR (1998) Spatio-temporal variation in coral recruitment at different scales on Heron Reef, southern Great Barrier Reef. *Coral Reefs,* **17**, 71-81.

Dupont S, Thorndyke MC (2009) Impact of CO 2-driven ocean acidification on invertebrates early life-history–What we know, what we need to know and what we can do. *Biogeosciences Discussions,* **6**, 3109-3131.

Durrant H, Clark GF, Dworjanyn SA, Byrne M, Johnston EL (2013) Seasonal variation in the effects of ocean warming and acidification on a native bryozoan, *Celleporaria nodulosa*. *Marine Biology,* **160**, 1903-1911.

Elbrecht V, Peinert B, Leese F (2017) Sorting things out: Assessing effects of unequal specimen biomass on DNA metabarcoding. *Ecology and evolution,* **7**, 6918-6926.

Ellingsen KE, Yoccoz NG, Tveraa T, et al (2020) The rise of a marine generalist predator and the fall of beta diversity. *Global Change Biology,* **26**, 2897-2907.

Enochs IC, Manzello DP (2012) Species richness of motile cryptofauna across a gradient of reef framework erosion. *Coral Reefs,* **31**, 653-661.

Enochs IC, Toth LT, Brandtneris VW, Afflerbach JC, Manzello DP (2011) Environmental determinants of motile cryptofauna on an eastern Pacific coral reef. *Marine Ecology Progress Series,* **438**, 105-118.

Fabricius KE, De'ath G, Noonan S, Uthicke S (2014) Ecological effects of ocean acidification and habitat complexity on reef-associated macroinvertebrate communities. *Proceedings of the Royal Society B: Biological Sciences,* **281**, 20132479.

Fabricius K, De'ath G (2001) Environmental factors associated with the spatial distribution of crustose coralline algae on the Great Barrier Reef. *Coral Reefs,* **19**, 303-309.

Fernández-Aldecoa RG, Ladah LB, Morgan SG, Dibble CD, Solana-Arellano E, Filonov A (2019) Delivery of zooplankton to the surf zone during strong internal tidal forcing and onshore winds in Baja California. *Marine Ecology Progress Series,* **625**, 15-26.

Field SF, Bulina MY, Kelmanson IV, Bielawski JP, Matz MV (2006) Adaptive evolution of multicolored fluorescent proteins in reef-building corals. *Journal of Molecular Evolution,* **62**, 332-339.

Finelli CM, Helmuth BS, Pentcheff ND, Wethey DS (2006) Water flow influences oxygen transport and photosynthetic efficiency in corals. *Coral Reefs,* **25**, 47-57.

Fisher R, O'Leary RA, Low-Choy S, et al (2015) Species richness on coral reefs and the pursuit of convergent global estimates. *Current Biology,* **25**, 500-505.

Floyd M, Mizuyama M, Obuchi M, et al (2020) Functional diversity of reef molluscs along a tropical-to-temperate gradient. *Coral Reefs,* **39**, 1361-1376.

Folkers M, Rombouts T (2020) Sponges revealed: a synthesis of their overlooked ecological functions within aquatic ecosystems. In: *YOUMARES 9-The Oceans: Our Research, Our Future*, (Springer) 181-193.

Fong P, Paul VJ (2011) Coral reef algae. In: *Coral reefs: an ecosystem in transition*, (Springer) 241-272.

Forsström T, Vasemägi A (2016) Can environmental DNA (eDNA) be used for detection and monitoring of introduced crab species in the Baltic Sea? *Marine pollution bulletin,* **109**, 350-355.

Francis FT, Filbee-Dexter K, Yan HF, Côté IM (2019) Invertebrate herbivores: Overlooked allies in the recovery of degraded coral reefs? *Global Ecology and Conservation,* **17**, e00593.

Gaino E, Sara M (1994) Siliceous spicules of *Tethya seychellensis* (Porifera) support the growth of a green alga: a possible light conducting system. *Marine Ecology Progress Series,* **108**, 147-152.

Gao X, Lee JR, Park SK, Kim NG, Choi HG (2019) Detrimental effects of sediment on attachment, survival and growth of the brown alga Sargassum thunbergii in early life stages. *Phycological Research,* **67**, 77-81.

García-Hernández JE, Hammerman NM, Cruz-Motta JJ, Schizas NV (2019) Associated organisms inhabiting the calcareous sponge Clathrina lutea in La Parguera, Puerto Rico. *Caribbean Journal of Science,* **49**, 239-254.

Gelis ERE, Kamal MM, Subhan B, Bachtiar I, Sani LMI, Madduppa H (2021) Environmental biomonitoring of reef fish community structure with eDNA metabarcoding in the Coral Triangle. *Environmental Biology of Fishes,* **104**, 887-903.

Gelman A, Hill J (2006) Data analysis using regression and multilevel/hierarchical models. Cambridge University Press.

Giachini Tosetto E, Bertrand A, Neumann-Leitão S, Nogueira Júnior M (2022) The Amazon River plume, a barrier to animal dispersal in the Western Tropical Atlantic. *Scientific reports,* **12**, 1-12.

Gibson R, Atkinson R, Gordon J, Smith I, Hughes D (2011) Coral-associated invertebrates: diversity, ecological importance and vulnerability to disturbance. *Oceanogr.Mar.Biol,* **49**, 43-104.

Ginsburg RN (1983) Geological and biological roles of cavities in coral reefs. *Perspectives on coral reefs. Australian Institute of Marine Science, Townsville,* 148-153.

Glynn PW, Enochs IC (2011) Invertebrates and their roles in coral reef ecosystems. *Coral reefs: an ecosystem in transition,* (Springer) 273-325.

Glynn PW, Manzello DP (2015) Bioerosion and coral reef growth: a dynamic balance. In: *Coral reefs in the Anthropocene*, (Springer) 67-97.

Goldberg CS, Turner CR, Deiner K, et al (2016) Critical considerations for the application of environmental DNA methods to detect aquatic species. *Methods in ecology and evolution,* **7**, 1299-1307.

Goldberg WM (2013) *The biology of reefs and reef organisms* University of Chicago Press.

Gómez-Lemos LA, Doropoulos C, Bayraktarov E, Diaz-Pulido G (2018) Coralline algal metabolites induce settlement and mediate the inductive effect of epiphytic microbes on coral larvae. *Scientific reports,* **8**, 1-11.

Gonzalez-Rivero M, Beijbom O, Rodriguez-Ramirez A, et al (2020) Monitoring of coral reefs using artificial intelligence: A feasible and cost-effective approach. *Remote Sensing,* **12**, 489.

Goreau TF, Hartman WD (1966) Sponge: effect on the form of reef corals. *Science,* **151**, 343-344.

Gouezo M, Olsudong D, Fabricius K, Harrison P, Golbuu Y, Doropoulos C (2020) Relative roles of biological and physical processes influencing coral recruitment during the lag phase of reef community recovery. *Scientific reports,* **10**, 1-12.

Gove JM, Williams GJ, McManus MA, Clark SJ, Ehses JS, Wedding LM (2015) Coral reef benthic regimes exhibit non-linear threshold responses to natural physical drivers. *Marine Ecology Progress Series,* **522**, 33-48.

Graham NA, Wilson SK, Carr P, Hoey AS, Jennings S, MacNeil MA (2018) Seabirds enhance coral reef productivity and functioning in the absence of invasive rats. *Nature,* **559**, 250-253.

Gratwicke B, Speight MR (2005) Effects of habitat complexity on Caribbean marine fish assemblages. *Marine Ecology Progress Series,* **292**, 301-310.

Guan Y, Hohn S, Merico A (2015) Suitable environmental ranges for potential coral reef habitats in the tropical ocean. *PloS one,* **10**, e0128831.

Guillemot N, Kulbicki M, Chabanet P, Vigliola L (2011) Functional redundancy patterns reveal non-random assembly rules in a species-rich marine assemblage. *PloS one,* **6**, e26735.

Harriott VJ, Fisk DA (1987) A comparison of settlement plate types for experiments on the recruitment of scleractinian corals. *Mar Ecol Prog Ser,* **37**, 201-208.

Harris JL, Hosegood P, Robinson E, Embling CB, Hilbourne S, Stevens GM (2021) Fine-scale oceanographic drivers of reef manta ray (Mobula alfredi) visitation patterns at a feeding aggregation site. *Ecology and Evolution,* **11**, 4588-4604.

Harrison JB, Sunday JM, Rogers SM (2019) Predicting the fate of eDNA in the environment and implications for studying biodiversity. *Proceedings of the Royal Society B,* **286**, 20191409.

Harrison PL, Wallace CC (1990) Reproduction, dispersal and recruitment of scleractinian corals. *Ecosystems of the world,* **25**, 133-207.

Hays GC, Koldewey HJ, Andrzejaczek S, et al (2020) A review of a decade of lessons from one of the world's largest MPAs: conservation gains and key challenges. *Marine Biology,* **167**, 1-22.

Hazeri G, Rahayu DL, Subhan B, et al (2019) Latitudinal species diversity and density of cryptic crustacean (Brachyura and Anomura) in micro-habitat Autonomous Reef Monitoring Structures across Kepulauan Seribu, Indonesia. *Biodiversitas Journal of Biological Diversity,* **20**.

He Q, Silliman BR (2019) Climate change, human impacts, and coastal ecosystems in the Anthropocene. *Current Biology,* **29**, 1021-1035.

Head CE, Bayley DT, Rowlands G, et al (2019) Coral bleaching impacts from back-to-back 2015–2016 thermal anomalies in the remote central Indian Ocean. *Coral Reefs,* **38**, 605-618.

Head CE, Bonsall MB, Jenkins TL, et al (2018) Exceptional biodiversity of the cryptofaunal decapods in the Chagos Archipelago, central Indian Ocean. *Marine Pollution Bulletin,* **135**, 636-647.

Head CE, Bonsall MB, Koldewey H, Pratchett MS, Speight M, Rogers AD (2015) High prevalence of obligate coral-dwelling decapods on dead corals in the Chagos Archipelago, central Indian Ocean. *Coral Reefs,* **34**, 905-915.

Henkel TP, Pawlik JR (2011) Host specialization of an obligate sponge-dwelling brittlestar. *Aquatic Biology,* **12**, 37-46.

Hestetun JT, Bye-Ingebrigtsen E, Nilsson RH, Glover AG, Johansen P, Dahlgren TG (2020) Significant taxon sampling gaps in DNA databases limit the operational use of marine macrofauna metabarcoding. *Marine Biodiversity,* **50**, 1-9.

Higgins E, Metaxas A, Scheibling RE (2022) A systematic review of artificial reefs as platforms for coral reef research and conservation. *PloS one,* **17**, e0261964.

Higgins E, Scheibling RE, Desilets KM, Metaxas A (2019) Benthic community succession on artificial and natural coral reefs in the northern Gulf of Aqaba, Red Sea. *PloS one,* **14**, e0212842.

Hleap JS, Littlefair JE, Steinke D, Hebert PD, Cristescu ME (2021) Assessment of current taxonomic assignment strategies for metabarcoding eukaryotes. *Molecular Ecology Resources,* **21**, 2190-2203.

Ho M, Carpenter RC (2017) Differential growth responses to water flow and reduced pH in tropical marine macroalgae. *Journal of experimental marine biology and ecology,* **491**, 58-65.

Ho M, McBroom J, Bergstrom E, Diaz-Pulido G (2021) Physiological responses to temperature and ocean acidification in tropical fleshy macroalgae with varying affinities for inorganic carbon. *ICES Journal of Marine Science,* **78**, 89-100.

Hu Y, Beggs H, Wang XH (2021) Intercomparison of high-resolution SST climatologies over the Australian region. *Journal of Geophysical Research: Oceans,* **126**, e2021JC017221.

Hughes TP, Baird AH, Bellwood DR, et al (2003) Climate change, human impacts, and the resilience of coral reefs. *Science,* **301**, 929-933.

Hughes TP, Barnes ML, Bellwood DR, et al (2017) Coral reefs in the Anthropocene. *Nature,* **546**, 82-90.

Hughes TP, Bellwood DR, Connolly SR (2002) Biodiversity hotspots, centres of endemicity, and the conservation of coral reefs. *Ecology Letters,* **5**, 775-784.

Hulsen T, de Vlieg J, Alkema W (2008) BioVenn–a web application for the comparison and visualization of biological lists using area-proportional Venn diagrams. *BMC genomics,* **9**, 1-6.

Hurley KK, Timmers MA, Godwin LS, Copus JM, Skillings DJ, Toonen RJ (2016) An assessment of shallow and mesophotic reef brachyuran crab assemblages on the south shore of O ʻahu, Hawai ʻi. *Coral Reefs,* **35**, 103-112.

Ip YCA, Chang JJM, Oh RM, et al (2022) Seq'and ARMS shall find: DNA (meta) barcoding of Autonomous Reef Monitoring Structures across the tree of life uncovers hidden cryptobiome of tropical urban coral reefs. *Molecular ecology,* **0**, 1-20.

IPCC (2022). Climate change 2022: Mitigation of climate change. In *Contribution of Working Group III to the Sixth Assessment Report of the Intergovernmental Panel on Climate Change* (Cambridge: Cambridge University Press)

Jackson J, Winston JE (1982) Ecology of cryptic coral reef communities. I. Distribution and abundance of major groups of encrusting organisms. *Journal of experimental marine biology and ecology,* **57**, 135-147.

Jackson JB, Hughes TP (1985) Adaptive strategies of coral-reef invertebrates: coral-reef environments that are regularly disturbed by storms and by predation often favor the very organisms most susceptible to damage by these processes. *American Scientist,* **73**, 265-274.

Januchowski-Hartley FA, Graham NA, Wilson SK, Jennings S, Perry CT (2017) Drivers and predictions of coral reef carbonate budget trajectories. *Proceedings of the Royal Society B: Biological Sciences,* **284**, 20162533.

Johnson MD, Price NN, Smith JE (2022) Calcification accretion units (CAUs): A standardized approach for quantifying recruitment and calcium carbonate accretion in marine habitats. *Methods in Ecology and Evolution,* **13**, 1436-1446.

Josefson AB (2016) Species sorting of benthic invertebrates in a salinity gradient–importance of dispersal limitation. *PLoS One,* **11**, e0168908.

Kahn AS, Yahel G, Chu JW, Tunnicliffe V, Leys SP (2015) Benthic grazing and carbon sequestration by deep-water glass sponge reefs. *Limnology and Oceanography,* **60**, 78-88.

Kennedy EV, Ordoñez A, Lewis BE, Diaz-Pulido G (2017) Comparison of recruitment tile materials for monitoring coralline algae responses to a changing climate. *Marine Ecology Progress Series,* **569**, 129-144.

Klumpp DW, McKinnon AD, Mundy CN (1988) Motile cryptofauna of a coral reef: Abundance, distribution and trophic potential. *Marine Ecology Progress Series,* **45**, 95-108.

Klumpp DW, Pulfrich A (1989) Trophic significance of herbivorous macroinvertebrates on the central Great Barrier Reef. *Coral Reefs,* **8**, 135-144.

Knowlton N, Brainard RE, Fisher R, Moews M, Plaisance L, Caley MJ (2010) Coral reef biodiversity. *Life in the world's oceans: diversity distribution and abundance,* 65-74.

Knowlton N, Jackson JBC (2008) Shifting baselines, local impacts, and global change on coral reefs. *PLoS biology,* **6**, e54.

Kobluk DR (1988) Cryptic faunas in reefs: ecology and geologic importance. *Palaios,* 379-390.

Koldewey HJ, Curnick D, Harding S, Harrison LR, Gollock M (2010) Potential benefits to fisheries and biodiversity of the Chagos Archipelago/British Indian Ocean Territory as a no-take marine reserve. *Marine pollution bulletin,* **60**, 1906-1915.

Koldewey H, Atchison-Balmond N, Graham N, et al (2021) Key climate change effects on the coastal and marine environment around the Indian Ocean UK Overseas Territories. *MCCIP Science Review 2021,* 2.

Komai T, Gotoh RO, Sado T, Miya M (2019) Development of a new set of PCR primers for eDNA metabarcoding decapod crustaceans. *Metabarcoding and Metagenomics,* **3**, e33835.

Kornder NA, Cappelletto J, Mueller B, et al (2021) Implications of 2D versus 3D surveys to measure the abundance and composition of benthic coral reef communities. *Coral Reefs,* 1-17.

Kovalenko KE, Thomaz SM, Warfe DM (2012) Habitat complexity: approaches and future directions. *Hydrobiologia,* **685**, 1-17.

Kramer MJ, Bellwood DR, Bellwood O (2014) Benthic Crustacea on coral reefs: a quantitative survey. *Marine Ecology Progress Series,* **511**, 105-116.

Kramer MJ, Bellwood O, Bellwood DR (2013) The trophic importance of algal turfs for coral reef fishes: the crustacean link. *Coral Reefs,* **32**, 575-583.

Kriegisch N, Reeves SE, Johnson CR, Ling SD (2019) Top-down sea urchin overgrazing overwhelms bottom-up stimulation of kelp beds despite sediment enhancement. *Journal of Experimental Marine Biology and Ecology,* **514**, 48-58.

Kroeker KJ, Micheli F, Gambi MC (2013) Ocean acidification causes ecosystem shifts via altered competitive interactions. *Nature Climate Change,* **3**, 156-159.

Kubicek A, Breckling B, Hoegh-Guldberg O, Reuter H (2019) Climate change drives trait-shifts in coral reef communities. *Scientific Reports,* **9**, 1-10.

Lange ID, Benkwitt CE, McDevitt-Irwin JM, et al (2021) Wave exposure shapes reef community composition and recovery trajectories at a remote coral atoll. *Coral Reefs,* **40**, 1819-1829.

Lange ID, Perry CT (2019) Bleaching impacts on carbonate production in the Chagos Archipelago: influence of functional coral groups on carbonate budget trajectories. *Coral Reefs,* **38**, 619-624.

Lange ID, Perry CT, Alvarez-Filip L (2020) Carbonate budgets as indicators of functional reef "health": A critical review of data underpinning census-based methods and current knowledge gaps. *Ecological Indicators,* **110**, 105857.

Lange ID, Perry CT, Stuhr M (2022) Recovery trends of reef carbonate budgets at remote coral atolls 6 years post-bleaching. *Limnology and Oceanography.*

Leduc N, Lacoursière-Roussel A, Howland KL, et al (2019) Comparing eDNA metabarcoding and species collection for documenting Arctic metazoan biodiversity. *Environmental DNA,* **1**, 342-358.

Leichter JJ, Shellenbarger G, Genovese SJ, Wing SR (1998) Breaking internal waves on a Florida (USA) coral reef: a plankton pump at work? *Marine Ecology Progress Series,* **166**, 83-97.

Leonard C, Hédouin L, Lacorne MC, et al (2022) Performance of innovative materials as recruitment substrates for coral restoration. *Restoration Ecology,* e13625.

Leray M, Ho S, Lin I, Machida RJ (2018) MIDORI server: a webserver for taxonomic assignment of unknown metazoan mitochondrial-encoded sequences using a curated database. *Bioinformatics,* **34**, 3753-3754.

Leray M, Knowlton N (2016) Censusing marine eukaryotic diversity in the twenty-first century. *Philosophical Transactions of the Royal Society B: Biological Sciences,* **371**, 20150331.

Leray M, Knowlton N (2015) DNA barcoding and metabarcoding reveal patterns of diversity in cryptic benthic communities. *Proceedings of the National Academy of Sciences,* **112**, 2076-2081.

Leray M, Yang JY, Meyer CP, et al (2013) A new versatile primer set targeting a short fragment of the mitochondrial COI region for metabarcoding metazoan diversity: application for characterizing coral reef fish gut contents. *Frontiers in Zoology,* **10**, 1-14.

Lesser MP (2006) Benthic–pelagic coupling on coral reefs: feeding and growth of Caribbean sponges. *Journal of Experimental Marine Biology and Ecology,* **328**, 277-288.

Lesser MP, Slattery M, Leichter JJ (2009) Ecology of mesophotic coral reefs. *Journal of Experimental Marine Biology and Ecology,* **375**, 1-8.

Levy N, Simon-Blecher N, Ben-Ezra S, et al (2023) Evaluating biodiversity for coral reef reformation and monitoring on complex 3D structures using environmental DNA (eDNA) metabarcoding. *Science of The Total Environment,* **856**, 159051.

Lindhart M, Monismith SG, Khrizman A, Mucciarone D, Dunbar R (2021) How consistent are estimates of roughness parameters on a rough coral reef? *Journal of Geophysical Research: Oceans,* **126**, e2021JC017825.

Littler MM, Littler DS (2013) The nature of crustose coralline algae and their interactions on reefs. *Research and discoveries: the revolution of science through SCUBA.*199.

Littler MM, Littler DS (1995) A colonial tunicate smothers corals and coralline algae on the Great Astrolabe Reef, Fiji. *Coral Reefs,* **14**, 148-149.

Liu G, Matrosova LE, Penland C, et al (2008) NOAA Coral Reef Watch coral bleaching outlook system. 951-955.

Logan A, Mathers SM, Thomas M (1984) Sessile invertebrate coelobite communities from reefs of Bermuda: species composition and distribution. *Coral Reefs,* **2**, 205-213.

Loh T, Pawlik JR (2014) Chemical defenses and resource trade-offs structure sponge communities on Caribbean coral reefs. *Proceedings of the National Academy of Sciences,* **111**, 4151-4156.

Lombardi C, Taylor PD, Cocito S (2020) Bryozoans: The 'forgotten' bioconstructors. In: *Perspectives on the Marine Animal Forests of the World*, (Springer), 193-217.

Longenecker K (2021) First record of two sublittoral amphipods from Hawai 'i. *Marine Biodiversity Records,* **14**, 1-4.

Longenecker K (2022) A new species of Mesanthura Barnard (Isopoda, Cymothoida, Anthuridae) from the Hawaiian Islands.

Longenecker K, Myers A (2021) New species of Bemlos Shoemaker (Amphipoda, Senticaudata, Aoridae) from the Hawaiian Islands and Madagascar.

Lopes AR, Faleiro F, Rosa IC, et al (2018) Physiological resilience of a temperate soft coral to ocean warming and acidification. *Cell Stress and Chaperones,* **23**, 1093-1100.

Luong J, Glick P, Ong A, et al (2019) Eversion and retraction of a soft robot towards the exploration of coral reefs. In *2019 2nd IEEE International Conference on Soft Robotics (RoboSoft)* 801-807.

Luter HM, Duckworth AR, Wolff CW, Evans-Illidge E, Whalan S (2016) Recruitment variability of coral reef sessile communities of the far north Great Barrier Reef. *PLoS One,* **11**, e0153184.

Lyons KG, Brigham CA, Traut BH, Schwartz MW (2005) Rare species and ecosystem functioning. *Conservation Biology,* **19**, 1019-1024.

Macdonald III KS, Ríos R, Duffy JE (2006) Biodiversity, host specificity, and dominance by eusocial species among sponge-dwelling alpheid shrimp on the Belize Barrier Reef. *Diversity and Distributions,* **12**, 165-178.

Maestro M, Pérez-Cayeiro ML, Chica-Ruiz JA, Reyes H (2019) Marine protected areas in the 21st century: Current situation and trends. *Ocean & Coastal Management,* **171**, 28-36.

Makiola A, Compson ZG, Baird DJ, et al (2020) Key questions for next-generation biomonitoring. *Frontiers in Environmental Science,* **7**, 197.

Maldonado M (2016) Sponge waste that fuels marine oligotrophic food webs: a re-assessment of its origin and nature. *Marine Ecology,* **37**, 477-491.

Maldonado M, Giraud K, Carmona C (2008) Effects of sediment on the survival of asexually produced sponge recruits. *Marine Biology,* **154**, 631-641.

Mallela J (2007) Coral reef encruster communities and carbonate production in cryptic and exposed coral reef habitats along a gradient of terrestrial disturbance. *Coral Reefs,* **26**, 775-785.

Mallela J (2018) The influence of micro-topography and external bioerosion on coral-reef-building organisms: recruitment, community composition and carbonate production over time. *Coral Reefs,* **37**, 227-237.

Mallela J (2013) Calcification by reef-building sclerobionts. *PLoS One,* **8**, e60010.

Mallela J, Milne BC, Martinez-Escobar D (2017) A comparison of epibenthic reef communities settling on commonly used experimental substrates: PVC versus ceramic tiles. *Journal of experimental marine biology and ecology,* **486**, 290-295.

Marcelino VR, Verbruggen H (2016) Multi-marker metabarcoding of coral skeletons reveals a rich microbiome and diverse evolutionary origins of endolithic algae. *Scientific Reports,* **6**, 1-9.

McCloskey LR (1970) The dynamics of the community associated with a marine scleractinian coral. *Internationale Revue der gesamten Hydrobiologie und Hydrographie,* **55**, 13-81.

McElroy ME, Dressler TL, Titcomb GC, et al (2020) Calibrating environmental DNA metabarcoding to conventional surveys for measuring fish species richness. *Frontiers in Ecology and Evolution,* **8**, 276.

McGill BJ (2010) Matters of scale. *Science,* **328**, 575-576.

McMurdie PJ, Holmes S (2014) Waste not, want not: why rarefying microbiome data is inadmissible. *PLoS Computational Biology,* **10**, e1003531.

McMurdie PJ, Holmes S (2013) phyloseq: an R package for reproducible interactive analysis and graphics of microbiome census data. *PloS one,* **8**, e61217.

Meesters E, Knijn R, Willemsen P, Pennartz R, Roebers G, van Soest Rv (1991) Sub-rubble communities of Curaçao and Bonaire coral reefs. *Coral Reefs,* **10**, 189-197.

Menegotto A, Dambros CS, Netto SA (2019) The scale-dependent effect of environmental filters on species turnover and nestedness in an estuarine benthic community. *Ecology,* **100**, e02721.

Meyer C, Davies N, Meyer J, Moritz C, Planes S, Roderick G (2006) The Moorea Biocode Project. S1-B.

Middelfart PU, Kirkendale LA, Wilson NG (2016) Australian tropical marine micromolluscs: an overwhelming bias. *Diversity,* **8**, 17.

Miloslavich P, Bax NJ, Simmons SE, et al (2018) Essential ocean variables for global sustained observations of biodiversity and ecosystem changes. *Global Change Biology,* **24**, 2416-2433.

Miyazawa E, Montilla LM, Agudo-Adriani EA, Ascanio A, Mariño-Briceño G, Croquer A (2020) On the importance of spatial scales on beta diversity of coral assemblages: a study from Venezuelan coral reefs. *PeerJ,* **8**, e9082.

Moews-Asher M, Castor CB, Reardon K, Timmers MA (2018) Field Guide to Cryptic Marine Invertebrates of the Philippines: A Sample of Biodiversity from Autonomous Reef Monitoring Structures.

Molodtsova TN, Britayev TA, Martin D (2016) Cnidarians and their polychaete symbionts. In: *The Cnidaria, past, present and future*, (Springer) 387-413.

Monroy-Velázquez LV, Rodríguez-Martínez RE, Blanchon P, Alvarez F (2020) The use of artificial substrate units to improve inventories of cryptic crustacean species on Caribbean coral reefs. *PeerJ,* **8**, e10389.

Mortimer JA, Esteban N, Guzman AN, Hays GC (2020) Estimates of marine turtle nesting populations in the south-west Indian Ocean indicate the importance of the Chagos Archipelago. *Oryx,* **54**, 332-343.

Mortimer, J.A. & Donnelly, M. (2008) *Eretmochelys imbricata*. In The IUCN Red List of Threatened Species. [accessed 6 January 2023]

Mouillot D, Bellwood DR, Baraloto C, et al (2013) Rare species support vulnerable functions in high-diversity ecosystems. *PLoS biology,* **11**, e1001569.

Muldrow M, Parsons E, Jonas R (2020) Shifting baseline syndrome among coral reef scientists. *Humanities and Social Sciences Communications,* **7**, 1-8.

Mundy CN (2000) An appraisal of methods used in coral recruitment studies. *Coral Reefs,* **19**, 124-131.

Murali A, Bhargava A, Wright ES (2018) IDTAXA: a novel approach for accurate taxonomic classification of microbiome sequences. *Microbiome,* **6**, 1-14.

Natural History Museum (2014). *Specimens* (from *Collection specimens*) [Data set resource]. Natural History Museum. https://data.nhm.ac.uk/dataset/collection-specimens/resource/05ff2255-c38a-40c9-b657-4ccb55ab2feb

Nash KL, Graham NA, Wilson SK, Bellwood DR (2013) Cross-scale habitat structure drives fish body size distributions on coral reefs. *Ecosystems,* **16**, 478-490.

Nelson HR, Altieri AH (2019) Oxygen: the universal currency on coral reefs. *Coral Reefs,* **38**, 177-198.

Neo ML, Eckman W, Vicentuan K, Teo SL, Todd PA (2015) The ecological significance of giant clams in coral reef ecosystems. *Biological Conservation,* **181**, 111-123.

Nguyen BN, Shen EW, Seemann J, et al (2020) Environmental DNA survey captures patterns of fish and invertebrate diversity across a tropical seascape. *Scientific Reports,* **10**, 1-14.

Nichols PK, Timmers M, Marko PB (2021) Hide 'n seq: Direct versus indirect metabarcoding of coral reef cryptic communities. *Environmental DNA,* **4**, 93-107.

Nichols RV, Vollmers C, Newsom LA, et al (2018) Minimizing polymerase biases in metabarcoding. *Molecular Ecology Resources,* **18**, 927-939.

Obst M, Exter K, Allcock AL, et al (2020) A marine biodiversity observation network for genetic monitoring of hard-bottom communities (ARMS-MBON). *Frontiers in Marine Science,* **7**, 1031.

Obura DO, Aeby G, Amornthammarong N, et al (2019) Coral reef monitoring, reef assessment technologies, and ecosystem-based management. *Frontiers in Marine Science,* **6**, 580.

Oksanen J, Blanchet FG, Kindt R, et al (2013) Package 'vegan'. *Community ecology package, version,* **2**, 1-295.

Osman RW, Whitlatch RB (2004) The control of the development of a marine benthic community by predation on recruits. *Journal of experimental marine biology and ecology,* **311**, 117-145.

Paknia O, Koch A (2015) Lack of well-maintained natural history collections and taxonomists in megadiverse developing countries hampers global biodiversity exploration. *Organisms Diversity & Evolution,* **15**, 619-629.

Palmer CV, Modi CK, Mydlarz LD (2009) Coral Fluorescent Proteins as Antioxidants. *PLOS ONE,* **4**, e7298.

Palomino-Alvarez LA, Vital XG, Castillo-Cupul RE, et al (2021) Evaluation of the Use of Autonomous Reef Monitoring Structures (ARMS) for Describing the Species Diversity of Two Coral Reefs in the Yucatan Peninsula, Mexico. *Diversity,* **13**, 579.

Pan X, Wong GT, DeCarlo TM, Tai J, Cohen AL (2017) Validation of the remotely sensed nighttime sea surface temperature in the shallow waters at the Dongsha Atoll. *Terrestrial, Atmospheric and Oceanic Sciences,* **28**, 517-524.

Pawka SS (1983) Island shadows in wave directional spectra. *Journal of Geophysical Research: Oceans,* **88**, 2579-2591.

Pawlik JR, Loh T, McMurray SE, Finelli CM (2013) Sponge communities on Caribbean coral reefs are structured by factors that are top-down, not bottom-up. *PLoS One,* **8**, e62573.

Pawlik JR, McMurray SE (2020) The emerging ecological and biogeochemical importance of sponges on coral reefs. *Annual Review of Marine Science,* **12**, 315-337.

Pearman JK, Anlauf H, Irigoien X, Carvalho S (2016) Please mind the gap – Visual census and cryptic biodiversity assessment at central Red Sea coral reefs. *Marine Environmental Research,* **118**, 20-30.

Pearman JK, Aylagas E, Voolstra CR, Anlauf H, Villalobos R, Carvalho S (2019) Disentangling the complex microbial community of coral reefs using standardized Autonomous Reef Monitoring Structures (ARMS). *Molecular Ecology,* **28**, 3496-3507.

Pearman JK, Chust G, Aylagas E, et al (2020) Pan-regional marine benthic cryptobiome biodiversity patterns revealed by metabarcoding Autonomous Reef Monitoring Structures. *Molecular Ecology,* **29**, 4882-4897.

Pearman JK, Leray M, Villalobos R, et al (2018) Cross-shelf investigation of coral reef cryptic benthic organisms reveals diversity patterns of the hidden majority. *Scientific Reports,* **8**, 1-17.

Peck LS, Clark MS, Power D, Reis J, Batista FM, Harper EM (2015) Acidification effects on biofouling communities: winners and losers. *Global Change Biology,* **21**, 1907-1913.

Pecquet A, Dorey N, Chan KYK (2017) Ocean acidification increases larval swimming speed and has limited effects on spawning and settlement of a robust fouling bryozoan, Bugula neritina. *Marine Pollution Bulletin,* **124**, 903-910.

Pennesi C, Danovaro R (2017) Assessing marine environmental status through microphytobenthos assemblages colonizing the Autonomous Reef Monitoring Structures (ARMS) and their potential in coastal marine restoration. *Marine Pollution Bulletin,* **125**, 56-65.

Pereira HM, Ferrier S, Walters M, et al (2013) Essential biodiversity variables. *Science,* **339**, 277-278.

Perry CT, Morgan KM (2017) Bleaching drives collapse in reef carbonate budgets and reef growth potential on southern Maldives reefs. *Scientific reports,* **7**, 1-9.

Pilly SS, Richardson LE, Turner JR, Roche RC (2022) Atoll-dependent variation in depth zonation of benthic communities on remote reefs. *Marine environmental research,* **173**, 105520.

Pistevos JC, Calosi P, Widdicombe S, Bishop JD (2011) Will variation among genetic individuals influence species responses to global climate change? *Oikos,* **120**, 675-689.

Plaisance L, Caley MJ, Brainard RE, Knowlton N (2011) The diversity of coral reefs: what are we missing? *PloS one,* **6**, e25026.

Plaisance L, Matterson K, Fabricius K, Drovetski S, Meyer C, Knowlton N (2021) Effects of low pH on the coral reef cryptic invertebrate communities near CO2 vents in Papua New Guinea. *Plos one,* **16**, e0258725.

Polanco Fernández A, Marques V, Fopp F, et al (2021) Comparing environmental DNA metabarcoding and underwater visual census to monitor tropical reef fishes. *Environmental DNA,* **3**, 142-156.

Porzio L, Buia MC, Hall-Spencer JM (2011) Effects of ocean acidification on macroalgal communities. *Journal of Experimental Marine Biology and Ecology,* **400**, 278-287.

Pratchett MS (2001) Influence of coral symbionts on feeding preferences of crown-of-thorns starfish Acanthaster planci in the western Pacific. *Marine Ecology Progress Series,* **214**, 111-119.

Price A, Harris A, Mcgowan A, Venkatachalam AJ, Sheppard C (2010) Chagos feels the pinch: assessment of holothurian (sea cucumber) abundance, illegal harvesting and conservation prospects in British Indian Ocean Territory. *Aquatic Conservation: Marine and Freshwater Ecosystems,* **20**, 117-126.

Quast C, Pruesse E, Yilmaz P, et al (2012) The SILVA ribosomal RNA gene database project: improved data processing and web-based tools. *Nucleic acids research,* **41**, D590-D596.

R Core Team (2022) R: A language and environment for statistical computing (Vienna, Austria: R Foundation for Statistical Computing). Available at: https://www.R-project.org/.

Randall CJ, Giuliano C, Heyward AJ, Negri AP (2021) Enhancing coral survival on deployment devices with microrefugia. *Frontiers in Marine Science,* , 478.

Ransome E, Geller JB, Timmers M, et al (2017) The importance of standardization for biodiversity comparisons: A case study using autonomous reef monitoring structures (ARMS) and metabarcoding to measure cryptic diversity on Mo'orea coral reefs, French Polynesia. *PloS one,* **12**, e0175066.

Reaka-Kudla ML (1997) The global biodiversity of coral reefs: a comparison with rain forests. *Biodiversity II: Understanding and protecting our biological resources,* **2**, 551.

Reid BN, Servis JA, Timmers M, Rohwer F, Naro-Maciel E (2022) 18S rDNA amplicon sequence data (V1–V3) of the Palmyra Atoll National Wildlife Refuge, Central Pacific. *Metabarcoding and Metagenomics,* **6**, e78762.

Reid EC, DeCarlo TM, Cohen AL, et al (2019) Internal waves influence the thermal and nutrient environment on a shallow coral reef. *Limnology and Oceanography,* **64**, 1949-1965.

Reverter M, Helber SB, Rohde S, de Goeij JM, Schupp PJ (2022) Coral reef benthic community changes in the Anthropocene: Biogeographic heterogeneity, overlooked configurations, and methodology. *Global Change Biology,* **28**, 1956-1971.

Richards ZT, Stat M, Heydenrych M, DiBattista JD (2022) Environmental DNA for Biodiversity Monitoring of Coral Reefs. In: *Coral Reef Conservation and Restoration in the Omics Age,* (Springer) 203-224.

Richardson RT, Bengtsson-Palme J, Gardiner MM, Johnson RM (2018) A reference cytochrome c oxidase subunit I database curated for hierarchical classification of arthropod metabarcoding data. *PeerJ,* **6**, e5126.

Richter C, Wunsch M, Rasheed M, KoÈtter I, Badran MI (2001) Endoscopic exploration of Red Sea coral reefs reveals dense populations of cavity-dwelling sponges. *Nature,* **413**, 726-730.

Ripley B, Venables B, Bates DM, et al (2013) Package 'mass'. *Cran r,* **538**, 113-120.

Rix L, de Goeij JM, Mueller CE, et al (2016) Coral mucus fuels the sponge loop in warm-and cold-water coral reef ecosystems. *Scientific reports,* **6**, 1-11.

Roche RC, Pratchett MS, Carr P, et al (2015) Localized outbreaks of *Acanthaster planci* at an isolated and unpopulated reef atoll in the Chagos Archipelago. *Marine Biology,* **162**, 1695-1704.

Rodolfo-Metalpa R, Lombardi C, Cocito S, Hall-Spencer JM, Gambi MC (2010) Effects of ocean acidification and high temperatures on the bryozoan *Myriapora truncata* at natural CO2 vents. *Marine Ecology,* **31**, 447-456.

Rodriguez SR, Ojeda FP, Inestrosa NC (1993) Settlement of benthic marine invertebrates. *Marine Ecology Progress Series,* **97**, 193-207.

Roth F, Wild C, Carvalho S, et al (2019) An *in situ* approach for measuring biogeochemical fluxes in structurally complex benthic communities. *Methods in Ecology and Evolution,* **10**, 712-725.

Roth SK, Powell A, Smith DJ, Roth F, Schierwater B (2018) The highly competitive ascidian *Didemnum sp.* threatens coral reef communities in the Wakatobi Marine National Park, Southeast Sulawesi, Indonesia. *Regional Studies in Marine Science,* **24**, 48-54.

Rothans TC, Miller AC (1991) A link between biologically imported particulate organic nutrients and the detritus food web in reef communities. *Marine Biology,* **110**, 145-150.

Safaie A, Silbiger NJ, McClanahan TR, et al (2018) High frequency temperature variability reduces the risk of coral bleaching. *Nature communications,* **9**, 1-12.

Salinas-de-León P, Costales-Carrera A, Zeljkovic S, Smith DJ, Bell JJ (2011) Scleractinian settlement patterns to natural cleared reef substrata and artificial settlement panels on an Indonesian coral reef. *Estuarine, Coastal and Shelf Science,* **93**, 80-85.

Samoilys M, Roche R, Koldewey H, Turner J (2018) Patterns in reef fish assemblages: Insights from the Chagos Archipelago. *PloS one,* **13**, e0191448.

Sanabria-Fernandez JA, Lazzari N, Riera R, Becerro MA (2018) Building up marine biodiversity loss: artificial substrates hold lower number and abundance of low occupancy benthic and sessile species. *Marine environmental research,* **140**, 190-199.

Scheffers SR, de Goeij J, van Duyl FC, Bak RP (2003) The cave-profiler: a simple tool to describe the 3-D structure of inaccessible coral reef cavities. *Coral Reefs,* **22**, 49-53.

Scheffers SR, Van Soest RW, Nieuwland G, Bak RP (2010) Coral reef framework cavities: Is functional similarity reflected in composition of the cryptic macrofaunal community? *Atoll Research Bulletin,* **583**, 1-24.

Schleussner C, Deryng D, D'haen S, et al (2018) 1.5 C hotspots: climate hazards, vulnerabilities, and impacts. *Annual Review of Environment and Resources,* **43**, 135-163.

Schönberg C, Ortiz JC (2008) Is sponge bioerosion increasing. **8**, 7-11.

Schott FA, Xie S, McCreary Jr JP (2009) Indian Ocean circulation and climate variability. *Reviews of Geophysics,* **47**.

Sepulveda AJ, Schabacker J, Smith S, Al-Chokhachy R, Luikart G, Amish SJ (2019) Improved detection of rare, endangered and invasive trout in using a new large-volume sampling method for eDNA capture. *Environmental DNA,* **1**, 227-237.

Seminoff, J.A. (2004) *Chelonia mydas*. In The IUCN Red List of Threatened Species. [accessed 6 January 2023].

Servis JA, Reid BN, Timmers MA, Stergioula V, Naro-Maciel E (2020) Characterizing coral reef biodiversity: genetic species delimitation in brachyuran crabs of Palmyra Atoll, Central Pacific. *Mitochondrial DNA Part A,* **31**, 178-189.

Sheppard CR, Ateweberhan M, Bowen BW, et al (2012) Reefs and islands of the Chagos Archipelago, Indian Ocean: why it is the world's largest no-take marine protected area. *Aquatic Conservation: Marine and Freshwater Ecosystems,* **22**, 232-261.

Sheppard CR, Ateweberhan M, Chen AC, et al (2013) Coral reefs of the Chagos Archipelago, Indian Ocean. In: *Coral reefs of the United Kingdom overseas territories*, (Springer), 241-252.

Sheppard CR, Spalding M, Bradshaw C, Wilson S (2002) Erosion vs. recovery of coral reefs after 1998 El Niño: Chagos reefs, Indian Ocean. *AMBIO: A Journal of the human environment,* **31**, 40-48.

Sheppard C, Sheppard A (2019) British Indian Ocean Territory (Chagos Archipelago). In: *World seas: An environmental evaluation*, (Elsevier) 237-252.

Sheppard C, Sheppard A, Fenner D (2020) Coral mass mortalities in the Chagos Archipelago over 40 years: Regional species and assemblage extinctions and indications of positive feedbacks. *Marine pollution bulletin,* **154**, 111075.

Sheppard C, Sheppard A, Mogg A, et al (2017) Coral bleaching and mortality in the Chagos Archipelago. *Atoll Research Bulletin,* **613**, 1-26.

Shinzato C, Zayasu Y, Kanda M, et al (2018) Using seawater to document coral-zoothanthella diversity: a new approach to coral reef monitoring using environmental DNA. *Frontiers in Marine Science,* **5**, 28.

Siddik AA, Al-Sofyani AA, Ba-Akdah MA, Satheesh S (2019) Invertebrate recruitment on artificial substrates in the Red Sea: role of substrate type and orientation. *Journal of the Marine Biological Association of the United Kingdom,* **99**, 741-750.

Siddik AA, Satheesh S (2021) Interactive effects of light and substrate colour on the recruitment of marine invertebrates on artificial materials. *Community Ecology,* **22**, 69-78.

Sing Wong A, Vrontos S, Taylor ML (2022) An assessment of people living by coral reefs over space and time. *Global Change Biology,* **28**, 7139-7153.

Singer G, Fahner NA, Barnes JG, McCarthy A, Hajibabaei M (2019) Comprehensive biodiversity analysis via ultra-deep patterned flow cell technology: a case study of eDNA metabarcoding seawater. *Scientific reports,* **9**, 1-12.

Sipos R, Székely AJ, Palatinszky M, Révész S, Márialigeti K, Nikolausz M (2007) Effect of primer mismatch, annealing temperature and PCR cycle number on 16S rRNA gene-targetting bacterial community analysis. *FEMS microbiology ecology,* **60**, 341-350.

Small A, Adey WH, Spoon D (1998) Are current estimates of coral reef biodiversity too low? The view through the window of a microcosm. *Atoll Research Bulletin,* **458**, 1-20.

Smith EG, D'Angelo C, Salih A, Wiedenmann J (2013) Screening by coral green fluorescent protein (GFP)-like chromoproteins supports a role in photoprotection of zooxanthellae. *Coral Reefs,* **32**, 463-474.

Smith EG, D'angelo C, Sharon Y, Tchernov D, Wiedenmann J (2017) Acclimatization of symbiotic corals to mesophotic light environments through wavelength transformation by fluorescent protein pigments. *Proceedings of the Royal Society B: Biological Sciences,* **284**, 20170320.

Socolar JB, Gilroy JJ, Kunin WE, Edwards DP (2016) How should beta-diversity inform biodiversity conservation? *Trends in ecology & evolution,* **31**, 67-80.

Souter DW, Linden O (2000) The health and future of coral reef systems. *Ocean & Coastal Management,* **43**, 657-688.

Spalding M, Spalding MD, Ravilious C, Green EP (2001) *World atlas of coral reefs* University of California Press.

St. Pierre JI, Kovalenko KE (2014) Effect of habitat complexity attributes on species richness. *Ecosphere,* **5**, 1-10.

Stat M, Huggett MJ, Bernasconi R, et al (2017) Ecosystem biomonitoring with eDNA: metabarcoding across the tree of life in a tropical marine environment. *Scientific Reports,* **7**, 1-11.

Stauffer S, Jucker M, Keggin T, et al (2021) How many replicates to accurately estimate fish biodiversity using environmental DNA on coral reefs? *Ecology and Evolution,* **11**, 14630-14643.

Stein A, Gerstner K, Kreft H (2014) Environmental heterogeneity as a universal driver of species richness across taxa, biomes and spatial scales. *Ecology Letters,* **17**, 866-880.

Steiner Z, Turchyn AV, Harpaz E, Silverman J (2018) Water chemistry reveals a significant decline in coral calcification rates in the southern Red Sea. *Nature Communications,* **9**, 1-8.

Stella JS, Wolfe K, Roff G, et al (2022) Functional and phylogenetic responses of motile cryptofauna to habitat degradation. *Journal of Animal Ecology,* **91**, 2203-2219.

Stewart HL, Carpenter RC (2003) The effects of morphology and water flow on photosynthesis of marine macroalgae. *Ecology,* **84**, 2999-3012.

Stewart HL, Holbrook SJ, Schmitt RJ, Brooks AJ (2006) Symbiotic crabs maintain coral health by clearing sediments. *Coral Reefs,* **25**, 609-615.

Steyaert M, Lindhart M, Khrizman A, et al (2022) Remote reef cryptobenthic diversity: integrating Autonomous Reef Monitoring Structures (ARMS) and in-situ environmental parameters. *Frontiers in Marine Science,* **9**, 2460.

Steyaert M, Mogg A, Dunn N, Dowell R, Head CE (2022) Observations of coral and cryptobenthic sponge fluorescence and recruitment on autonomous reef monitoring structures (ARMS). *Coral Reefs,* **41**, 877-883.

Stoeck T, Bass D, Nebel M, et al (2010) Multiple marker parallel tag environmental DNA sequencing reveals a highly complex eukaryotic community in marine anoxic water. *Molecular ecology,* **19**, 21-31.

Storlazzi CD, Field ME, Bothner MH (2011) The use (and misuse) of sediment traps in coral reef environments: theory, observations, and suggested protocols. *Coral Reefs,* **30**, 23-38.

Stubler AD, Furman BT, Peterson BJ (2014) Effects of pCO2 on the interaction between an excavating sponge, *Cliona varians*, and a hermatypic coral, Porites furcata. *Marine Biology,* **161**, 1851-1859.

Sundar VC, Yablon AD, Grazul JL, Ilan M, Aizenberg J (2003) Fibre-optical features of a glass sponge. *Nature,* **424**, 899-900.

Sundberg P, Axberg A, Daragmeh N, Panova M, Obst M (2022) Genetic methods in environmental monitoring: Early detection and monitoring of non-indigenous species based on DNA. Rapport 2022: 4, Swedish Agency for Marine and Water Management.

Sura SA, Delgadillo A, Franco N, Gu K, Turba R, Fong P (2019) Macroalgae and nutrients promote algal turf growth in the absence of herbivores. *Coral Reefs,* **38**, 425-429.

Swezey DS, Bean JR, Hill TM, Gaylord B, Ninokawa AT, Sanford E (2017) Plastic responses of bryozoans to ocean acidification. *Journal of Experimental Biology,* **220**, 4399-4409.

Takada Y, Abe O, Shibuno T (2007) Colonization patterns of mobile cryptic animals into interstices of coral rubble. *Marine Ecology Progress Series,* **343**, 35-44.

Takada Y, Abe O, Hashimoto K, Shibuno T (2016) Colonization of coral rubble by motile cryptic animals: differences between contiguous versus raised substrates from the bottom. *Journal of Experimental Marine Biology and Ecology,* **475**, 62-72.

Tebben J, Motti CA, Siboni N, et al (2015) Chemical mediation of coral larval settlement by crustose coralline algae. *Scientific Reports,* **5**, 1-11.

Tebbett SB, Bellwood DR, Purcell SW (2018) Sediment addition drives declines in algal turf yield to herbivorous coral reef fishes: implications for reefs and reef fisheries. *Coral Reefs,* **37**, 929-937.

Tebbett SB, Streit RP, Bellwood DR (2019) Expansion of a colonial ascidian following consecutive mass coral bleaching at Lizard Island, Australia. *Marine Environmental Research,* **144**, 125-129.

Tews J, Brose U, Grimm V, et al (2004) Animal species diversity driven by habitat heterogeneity/diversity: the importance of keystone structures. *Journal of Biogeography,* **31**, 79-92.

Thomsen PF, Willerslev E (2015) Environmental DNA–An emerging tool in conservation for monitoring past and present biodiversity. *Biological Conservation,* **183**, 4-18.

Tickler DM, Letessier TB, Koldewey HJ, Meeuwig JJ (2017) Drivers of abundance and spatial distribution of reef-associated sharks in an isolated atoll reef system. *PloS one,* **12**, e0177374.

Timmers MA, Jury CP, Vicente J, Bahr KD, Webb MK, Toonen RJ (2021) Biodiversity of coral reef cryptobiota shuffles but does not decline under the combined stressors of ocean warming and acidification. *Proceedings of the National Academy of Sciences,* **118**.

Timmers MA, Vicente J, Webb M, Jury CP, Toonen RJ (2020) Sponging up diversity: Evaluating metabarcoding performance for a taxonomically challenging phylum within a complex cryptobenthic community. *Environmental DNA,* **4**, 239-253.

Treibitz T, Neal BP, Kline DI, et al (2015) Wide field-of-view fluorescence imaging of coral reefs. *Scientific reports,* **5**, 1-9.

Trivedi S, Aloufi AA, Ansari AA, Ghosh SK (2016) Role of DNA barcoding in marine biodiversity assessment and conservation: an update. *Saudi Journal of Biological Sciences,* **23**, 161-171.

Tsuji S, Takahara T, Doi H, Shibata N, Yamanaka H (2019) The detection of aquatic macroorganisms using environmental DNA analysis - A review of methods for collection, extraction, and detection. *Environmental DNA,* **1**, 99-108.

Tyler JC, Böhlke JE (1972) Records of sponge-dwelling fishes, primarily of the Caribbean. *Bulletin of Marine Science,* **22**, 601-642.

Valles H, Kramer DL, Hunte W (2006) A standard unit for monitoring recruitment of fishes to coral reef rubble. *Journal of Experimental Marine Biology and Ecology,* **336**, 171-183.

van der Loos LM, Nijland R (2021) Biases in bulk: DNA metabarcoding of marine communities and the methodology involved. *Molecular Ecology,* **30**, 3270-3288.

Vaz-Pinto F, Torrontegi O, Prestes A, Álvaro NV, Neto AI, Martins GM (2014) Invasion success and development of benthic assemblages: effect of timing, duration of submersion and substrate type. *Marine Environmental Research,* **94**, 72-79.

Venables WN, Ripley BD (2002) Modern applied statistics with S. fourth Edition (Springer).

Vicente J, Timmers MA, Webb MK, Bahr KD, Jury CP, Toonen RJ (2022) Ecological succession of the sponge cryptofauna in Hawaiian reefs add new insights to detritus production by pioneering species. *Scientific Reports,* **12**, 1-14.

Vicente J, Webb MK, Paulay G, et al (2021) Unveiling hidden sponge biodiversity within the Hawaiian reef cryptofauna. *Coral Reefs,* **41**, 1-16.

Villalobos R, Aylagas E, Pearman JK, et al (2022) Inter-annual variability patterns of reef cryptobiota in the central Red Sea across a shelf gradient. *Scientific reports,* **12**, 1-17.

Wang YI, Naumann U, Wright ST, Warton DI (2012a) mvabund–an R package for model-based analysis of multivariate abundance data. *Methods in Ecology and Evolution,* **3**, 471-474.

Wangensteen OS, Palacín C, Guardiola M, Turon X (2018) DNA metabarcoding of littoral hard-bottom communities: high diversity and database gaps revealed by two molecular markers. *PeerJ,* **6**, e4705.

Warton DI (2008) Penalized normal likelihood and ridge regularization of correlation and covariance matrices. *Journal of the American Statistical Association,* **103**, 340-349.

Warton DI, Wright ST, Wang Y (2012) Distance-based multivariate analyses confound location and dispersion effects. *Methods in Ecology and Evolution,* **3**, 89-101.

Weiss A, Martindale RC (2017) Crustose coralline algae increased framework and diversity on ancient coral reefs. *PLoS One,* **12**, e0181637.

West KM, Adam AA, White N, et al (2022) The applicability of eDNA metabarcoding approaches for sessile benthic surveying in the Kimberley region, north-western Australia. *Environmental DNA,* **4**, 34-49.

West KM, Stat M, Harvey ES, et al (2020) eDNA metabarcoding survey reveals fine-scale coral reef community variation across a remote, tropical island ecosystem. *Molecular ecology,* **29**, 1069-1086.

Whittaker RJ, Willis KJ, Field R (2001) Scale and species richness: towards a general, hierarchical theory of species diversity. *Journal of Biogeography,* **28**, 453-470.

Wickham H (2016) *ggplot2: elegant graphics for data analysis.* (Springer), ISBN 978-3-319-24277-4

Williams GJ, Gove JM, Eynaud Y, Zgliczynski BJ, Sandin SA (2015) Local human impacts decouple natural biophysical relationships on Pacific coral reefs. *Ecography,* **38**, 751-761.

Williams GJ, Graham NA (2019) Rethinking coral reef functional futures. *Functional Ecology,* **33**, 942-947.

Williams ID, Richards BL, Sandin SA, et al (2011) Differences in reef fish assemblages between populated and remote reefs spanning multiple archipelagos across the central and western Pacific. *Journal of Marine Biology,* **2011**.

Williams J, Pettorelli N, Hartmann A, Quinn A, Plaisance L, O'Mahoney M, Meyer C, Fabricius K, Knowlton N, Ransome E (2023) Decline of a distinct coral reef holobiont community under ocean acidification. *Manuscript in preparation*.

Willis AD, Martin BD (2018) DivNet: Estimating diversity in networked communities. *BioRxiv,* 305045.

Willis A, Bunge J (2015) Estimating diversity via frequency ratios. *Biometrics,* **71**, 1042-1049.

Wizemann A, Nandini SD, Stuhldreier I, et al (2018) Rapid bioerosion in a tropical upwelling coral reef. *PloS one,* **13**, e0202887.

Wolfe K, Kenyon TM, Mumby PJ (2021) The biology and ecology of coral rubble and implications for the future of coral reefs. *Coral Reefs,* **40**, 1769-1806.

Wolfe K, Mumby PJ (2020) RUbble Biodiversity Samplers: 3D-printed coral models to standardize biodiversity censuses. *Methods in Ecology and Evolution,* **11**, 1395-1400.

Woodhead AJ, Hicks CC, Norström AV, Williams GJ, Graham NA (2019) Coral reef ecosystem services in the Anthropocene. *Functional Ecology,* **33**, 1023-1034.

Worm B, Barbier EB, Beaumont N, et al (2006) Impacts of biodiversity loss on ocean ecosystem services. *Science,* **314**, 787-790.

Wulff J (2016) Sponge contributions to the geology and biology of reefs: past, present, and future. In: *Coral reefs at the crossroads* (Springer), 103-126.

Wulff J (2001) Assessing and monitoring coral reef sponges: why and how? *Bulletin of Marine Science,* **69**, 831-846.

Wulff JL (1984) Sponge-mediated coral reef growth and rejuvenation. *Coral Reefs,* **3**, 157-163.

Wyatt AS, Leichter JJ, Toth LT, Miyajima T, Aronson RB, Nagata T (2020) Heat accumulation on coral reefs mitigated by internal waves. *Nature Geoscience,* **13**, 28-34.

Yakovis EL, Artemieva AV, Fokin MV, Varfolomeeva MA, Shunatova NN (2007) Effect of habitat architecture on mobile benthic macrofauna associated with patches of barnacles and ascidians. *Marine Ecology Progress Series,* **348**, 117-124.

Yang HS, Jöst AB, Kim T, et al (2021) Research on the application of the Autonomous Reef Monitoring Structures (ARMS) for the change of marine ecosystem and biodiversity diagnosis in Jeju Island. 년도 한국해양학회 추계학술대회, 185-185.

Zawada DG, Mazel CH (2014) Fluorescence-Based Classification of Caribbean Coral Reef Organisms and Substrates. *PLOS ONE,* **9**, e84570.

Zawada KJ, Madin JS, Baird AH, Bridge TC, Dornelas M (2019) Morphological traits can track coral reef responses to the Anthropocene. *Functional Ecology,* **33**, 962-975.

Zimmerman TL, Martin JW (2004) Artificial reef matrix structures (ARMS): an inexpensive and effective method for collecting coral reef-associated invertebrates. *Gulf and Caribbean Research,* **16**, 59-64.

Zweifler A, Akkaynak D, Mass T, Treibitz T (2017) *In situ* analysis of coral recruits using fluorescence imaging. *Frontiers in Marine Science,* **4**, 273.

Zweng RC, Koch MS, Bowes G (2018) The role of irradiance and C-use strategies in tropical macroalgae photosynthetic response to ocean acidification. *Scientific Reports,* **8**, 1-11.

APPENDIX

A. Supplementary Material for Chapter 2

A.i Barcoding of 2019 motiles (>2mm)

Background & Methods

A total of 755 motile specimens (incl. crustaceans, echinoderms, molluscs, annelids) across 304 morphospecies samples were collected across all ARMS retrieved in 2019 (see Chapter 2 Methods section) and individually photographed with unique identification numbers.

DNA was extracted from 304 individual specimen using QIAGEN's DNEasy Blood & Tissue kit (96-well) and quantified using the QuBit dsDNA Broad Range assay kit, following manufacturers' protocols. The 658bp Folmer region of the cytochrome oxidase I (COI) was targeted and amplified via polymerase chain reaction (PCR) using the degenerated primer set dgLCO1490/dgHCO2198 (Meyer, 2003). PCR reactions were carried in 20µL volumes including 2µL of DNA, 0.5µL of forward and 0.5µL of reverse primers, 4µL of 5X HOTFIRPol Blend Master Mix (12.5mM $MgCl_2$) and 13µL of PCR-grade H_2O. Based on first gel results, PCRs were rerun using more or less DNA where needed, e.g., by diluting DNA concentrations by 10 or 100 times if gel smears were observed. For sampled with successful amplification, PCRs were run once again in duplicates, and resulting DNA products were quantified using the QuBit dsDNA High Sensitivity assay, following manufacturer's protocols, and normalized to a final concentration of 10ng/µL. Sanger sequencing was carried out externally by using the PlateSeq service from Eurofins Genomics (Germany). The PlateSeq kit PCR service includes DNA purification and Sanger sequencing for each individual samples.

Samples with sequences of high quality were then inspected using Geneious Prime (version 2022.2.2) (https://www.geneious.com), and sequences were trimmed to remove low quality bases on either hand of sequences. Sequences were then assigned taxonomy using the megaBLAST tool within Geneious Prime, and the top hit was retained (highest % query cover and % identity match).

Results

A total of 160 samples were sent for sequencing after successful PCRs, and of these, a total of 123 sequenced samples were of high quality (contiguous read length (CRL) > 500 nucleotides), 13 were of medium quality (CRL > 100 < 500 n) and 24 had poor/failed sequencing (CRL < 100 n). The top taxonomy hit for each sequence was then compared to photograph of individual specimen taken at the time of field sampling collections, to determine if broad taxonomy matched (Table A.i.i). Of these, a total of 95 specimen matched with images taken in the field, whilst for others, either images were not found, or broad taxonomy did not match (Table A.i.i).

Table A.i.i. Summary of taxonomy assignments for successfully barcoded motile specimen collected from 2019 ARMS. The megaBLAST identity match and query percentages, and the taxonomy, of the top match hits for each voucher sample is provided, along whether these identifications match the original field sample photo.

Voucher ID	% Identical Sites	Query coverage	Species	Photo ID match
ARMS19M_338	100.00%	100.00%	Cephalopholis urodeta	Yes
ARMS19S_223	99.50%	100.00%	Porites harrisoni	na
ARMS19M_357	99.40%	100.00%	Eviota guttata	Yes
ARMS19S_206	99.10%	100.00%	Haliclona tubifera	na
ARMS19M_45	99.00%	100.00%	Decapoda sp.	Yes
ARMS19M_212	91.10%	100.00%	Istigobius sp.	No
ARMS19M_107	82.70%	100.00%	Cottus koreanus	Maybe
ARMS19M_222	82.30%	100.00%	Eratoena sandwichensis	Yes
ARMS19M_110	80.20%	99.85%	Marphysa sp.	Yes
ARMS19M_261	98.10%	99.84%	Discodoris confusa	Yes
ARMS19M_442.2	99.20%	99.69%	Palaemonella rotumana	Yes
ARMS19M_215	85.60%	99.69%	Achelia hoekii	Yes
ARMS19M_136	80.40%	99.69%	Marphysa sp.	Yes
ARMS19M_137	80.40%	99.69%	Marphysa sp.	Yes
ARMS19M_207	99.20%	99.68%	Decapoda sp.	Yes
ARMS19M_022	98.90%	99.68%	Decapoda sp.	Yes
ARMS19M_442.1	98.10%	99.68%	Decapoda sp.	Yes
ARMS19S_191	99.10%	99.37%	Ophiothela tigris	Yes
ARMS19M_246	92.90%	99.22%	Galathea mauritiana	Yes
ARMS19M_052	99.40%	99.21%	Brachyura sp.	Yes
ARMS19M_119	99.20%	99.21%	Decapoda sp.	Yes
ARMS19M_446	99.00%	99.21%	Decapoda sp.	Yes
ARMS19M_167	99.80%	99.20%	Gastropoda sp.	Yes
ARMS19M_221	99.80%	99.20%	Calcinus pulcher	Yes
ARMS19M_332	99.80%	99.20%	Cerithium egenum	na
ARMS19M_151	96.00%	99.20%	Gyrineum lacunatum	No
ARMS19M_355	99.80%	99.18%	Cirrhilabrus exquisitus	Yes
ARMS19M_103	99.50%	99.07%	Palaemonella rotumana	Yes
ARMS19M_439	99.70%	99.06%	Calcinus rosaceus	Yes
ARMS19M_159	92.60%	99.00%	Decapoda sp.	Maybe
ARMS19S_135	80.50%	98.95%	Calloporina angustipora	na
ARMS19S_224	88.60%	98.87%	Nevianipora sp.	na
ARMS19M_121	99.20%	98.76%	Palaemonella rotumana	Yes
ARMS19M_208.1	92.90%	98.73%	Stomatella sp.	Yes
ARMS19M_046	85.90%	98.52%	Pagurixus laevimanus	Yes
ARMS19M_068	96.50%	98.29%	Gastropoda sp.	Yes
ARMS19M_071	84.80%	98.13%	Mopalia spectabilis	Yes
ARMS19S_002	99.70%	97.98%	Brachyura sp.	No
ARMS19M_255	95.40%	97.98%	Cerithium munitum	Yes
ARMS19M_256	93.80%	97.98%	Hippolytidae sp.	Yes
ARMS19S_018	95.70%	97.97%	Gastropoda sp.	Yes
ARMS19M_330	98.70%	97.96%	Decapoda sp.	Yes
ARMS19M_142	100.00%	97.95%	Calcinus pulcher	Yes
ARMS19M_173	93.80%	97.83%	Hippolytidae sp.	Yes
ARMS19M_132	93.70%	97.83%	Hippolytidae sp.	Yes
ARMS19M_321	94.40%	97.82%	Pleurobranchidae sp.	Yes
ARMS19M_122	99.80%	97.81%	Cerithium egenum	Yes
ARMS19M_252	92.90%	97.81%	Galathea mauritiana	Yes
ARMS19M_177.2	98.90%	97.80%	Arthropoda sp.	Yes
ARMS19S_001	85.20%	97.80%	Pseudoplesiops sp.	Yes
ARMS19M_013	98.70%	97.76%	Graphicomassa adiostina	Yes
ARMS19S_008	98.10%	97.67%	Decapoda sp.	Yes
ARMS19S_010	98.10%	97.67%	Decapoda sp.	Yes
ARMS19M_128	96.20%	97.67%	Phylladiorhynchus sp.	Yes
ARMS19M_117	91.70%	97.67%	Favartia sp.	Yes
ARMS19M_250	91.70%	97.67%	Favartia sp.	na
ARMS19M_124	99.70%	97.66%	Cerithium egenum	Yes
ARMS19M_213	89.50%	97.66%	Caridea sp.	Yes
ARMS19S_020	98.90%	97.65%	Graphicomassa adiostina	Yes

ARMS19S_012	98.30%	97.55%	Decapoda sp.	Yes
ARMS19S_005	92.80%	97.55%	Galathea mauritiana	Yes
ARMS19M_014	99.00%	97.53%	Graphicomassa adiostina	Yes
ARMS19M_210	83.40%	97.52%	Janolus sp.	Yes
ARMS19M_236	94.90%	97.51%	Gastropoda sp.	Yes
ARMS19M_101	92.60%	97.50%	Pagurixus sp.	Yes
ARMS19M_056	86.50%	97.48%	Vexillum sp.	na
ARMS19S_016	100.00%	97.39%	Saron marmoratus	No
ARMS19M_055	89.30%	97.39%	Emarginula sp.	na
ARMS19M_062	100.00%	97.38%	Epiactaea nodulosa	Yes
ARMS19S_022	98.70%	97.38%	Graphicomassa adiostina	Yes
ARMS19S_007.1	85.50%	97.38%	Pseudoplesiops sp.	No
ARMS19M_089	97.50%	97.37%	Turbo cepoides	Yes
ARMS19M_147	93.00%	97.37%	Micropagurus devaneyi	No
ARMS19S_004	99.80%	97.36%	Saron marmoratus	No
ARMS19M_335	99.70%	97.36%	Fusigobius duospilus	Yes
ARMS19M_449	96.00%	97.36%	Gyrineum lacunatum	Yes
ARMS19S_017	95.70%	97.36%	Gastropoda sp.	Yes
ARMS19M_011	92.40%	97.36%	Cerithium echinatum	Yes
ARMS19M_254	91.50%	97.36%	Istigobius rigilius	Yes
ARMS19M_226	89.00%	97.36%	Caridea sp.	Yes
ARMS19M_054	100.00%	97.34%	Carupa tenuipes	na
ARMS19M_209	100.00%	97.33%	Exoclimenella maldivensis	Yes
ARMS19M_087	87.70%	97.21%	Vexillum roseum	Yes
ARMS19M_149	92.90%	97.20%	Stomatella sp.	Yes
ARMS19M_208.2	92.90%	97.20%	Stomatella sp.	Yes
ARMS19M_155	86.20%	97.20%	Polyplacophora sp.	Yes
ARMS19M_437	94.90%	97.07%	Glossodoris cf.	Yes
ARMS19M_150	92.90%	97.05%	Stomatella sp.	Yes
ARMS19M_452	81.60%	96.89%	Dallocardia muricata	Yes
ARMS19M_106	83.60%	96.72%	Perinereis sp.	Yes
ARMS19M_072	92.40%	96.71%	Monoplex comptus	Yes
ARMS19M_148	92.50%	96.70%	Monoplex comptus	Yes
ARMS19M_168	92.50%	96.55%	Monoplex comptus	Yes
ARMS19S_189	98.70%	96.35%	Graphicomassa adiostina	na
ARMS19M_070	92.50%	96.31%	Reticutriton pfeifferianus	na
ARMS19S_088	100.00%	96.30%	Calliactis polypus	Maybe
ARMS19M_445	94.80%	96.21%	Polychaeta sp.	Yes
ARMS19M_120	98.90%	96.19%	Arthropoda sp.	Yes
ARMS19M_006	97.60%	96.17%	Thranita coeruleipes	Yes
ARMS19M_102	99.00%	96.14%	Decapoda sp.	Yes
ARMS19M_214	96.00%	96.12%	Phylladiorhynchus sp.	Yes
ARMS19M_248	92.40%	95.88%	Cerithium echinatum	Yes
ARMS19M_112	93.70%	95.48%	Paguridae sp.	Yes
ARMS19M_049	86.70%	95.29%	Vexillum sp.	Yes
ARMS19M_331	99.50%	95.27%	Cuapetes grandis	Yes
ARMS19M_325	99.80%	95.12%	Cuapetes grandis	Yes
ARMS19M_043	84.60%	95.00%	Arthropoda sp.	Yes
ARMS19M_313	94.60%	94.88%	Polychaeta sp.	Yes
ARMS19M_111	94.80%	94.32%	Polychaeta sp.	Yes
ARMS19S_073	80.20%	93.89%	Calloporina angustipora	Yes
ARMS19M_067	98.70%	93.77%	Talostolida teres	Yes
ARMS19S_009	99.20%	93.64%	Cuapetes grandis	Yes
ARMS19S_007.2	98.80%	93.16%	Monoplex comptus	Yes
ARMS19M_230	86.50%	92.87%	Periclimenes diversipes	Yes
ARMS19M_177.1	98.60%	91.67%	Arthropoda sp.	Yes
ARMS19M_239	85.20%	89.78%	Parapallene bermudensis	Yes
ARMS19M_082	80.60%	86.33%	Zerconidae sp.	No
ARMS19S_011	99.80%	78.89%	Ophiothrix trilineata	No
ARMS19S_060	74.70%	52.67%	Oedothorax fuscus	No
ARMS19M_440	75.90%	39.49%	Hemicycla fulgida	na
ARMS19S_095	79.70%	22.39%	Hypsibius klebelsbergi	No

Table A.1. GPS coordinates for reef sampling sites across the Chagos Marine Protected Area.

Reef site	Atoll	Latitude	Longitude
Ile Anglaise	Salomon	5° 20.32' S	72° 12.80' E
Ile du Coin	Perhos Banos	5° 27.023' S	71° 46.043' E
Moresby	Perhos Banos	5° 14.13' S	71° 50.02' E

Table A.2. Summary of COI sequence reads retained through DADA2 pipeline steps for individual metabarcoding samples. Sample metadata is also provided to indicate sampling year, sample site and fraction. Note: 2019 and 2021 samples were sequenced on separate MiSeq runs. Reads through pipeline steps are also presented for eDNA samples (see Chapter 4). denoisedF = denoised forward reads ; denoisedR = denoised reverse reads; nonchim = non-chimeric reads.

sample ID	site	year	fraction	input	filtered	denoisedF	denoisedR	merged	nonchim
2019-coi-A1_S1	Coin	2019	100-500um	196541	180768	179322	179180	170628	169452
2019-coi-A2_S2	Coin	2019	100-500um	103733	95490	94439	94470	88948	88134
2019-coi-A3_S3	Moresby	2019	100-500um	193410	180347	178916	178763	170772	168933
2019-coi-A4_S4	Anglaise	2019	100-500um	142059	133794	132539	132655	128078	126769
2019-coi-A5_S5	Anglaise	2019	100-500um	122297	114491	113331	113207	108943	107104
2019-coi-A6_S6	Anglaise	2019	100-500um	149057	137289	135944	135813	129953	128908
2019-coi-A7_S7	Coin	2019	100-500um	182088	170450	168864	168885	164709	163188
2019-coi-A8_S8	Moresby	2019	100-500um	208313	194041	192689	192440	180793	179200
2019-coi-A9_S9	Moresby	2019	100-500um	229186	214519	212552	212677	204228	201503
2019-coi-A1_S10	Coin	2019	500um-2mm	222023	207577	206732	206646	203513	202991
2019-coi-A2_S11	Coin	2019	500um-2mm	174441	162677	161805	161814	158215	158107
2019-coi-A3_S12	Moresby	2019	500um-2mm	160557	149821	149348	149436	147944	146731
2019-coi-A4_S13	Anglaise	2019	500um-2mm	179598	169252	168623	168658	166689	165975
2019-coi-A5_S14	Anglaise	2019	500um-2mm	190609	182005	181177	181352	178452	177693
2019-coi-A6_S15	Anglaise	2019	500um-2mm	228033	212568	211869	211993	208550	207973
2019-coi-A7_S16	Coin	2019	500um-2mm	263636	249937	249126	249074	247187	246712
2019-coi-A8_S17	Moresby	2019	500um-2mm	185862	174735	173928	173891	171466	170375
2019-coi-A9_S18	Moresby	2019	500um-2mm	61623	57479	57295	57279	56909	56783
2019-coi-A1_S19	Coin	2019	sessile	210537	194520	192975	193059	187382	185745
2019-coi-A2_S20	Coin	2019	sessile	133568	124702	123577	123653	119231	116640
2019-coi-A3_S21	Moresby	2019	sessile	148682	139749	139125	139131	136399	135345
2019-coi-A4_S22	Anglaise	2019	sessile	153800	145312	144203	144180	141207	138058
2019-coi-A5_S23	Anglaise	2019	sessile	145197	137375	136350	136211	133614	132749
2019-coi-A6_S24	Anglaise	2019	sessile	228529	214584	213352	213387	209692	209222
2019-coi-A7_S25	Coin	2019	sessile	174216	164057	163250	163303	161534	161153
2019-coi-A8_S26	Moresby	2019	sessile	154544	145630	144644	144657	139931	138710
2019-coi-A9_S27	Moresby	2019	sessile	130943	122557	121393	121485	118656	117382
2021-coi-A2_S2	Anglaise	2021	100-500um	269635	244363	242470	242575	233481	231545
2021-coi-A3_S3	Anglaise	2021	100-500um	332937	298559	296563	296063	288206	285683
2021-coi-A4_S4	Moresby	2021	100-500um	367779	339433	337478	337494	325943	321169
2021-coi-A5_S5	Moresby	2021	100-500um	252882	230844	229174	228830	219950	218279
2021-coi-A6_S6	Moresby	2021	100-500um	127717	116139	114621	114474	109870	108958
2021-coi-A7_S7	Coin	2021	100-500um	250233	228975	227428	227398	221132	219735
2021-coi-A8_S8	Coin	2021	100-500um	110988	101765	100851	100782	98337	97595
2021-coi-A9_S9	Coin	2021	100-500um	1304419	1200296	1195774	1195512	1170521	1156638
2021-coi-A2_S11	Anglaise	2021	500um-2mm	216441	204007	203612	203704	201254	200124
2021-coi-A3_S12	Anglaise	2021	500um-2mm	159400	140403	139597	139609	136306	135780
2021-coi-A4_S13	Moresby	2021	500um-2mm	246465	230663	230322	230309	226659	224182
2021-coi-A5_S14	Moresby	2021	500um-2mm	214996	184925	184019	184070	180941	179690
2021-coi-A6_S15	Moresby	2021	500um-2mm	334717	312677	311981	311947	309275	304860
2021-coi-A7_S16	Coin	2021	500um-2mm	369704	337769	336581	336412	333487	332199
2021-coi-A8_S17	Coin	2021	500um-2mm	131119	120013	119455	119282	116429	116094
2021-coi-A9_S18	Coin	2021	500um-2mm	153997	139329	138469	138343	135006	134598
2021-coi-A1_S19	Anglaise	2021	sessile	207788	192858	192187	191984	189847	189450
2021-coi-A2_S20	Anglaise	2021	sessile	328887	309615	308849	308931	306396	304812
2021-coi-A4_S22	Moresby	2021	sessile	326247	299960	299162	299152	296542	295400
2021-coi-A5_S23	Moresby	2021	sessile	338255	315553	314692	314626	311251	310335
2021-coi-A6_S24	Moresby	2021	sessile	204240	181174	180209	179994	177498	175988
2021-coi-A7_S25	Coin	2021	sessile	401452	375267	374475	374507	371078	369018
2021-coi-A8_S26	Coin	2021	sessile	136698	125998	125339	125309	122739	122128
2021-coi-A9_S27	Coin	2021	sessile	212218	201179	200907	200823	199847	199636
2021-coi-A1_S28	Anglaise	2021	eDNA	355595	334605	332648	332515	325087	319584
2021-coi-A2_S29	Anglaise	2021	eDNA	390247	367873	365754	365826	356388	350296
2021-coi-A3_S30	Anglaise	2021	eDNA	254985	238977	237696	237846	233895	231390
2021-coi-A4_S31	Moresby	2021	eDNA	328789	306955	305376	305431	298842	293638
2021-coi-A5_S32	Moresby	2021	eDNA	292970	275623	274072	273835	268278	264556
2021-coi-A6_S33	Moresby	2021	eDNA	470132	448391	445819	445736	436549	429237
2021-coi-A7_S34	Coin	2021	eDNA	297724	283863	282416	282264	277511	275019
2021-coi-A8_S35	Coin	2021	eDNA	627881	592942	591347	591246	583320	568203
2021-coi-A9_S36	Coin	2021	eDNA	686678	633366	632481	631360	618251	585124
2021-coi-neg_S40	eDNA negative	2021	eDNA	8273	7737	7658	7649	7540	7540

Table A.3. Summary of 18S sequence reads retained through DADA2 pipeline steps for individual metabarcoding samples. Sample metadata is also provided to indicate sampling year, sample site and fraction. Note: 2019 and 2021 samples were sequenced on separate MiSeq runs. Reads through pipeline steps are also presented for eDNA samples (see Chapter 4). denoisedF = denoised forward reads ; denoisedR = denoised reverse reads; nonchim = non-chimeric reads.

sample ID	site	year	fraction	input	filtered	denoisedF	denoisedR	merged	nonchim
2019-18s-A1_S28	Coin	2019	100-500um	167353	134318	133372	133010	118236	112729
2019-18s-A2_S29	Coin	2019	100-500um	224192	178772	177590	177686	155209	150695
2019-18s-A3_S30	Moresby	2019	100-500um	988313	767535	763347	762668	645895	603362
2019-18s-A4_S31	Anglaise	2019	100-500um	94482	76361	75833	75744	62994	61466
2019-18s-A5_S32	Anglaise	2019	100-500um	179388	139231	138412	138487	122226	120553
2019-18s-A6_S33	Anglaise	2019	100-500um	122028	97770	97138	97150	81020	79702
2019-18s-A7_S34	Coin	2019	100-500um	178413	146968	146074	146213	139045	136625
2019-18s-A8_S35	Moresby	2019	100-500um	193491	154059	153036	152561	136205	129222
2019-18s-A9_S36	Moresby	2019	100-500um	151599	117546	116777	116887	103215	102292
2019-18s-A1_S37	Coin	2019	500um-2mm	137146	108930	108382	108362	99716	97282
2019-18s-A2_S38	Coin	2019	500um-2mm	151022	99562	98971	98772	89917	82023
2019-18s-A3_S39	Moresby	2019	500um-2mm	137174	113122	112799	112618	105729	98052
2019-18s-A4_S40	Anglaise	2019	500um-2mm	100237	86806	86538	86422	75937	71800
2019-18s-A5_S41	Anglaise	2019	500um-2mm	136916	118688	118416	118513	112981	112334
2019-18s-A6_S42	Anglaise	2019	500um-2mm	148699	129982	129610	129767	122529	120478
2019-18s-A7_S43	Coin	2019	500um-2mm	164112	138189	137780	137707	133541	128932
2019-18s-A8_S44	Moresby	2019	500um-2mm	165338	144089	143714	143682	125211	122589
2019-18s-A9_S45	Moresby	2019	500um-2mm	142051	125522	125209	125302	117370	117136
2019-18s-A1_S46	Coin	2019	sessile	123339	106169	105465	105716	99820	99402
2019-18s-A2_S47	Coin	2019	sessile	228827	188244	187290	187639	167009	166033
2019-18s-A3_S48	Moresby	2019	sessile	86526	69970	69571	69726	66270	66057
2019-18s-A4_S49	Anglaise	2019	sessile	114562	95694	95093	95352	90682	90392
2019-18s-A5_S50	Anglaise	2019	sessile	113558	94554	94054	94229	89289	88952
2019-18s-A6_S51	Anglaise	2019	sessile	109706	90969	90449	90649	84038	83852
2019-18s-A7_S52	Coin	2019	sessile	123434	105072	104655	104824	101519	100987
2019-18s-A8_S53	Moresby	2019	sessile	124770	107336	106865	107002	101847	101295
2019-18s-A9_S54	Moresby	2019	sessile	112485	90622	90141	90338	84153	83874
2021-18s-A1_S1	Anglaise	2021	100-500um	386559	297654	295830	296102	259599	258014
2021-18s-A2_S2	Anglaise	2021	100-500um	382838	287105	285581	285909	248184	247143
2021-18s-A3_S3	Anglaise	2021	100-500um	524643	462539	461072	461244	421926	412644
2021-18s-A4_S4	Moresby	2021	100-500um	415610	321704	320114	320310	279996	277025
2021-18s-A5_S5	Moresby	2021	100-500um	472280	373575	371699	371693	289501	287127
2021-18s-A6_S6	Moresby	2021	100-500um	441059	326264	324113	324768	261044	259622
2021-18s-A7_S7	Coin	2021	100-500um	475060	359298	357708	357732	319123	316578
2021-18s-A8_S8	Coin	2021	100-500um	368090	272750	271044	271365	219211	218212
2021-18s-A9_S9	Coin	2021	100-500um	207072	153506	152219	152281	125818	124353
2021-18s-A1_S10	Anglaise	2021	500um-2mm	129041	99649	99363	99403	84851	84382
2021-18s-A2_S11	Anglaise	2021	500um-2mm	181725	152540	152142	152246	142756	142050
2021-18s-A3_S12	Anglaise	2021	500um-2mm	381344	322466	321294	321547	297465	288677
2021-18s-A4_S13	Moresby	2021	500um-2mm	182692	149142	148548	148706	132253	129558
2021-18s-A5_S14	Moresby	2021	500um-2mm	154133	121221	120776	120797	108835	106897
2021-18s-A6_S15	Moresby	2021	500um-2mm	183906	142199	141534	141609	126638	121213
2021-18s-A7_S16	Coin	2021	500um-2mm	239933	127040	126248	126381	117635	117097
2021-18s-A8_S17	Coin	2021	500um-2mm	250148	154891	153827	154130	123147	121129
2021-18s-A9_S18	Coin	2021	500um-2mm	356189	239590	238509	238785	172351	170551
2021-18s-A1_S19	Anglaise	2021	sessile	421713	368369	365824	365273	336044	306451
2021-18s-A2_S20	Anglaise	2021	sessile	317151	278150	276976	277143	254406	246593
2021-18s-A3_S21	Anglaise	2021	sessile	190401	151972	151516	151617	145812	144868
2021-18s-A4_S22	Moresby	2021	sessile	134054	117025	116399	116529	110802	105630
2021-18s-A5_S23	Moresby	2021	sessile	220074	181137	180429	180248	165544	161803
2021-18s-A6_S24	Moresby	2021	sessile	268608	214508	212822	212615	184002	178402
2021-18s-A7_S25	Coin	2021	sessile	125153	101641	101111	101217	94687	94381
2021-18s-A8_S26	Coin	2021	sessile	185006	143026	141520	141244	124343	114343
2021-18s-A9_S27	Coin	2021	sessile	446745	352608	351417	351735	311478	307269
2021-18s-A1_S28	Anglaise	2021	eDNA	300395	268282	266333	266296	258080	255230
2021-18s-A2_S29	Anglaise	2021	eDNA	264851	241723	239710	239697	230904	227418
2021-18s-A3_S30	Anglaise	2021	eDNA	376195	329856	327848	327956	320706	313323
2021-18s-A4_S31	Moresby	2021	eDNA	258185	231702	230198	230108	225109	222819
2021-18s-A5_S32	Moresby	2021	eDNA	202303	170823	169023	168806	161613	156290
2021-18s-A6_S33	Moresby	2021	eDNA	241715	213741	211277	211046	201497	197461
2021-18s-A7_S34	Coin	2021	eDNA	260655	220652	218711	218621	195403	191653
2021-18s-A8_S35	Coin	2021	eDNA	293532	255159	252919	251783	240788	225581
2021-18s-A9_S36	Coin	2021	eDNA	255237	219648	218824	218781	215058	210190

Table A.4. List of marine metazoan species identified on ARMS using metabarcoding, including both fully described and un-described species.

Phylum	Family	Species
Annelida	Amphinomidae	*Eurythoe cf. complanata ET_2017*
		Eurythoe sp. HAW02
	Dorvilleidae	*Dorvilleidae sp. BMOO_13194*
	Polynoidae	*Polynoidae sp. C_0726*
	Syllidae	*Proceraea madeirensis*
Arthropoda	Acartiidae	*Acartia negligens*
		Alpheus sp. PNG1352b
	Calanidae	*Cosmocalanus darwinii*
		Undinula vulgaris
	Calocalanidae	*Calocalanus pavo*
		Calocalanus plumulosus
		Candacia curta
	Centropagidae	*Centropages furcatus*
	Clausocalanidae	*Clausocalanus furcatus*
	Corycaeidae	*Farranula gibbula*
	Diogenidae	*Calcinus pulcher*
	Eucalanidae	*Eucalanus pseudattenuatus*
		Euchaeta rimana
	Galatheidae	*Galatheidae sp. KSA_C171*
		Galatheidae sp. PNG_0270e
	Hippolytidae	*Hippolytidae sp. USNM 1467165*
		Lysmata ternatensis
		Saron marmoratus
	Oithonidae	*Oithona attenuata*
		Oithona simplex
	Palaemonidae	*Conchodytes meleagrinae*
		Coralliocaris superba
		Cuapetes grandis
		Exoclimenella maldivensis
		Palaemonella rotumana
		Periclimenaeus rastrifer
		Periclimenella agattii
		Periclimenes sp. PNG_0028a
	Paracalanidae	*Paracalanus denudatus*
		Paracalanus gracilis
		Paracalanus indicus
		Paracalanus parvus
		Paracalanus quasimodo
		Paracalanus tropicus
	Pontellidae	*Pontella fera*
	Portunidae	*Portunidae sp. KSA_1038*
		Thalamita admete
	Sapphirinidae	*Copilia hendorffi*
		Copilia mirabilis
	Temoridae	*Temora discaudata*
	unknown	*Amphipoda sp. LPdivOTU470*

	unknown	*Amphipoda sp. LPdivOTU63*
	unknown	*Anomura sp. LPdivOTU441*
	unknown	*Anomura sp. LPdivOTU90*
	unknown	*Arthropoda sp. KSA_1073*
	unknown	*Brachyura sp. LPdivOTU248*
	unknown	*Brachyura sp. LPdivOTU261*
	unknown	*Brachyura sp. LPdivOTU284*
	unknown	*Brachyura sp. LPdivOTU364*
	unknown	*Brachyura sp. LPdivOTU422*
	unknown	*Brachyura sp. LPdivOTU446*
	unknown	*Brachyura sp. LPdivOTU495*
	unknown	*Brachyura sp. LPdivOTU522*
	unknown	*Brachyura sp. LPdivOTU59*
	unknown	*Brachyura sp. LPdivOTU67*
	unknown	*Calanoida sp. KJ641*
	unknown	*Caridea sp. LPdivOTU188*
	unknown	*Caridea sp. LPdivOTU475*
	unknown	*Caridea sp. LPdivOTU66*
	unknown	*Copepoda sp. IP0237*
	unknown	*Decapoda sp. C_0240*
	unknown	*Decapoda sp. JOD_0428*
	unknown	*Decapoda sp. KSA_1414*
	unknown	*Decapoda sp. KSA_1622*
	unknown	*Decapoda sp. SHR066*
	unknown	*Decapoda sp. SHR171*
	unknown	*Decapoda sp. SHR207*
	Xanthidae	*Liomera monticulosa*
		Luniella spinipes
		Platypodia semigranosa
		Xanthias punctatus
Chaetognatha	Sagittidae	*Sagitta sp. ZP285*
Chordata	Acanthuridae	*Acanthurus leucosternon*
		Acanthurus lineatus
		Acanthurus nigricauda
		Ctenochaetus striatus
		Naso brevirostris
		Naso unicornis
		Zebrasoma desjardinii
	Balistidae	*Melichthys niger*
	Carangidae	*Alectis indica*
		Caranx melampygus
		Decapterus macarellus
	Chaetodontidae	*Chaetodon auriga*
		Chaetodon trifasciatus
	Gobiidae	*Fusigobius neophytus*
	Holocentridae	*Myripristis berndti*
		Myripristis vittata
		Neoniphon sammara
		Sargocentron caudimaculatum
	Kyphosidae	*Kyphosus cinerascens*
	Labridae	*Chlorurus gibbus*
		Chlorurus sordidus

		Epibulus insidiator
		Halichoeres hortulanus
		Scarus niger
	Lethrinidae	*Monotaxis grandoculis*
	Lutjanidae	*Lutjanus malabaricus*
		Macolor macularis
		Macolor niger
	Mullidae	*Parupeneus macronemus*
		Parupeneus trifasciatus
	Pomacentridae	*Amblyglyphidodon leucogaster*
		Chromis viridis
		Plectroglyphidodon lacrymatus
	Scombridae	*Euthynnus affinis*
		Gymnosarda unicolor
	Serranidae	*Plectropomus areolatus*
		Pseudanthias sp. KSA_1890
	Tetraodontidae	*Canthigaster janthinoptera*
Cnidaria	Agariciidae	*Pavona explanulata*
		Pavona venosa
	Aiptasiidae	*Exaiptasia diaphana*
	Alcyoniidae	*Sarcophyton ehrenbergi*
		Sarcophyton glaucum
		Sinularia brassica
	Aliciidae	*Triactis producta*
	Astrocoeniidae	*Palauastrea sp. YC_2017*
	Boloceroididae	*Boloceroides mcmurrichi*
	Clytiidae	*Clytia gracilis*
	Diphyidae	*Diphyes sp. HAW01*
	Euphylliidae	*Galaxea fascicularis*
	Fungiidae	*Lithophyllon concinna*
		Lobactis scutaria
	Hormathiidae	*Calliactis polypus*
	Isophelliidae	*Telmatactis sp. HAW01*
	Merulinidae	*Cyphastrea serailia*
		Dipsastraea pallida
		Leptoria irregularis
		Paragoniastrea australensis
		Platygyra verweyi
	Nephtheidae	*Litophyton acuticonica*
		Stereonephthya sp. C CSM_2013
	Oceaniidae	*Turritopsoides sp. MA207*
	Pectiniidae	*Physophyllia ayleni*
	Pelagiidae	*Pelagia noctiluca*
	Phymanthidae	*Phymanthus sp. IP0414*
	Plexauridae	*Rumphella sp. A CSM_2013*
	Pocilloporidae	*Pocillopora woodjonesi*
	Poritidae	*Porites monticulosa*
		Porites okinawensis
		Porites rus
	Prayidae	*Rosacea sp. 3 BO_2009*
	Siderastreidae	*Psammocora nierstraszi*
	Sphaerocorynidae	*Sphaerocoryne sp. USNM IZ 1450222*

	unknown	*Leptastrea transversa*
	Xeniidae	*Ovabunda faraunensis*
Echinodermata	Acanthasteridae	*Acanthaster planci*
	Cidaridae	*Eucidaris metularia*
	Corellidae	*Corella minuta*
	Diadematidae	*Echinothrix calamaris*
		Echinothrix diadema
	Holothuriidae	*Bohadschia subrubra*
		Holothuria atra
		Holothuria scabra
		Holothuriidae sp. USNM IZ 1449044
	Ophiactidae	*Ophiactis aff. savignyi HAW02*
		Ophiactis savignyi
	Ophidiasteridae	*Linckia multifora*
	Ophiocomidae	*Breviturma brevipes*
		Breviturma doederleini
		Ophiocoma erinaceus
	Ophionereidae	*Ophionereis porrecta*
	Ophiotrichidae	*Macrophiothrix longipeda*
		Ophiothela tigris
		Ophiothrix trilineata
	Stichopodidae	*Stichopus chloronotus*
	Toxopneustidae	*Toxopneustes pileolus*
Mollusca	Aeolidiidae	*Limenandra sp. A LC_2013*
	Aglajidae	*Niparaya regiscorona*
	Aplysiidae	*Aplysia parvula*
	Cerithiidae	*Cerithium egenum*
	Chromodorididae	*Goniobranchus vibratus*
	Columbellidae	*Euplica ionida*
		Seminella peasei
	Hydrobiidae	*Rissoina sp. PNG2285*
	Littorinidae	*Littoraria undulata*
	Muricidae	*Maculotriton serriale*
	Octopodidae	*Octopus cyanea*
	Plakobranchidae	*Thuridilla livida*
	Pleurobranchidae	*Pleurobranchus forskalii*
	Ranellidae	*Cymatiinae sp. BMOO_02358*
	Rissoidae	*Rissoina honoluluensis*
	Tellinidae	*Loxoglypta clathrata*
	Terebridae	*Myurella affinis*
	Trinchesiidae	*Phestilla lugubris*
		Phestilla sibogae
	Turridae	*Carinapex minutissima*
	unknown	*Gastropoda sp. IOP_0552*
	unknown	*Gastropoda sp. IOP_0601*
	unknown	*Gastropoda sp. KSA_1781*
	unknown	*Mollusca sp. IOP_0387*
	Vermetidae	*Cupolaconcha meroclista*
		Petaloconchus keenae
Porifera	Astroscleridae	*Astrosclera willeyana*
	Biemnidae	*Biemna fistulosa*
		Neofibularia hartmani

	Callyspongiidae	*Callyspongia fallax*
		Callyspongia subarmigera
	Chalinidae	*Chalinidae sp. 2 JV_2020*
		Cladocroce burapha
		Haliclona sp. 1 PRT_2020
		Haliclona sp. 22 JV_2020
	Coelosphaeridae	*Lissodendoryx hawaiiana*
	Dictyodendrillidae	*Dictyodendrilla cavernosa*
	Geodiidae	*Geodia californica*
	Halichondriidae	*Hymeniacidon sp. 1 JV_2020*
	Iotrochotidae	*Iotrochota acerata*
	Microcionidae	*Clathria sp. 2 PRT_2020*
	Mycalidae	*Mycale cecilia*
		Mycale mirabilis
	Niphatidae	*Gelliodes wilsoni*
	Oscarellidae	*Oscarella sp. 3 JV_2020*
	Plakinidae	*Plakina sp. 1 JV_2020*
		Plakortis halichondrioides
	Pseudoceratinidae	*Pseudoceratina purpurea*
	Spirastrellidae	*Spirastrella sp. SPS.2*
	Spongiidae	*Hyattella sinuosa*
	Suberitidae	*Suberitidae sp. 1 JV_2020*
		Suberitidae sp. 3 JV_2020
		Suberitidae sp. 5 JV_2020
	Tedaniidae	*Tedania ignis*
		Tedania tubulifera
	Tethyidae	*Tethya minuta*
		Tethya sp. 3 JV_2020
	Tetillidae	*Cinachyra sp. CJ_2016*
	Theonellidae	*Theonella swinhoei*
		Theonella xantha
	unknown	*Haplosclerida sp. 2 JV_2020*
	unknown	*Haplosclerida sp. 8 JV_2020*
	unknown	*Haplosclerida sp. DGM_2019*
	unknown	*Poecilosclerida sp. DGM_2019*
	unknown	*Terpios gelatinosus*
	unknown	*Terpios hoshinota*
Sipuncula	Phascolosomatidae	*Phascolosoma nigrescens*

Table A.5. Summary table of multivariate GLM on the effect of site, year and both variables interacting, on the abundance of metazoan orders in the COI metabarcoding dataset. Only orders which were found to have their abundance significantly ($p<0.05$) determined by variables are shown in this table and highlighted in green. The abundance of individual orders is based on the accumulative number of cOTUs present for each order-level group, and so does not include read abundances. P-values and test scores are presented for each GLM.

Phylum	Order	Site		Year		Site * Year	
		p-value	test	p-value	test	p-value	test
Porifera	Agelasida	0.001	17.73	0.037	4.69	0.487	0.69
Arthropoda	Amphipoda	0.028	7.54	0.005	8.89	0.976	0.01
Echinodermata	Aspidochirotida	0.033	7.56	0.018	5.90	0.714	0.93
Nemertea	Monostilifera	0.016	9.96	0.009	7.17	0.436	0.58
Chordata	Syngnathiformes	0.01	9.96	0.007	8.34	0.729	0.00
Cnidaria	Trachymedusae	0.019	7.03	0.022	6.41	0.721	0.00
Mollusca	Triphoridae	0.001	18.76	0.025	5.36	0.911	0.00
Cnidaria	Corallimorpharia	0.748	0.72	0.034	5.25	0.047	5.63
Chordata	Aplousobranchia	0.394	2.01	0.039	4.73	0.089	5.93
Cnidaria	Coronatae	0.308	3.14	0.043	4.73	0.77	0.00
Bryozoa	Ctenostomatida	0.277	2.58	0.016	6.29	0.07	5.79
Nematoda	Enoplida	0.378	2.17	0.044	4.53	0.372	2.42
Chordata	Gobiiformes	0.78	0.41	0.019	6.41	0.893	0.00
Mollusca	Littorinimorpha	0.348	2.23	0.038	4.47	0.877	0.37
Ctenophora	Platyctenida	0.094	5.47	0.011	8.15	0.615	0.00
Arthropoda	Sarcoptiformes	0.383	2.22	0.001	15.78	0.679	0.00
Cnidaria	Scleractinia	0.857	0.53	0.02	6.84	0.739	0.00
Arthropoda	Tanaidacea	0.063	6.63	0.037	4.73	0.507	0.00
Cnidaria	Actiniaria	0.001	36.03	0.575	0.35	0.4	0.17
Cnidaria	Alcyonacea	0.029	7.76	0.11	2.72	0.61	1.20
Echinodermata	Amphilepidida	0.025	6.76	0.691	0.25	0.719	0.00
Cnidaria	Anthoathecata	0.001	21.39	0.118	2.39	0.906	0.00
Echinodermata	Camarodonta	0.006	13.87	0.822	0.05	0.123	3.08
Mollusca	Cerithiidae	0.03	6.76	0.649	0.25	0.599	0.00
Bryozoa	Cyclostomatida	0.021	8.61	0.556	0.36	0.37	2.60
Annelida	Eunicida	0.002	14.51	0.089	2.97	0.25	3.51
Mollusca	Heterostropha	0.013	10.03	0.604	0.33	0.306	1.24
Arthropoda	Isopoda	0.026	7.38	0.069	3.98	0.68	0.00
Chordata	Lutjaniformes	0.048	5.18	0.745	0.01	0.678	0.00
Mollusca	Neogastropoda	0.001	29.76	0.338	0.92	0.103	4.94
Mollusca	Nudibranchia	0.001	22.20	0.764	0.08	0.561	1.34
Annelida	Paraonidae	0.002	18.24	0.415	0.84	0.175	2.21
Mollusca	Pleurobranchida	0.038	7.36	0.244	1.43	0.74	0.66
Mollusca	Pleurotomariida	0.011	4.72	0.18	2.62	0.673	0.00
Arthropoda	Poecilostomatoida	0.002	17.25	0.369	0.92	0.517	1.83
Porifera	Polymastiida	0.001	17.15	0.908	0.02	0.598	0.00
Mollusca	Pteropoda	0.023	8.52	0.961	0.01	0.308	2.55
Echinodermata	Spatangoida	0.023	7.79	0.107	3.19	0.326	2.45
Annelida	Spionida	0.006	12.16	0.411	0.79	0.315	2.55
Porifera	Biemnida	0.073	5.55	0.585	0.34	0.027	8.27
Porifera	Bubarida	0.387	2.19	0.099	2.72	0.008	12.82
Arthropoda	Euphausiacea	0.625	1.82	0.783	0.01	0.034	3.36
Platyhelminthes	Polycladida	0.396	2.66	0.663	0.25	0.03	4.09
Mollusca	Siphonariida	0.647	1.82	0.861	0.01	0.038	3.36
Echinodermata	Valvatida	0.657	0.89	0.165	2.22	0.001	23.48

Table A.6. Summary table of multivariate GLM on the effect of site, year and both variables interacting, on the abundance of metazoan orders in the 18S metabarcoding dataset. Only orders which were found to have their abundance significantly ($p<0.05$) determined by variables are shown in this table and highlighted in green. The abundance of individual orders is based on the accumulative number of cOTUs present for each order-level group, and so does not include read abundances. P-values and test scores are presented for each GLM.

Phylum	Order	Site		Year		Site * Year	
		p-value	test	p-value	test	p-value	test
Arthropoda	Calanoida	0.694	0.78	0.002	13.14	0.003	13.81
Cnidaria	Alcyonacea	0.02	9.55	0.69	0.13	0.008	8.88
Arthropoda	Siphonostomatoida	0.001	23.50	0.972	0.00	0.002	11.06
Gastrotricha	Chaetonotida	0.001	17.50	0.365	1.04	0.03	1.79
Chaetognatha	Phragmophora	0.009	11.35	0.002	12.81	0.599	0.59
Chaetognatha	Aphragmophora	0.018	9.13	0.01	6.47	0.088	5.47
Bryozoa	Ctenostomatida	0.003	13.22	0.002	15.50	0.625	0.46
Arthropoda	Sessilia	0.014	9.67	0.002	8.85	0.412	1.46
Arthropoda	Pedunculata	0.036	7.23	0.009	7.44	0.693	0.00
Platyhelminthes	Prolecithophora	0.01	9.00	0.002	10.75	0.697	0.00
Cnidaria	Leptothecata	0.001	21.10	0.001	13.92	0.161	2.26
Nematozoa	Monhysterida	0.647	0.92	0.018	7.29	0.096	4.06
Nematozoa	Desmoscolecida	0.768	0.52	0.011	7.69	0.228	3.53
Rotifera	Adinetida	0.344	2.71	0.002	12.49	0.912	0.00
Nematozoa	Tylenchida	0.679	1.33	0.003	9.07	0.659	0.00
Nematozoa	Ascaridida	0.633	1.08	0.005	10.44	0.13	3.43
Nematozoa	Spirurida	0.553	1.49	0.009	9.40	0.454	1.83
Nematozoa	Araeolaimida	0.158	4.88	0.017	7.44	0.741	0.00
Nematozoa	Desmodorida	0.197	4.20	0.032	5.85	0.485	0.80
Entoprocta	Loxosomatidae	0.28	3.02	0.044	4.34	0.803	0.00
Arthropoda	Harpacticoida	0.426	1.86	0.01	7.44	0.703	0.00
Scalidophora	Cyclorhagida	0.811	0.56	0.001	11.22	0.791	0.77
Arthropoda	Halocyprida	0.178	3.80	0.001	20.31	0.11	4.77
Porifera	Homosclerophorida	0.091	4.92	0.018	5.87	0.649	0.00
Mollusca	Caenogastropoda	0.768	0.70	0.002	12.16	0.262	3.11
Tunicata	Copelata	0.711	0.74	0.005	11.07	0.445	2.35
Porifera	Poecilosclerida	0.335	2.47	0.039	4.66	0.401	2.33
Nemertea	Palaeonemertea	0.955	0.00	0.005	9.07	0.994	0.00
Cnidaria	Carybdeida	0.057	7.08	0.004	10.75	0.548	0.00
Nemertea	Monostilifera	0.278	2.72	0.004	10.75	0.578	0.00
Nemertea	Heteronemertea	0.071	6.35	0.009	7.29	0.153	0.56
Annelida	Phascolosomatiformes	0.19	3.49	0.038	4.88	0.444	2.36
Nemertea	Polystilifera	0.016	9.18	0.742	0.13	0.128	4.88
Mollusca	Arcoida	0.017	9.42	0.307	1.22	0.278	1.64
Porifera	Dictyoceratida	0.038	7.61	0.119	2.34	0.505	1.86
Mollusca	Myoida	0.001	25.77	0.548	0.43	0.221	0.91
Annelida	Capitellida	0.041	6.77	0.192	2.11	0.273	0.43
Porifera	Clathrinida	0.002	14.27	0.127	2.44	0.13	0.41
Porifera	Hadromerida	0.019	9.18	0.215	1.86	0.868	0.36
Arthropoda	Podocopida	0.024	7.00	0.514	0.36	0.733	0.00
Arthropoda	Leptostraca	0.003	12.12	0.094	2.79	0.406	2.64
Mollusca	Pholadomyoida	0.001	15.30	0.218	1.43	0.197	2.98
Porifera	Axinellida	0.001	14.95	0.314	1.19	0.878	0.36
Cnidaria	Coronatae	0.006	10.44	0.28	1.28	0.683	1.08
Rotifera	Ploimida	0.016	8.90	0.172	2.05	0.322	2.74
Gnathostomulida	Bursovaginoidea	0.011	10.06	0.066	3.50	0.499	0.64
Ctenophora	Platyctenida	0.011	9.22	0.089	3.24	0.199	0.29
Platyhelminthes	Mediofusata	0.001	23.98	0.263	1.28	0.379	1.94
Annelida	Phyllodocida	0.006	11.57	0.518	0.49	0.056	4.40

Table A.7. Percentage overlap of COI and 18S cOTU sequence variants between ARMS triplicates per site and per sampling year.

COI	Site	% overlap in 2019	% overlap in 2021
	Moresby	20.51	20.45
	Ile Anglaise	23.37	9.87
	Ile du Coin	17.47	17.37
	All site average	20.45	15.9
18S	**Moresby**	31.76	32.16
	Ile Anglaise	32.24	28.38
	Ile du Coin	25.1	33.79
	All site average	29.7	31.4

B. Supplementary Material for Chapter 3

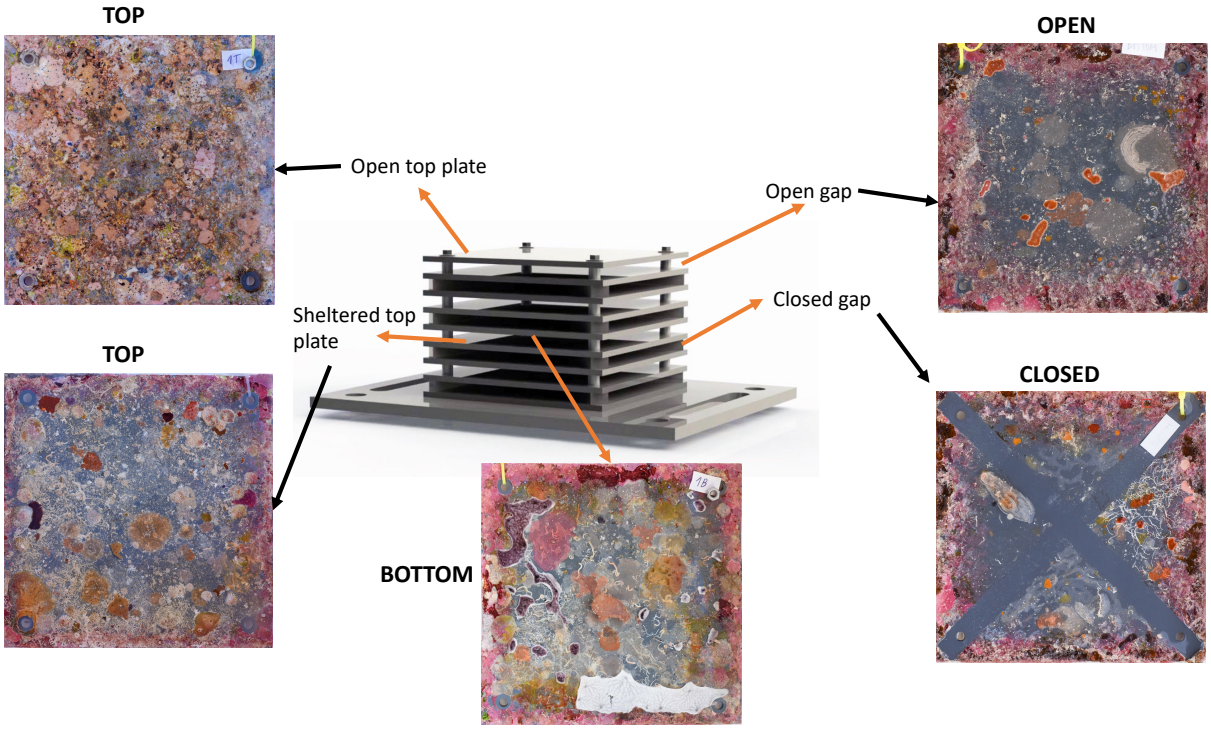

Figure B.1. Summary graphic of Autonomous Reef Monitoring Structures (ARMS), with example photographs of each plate surface type. The ARMS graphic was designed by drawn by D. Merritt and obtained from the Smithsonian Global ARMS Program 'ARMS Assembly Protocol'. Photographs of ARMS plate faces are from this study's dataset.

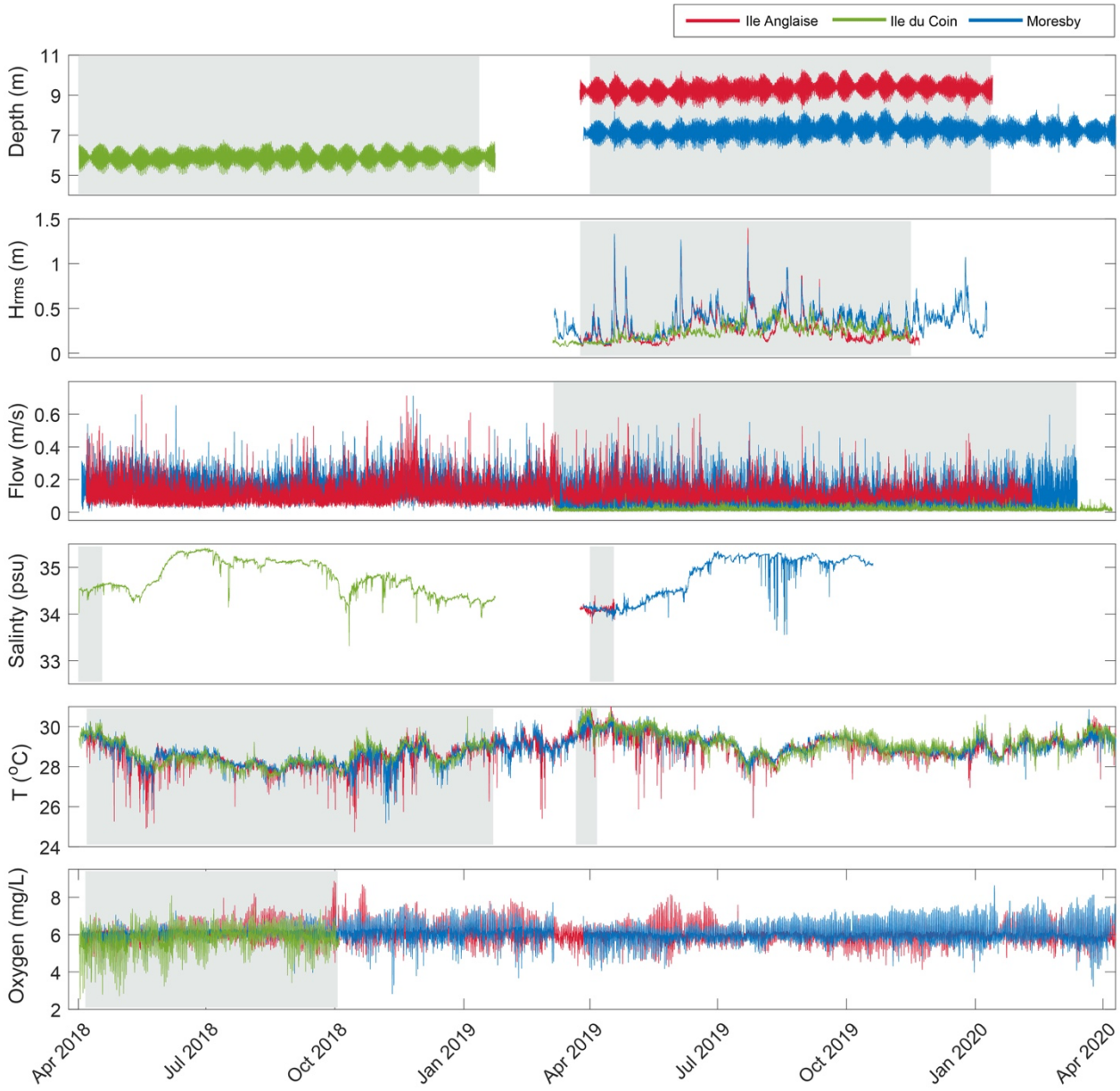

Figure B.2. Long term environmental conditions measured at the three sites between April 2018 and April 2020 for a) depth, b) root-mean-square wave heights, c) flow velocity, d) salinity, e) temperature, and f) dissolved oxygen. Timeseries are not complete due to limited battery life of instruments and instrument availability. Grey background portions indicate the time ranges for which data was compared between the three sites. For specific dates see Supplementary Table S4. Note that due to the lack of overlap in time range of the data of depth and salinity between Ile du Coin and the other two sites, similar calendar dates from different years were used to compare between the sites - 2018 in Ile du Coin and 2019 in Ile Anglaise and Moresby.

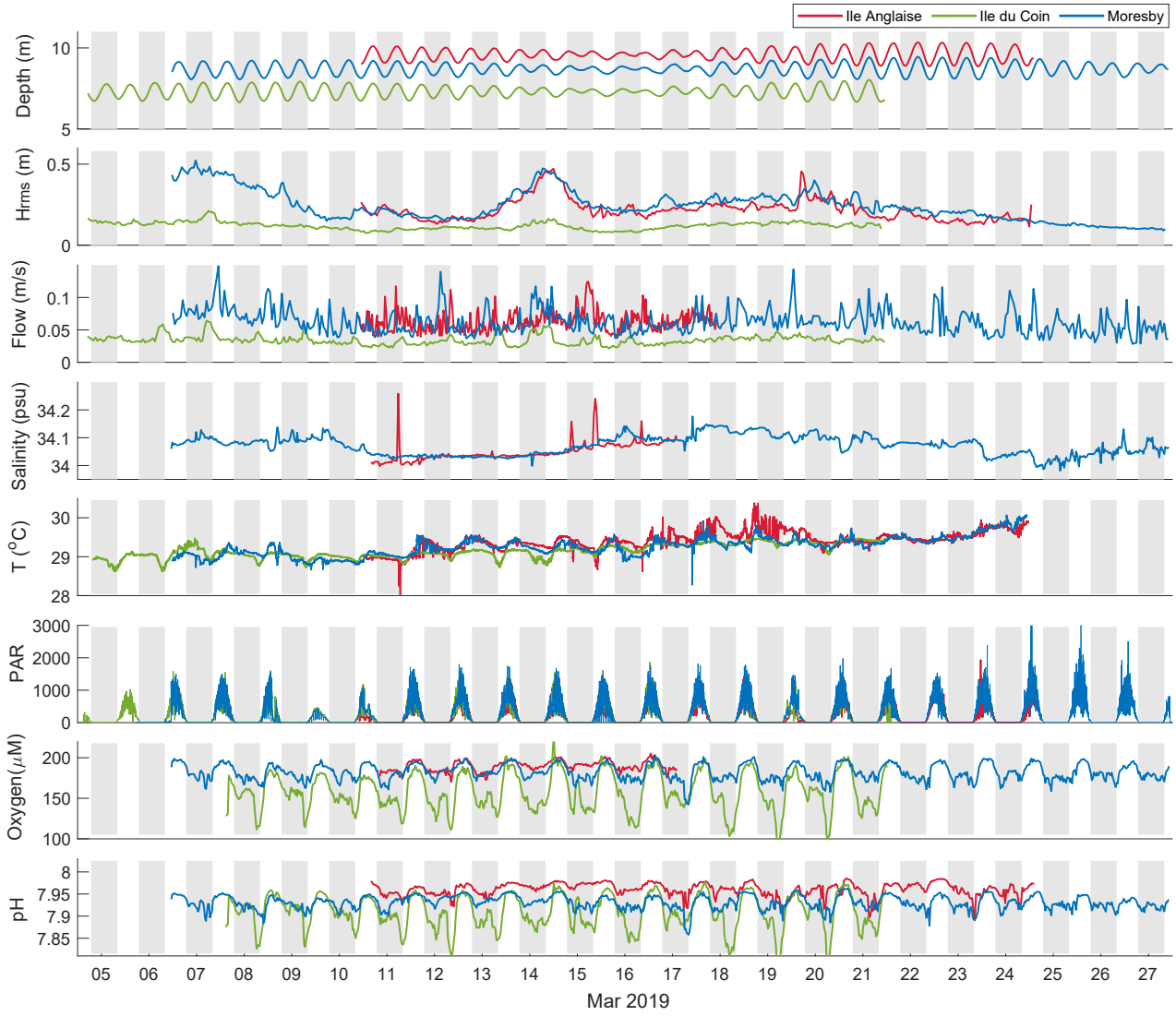

Figure B.3. Short-term deployments across the three sites during the month of March 2019 for a) depth, b) root-mean-square wave heights, c) flow velocity (1 meter above the seabed), d) salinity, e) temperature, f) dissolved oxygen, g) PAR, and h) pH. Grey bars represent night-time periods, and white background represents daytime periods. For Ile du Coin and Moresby, measurements were taken 500-700 m from the ARMS.

Table B.1. Latitudinal and longitudinal coordinates for ARMS devices and environmental instruments across sampling site in the Chagos Archipelago Marine Protected Area.

Reef site	Device	Latitude	Longitude
Ile Anglaise	ARMS (n=3) + Instruments	5° 20.32' S	72° 12.80' E
Ile du Coin	ARMS (n=3) + Instruments	5° 27.023' S	71° 46.043' E
Ile du Coin	Instruments	5° 26.014' S	71° 45.012' E
Moresby	ARMS (n=3)	5° 14.13' S	71° 50.02' E
Moresby	Instruments	5° 14.08' S	71° 49.63' E

Table B.2. CoralNet labelset for ARMS image analysis, with matching short codes and identification descriptions.

Label name	Short Code	Description
ARMS-CREP-Coral	_CO	Stony corals or hard corals of Order Scleratinia
ARMS-CREP-Bivalve	_BI	Live or empty shells of Class Bivalvia (incl. Mussels, clams and oysters).
ARMS-CREP-Bryozoan	_BRY	Encrusting or branching colonies of Class Bryozoa (commonly called 'moss-animals'). Live or dead colonies are included (with or without zooids).
ARMS-CREP-Calcareous Worm Tube	_CAWT	Annelid worms living in solid secreted tubes of calcium carbonate. Empty or broken tubes are included.
ARMS-CREP-Corallimorph	_CMOR	Solitary or colonial of anemone-like animals or the Order Corallimorpharia.
ARMS-CREP-Eggs	_EGG	Egg masses deposited by mobile fauna.
ARMS-CREP-Foraminifera	_FORM	Small single-cell protist with shells or tests of various shapes. Colour may be white, pink or red (including Homotrema sp.).
ARMS-CREP-Gastropoda	_GAS	Molluscs of the Class Gastropoda, including snails, slugs and limpets. Empty gastropod shells are included.
ARMS-CREP-Hydrocoral	_HYCO	Non-scleractinian colonial corals with hard skeletons of the Class Hydrozoa.
ARMS-CREP-Hydrozoa	_HYD	Hydroid-stage animals of the Class Hydrozoa, the majority of which are colonial.
ARMS-CREP-Octocoral	_OCTO	Gorgonian corals including sea fans, sea pens and octocorals. Majority are colonial or stoloniferous, and a number of tentacles in a multiple of eight.
ARMS-CREP-Soft Worm Tube	_SOWT	Annelid worms living in soft secreted tubes. Empty tubes are included. Tubes often sand coloured and contain sediment particles. Can be hard to discern from loose sediment, and can be identified but their round or tubular forms.
ARMS-CREP-Sponge	_SP	Branching, encrusting and burrowing animals of the Phylum Porifera. Sponges can often be confused with colonial ascidians but are identified by the presence of visible spicules, channels and large pores.
ARMS-CREP-Tunicate Colonial	_TUNC	Colonial ascidians of the sub-Phylum Tunicata. This includes colonies or chains of individual zooids. Often confused with sponges, these are distinguishable by smooth 'tunic' and multiple regular siphons.
Tunicate (solitary)	Tun_sol	Solitary ascidians of the sub-Phylum Tunicata. Often large in size and have two conspicuous siphons for filtering.
ARMS-CREP-Zoanthid	_ZO	Colonial anemone-like animals of the Order Zoanthidea. These lack 'hard' skeletons and have a number of tentacles in a multiple of six.
ARMS-CREP-Sediment	_SED	Sediment which either obscures organisms or rests on the plate. This includes coarse and fine sand.
Excavating Bite Scar	BiteScar	Bare substrate created by the excavation of surrounding sessile substrate by grazers or predators. Includes visible bite and scrape marks of parrotfish and molluscs.
ARMS-CREP-Mobile Fauna	_MOBF	Category encompassing organisms which do not permanently attach themselves to sessile substrate, including but not limited to echinoderms, fish, nudibranchs, free-living worms.
ARMS-CREP-No Recruitment	_NR	Bare plate surface in an area where colonisation is possible (not obstructed by cross-bars, spacers and bolts).
ARMS-CREP-Unavailable	_UNAV	Survey point located on an area where colonisation is not possible (obstructed by cross-bars, spacers, bolts or off the plate).
ARMS-CREP-Unclassified/Unknown	_UNK	Survey point for specimens that cannot be identified to other labels with confidence.
ARMS-CREP-Blue-green macroalga	_BGMA	Cyanobacteria often seen as fine filamentous tufts or mats over a portion of plates/ Can be observed in different colours including but not limited to deep purple, white, pale yellow and red.
ARMS-CREP-Brown encrusting macroalgae	_BREN	Brown macroalgae observed as encrusting often on the outer edges of plates. Can either be completely attached to the plate, or partly attached and lifting off around edges. Often observed in blade-like or fan-like forms (e.g. Lobophora spp.)
ARMS-CREP-Brown upright macroalgae	_BRUP	Brown algae in upright forms, of the Class Phaeophyta. Colours may range from pale beige to dark brown or near black. Forms include filaments, blades or flattened branches (e.g. Dictyopteris or Dictyota spp.).
ARMS-CREP-CCA	_CCA	Crustose coralline algae, usually observed in hard pink or lavender patches.
ARMS-CREP-Green encrusting macroalgae	_GREN	Green macroalgae observed as encrusting often on the outer edges of plates.
ARMS-CREP-Green upright macroalgae	_GRUP	Green macroalgae not in encrusting forms, colours ranging from yellow-green, to grass green or black-green tones. Forms include blades, fans, branching, filamentous, bubble, calcified discs (e.g. Halimeda spp.) and flattened fronds.
ARMS-CREP-Red encrusting macroalgae	_RDEN	Red macroalgae observed as encrusting often on the outer edges of plates. Can either be completely attached to the plate, or partly attached and lifting off around edges. Often observed in blade-like or fan-like forms (e.g. Peyssonnelia spp.) and can vary in colour from scarlet red to wine red and maroon tones.
ARMS-CREP-Red upright macroalgae	_RDUP	Red upright macroalgae of the Phylum Rhodophyta, can vary in forms and colours from scarlet red to wine red and maroon tones (e.g. Asparagopsis spp.)

Table B.3. Timeline of the instruments measuring environmental data deployed long-term and short-term at each site. ARMS were deployed at all sites in March 2018 and retrieved in March 2019.

	2018									2019											2020			
	A	M	J	J	A	S	O	N	D	J	F	M	A	M	J	J	A	S	O	N	D	J	F	M	A
Ile Anglaise																								
Temperature	SBE56 (sampling interval 30 sec)											SBE56 (sampling interval 30 sec)												
Salinity												SBE 37 (sampling interval 10 min)												
Flow velocity	ADP																							
PAR																								
Dissolved O2	miniDOT (sampling interval																							
pH																								
Waves												RBR Virtuoso												
Ile du Coin																								
Temperature	SBE37 (sampling interval 10 min)											SBE56 (sampling interval 30 sec)												
Salinity	SBE 37 (sampling interval 10 min)																							
Flow velocity												ADCP												
PAR																								
Dissolved O2	miniDOT																							
pH																								
Waves												RBR solo												
Moresby																								
Temperature	SBE56 (sampling interval 30 sec)											SBE56 (sampling interval 30 sec)												
Salinity												SBE 37 (sampling interval 10 min)												
Flow velocity	ADCP																							
PAR																								
Dissolved O2	miniDOT																							
pH																								
Waves												RBR solo												

Table B.4. Long-term deployment dates and information for the deployment of instruments.

	Site	Instrument	Sampling interval	Range	Range where mean/sd/etc. were caluclated
Depth	Ile Anglaise	SBE 37-SM/SMP (Sea-Bird Scientific)	10 min	March 24, 2019 - January 13, 2020	April 1, 2019 - January 23, 2020
	Ile du Coin	SBE 37-SM/SMP (Sea-Bird Scientific)	10 min	April 1, 2018 - January 23, 2019	April 1, 2018 - January 23, 2019
	Moresby	SBE 37-SM/SMP (Sea-Bird Scientific)	10 min	March 27, 2019 onward	April 1, 2019 - January 23, 2020
Waves	Ile Anglaise	RBR Virtuoso (Ruskin)	1 Hz	March 24 - November 21, 2019	March 24 - November 21, 2019
	Ile du Coin	RBR Solo (Ruskin)	1 Hz	March 5- November 15, 2019	March 5- November 15, 2019
	Moresby	RBR Solo (Ruskin)	1 Hz	March 6 - January 9, 2020	March 6 - January 9, 2020
Flow velocity	Ile Anglaise	Acoustic Doppler Profiler (ADP; Nortek)	30 min	April 6, 2018 - February 10, 2020	March 12, 2019 - February 10, 2020
	Ile du Coin	Acoustic Doppler Current Profiler (ADCP; RD Instruments)	20 min	March 5, 2019 to April 7, 2020	March 5, 2019 - April 7, 2020
	Moresby	Acoustic Doppler Current Profiler (ADCP; RD Instruments)	20 min	April 3, 2018 - March 13, 2020	March 6, 2019 - April 13, 2020
Salinity	Ile Anglaise	SBE 37-SM/SMP (Sea-Bird Scientific)	10 min	March 24, 2019 - January 13, 2020	April 1, 2019 - April 18, 2019
	Ile du Coin	SBE 37-SM/SMP (Sea-Bird Scientific)	10 min	April 1, 2018 - January 23, 2019	April 1, 2018 - April 18, 2018
	Moresby	SBE 37-SM/SMP (Sea-Bird Scientific)	10 min	March 27, 2019 onward	April 1, 2019 - April 18, 2019
Temperature	Ile Anglaise	SBE 56 (Sea-Bird Scientific)	30 sec	April 6, 2018 onward	April 7, 2018 - April 7, 2019, excluding Jan 23-Mar 22, 2019
	Ile du Coin	SBE 37-SM/SMP (Sea-Bird Scientific)	10 min	April 7, 2018 - January 23, 2019	April 7, 2018 - January 23, 2019
		SBE 56 (Sea-Bird Scientific)	30 sec	March 22, 2019 on wards	March 22, 2019 - April 7, 2019
	Moresby	SBE 56 (Sea-Bird Scientific)	30 sec	April 3, 2018 onward	April 7, 2018 - April 7, 2019, excluding Jan 23-Mar 22, 2019
Dissolved Oxygen	Ile Anglaise	miniDOT (PME)	5 min	April 6, 2018 - March 10, 2019	April 6, 2018 - October 3, 2018
		miniDOT (PME)	10 min	March 10, 2019 - onward	
	Ile du Coin	miniDOT (PME)	5 min	April 1, 2018 - October 4, 2018	April 6, 2018 - October 3, 2018
	Moresby	miniDOT (PME)	5 min	April 3, 2018 - March 6, 2019	April 6, 2018 - October 3, 2018
		miniDOT (PME)	10 min	March 27, 2019 - onward	

Table B.5. Short-term deployment dates and information for the deployment of instruments.

	Site	Instrument	Sampling interval	Range	Range used for calculations
	Ile Anglaise	RBR Solo (Ruskin)	10 min	March 10 - March 24, 2019	-
	Ile du Coin	RBR Solo (Ruskin)	10 min	March 5 - March 21, 2019	-
Depth	Moresby	RBR Solo (Ruskin)	10 min	March 6 - March 27, 2019	-
	Ile Anglaise	RBR Solo (Ruskin)	1 Hz	March 10 - March 24, 2019	-
	Ile du Coin	RBR Solo (Ruskin)	1 Hz	March 5 - March 21, 2019	-
Waves	Moresby	RBR Solo (Ruskin)	1 Hz	March 6 - March 27, 2019	-
	Ile Anglaise	Acoustic Doppler Profiler (ADP; Nortek)	30 min	March 10 - March 24, 2019	-
	Ile du Coin	Acoustic Doppler Velocimeter (ADV; Nortek)	1 hour	March 5 - March 21, 2019	-
Flow velocity	Moresby	Acoustic Doppler Velocimeter (ADV; Nortek)	1 hour	March 6 - March 27, 2019	-
	Ile Anglaise	SBE 37-SM/SMP (Sea-Bird Scientific)	1 min (20 min ave)	March 10 - March 17, 2019	-
	Ile du Coin	SeapHOx V2 (Sea-Bird Scientific)	30 sec (15 min ave)	Malfunctioned	-
Salinity	Moresby	SeapHOx V2 (Sea-Bird Scientific)	30 sec (15 min ave)	March 6 - March 27, 2019	-
	Ile Anglaise	SBE 37, SBE 56 (Sea-Bird Scientific)	30 sec	March 10 - March 24, 2019	-
	Ile du Coin	SBE 37, SBE 56 (Sea-Bird Scientific)	30 sec	March 5 - March 21, 2019	-
Temperature	Moresby	SBE 37, SBE 56 (Sea-Bird Scientific)	30 sec	March 6 - March 24, 2019	-
	Ile Anglaise	miniPAR (PME)	1 min	March 10 - March 24, 2019	March 10 - March 21, 2019
	Ile du Coin	miniPAR (PME)	1 min	March 5 - March 21, 2019	March 10 - March 21, 2019
PAR	Moresby	miniPAR (PME)	1 min	March 6 - March 27, 2019	March 10 - March 21, 2019
	Ile Anglaise	SBE 37-SM/SMP/SMP-ODO	1 min (20 min ave)	March 10 - March 24, 2019	-
	Ile du Coin	SBE 37-SM/SMP/SMP-ODO	30 sec (15 min ave)	March 7 - March 21, 2019	-
Dissolved Oxygen	Moresby	SBE 37-SM/SMP/SMP-ODO	30 sec (15 min ave)	March 6 - March 27, 2019	-
	Ile Anglaise	SeaFET (Sea-Bird Scientific)	10 sec (20 min ave)	March 10 - March 24, 2019	March 10 - March 20, 2019
	Ile du Coin	SeapHOx V2 (Sea-Bird Scientific)	30 sec (15 min ave)	March 7 - March 21, 2019	March 10 - March 20, 2019
pH	Moresby	SeapHOx V2 (Sea-Bird Scientific)	30 sec (15 min ave)	March 6 - March 27, 2019	March 10 - March 20, 2019

Table B.6. Due to the length of this table, please find in Supplementary Information of published article instead: https://doi.org/10.3389/fmars.2022.932375

Table B.7. Environmental data summary.

		Ile Anglaise	*Ile du Coin*	*Moresby*	Time range	Comments
Temperature (long term)	Mean	28.5138	29.3977	28.5764	7 Apr 2018 00:00 - 6 Apr 2019 23:59 excluding Jan 23-Mar 22!	
	SD	0.6049	0.9419	0.5844		
	Min	24.7389	27.164	25.1754		
	Max	30.9043	30.9801	30.9263		
Salinity	Mean	34.0761	34.5334	34.0801	1 Apr 12:00 - 18 Apr 11:50. Ile Anglaise and Moresby for 2019 and Ile du Coin for 2018.	Average for overlapping days - full 24h
	SD	0.0485	0.0623	0.044		
	Min	33.7972	34.0219	33.8516		
	Max	34.3988	34.6647	34.2321		
Depth (long term)	Mean	9.3098	5.8716	7.224	1 Apr 12:00 - 12 Jan 11:50.	Overlapping days in the year - 2018 (Coin), 2019 (Anglaise, Moresby)
	SD	0.3401	0.3146	0.338		
	Min	8.223	4.967	6.131		
	Max	10.294	6.775	8.377		
Dissolved oxygen (long term)	Mean	6.1271	5.8684	6.1242	6 Apr 16:03 - 3 Oct 15:58	Average for overlapping days - full 24h
	SD	0.4123	0.5988	0.2744		
	Min	4.5018	2.7096	3.9168		
	Max	8.8656	8.0878	7.2851		
pH (short term)	Mean	7.9607	7.9082	7.9327	10 Apr 16:00 - 20 Mar 15:59	Average for overlapping days - full 24h
	SD	0.0137	0.0401	0.0163		
	Min	7.9155	7.7778	7.8579		
	Max	7.9855	7.9772	7.9623		
PAR (short term)	Mean	189.333	214.718	235.438	10 Mar 10:01 - 21 March 10:00	Average for overlapping days - full 24h
	Mean Max	1089.088	1354.21	1579.523		
	SD mean max	387.667	312.488	368.706		
Velocity (long term)	Mean	0.1165	0.0185	0.1012	5 Mar 2019 - 7 Apr 2020 (Coin), 6 Mar 2019 - 13 Mar 2020 (Moresby), 12 Mar 2019 - 10 Feb 2020 (Anglaise)	
	SD	0.069	0.0102	0.0722		
	Min	0.02	0.0036	0.0043		
	Max	0.7181	0.1154	0.596		
Waves (long term)	Mean	0.2676	0.2316	0.3506	5 Mar 2019 - 15 Nov 2019 (Coin), 6 Mar 2019 - 8 Jan 2020 (Moresby), 24 Mar 2019 - 21 Nov 209 (Anglaise)	
	SD	0.158	0.0874	0.1506		
	Min	0.0744	0.0716	0.0903		
	Max	1.3975	0.5728	1.3327		

Table B.8. Values from an overall summary and analysis of deviance of a generalised linear model (GLM) of live sessile cover (%) with ARMS plate face (top and bottom) and sampling sites (Ile du Coin, Moresby, Ile Anglaise)(family = quasibinomial).

Summary				
Call: glm(formula = perc_recruitment_available_space_2 ~ site + top_bottom, family = quasibinomial, data = cn_photo_analysis_2)				

	Estimate	Std.Error	t value	Pr(>| t |)
Coefficients:				
(Intercept)	1.465678	0.115186	12.724	<2e-16 ***
site(Ile du Coin)	-0.580871	0.127268	-4.564	1.12e-05 ***
site(Moresby)	-0.009891	0.132424	-0.075	0.941
top_bottom(top)	-0.8268	0.10449	-7.913	8.36e-13 ***

(Dispersion parameter for quasibinomial family taken to be 0.07449642)				
Null deviance: 17.475 on 137 degrees of freedom				
Residual deviance: 10.542 on 134 degrees of freedom				
AIC: NA				
Number of Fisher iterations: 4				

Analysis of Deviance				
Model: quasibinomial, link: logit				
Response: proportion of recruitment on available space				
	DF	Deviance	Residual DF	Residual Deviance
NULL			137	17.475
site	2	2.1193	135	15.355
top_bottom	1	4.8132	134	10.542

Table B.9. Multivariate GLM output for all sessile groups. Significant values are highlighted in bold font.

Predictors	Hard coral		Bivalve		Bryozoan		Calcified tube worms	
	Dev.	Pr(>Dev)	Dev.	Pr(>Dev)	Dev.	Pr(>Dev)	Dev.	Pr(>Dev)
Site	5.26	0.57	9.23	0.22	17.62	**0.016***	12.1	0.12
Plate face	9.54	0.1	7.01	0.22	9.78	0.1	23.9	**0.001*****
Site : plate face	7.05	0.56	7.11	0.56	2.4	0.96	0.7	1
	Foraminifera		Gastropoda		Hydrozoa		Octocoral	
	Dev.	Pr(>Dev)	Dev.	Pr(>Dev)	Dev.	Pr(>Dev)	Dev.	Pr(>Dev)
Site	4.36	0.66	17.95	**0.014***	1.47	0.92	12.07	0.12
Plate face	2.88	0.66	0.73	0.89	0.03	0.89	0.24	0.89
Site : plate face	8.89	0.39	2.25	0.96	11.47	0.21	0.08	1
	Soft-tube worms		Sponge		Colonial tunicates		Solitary tunicates	
	Dev.	Pr(>Dev)	Dev.	Pr(>Dev)	Dev.	Pr(>Dev)	Dev.	Pr(>Dev)
Site	0.25	0.99	0.14	1	0.14	1	1.36	0.92
Plate face	62.38	**0.001*****	4.98	0.36	31.14	**0.001*****	4.24	0.43
Site : plate face	5.22	0.73	11.74	0.2	15.49	0.06	0.11	1
	Blue-green macroalgae		Brown encrusting macroalgae		Brown upright macroalgae		CCA	
	Dev.	Pr(>Dev)	Dev.	Pr(>Dev)	Dev.	Pr(>Dev)	Dev.	Pr(>Dev)
Site	12.41	0.11	19.66	**0.008****	7.84	0.3	1.79	0.92
Plate face	5.6	0.31	1.07	0.89	2.1	0.77	22.01	**0.002****
Site : plate face	0.36	1	7.14	0.56	5.71	0.69	20.86	**0.014***
	Green encrusting macroalgae		Green upright macroalgae		Red encrusting macroalgae		Red upright macroalgae	
	Dev.	Pr(>Dev)	Dev.	Pr(>Dev)	Dev.	Pr(>Dev)	Dev.	Pr(>Dev)
Site	1.99	0.91	1.65	0.92	2.59	0.85	3.52	0.76
Plate face	21.92	**0.002****	0.97	0.89	16.88	**0.003****	2.03	0.77
Site : plate face	17.18	**0.04***	4.85	0.74	20.3	**0.014***	0.45	1

Table B.10. Summary of outputs from permutation-based ANOVA tests on the effect of the constraints of environmental factors on db-RDA ordinations of benthic communities. Df = degrees of freedom, Sum of Sq = Sum of Squares, F = F-statistic, Pr(>F) = p-value.

Model	Factor	Df	Sum of Sq.	F	Pr(>F)
Temperature	In-situ	1	0.062	3.3	0.017*
	Ex-situ	1	0.056	2.98	0.025*
	(Residual)	15	0.28		
pH & Oxygen	pH	1	0.05	2.74	0.043*
	Oxygen	1	0.07	3.54	0.017*
	(Residual)	15	0.28		
PAR & Salinity	PAR	1	0.05	2.85	0.033*
	Salinity	1	0.06	3.44	0.019*
	(Residual)	15	0.28		
Velocity & Wave heights	Velocity	1	0.06	3.3	0.016*
	Wave heights	1	0.06	3	0.026*
	(Residual)	15	0.28		

B.i Supplementary Methods and Results for Chapter 3

Degree Heating Day analysis

A bleaching threshold value and the number of Degree Heating Days (DHD) were calculated across sites to determine the extent of temperature stress on surrounding reef benthos. DHD is a metric developed to describe the cumulative heat stress on a given reef (Wyatt et al., 2020). Reefs are assigned bleaching thresholds equivalent to the maximum monthly mean (MMM) SST, and any recorded temperature exceeding the MMM+1°C (the bleaching threshold) contributes to bleaching risk. Degree heating days are calculated as:

$$DHD = \sum_{i=1}^{n} \frac{max(0, T - T_b)}{n_D},$$

where n_D is the number of samples in a day (for 30 seconds sampling, n_D =2,880), T-T_b is the bleaching threshold exceedance (note that if $T_b > T$ the contribution is zero), and by convention, the summation is over the preceding 12 days (for 30s sampling, n = 34,560).

DHD was then calculated for Ile Anglaise and Moresby using the new temperature time series (with internal wave signal removed) to estimate the heat stress on outer-reef sites in the absence of internal waves.

Results

For the three sites in this study, the MMM was 29.3°C, and the bleaching threshold (T_b) was thus 30.3°C. Overall, 2018 and 2019 had relatively few periods of time where temperatures were above the bleaching threshold, most of which were between February and April 2019 (Supplementary Figure 1). At Ile Anglaise and Moresby, maximum Degree Heating Days (DHD) was 0.32°C-days and 0.46°C-days, respectively. Maximum DHD in the sheltered Ile du Coin reef was 1.7°C-days, a three to four-fold increase compared to exposed reef sites. While relatively short periods of heat stress were observed at the two sites, internal waves decreased heat stress by 13% at Ile Anglaise, and 8% at Moresby.

Turbidity

A measure of turbidity was calculated for each site based on the Beer-Lambert Law (McNaught and Wilkinson, 1997), by calculating light attenuation coefficients as:

$$I = I_0 \exp(-mD),$$

where I is the measured light intensity taken as the mean PAR measured at each site, I_0 is the incident light intensity on the water surface, m is the attenuation coefficient and D is the mean measured depth at each site. For the comparison between sites, we used the value of m as a normalised light attenuation coefficient. I_0 was assumed to be constant for all three sites (I_0=3000 µmol m^{-2} s^{-1}).

Results

Calculated light attenuation coefficients indicate that Ile Anglaise had the clearest water (0.288), followed by Moresby (0.293), and that the highest water turbidity was found in Ile du Coin (0.362).

C. Supplementary Material for Chapter 4

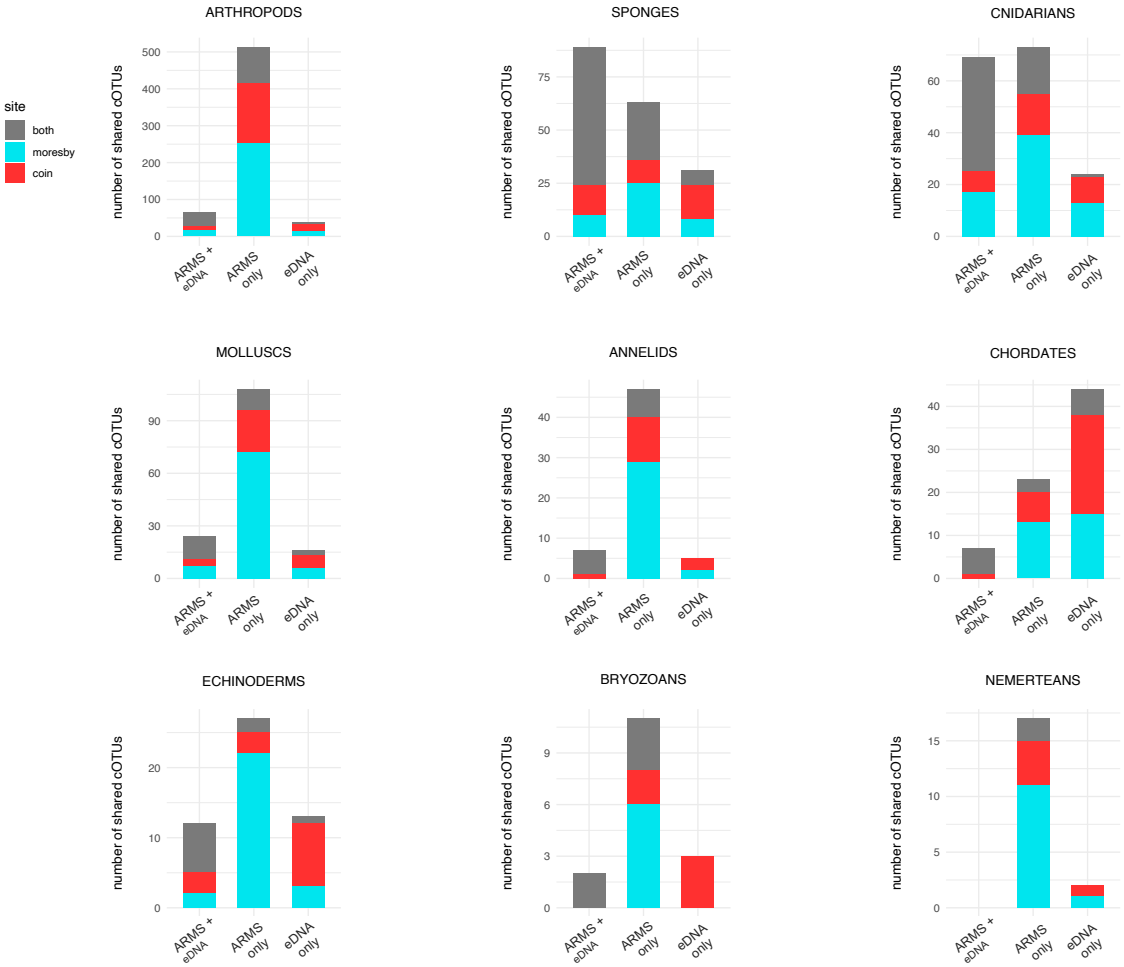

Figure C.1. Stacked barplots displaying the number of COI cOTUs across individual metazoan phyla which are either found in both eDNA and ARMS samples, or uniquely in ARMS or eDNA samples. The number of these cOTUs found either in the ocean-facing site Moresby (blue) or lagoonal site Ile du Coin (red), or in both (grey) is also displayed in each plot. This data was obtained from rarefied samples.

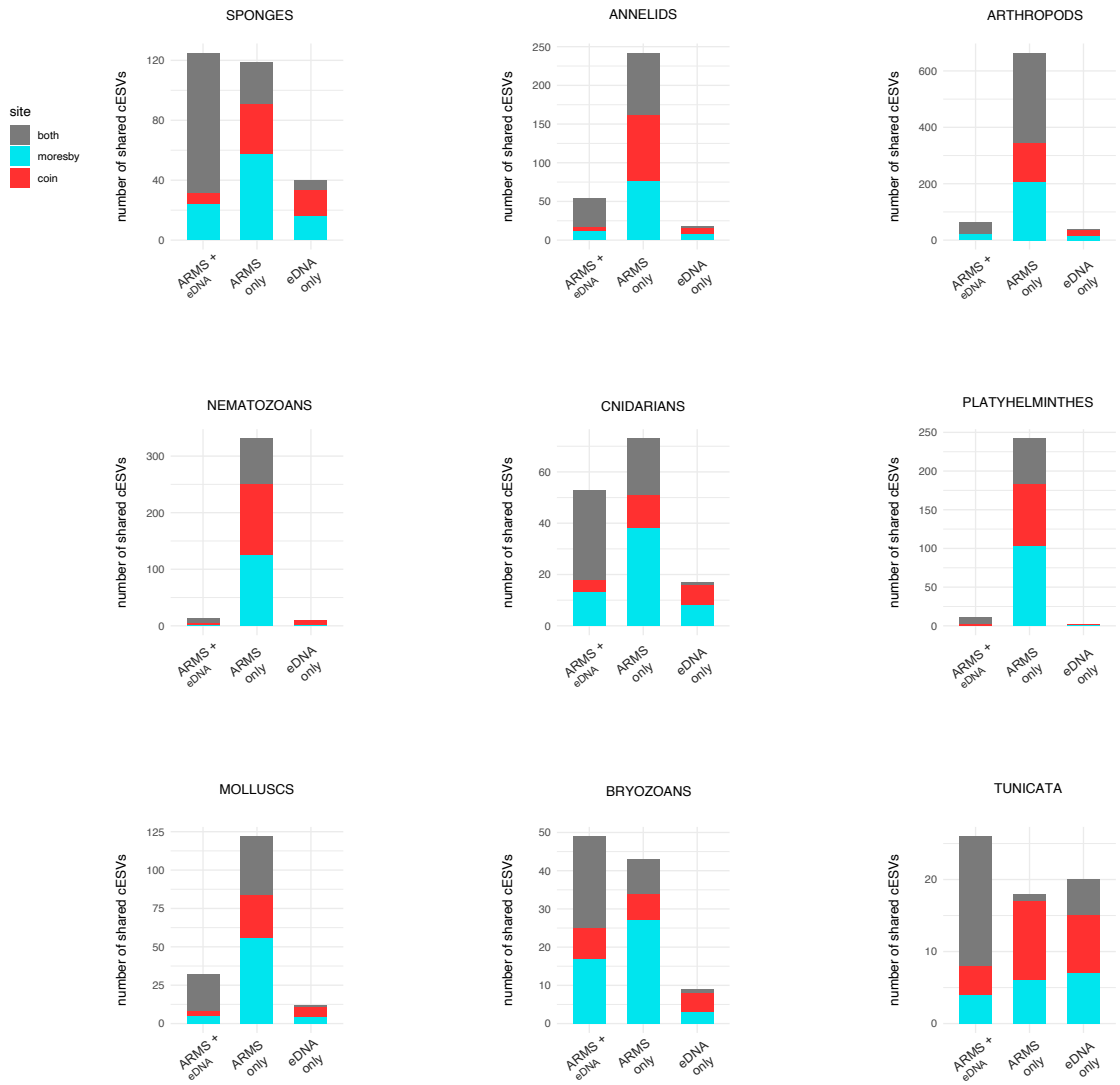

Figure C.2. Stacked barplots displaying the number of 18S cESVs across individual metazoan phyla which are either found in both eDNA and ARMS samples, or uniquely in ARMS or eDNA samples. The number of these cESVs found either in the ocean-facing site Moresby (blue) or lagoonal site Ile du Coin (red), or in both (grey) is also displayed in each plot. This data was obtained from rarefied samples.

Table C.1. Metazoan COI curated OTU sequence variants found to have significant differential abundances between eDNA and ARMS samples. Base mean values of abundance, log2FoldChange (log2FC) values and adjusted p-values are displayed for each cOTU, along with taxonomic assignments at phylum, class, order, family and genus level.

OTU_id	Base Mean	log2 FC	P-value	Phylum	Order	Genus
OTU_234851	77.36	-23.76	1E-10	Annelida	Phyllodocida	Trypanosyllis
OTU_10047	21.51	-21.82	1E-08	Annelida	Eunicida	Eunice
OTU_11300	18.48	-21.62	2E-08	Annelida	Eunicida	Palola
OTU_10470	204.69	-11.13	4E-05	Annelida	Phyllodocida	Opisthosyllis
OTU_9945	139.61	-10.41	2E-04	Annelida	Phyllodocida	Platynereis
OTU_10511	103.11	-9.97	1E-04	Annelida	order_family_genus_Polychaeta sp. C_0712	genus_Polychaeta sp. C_0712
OTU_13823	98.01	-9.90	6E-05	Annelida	Phyllodocida	unclassified_Polynoidae
OTU_20144	94.93	-9.85	2E-04	Annelida	Phyllodocida	Phyllodoce
OTU_20105	86.33	-9.72	1E-03	Annelida	Phyllodocida	unclassified_Phyllodocidae
OTU_105111	45.65	-8.97	3E-02	Annelida	order_family_genus_Polychaeta sp. C_0712	genus_Polychaeta sp. C_0712
OTU_10248	326.11	-8.74	1E-03	Annelida	Phyllodocida	Nereis
OTU_864	32.54	-8.31	2E-02	Annelida	Terebellida	genus_Terebellidae sp. JOD_0458
OTU_10365	836.66	-8.18	1E-05	Annelida	order_family_genus_Polychaeta sp. C_0118	genus_Polychaeta sp. C_0118
OTU_10397	761.23	-8.11	4E-02	Annelida	order_family_genus_Annelida sp. BOLD_ACQ2837	genus_Annelida sp. BOLD_ACQ2837
OTU_23485	26.11	-7.99	5E-02	Annelida	Phyllodocida	Trypanosyllis
OTU_18105	23.12	-7.82	2E-02	Annelida	Phyllodocida	Pisione
OTU_29040	50.71	-7.24	5E-03	Annelida	Eunicida	Lysidice
OTU_12676	10.47	7.66	5E-03	Annelida	order_family_genus_Polychaeta sp. LVSF009	genus_Polychaeta sp. LVSF009
OTU_16787	931.11	-26.85	9E-17	Arthropoda	Decapoda	Cuapetes
OTU_9985	631.66	-26.43	2E-11	Arthropoda	Decapoda	genus_Caridea sp. LPdivOTU66
OTU_16839	622.95	-25.72	6E-11	Arthropoda	Decapoda	genus_Decapoda sp. SHR162
OTU_9090	184.58	-24.74	2E-10	Arthropoda	Decapoda	genus_Decapoda sp. C_0240
OTU_10899	98.74	-23.89	7E-10	Arthropoda	Decapoda	genus_Caridea sp. LPdivOTU374
OTU_10929	50.40	-23.18	3E-09	Arthropoda	Decapoda	unclassified_Xanthidae
OTU_10274	81.96	-23.18	2E-09	Arthropoda	Decapoda	unclassified_Porcellanidae
OTU_18187	12.82	-21.34	5E-08	Arthropoda	Decapoda	Periclimenella
OTU_126031	12.73	-21.32	5E-08	Arthropoda	Decapoda	unclassified_Hippolytidae
OTU_17227	11.68	-19.45	5E-07	Arthropoda	Decapoda	unclassified_Alpheidae
OTU_12603	1543.05	-13.88	2E-07	Arthropoda	Decapoda	unclassified_Hippolytidae
OTU_10878	587.18	-12.48	7E-08	Arthropoda	Decapoda	genus_Decapoda sp. KSA_1358
OTU_17499	415.75	-11.98	2E-06	Arthropoda	Decapoda	genus_Decapoda sp. SHR084
OTU_241071	2012.45	-11.06	2E-04	Arthropoda	Amphipoda	Yhi
OTU_24107	196.71	-10.90	7E-04	Arthropoda	Amphipoda	Yhi
OTU_1107	185.43	-10.82	1E-05	Arthropoda	Decapoda	Pagurixus
OTU_5166	2991.24	-10.28	9E-06	Arthropoda	Decapoda	unclassified_Galatheidae
OTU_23998	123.30	-10.23	5E-03	Arthropoda	Decapoda	Periclimenaeus
OTU_24363	207.27	-9.27	9E-04	Arthropoda	order_family_genus_Arthropoda sp. LPdivOTU418	genus_Arthropoda sp. LPdivOTU418
OTU_5163	27.70	-8.08	2E-02	Arthropoda	Decapoda	unclassified_Galatheidae
OTU_18068	19.62	-7.58	2E-02	Arthropoda	Decapoda	unclassified_Galatheidae
OTU_3734	753.39	6.49	1E-03	Arthropoda	order_family_genus_Copepoda sp. IP0237	genus_Copepoda sp. IP0237
OTU_26824	185.47	7.15	7E-04	Arthropoda	Calanoida	Bestiolina
OTU_37341	387.54	7.25	4E-02	Arthropoda	order_family_genus_Copepoda sp. IP0237	genus_Copepoda sp. IP0237
OTU_10828	52.34	7.51	5E-02	Arthropoda	Poecilostomatoida	Copilia
OTU_268241	261.34	7.58	6E-05	Arthropoda	Calanoida	Bestiolina
OTU_1444	161.18	7.61	6E-05	Arthropoda	Calanoida	Paracalanus
OTU_6118	518.20	9.11	2E-04	Arthropoda	Calanoida	Delibus
OTU_24746	206.79	9.95	6E-04	Arthropoda	Calanoida	Calocalanus
OTU_10940	116.69	-10.15	5E-07	Bryozoa	Ctenostomatida	Nolella
OTU_26382	55.43	-9.08	2E-02	Bryozoa	Cheilostomatida	Poricella
OTU_11458	45.40	-8.79	3E-04	Bryozoa	Cheilostomatida	Catenicella
OTU_6970	34.94	-8.41	1E-02	Bryozoa	Cheilostomatida	Torquatella
OTU_11953	19.16	-7.54	1E-02	Bryozoa	Cyclostomatida	Proboscina
OTU_69701	212.73	-7.01	5E-03	Bryozoa	Cheilostomatida	Torquatella
OTU_109401	58.65	-3.88	5E-02	Bryozoa	Ctenostomatida	Nolella
OTU_28211	4.41	6.38	4E-02	Cercozoa	order_family_Bigelowiella	Bigelowiella
OTU_2821	5.06	6.61	3E-02	Cercozoa	order_family_Bigelowiella	Bigelowiella
OTU_20367	7.72	-6.23	3E-02	Chordata	Enterogona	Didemnum
OTU_16419	5.79	6.80	2E-02	Chordata	Acanthuriformes	Ctenochaetus
OTU_24039	6.24	6.91	2E-02	Chordata	Perciformes	Nemanthias
OTU_809	6.85	7.04	2E-02	Chordata	Labriformes	Chlorurus
OTU_8091	14.40	7.41	4E-02	Chordata	Labriformes	Chlorurus
OTU_12276	23.81	-21.95	1E-08	Cnidaria	Corallimorpharia	Corynactis
OTU_5054	138.81	-10.40	2E-03	Cnidaria	Alcyonacea	unclassified_Primnoidae
OTU_24531	24.21	-8.05	2E-03	Cnidaria	Anthoathecata	Pandeopsis
OTU_18314	102.61	-6.11	1E-02	Cnidaria	Leptothecata	Clytia
OTU_16762	93.85	-4.78	1E-02	Cnidaria	Leptothecata	Clytia
OTU_1155	8.35	5.95	5E-02	Cnidaria	Alcyonacea	Ovabunda
OTU_28862	92.20	7.26	5E-02	Cnidaria	Scleractinia	Galaxea
OTU_20273	11.93	7.82	5E-03	Cnidaria	Scleractinia	unclassified_Merulinidae
OTU_10472	58.36	-21.22	4E-08	Echinodermata	Amphilepidida	Amphipholis

OTU_1156	200.81	-10.93	2E-05	Echinodermata	Amphilepidida	Ophiothrix
OTU_1302	519.47	-12.31	1E-07	Entoprocta	order_Barentsiidae	Barentsia
OTU_24171	30.98	-8.41	5E-02	Entoprocta	order_Loxosomatidae	Loxomitra
OTU_5580	15.71	-7.43	8E-03	Entoprocta	order_Loxosomatidae	Loxosomella
OTU_5639	13.06	-7.17	2E-03	Entoprocta	order_Loxosomatidae	Loxomitra
OTU_1301	6.51	-5.99	4E-02	Entoprocta	order_Barentsiidae	Barentsia
OTU_17044	46.53	-23.07	3E-09	Mollusca	Littorinimorpha	Petaloconchus
OTU_29064	16.44	-7.32	9E-03	Mollusca	order_family_genus_Mollusca sp. IOP_0387	genus_Mollusca sp. IOP_0387
OTU_10964	4.57	6.43	4E-02	Mollusca	Octopoda	Octopus
OTU_18120	24.24	-7.88	2E-02	Nemertea	order_Cephalotrichidae	Cephalothrix
OTU_8100	686.69	-26.52	1E-19	Porifera	Poecilosclerida	Iotrochota
OTU_27549	87.75	-23.73	8E-10	Porifera	Poecilosclerida	Clathria
OTU_12221	56.14	-23.12	2E-09	Porifera	Poecilosclerida	Phorbas
OTU_24664	51.51	-23.00	2E-09	Porifera	Bubarida	Dictyonella
OTU_25607	38.74	-22.61	4E-09	Porifera	Poecilosclerida	Clathria
OTU_26553	15.70	-21.39	3E-08	Porifera	Poecilosclerida	unclassified_Microcionidae
OTU_26230	77.17	-9.55	4E-04	Porifera	Haplosclerida	unclassified_Chalinidae
OTU_122211	205.20	-9.16	3E-02	Porifera	Poecilosclerida	Phorbas
OTU_27600	39.11	-8.57	2E-02	Porifera	Poecilosclerida	Mycale
OTU_26319	6148.25	-8.49	4E-04	Porifera	Haplosclerida	Callyspongia
OTU_27098	29.54	-8.17	1E-03	Porifera	Poecilosclerida	unclassified_Hymedesmiidae
OTU_8997	15.96	-7.28	3E-02	Porifera	order_family_genus_Verongimorpha sp. 1 JV_2020	genus_Verongimorpha sp. 1 JV_2020
OTU_26322	15.65	-7.25	3E-03	Porifera	Poecilosclerida	Clathria
OTU_26872	621.45	-7.20	2E-03	Porifera	Haplosclerida	genus_Chalinidae sp. HS0146
OTU_25038	885.59	-6.63	4E-06	Porifera	Haplosclerida	genus_Haplosclerida sp. 2 JV_2020
OTU_28688	161.14	-6.35	8E-03	Porifera	Chondrillida	genus_Chondrillida sp. 3 JV_2020
OTU_5872	727.90	-6.08	2E-03	Porifera	Homosclerophorida	Oscarella
OTU_25606	121.00	-5.05	2E-02	Porifera	Poecilosclerida	Ophlitaspongia
OTU_27081	77.37	-4.11	2E-02	Porifera	Haplosclerida	Callyspongia
OTU_13314	44.64	6.94	6E-03	Porifera	Verongiida	Ianthella
OTU_28591	9.09	7.45	8E-03	Porifera	Hadromerida	Spirastrella
OTU_24232	10.09	7.58	7E-03	Porifera	Clionaida	Spirastrella
OTU_840	228.10	8.61	5E-04	Porifera	Dendroceratida	Halisarca
OTU_285911	22.57	8.74	1E-03	Porifera	Hadromerida	Spirastrella

Table C.2. Metazoan 18S curated ESV sequence variants found to have significant differential abundances between eDNA and ARMS samples. Base mean values of abundance, log2FoldChange (log2FC) values and adjusted p-values are displayed for each cESV, along with taxonomic assignments at phylum, class, order, family and genus level.

ESV_id	Base Mean	Log2 FC	P-value	Phylum	Class	Order
ESV_94	351.832616	-24.92052542	1.26E-13	Annelida	Polychaeta	Phyllodocida
ESV_13	925.936618	-26.96106921	5.79E-12	Annelida	Polychaeta	Phyllodocida
ESV_190	201.604771	-24.8810828	1.79E-11	Annelida	Polychaeta	Phyllodocida
ESV_237	221.519107	-24.90826881	1.86E-11	Annelida	Polychaeta	Phyllodocida
ESV_352	145.015046	-24.44161682	1.86E-11	Annelida	Polychaeta	Phyllodocida
ESV_84	118.375223	-24.15481291	2.17E-10	Annelida	Polychaeta	Phyllodocida
ESV_239	70.1551382	-23.45420923	1.54E-09	Annelida	Polychaeta	Phyllodocida
ESV_589	62.491958	-23.2972778	1.78E-09	Annelida	Polychaeta	Phyllodocida
ESV_8	1896.07818	-14.215119	2.19E-09	Annelida	Polychaeta	Phyllodocida
ESV_17	1039.58229	-13.34821208	3.54E-09	Annelida	Polychaeta	Phyllodocida
ESV_415	35.9580222	-22.53765008	5.03E-09	Annelida	Polychaeta	Phyllodocida
ESV_96	274.779705	-11.42883825	4.27E-08	Annelida	Polychaeta	Phyllodocida
ESV_28	620.486794	-12.60355496	1.24E-07	Annelida	Polychaeta	Capitellida
ESV_330	300.108331	-11.55595319	2.61E-07	Annelida	Polychaeta	Phyllodocida
ESV_346	133.684828	-10.38975652	8.99E-07	Annelida	Polychaeta	Phyllodocida
ESV_25	797.32049	-12.96538544	1.03E-06	Annelida	Polychaeta	Phyllodocida
ESV_12	315.602445	-11.62803483	2.02E-06	Annelida	Polychaeta	Eunicida
ESV_200	316.987884	-11.63488909	6.20E-06	Annelida	Polychaeta	Phyllodocida
ESV_29	268.448619	-11.39499906	8.15E-06	Annelida	Polychaeta	Phyllodocida
ESV_34	1052.74038	-9.647408253	1.15E-05	Annelida	Polychaeta	Phyllodocida
ESV_366	96.1377057	-9.913499853	1.30E-05	Annelida	Polychaeta	Phascolosomatiformes
ESV_32	191.512795	-10.90789119	2.34E-05	Annelida	Polychaeta	Phyllodocida
ESV_76	141.319656	-10.46983169	3.20E-05	Annelida	Polychaeta	Phyllodocida
ESV_264	182.820743	-10.84073496	7.39E-05	Annelida	Polychaeta	Phyllodocida
ESV_286	183.822825	-10.8484352	8.41E-05	Annelida	Polychaeta	Spionida
ESV_773	108.997018	-10.09398022	9.33E-05	Annelida	Polychaeta	Capitellida
ESV_178	167.370632	-10.71346919	0.000101086	Annelida	Polychaeta	Phyllodocida
ESV_650	95.0693893	-9.897557616	0.000333514	Annelida	Polychaeta	Spionida
ESV_1006	48.8106781	-8.937543462	0.000401267	Annelida	Polychaeta	Phyllodocida
ESV_1181	33.0477365	9.009308348	0.000442577	Annelida	Polychaeta	Phyllodocida
ESV_622	107.18769	-10.07064565	0.0005309	Annelida	Polychaeta	Spionida
ESV_234	116.185185	-10.18719602	0.000814779	Annelida	Polychaeta	Phyllodocida
ESV_26	217.755656	-8.588000555	0.000861557	Annelida	Polychaeta	Terebellida
ESV_541	101.222782	-9.98830084	0.000872936	Annelida	Polychaeta	Phyllodocida
ESV_27	50.0438433	-8.972362491	0.000917628	Annelida	Polychaeta	Terebellida
ESV_858	95.9865637	-9.910973531	0.001116923	Annelida	Polychaeta	Terebellida
ESV_148	70.8376034	-9.471975896	0.001529536	Annelida	Polychaeta	Phyllodocida
ESV_108	161.95034	-10.6660419	0.001567581	Annelida	Polychaeta	Phyllodocida
ESV_918	66.590943	-9.383896251	0.001656142	Annelida	Polychaeta	Phyllodocida
ESV_602	50.2443142	-8.978453756	0.002786564	Annelida	Polychaeta	Spionida
ESV_294	51.0452504	-9.00134475	0.002976843	Annelida	Polychaeta	Phyllodocida
ESV_445	16.6264736	-7.383633085	0.003476224	Annelida	Polychaeta	Spionida
ESV_413	25.16302	-7.982507023	0.004183633	Annelida	Polychaeta	Sabellida
ESV_1766	34.2822329	-8.427778225	0.004472461	Annelida	Polychaeta	Spionida
ESV_1623	29.802769	-8.222654079	0.005606195	Annelida	Polychaeta	Aspidosiphonidormes
ESV_30	378.097432	-7.570403153	0.008105702	Annelida	Polychaeta	Phyllodocida
ESV_687	32.8993376	-8.36779247	0.010070968	Annelida	Polychaeta	Spionida
ESV_915	29.5212313	-8.210280578	0.010148236	Annelida	Polychaeta	Phyllodocida
ESV_318	30.2867808	-8.248487482	0.011712075	Annelida	Polychaeta	Phyllodocida
ESV_208	41.1984336	-8.691283416	0.012315335	Annelida	Polychaeta	Phyllodocida
ESV_36	230.848449	-4.407362648	0.012551962	Annelida	Polychaeta	Eunicida
ESV_1718	28.8094245	-6.25964892	0.014500082	Annelida	Polychaeta	Sabellida
ESV_278	41.901986	-8.716235372	0.017195025	Annelida	Polychaeta	Phyllodocida
ESV_505	14.1898489	-7.158140417	0.017380341	Annelida	Polychaeta	Phyllodocida
ESV_1095	42.4320279	-8.733449555	0.019709389	Annelida	Polychaeta	Eunicida
ESV_1316	16.6972529	-7.38933052	0.019873134	Annelida	Polychaeta	Phyllodocida
ESV_129	142.664434	-7.743272223	0.01987552	Annelida	Polychaeta	Capitellida
ESV_356	9.90338143	-6.640130671	0.025904284	Annelida	Polychaeta	Capitellida
ESV_1439	13.291566	-7.059891684	0.026859389	Annelida	Polychaeta	Sabellida
ESV_1708	13.4913335	-7.078265295	0.029702196	Annelida	Polychaeta	Capitellida
ESV_1158	53.9397336	-6.334152047	0.036508417	Annelida	Polychaeta	Spionida
ESV_598	29.7338908	-4.482786188	0.04356529	Annelida	Polychaeta	Capitellida
ESV_1230	8.28299724	-6.38335029	0.047889592	Annelida	Polychaeta	Phyllodocida
ESV_31	1069.61548	-4.992389107	0.048640306	Annelida	Polychaeta	Phyllodocida
ESV_188	1074.94117	-27.36201225	4.68E-13	Annelida	Polychaeta	Eunicida
ESV_81	1419.92952	-13.94884638	1.38E-11	Annelida	Polychaeta	Phyllodocida
ESV_3521	184.493526	-24.96511167	2.39E-11	Annelida	Polychaeta	Phyllodocida
ESV_305	197.763974	-25.05965314	2.81E-11	Annelida	Polychaeta	Phyllodocida
ESV_777	239.30805	-25.3191813	7.97E-11	Annelida	Polychaeta	Capitellida
ESV_1781	461.890563	-24.29842109	1.57E-10	Annelida	Polychaeta	Phyllodocida
ESV_109	1045.47518	-13.50716832	7.57E-10	Annelida	Polychaeta	Phyllodocida
ESV_174	1013.10397	-13.46182423	7.57E-10	Annelida	Polychaeta	Phyllodocida
ESV_841	986.86767	-13.42393838	7.57E-10	Annelida	Polychaeta	Phyllodocida
ESV_99	64.5772009	-23.53564517	1.28E-09	Annelida	Polychaeta	Sabellida
ESV_6871	57.0038796	-23.35375382	1.64E-09	Annelida	Polychaeta	Spionida
ESV_461	55.5280353	-23.33141797	1.66E-09	Annelida	Polychaeta	Spionida
ESV_1291	54.5058624	-23.26452078	1.84E-09	Annelida	Polychaeta	Capitellida
ESV_166	66.441018	-23.02195052	2.49E-09	Annelida	Polychaeta	Terebellida
ESV_2387	45.4930753	-23.05720694	2.49E-09	Annelida	Polychaeta	Opheliidae
ESV_9151	44.6984169	-23.03159056	2.49E-09	Annelida	Polychaeta	Phyllodocida
ESV_613	134.630093	-22.56604164	4.74E-09	Annelida	Polychaeta	Capitellida
ESV_105	558.119607	-12.60171163	7.31E-09	Annelida	Polychaeta	Phyllodocida
ESV_162	568.724909	-12.62870484	7.35E-09	Annelida	Polychaeta	Phyllodocida
ESV_412	24.8258777	-22.23604325	8.09E-09	Annelida	Polychaeta	Spionida
ESV_385	24.3845706	-22.21040105	8.35E-09	Annelida	Polychaeta	Spionida

ESV_1019	24.0894184	-22.1720989	8.82E-09	Annelida	Polychaeta	Spionida
ESV_2678	21.9100984	-22.06443411	1.06E-08	Annelida	Polychaeta	Phyllodocida
ESV_2081	17.4359708	-21.75538068	1.65E-08	Annelida	Polychaeta	Phyllodocida
ESV_103	24.99533	-21.71403186	1.75E-08	Annelida	Polychaeta	Sabellida
ESV_64	2529.4167	-11.87089932	1.75E-08	Annelida	Polychaeta	Capitellida
ESV_1772	13.6416845	-21.4276526	2.85E-08	Annelida	Polychaeta	Sabellida
ESV_9181	11.6499596	-21.21720624	3.94E-08	Annelida	Polychaeta	Phyllodocida
ESV_2998	22.0686962	-21.12431221	4.46E-08	Annelida	Polychaeta	Capitellida
ESV_361	1417.90833	-8.656841757	4.55E-08	Annelida	Polychaeta	Eunicida
ESV_688	10.1742483	-21.03243519	5.07E-08	Annelida	Polychaeta	Spionida
ESV_962	262.502421	-11.5133134	5.28E-08	Annelida	Polychaeta	Phyllodocida
ESV_421	305.405804	-11.7319483	6.82E-08	Annelida	Polychaeta	Phyllodocida
ESV_2341	192.640918	-11.06694218	1.44E-07	Annelida	Polychaeta	Phyllodocida
ESV_16	5347.48832	-11.82538375	8.03E-07	Annelida	Polychaeta	Phyllodocida
ESV_155	447.51593	-12.28311554	9.23E-07	Annelida	Polychaeta	Phyllodocida
ESV_1901	216.879105	-11.2381026	2.71E-06	Annelida	Polychaeta	Phyllodocida
ESV_2371	182.194783	-10.98678763	4.56E-06	Annelida	Polychaeta	Phyllodocida
ESV_2001	292.037352	-11.66725198	5.08E-06	Annelida	Polychaeta	Phyllodocida
ESV_233	135.057776	-10.55487976	8.58E-06	Annelida	Polychaeta	Phyllodocida
ESV_132	4733.02856	-10.51431843	9.25E-06	Annelida	Polychaeta	Phyllodocida
ESV_301	2470.5394	-8.945355042	1.85E-05	Annelida	Polychaeta	Phyllodocida
ESV_712	84.5813487	-9.879845032	3.52E-05	Annelida	Polychaeta	Phyllodocida
ESV_1283	88.03249	-9.937092919	4.74E-05	Annelida	Polychaeta	Spionida
ESV_341	464.182831	-12.33568261	5.60E-05	Annelida	Polychaeta	Phyllodocida
ESV_941	303.419019	-10.76031989	0.000124934	Annelida	Polychaeta	Phyllodocida
ESV_141	187.547879	-11.0284329	0.000406032	Annelida	Polychaeta	Phyllodocida
ESV_764	161.525609	-10.81278317	0.000406032	Annelida	Polychaeta	Spionida
ESV_1052	87.5379058	-9.928839243	0.000541618	Annelida	Polychaeta	Terebellida
ESV_121	2155.58905	-7.222905738	0.001010312	Annelida	Polychaeta	Eunicida
ESV_6021	50.4148604	-9.132931186	0.001237285	Annelida	Polychaeta	Spionida
ESV_956	107.660766	-10.22780792	0.001704785	Annelida	Polychaeta	Phyllodocida
ESV_1722	39.8114669	-8.792127713	0.001952749	Annelida	Polychaeta	Terebellida
ESV_761	624.525571	-5.258582972	0.002135943	Annelida	Polychaeta	Phyllodocida
ESV_16231	39.5909296	-8.783456765	0.002920775	Annelida	Polychaeta	Aspidosiphonidormes
ESV_704	152.143709	-10.72650241	0.00337637	Annelida	Polychaeta	Phyllodocida
ESV_906	146.568376	-10.67256078	0.00422392	Annelida	Polychaeta	Spionida
ESV_251	31.7194574	-8.466121062	0.004503931	Annelida	Polychaeta	Phyllodocida
ESV_300	63.3635948	-5.731537101	0.007409264	Annelida	Polychaeta	Phyllodocida
ESV_619	58.3454663	-9.344074564	0.007409264	Annelida	Polychaeta	Phyllodocida
ESV_311	281.211242	-10.87163282	0.007853047	Annelida	Polychaeta	Phyllodocida
ESV_942	65.0249738	-9.500060629	0.008315891	Annelida	Polychaeta	Spionida
ESV_558	16.015102	-7.475409372	0.008371669	Annelida	Polychaeta	Phyllodocida
ESV_5891	69.9148463	-9.604876384	0.009905919	Annelida	Polychaeta	Phyllodocida
ESV_1962	35.3631031	-8.6212469	0.010769434	Annelida	Polychaeta	Spionida
ESV_236	78.9615648	-5.232417001	0.010809449	Annelida	Polychaeta	Eunicida
ESV_2861	55.0069196	-9.258432536	0.013289395	Annelida	Polychaeta	Spionida
ESV_17661	8.03193072	-6.486040949	0.014496888	Annelida	Polychaeta	Spionida
ESV_2631	23.1915675	-8.011261683	0.015220799	Annelida	Polychaeta	Opheliidae
ESV_2336	27.6814578	-8.269375592	0.016105061	Annelida	Polychaeta	Sabellida
ESV_456	19.8643176	-7.78859251	0.01666785	Annelida	Polychaeta	Spionida
ESV_3461	25.774925	-8.164131133	0.019066445	Annelida	Polychaeta	Phyllodocida
ESV_220	16.2677807	-7.502153285	0.020210805	Annelida	Polychaeta	Eunicida
ESV_92	1327.07424	-5.084089603	0.034594495	Annelida	Polychaeta	Capitellida
ESV_193	133.116955	-6.761165261	0.038493541	Annelida	Polychaeta	Capitellida
ESV_4300	4.93662567	-5.786275523	0.045450814	Annelida	Polychaeta	Phyllodocida
ESV_213	249.714273	-25.17355196	8.85E-14	Arthropoda	Maxillopoda	Cyclopoida
ESV_336	138.255648	-24.37123623	1.79E-11	Arthropoda	Maxillopoda	Calanoida
ESV_243	117.287907	-24.14903735	1.24E-10	Arthropoda	Maxillopoda	Harpacticoida
ESV_302	65.9985301	-23.37056246	1.29E-10	Arthropoda	Maxillopoda	Harpacticoida
ESV_135	137.796309	-24.35492162	2.17E-10	Arthropoda	Maxillopoda	Calanoida
ESV_182	61.4980279	-23.10765714	2.74E-10	Arthropoda	Maxillopoda	unclassified_Copepoda
ESV_398	84.0040823	-23.69390045	4.65E-10	Arthropoda	Ostracoda	Podocopida
ESV_171	119.821641	-24.17250848	6.19E-10	Arthropoda	Maxillopoda	Calanoida
ESV_430	81.5243024	-23.65885204	1.24E-09	Arthropoda	Maxillopoda	Cyclopoida
ESV_698	83.643656	-23.59247513	1.32E-09	Arthropoda	Maxillopoda	Harpacticoida
ESV_564	74.8009513	-23.53839209	1.38E-09	Arthropoda	Maxillopoda	Cyclopoida
ESV_457	68.2003048	-23.40434105	1.59E-09	Arthropoda	Ostracoda	Podocopida
ESV_583	67.620187	-23.40477642	1.59E-09	Arthropoda	Maxillopoda	Cyclopoida
ESV_649	47.7729166	-22.93227697	2.93E-09	Arthropoda	Maxillopoda	Harpacticoida
ESV_204	43.256892	-22.79855231	3.54E-09	Arthropoda	Ostracoda	Podocopida
ESV_1245	42.5194346	-22.77324778	3.59E-09	Arthropoda	Maxillopoda	Cyclopoida
ESV_670	39.1919369	-22.6587425	4.22E-09	Arthropoda	Maxillopoda	Harpacticoida
ESV_1022	37.7050079	-22.61060877	4.51E-09	Arthropoda	Maxillopoda	Cyclopoida
ESV_1118	33.9606039	-22.46465053	5.66E-09	Arthropoda	Maxillopoda	Calanoida
ESV_751	32.6988361	-22.41927301	5.97E-09	Arthropoda	Maxillopoda	Cyclopoida
ESV_468	31.8322472	-22.38040219	6.32E-09	Arthropoda	Maxillopoda	Harpacticoida
ESV_1212	25.9618889	-22.10179582	9.85E-09	Arthropoda	Maxillopoda	Harpacticoida
ESV_705	25.7235098	-22.09437873	9.85E-09	Arthropoda	Maxillopoda	unclassified_Copepoda
ESV_957	28.9646942	-22.07867729	9.91E-09	Arthropoda	Ostracoda	Podocopida
ESV_1885	25.2129132	-22.01580058	1.07E-08	Arthropoda	Ostracoda	Podocopida
ESV_290	536.752269	-12.39465452	1.13E-08	Arthropoda	Maxillopoda	Harpacticoida
ESV_2044	23.0572008	-21.94614008	1.15E-08	Arthropoda	Maxillopoda	unclassified_Copepoda
ESV_399	21.3802725	-21.84426292	1.35E-08	Arthropoda	Maxillopoda	unclassified_Copepoda
ESV_969	52.7855558	-21.79052374	1.46E-08	Arthropoda	Maxillopoda	Harpacticoida
ESV_2065	21.2744542	-21.78807751	1.46E-08	Arthropoda	Maxillopoda	Cyclopoida
ESV_947	18.7666425	-21.66703467	1.77E-08	Arthropoda	Ostracoda	Podocopida
ESV_1130	17.3035274	-21.55648602	2.08E-08	Arthropoda	Maxillopoda	unclassified_Copepoda
ESV_1456	20.8217513	-21.45243878	2.47E-08	Arthropoda	Maxillopoda	unclassified_Copepoda
ESV_170	597.447391	-12.54919584	2.96E-08	Arthropoda	Maxillopoda	Harpacticoida
ESV_347	39.1888136	-21.25638371	3.38E-08	Arthropoda	Maxillopoda	Harpacticoida
ESV_692	21.0999297	-20.75226036	7.63E-08	Arthropoda	Maxillopoda	Cyclopoida
ESV_118	370.522908	-11.86004239	7.97E-08	Arthropoda	Ostracoda	Podocopida
ESV_1633	19.4598895	-20.08394214	2.21E-07	Arthropoda	Maxillopoda	Harpacticoida
ESV_484	599.82244	-12.55487035	3.39E-07	Arthropoda	Maxillopoda	Harpacticoida

ESV_110	1399.52763	-13.77703291	2.90E-06	Arthropoda	Maxillopoda	Harpacticoida
ESV_207	330.860045	-11.69657927	3.54E-06	Arthropoda	Maxillopoda	Harpacticoida
ESV_117	325.824013	-11.67444328	8.06E-06	Arthropoda	Ostracoda	Podocopida
ESV_179	447.065518	-12.13079503	1.44E-05	Arthropoda	Maxillopoda	Harpacticoida
ESV_197	402.380269	-11.97890029	2.34E-05	Arthropoda	Maxillopoda	Harpacticoida
ESV_134	195.676723	-10.93879413	3.63E-05	Arthropoda	Ostracoda	Podocopida
ESV_463	230.408127	-11.17470107	5.05E-05	Arthropoda	Maxillopoda	Harpacticoida
ESV_131	77.7244725	-9.607936031	6.28E-05	Arthropoda	Ostracoda	Podocopida
ESV_86	173.471793	-10.76518282	9.99E-05	Arthropoda	Ostracoda	Podocopida
ESV_616	104.829667	-10.03906643	0.000100009	Arthropoda	Maxillopoda	Harpacticoida
ESV_7	545.254737	-10.50221049	0.000106849	Arthropoda	Ostracoda	Podocopida
ESV_494	88.4630626	-9.794061216	0.000126363	Arthropoda	Maxillopoda	Pygophora
ESV_214	348.074482	-11.76971763	0.000142853	Arthropoda	Maxillopoda	Harpacticoida
ESV_940	84.4331953	-9.727191687	0.000164147	Arthropoda	Maxillopoda	Harpacticoida
ESV_335	290.654521	-11.5095007	0.000248312	Arthropoda	Ostracoda	Myodocopida
ESV_57	320.763516	-11.65177634	0.000270934	Arthropoda	Ostracoda	Podocopida
ESV_540	166.928446	-10.70975105	0.000287031	Arthropoda	Maxillopoda	Cyclopoida
ESV_978	65.5335305	-9.361529414	0.000325865	Arthropoda	Maxillopoda	Harpacticoida
ESV_222	339.453862	-11.73345034	0.000374959	Arthropoda	Maxillopoda	unclassified_Copepoda
ESV_708	83.3865823	-9.709010406	0.000412068	Arthropoda	Maxillopoda	Harpacticoida
ESV_677	95.13103	-9.899039848	0.000503416	Arthropoda	Maxillopoda	Harpacticoida
ESV_678	92.6420333	-9.860746278	0.000503416	Arthropoda	Maxillopoda	Harpacticoida
ESV_106	240.051874	-11.23369687	0.000580655	Arthropoda	Maxillopoda	Harpacticoida
ESV_586	101.740498	-9.99557832	0.000660812	Arthropoda	Ostracoda	Podocopida
ESV_597	89.8929691	-9.817244081	0.000715809	Arthropoda	Maxillopoda	Harpacticoida
ESV_806	104.140091	-10.02921687	0.000736717	Arthropoda	Maxillopoda	Cyclopoida
ESV_562	92.4238045	-9.857223917	0.001037961	Arthropoda	Maxillopoda	Harpacticoida
ESV_711	72.7980133	-9.512598007	0.001085008	Arthropoda	Maxillopoda	Harpacticoida
ESV_164	149.34185	-10.5491018	0.001440354	Arthropoda	Maxillopoda	Harpacticoida
ESV_173	635.91341	8.786626581	0.001606946	Arthropoda	Maxillopoda	Cyclopoida
ESV_1191	42.726801	-8.745152669	0.001656142	Arthropoda	Maxillopoda	unclassified_Copepoda
ESV_1469	44.0707379	-8.789890005	0.00181862	Arthropoda	Maxillopoda	Harpacticoida
ESV_1634	35.7561983	-8.488377624	0.00181862	Arthropoda	Maxillopoda	Harpacticoida
ESV_327	69.8153688	-9.451730523	0.002098227	Arthropoda	Maxillopoda	Harpacticoida
ESV_1062	37.9681307	-8.574958528	0.002128928	Arthropoda	Maxillopoda	Harpacticoida
ESV_1156	61.6403738	-9.272595407	0.00226299	Arthropoda	Maxillopoda	Harpacticoida
ESV_373	47.0268149	-8.882789413	0.002467251	Arthropoda	Ostracoda	Podocopida
ESV_497	29.1009804	-8.191358861	0.002697346	Arthropoda	Maxillopoda	Harpacticoida
ESV_1224	33.476084	-8.393592608	0.002810227	Arthropoda	Maxillopoda	Harpacticoida
ESV_1461	25.5333461	-8.002957542	0.0030746	Arthropoda	Maxillopoda	Harpacticoida
ESV_154	76.4653895	-8.620852872	0.003163843	Arthropoda	Maxillopoda	Harpacticoida
ESV_938	54.1480552	-9.086384422	0.003163843	Arthropoda	Maxillopoda	Harpacticoida
ESV_1231	50.5792796	-8.988053377	0.003182228	Arthropoda	Maxillopoda	Harpacticoida
ESV_612	49.2800926	-8.950332589	0.00349273	Arthropoda	Maxillopoda	Harpacticoida
ESV_216	82.2651535	-9.689176409	0.004224064	Arthropoda	Maxillopoda	Cyclopoida
ESV_527	31.4206092	-8.300119536	0.004699136	Arthropoda	Ostracoda	Podocopida
ESV_642	37.7965718	-8.568215458	0.005829951	Arthropoda	Maxillopoda	Harpacticoida
ESV_130	41.3567092	-8.69744626	0.006423506	Arthropoda	Ostracoda	Podocopida
ESV_303	105.765345	-10.05132866	0.006423506	Arthropoda	Maxillopoda	Harpacticoida
ESV_746	30.0479251	-8.237700238	0.006734256	Arthropoda	Maxillopoda	unclassified_Copepoda
ESV_930	28.922307	-8.182563327	0.006932578	Arthropoda	Maxillopoda	Harpacticoida
ESV_523	101.774225	-9.033434603	0.007167391	Arthropoda	Maxillopoda	Harpacticoida
ESV_478	25.8581962	-8.021216843	0.007844101	Arthropoda	Maxillopoda	Harpacticoida
ESV_823	35.1991357	-8.464229329	0.00786884	Arthropoda	Ostracoda	Podocopida
ESV_146	21.6359749	-7.763554817	0.008672385	Arthropoda	Ostracoda	Podocopida
ESV_529	84.9350216	-9.734980078	0.008833994	Arthropoda	Maxillopoda	Harpacticoida
ESV_1271	23.6586838	-7.893295825	0.009026963	Arthropoda	Maxillopoda	Cyclopoida
ESV_658	71.9405803	-9.495486149	0.009717661	Arthropoda	Maxillopoda	Harpacticoida
ESV_2469	20.0971273	-7.656997283	0.009956809	Arthropoda	Maxillopoda	unclassified_Copepoda
ESV_656	86.6405291	-9.763729517	0.010469293	Arthropoda	Maxillopoda	Harpacticoida
ESV_859	31.2597011	-8.294363059	0.011124069	Arthropoda	Maxillopoda	Harpacticoida
ESV_1025	29.7150064	-8.221418046	0.011364444	Arthropoda	Maxillopoda	Harpacticoida
ESV_1140	17.383172	-7.449542657	0.011411237	Arthropoda	Maxillopoda	Harpacticoida
ESV_763	57.9506406	-9.183757488	0.011731446	Arthropoda	Maxillopoda	Harpacticoida
ESV_1412	27.2722085	-8.09721686	0.011861408	Arthropoda	Maxillopoda	Harpacticoida
ESV_926	14.7298692	-7.209532309	0.012127208	Arthropoda	Ostracoda	Podocopida
ESV_1258	27.8997743	-8.130363724	0.012643878	Arthropoda	Maxillopoda	unclassified_Copepoda
ESV_1319	25.2861073	-7.988644748	0.01336121	Arthropoda	Maxillopoda	Harpacticoida
ESV_875	48.1356164	-8.91618995	0.013897701	Arthropoda	Maxillopoda	Harpacticoida
ESV_1586	25.4864895	-7.999895932	0.014292612	Arthropoda	Ostracoda	Podocopida
ESV_1133	39.5871566	-8.633237433	0.014624033	Arthropoda	Maxillopoda	Harpacticoida
ESV_1659	24.3183144	-7.927851743	0.014922783	Arthropoda	Ostracoda	Podocopida
ESV_61	322.068727	5.270833009	0.015553545	Arthropoda	Maxillopoda	Calanoida
ESV_2393	16.5109554	-7.375848209	0.016085635	Arthropoda	Maxillopoda	Harpacticoida
ESV_1128	55.5857118	-9.123687163	0.01631377	Arthropoda	Maxillopoda	Harpacticoida
ESV_2031	13.874482	-7.124594542	0.016707631	Arthropoda	Maxillopoda	Harpacticoida
ESV_1090	21.6407138	-7.76475667	0.017362995	Arthropoda	Maxillopoda	unclassified_Copepoda
ESV_1965	21.4609381	-7.750365854	0.017399521	Arthropoda	Pycnogonida	Pantopoda
ESV_606	38.6993606	-8.601737336	0.017502892	Arthropoda	Ostracoda	Podocopida
ESV_1422	41.285699	6.947183152	0.017577444	Arthropoda	Maxillopoda	Calanoida
ESV_1433	33.3805273	-8.388630647	0.017835429	Arthropoda	Maxillopoda	Cyclopoida
ESV_1226	21.1994349	-7.735136637	0.018007846	Arthropoda	Maxillopoda	Siphonostomatoida
ESV_839	43.0268518	-8.754460891	0.018521351	Arthropoda	Maxillopoda	Harpacticoida
ESV_939	17.8969065	-7.489422394	0.018732854	Arthropoda	Ostracoda	Podocopida
ESV_1525	15.4123426	-7.275833721	0.021712243	Arthropoda	Maxillopoda	Poecilostomatoida
ESV_3632	16.4242115	-7.365364463	0.022311393	Arthropoda	Maxillopoda	Harpacticoida
ESV_1050	26.6898078	-8.066194605	0.025754053	Arthropoda	Maxillopoda	Cyclopoida
ESV_1051	12.6463299	-6.987145923	0.02666981	Arthropoda	Ostracoda	Podocopida
ESV_703	13.6274115	-7.096028544	0.026669943	Arthropoda	Maxillopoda	Harpacticoida
ESV_770	12.3881562	-6.961957301	0.027986909	Arthropoda	Maxillopoda	Harpacticoida
ESV_2033	11.6083231	-6.868053363	0.029578743	Arthropoda	Ostracoda	Podocopida
ESV_2738	12.296973	-6.951471576	0.029746793	Arthropoda	Maxillopoda	Cyclopoida
ESV_23	2635.99838	7.276442071	0.029987618	Arthropoda	Maxillopoda	Calanoida
ESV_1509	11.3572963	-6.836335124	0.032164395	Arthropoda	Maxillopoda	Harpacticoida

ESV_44	100.100978	5.54880489	0.032282952	Arthropoda	Maxillopoda	Calanoida
ESV_2697	7.96616586	-6.325453755	0.035374248	Arthropoda	Ostracoda	Podocopida
ESV_635	37.998645	-8.574906658	0.037900519	Arthropoda	Maxillopoda	Harpacticoida
ESV_2238	8.92534365	-6.490009895	0.040288152	Arthropoda	Maxillopoda	Poecilostomatoida
ESV_2000	34.2297399	-8.424132324	0.04112775	Arthropoda	Maxillopoda	Harpacticoida
ESV_1112	8.58974927	-6.43532757	0.042022011	Arthropoda	Maxillopoda	Harpacticoida
ESV_138	414.993069	-7.832660974	0.042854453	Arthropoda	Maxillopoda	Harpacticoida
ESV_1217	31.9564858	-8.325467811	0.04356529	Arthropoda	Maxillopoda	Harpacticoida
ESV_1438	8.21236096	-6.370874738	0.044269288	Arthropoda	Maxillopoda	Harpacticoida
ESV_786	29.5953523	-8.214853644	0.046598264	Arthropoda	Maxillopoda	Cyclopoida
ESV_69	1414.95249	-13.94377594	1.30E-11	Arthropoda	Ostracoda	Podocopida
ESV_299	222.5894	-24.57105143	4.89E-11	Arthropoda	Ostracoda	Podocopida
ESV_3271	130.016509	-24.48529462	5.27E-11	Arthropoda	Maxillopoda	Harpacticoida
ESV_852	84.6314406	-23.90269513	7.57E-10	Arthropoda	Maxillopoda	Calanoida
ESV_136	602.26606	-12.71158559	1.11E-09	Arthropoda	Ostracoda	Podocopida
ESV_4571	63.9570351	-23.48849916	1.37E-09	Arthropoda	Ostracoda	Podocopida
ESV_1202	97.0510853	-23.41434354	1.49E-09	Arthropoda	Ostracoda	Myodocopida
ESV_1101	741.668485	-13.01189013	2.24E-09	Arthropoda	Maxillopoda	Harpacticoida
ESV_1061	38.9831344	-22.76211222	3.55E-09	Arthropoda	Maxillopoda	Harpacticoida
ESV_651	35.0281521	-22.68507035	3.96E-09	Arthropoda	Maxillopoda	Harpacticoida
ESV_7081	30.5939285	-22.47923721	5.51E-09	Arthropoda	Maxillopoda	Harpacticoida
ESV_1658	29.1502524	-22.4498382	5.73E-09	Arthropoda	Maxillopoda	Harpacticoida
ESV_2649	21.7505492	-22.05461741	1.06E-08	Arthropoda	Maxillopoda	unclassified_Copepoda
ESV_1887	20.8952754	-22.00584479	1.13E-08	Arthropoda	Maxillopoda	Cyclopoida
ESV_1632	19.505066	-21.91252845	1.28E-08	Arthropoda	Maxillopoda	Cyclopoida
ESV_5401	24.349404	-21.82628806	1.47E-08	Arthropoda	Maxillopoda	Cyclopoida
ESV_2901	299.160304	-11.70216628	3.02E-08	Arthropoda	Maxillopoda	Harpacticoida
ESV_1077	10.5178451	-21.07809766	4.74E-08	Arthropoda	Maxillopoda	Harpacticoida
ESV_161	363.033659	-11.98126032	5.86E-08	Arthropoda	Ostracoda	Podocopida
ESV_1341	294.806762	-11.68099212	1.07E-07	Arthropoda	Ostracoda	Podocopida
ESV_1641	760.337541	-13.0477121	9.49E-07	Arthropoda	Maxillopoda	Harpacticoida
ESV_2431	272.271015	-11.56629229	2.88E-06	Arthropoda	Maxillopoda	Harpacticoida
ESV_1701	179.929541	-10.96865817	2.90E-06	Arthropoda	Maxillopoda	Harpacticoida
ESV_417	274.344065	-11.57725931	3.31E-06	Arthropoda	Ostracoda	Podocopida
ESV_390	199.013653	-11.11412935	5.15E-06	Arthropoda	Maxillopoda	Harpacticoida
ESV_1182	288.679982	-11.65063122	7.58E-06	Arthropoda	Ostracoda	Podocopida
ESV_367	422.619231	-12.2003689	7.59E-06	Arthropoda	Ostracoda	Podocopida
ESV_6421	106.088842	-10.20691785	8.12E-06	Arthropoda	Maxillopoda	Harpacticoida
ESV_1171	189.271948	-11.04177927	8.76E-06	Arthropoda	Ostracoda	Podocopida
ESV_1349	85.9357799	-9.902551426	1.56E-05	Arthropoda	Maxillopoda	Harpacticoida
ESV_1531	61.1300399	-9.41224477	1.83E-05	Arthropoda	Maxillopoda	Harpacticoida
ESV_13191	70.1235413	-9.609313385	1.96E-05	Arthropoda	Maxillopoda	Harpacticoida
ESV_147	442.725583	-12.26744208	1.96E-05	Arthropoda	Ostracoda	Myodocopida
ESV_240	241.867691	-11.39541139	2.13E-05	Arthropoda	Ostracoda	Podocopida
ESV_4841	139.448146	-10.60117875	2.76E-05	Arthropoda	Maxillopoda	Harpacticoida
ESV_3981	243.216926	-11.40343993	3.02E-05	Arthropoda	Ostracoda	Podocopida
ESV_4971	178.599767	-10.95783315	4.66E-05	Arthropoda	Maxillopoda	Harpacticoida
ESV_406	198.010469	-11.10683021	5.01E-05	Arthropoda	Ostracoda	Podocopida
ESV_1301	122.225553	-10.41089198	7.52E-05	Arthropoda	Ostracoda	Podocopida
ESV_1426	61.4375008	-9.417271235	0.000124504	Arthropoda	Pycnogonida	Pantopoda
ESV_1589	59.0686026	-9.361797123	0.000165898	Arthropoda	Maxillopoda	Harpacticoida
ESV_363	277.385222	-11.59289353	0.000181277	Arthropoda	Ostracoda	Myodocopida
ESV_925	63.1474384	-9.458496108	0.000213427	Arthropoda	Maxillopoda	Harpacticoida
ESV_8591	127.679281	-10.47376196	0.000274577	Arthropoda	Maxillopoda	Harpacticoida
ESV_1174	75.0958629	-9.708144242	0.000293412	Arthropoda	Ostracoda	Podocopida
ESV_462	120.147336	-10.38589124	0.000293412	Arthropoda	Maxillopoda	unclassified_Copepoda
ESV_1045	112.350112	-10.28885286	0.000314676	Arthropoda	Ostracoda	Myodocopida
ESV_961	117.885502	-10.35861523	0.000323714	Arthropoda	Maxillopoda	Harpacticoida
ESV_1070	104.135243	-10.1797631	0.000406938	Arthropoda	Maxillopoda	unclassified_Copepoda
ESV_1279	61.5730408	-9.421992393	0.000406951	Arthropoda	Maxillopoda	Siphonostomatoida
ESV_3471	241.314371	-11.39203718	0.00042234	Arthropoda	Maxillopoda	Harpacticoida
ESV_442	215.948958	-11.23175484	0.000481124	Arthropoda	Ostracoda	Podocopida
ESV_674	155.274931	-10.75607542	0.000495458	Arthropoda	Maxillopoda	Calanoida
ESV_431	332.710666	-10.22816272	0.000497856	Arthropoda	Maxillopoda	Harpacticoida
ESV_349	142.150667	-10.62850573	0.00051151	Arthropoda	Ostracoda	Podocopida
ESV_1421	87.2239803	-9.923997836	0.000555458	Arthropoda	Maxillopoda	unclassified_Copepoda
ESV_1751	62.8396479	-9.450673154	0.000569538	Arthropoda	Maxillopoda	Harpacticoida
ESV_884	90.5309869	-9.977945763	0.000628076	Arthropoda	Ostracoda	Podocopida
ESV_1093	59.4359506	-9.371347718	0.000628399	Arthropoda	Maxillopoda	Harpacticoida
ESV_1943	26.6141824	-8.213049929	0.000736905	Arthropoda	Maxillopoda	Siphonostomatoida
ESV_2108	42.9646341	-8.902644508	0.000772093	Arthropoda	Maxillopoda	unclassified_Copepoda
ESV_1337	72.5350743	-9.658165239	0.000795472	Arthropoda	Maxillopoda	unclassified_Copepoda
ESV_4781	163.082359	-10.82671053	0.000833633	Arthropoda	Maxillopoda	Harpacticoida
ESV_102	74.3314146	-9.693584799	0.000890571	Arthropoda	Maxillopoda	Harpacticoida
ESV_1299	79.7628496	-9.795083217	0.000908442	Arthropoda	Maxillopoda	Harpacticoida
ESV_652	137.828808	-10.5841503	0.000986973	Arthropoda	Maxillopoda	Harpacticoida
ESV_75	42.0648381	-8.872708098	0.000986973	Arthropoda	Ostracoda	Podocopida
ESV_7631	46.0400144	-9.002880465	0.000986973	Arthropoda	Maxillopoda	Harpacticoida
ESV_1547	66.3053964	-9.528260587	0.001013194	Arthropoda	Maxillopoda	Harpacticoida
ESV_1275	64.8683675	-9.496890028	0.001094632	Arthropoda	Maxillopoda	Harpacticoida
ESV_1931	41.3533453	-8.847497593	0.001104325	Arthropoda	Maxillopoda	Harpacticoida
ESV_5621	58.6173563	-9.350906194	0.001121117	Arthropoda	Maxillopoda	Harpacticoida
ESV_11121	23.1250758	-7.043516576	0.001186605	Arthropoda	Maxillopoda	Harpacticoida
ESV_1725	49.9743874	-9.120717856	0.001306121	Arthropoda	Maxillopoda	unclassified_Copepoda
ESV_864	138.759867	-10.59377267	0.001431938	Arthropoda	Ostracoda	Podocopida
ESV_217	30.7435076	-8.419439043	0.00158925	Arthropoda	Ostracoda	Podocopida
ESV_5831	56.9858758	-9.310359154	0.001609005	Arthropoda	Maxillopoda	Cyclopoida
ESV_3021	41.4890604	-8.851589559	0.001689646	Arthropoda	Maxillopoda	Harpacticoida
ESV_1691	24.0099685	-8.063618489	0.00204334	Arthropoda	Maxillopoda	Harpacticoida
ESV_1852	38.8566376	-8.757419678	0.002337582	Arthropoda	Ostracoda	Podocopida
ESV_1338	34.4441007	-8.583886847	0.00259038	Arthropoda	Ostracoda	Podocopida
ESV_12711	39.2072148	-8.77111653	0.002677312	Arthropoda	Maxillopoda	Cyclopoida
ESV_2106	38.1743624	-8.731994276	0.002696	Arthropoda	Maxillopoda	Harpacticoida
ESV_5971	27.9534688	-8.282802735	0.003333245	Arthropoda	Maxillopoda	Harpacticoida

ESV_12261	29.1793286	-8.345513209	0.003531639	Arthropoda	Maxillopoda	Siphonostomatoida
ESV_1802	25.2916491	-8.139008531	0.003914693	Arthropoda	Maxillopoda	Cyclopoida
ESV_1353	34.4126062	-8.583065429	0.004069266	Arthropoda	Maxillopoda	Harpacticoida
ESV_389	25.3106767	-8.139312554	0.004451254	Arthropoda	Ostracoda	Podocopida
ESV_11301	15.5838227	-7.440942531	0.004832191	Arthropoda	Maxillopoda	unclassified_Copepoda
ESV_2951	11.0190069	-6.939572635	0.005614206	Arthropoda	Maxillopoda	Harpacticoida
ESV_921	20.6948398	-7.848463782	0.006013233	Arthropoda	Maxillopoda	Harpacticoida
ESV_1777	19.3673338	-7.754362608	0.006596368	Arthropoda	Maxillopoda	Harpacticoida
ESV_3346	16.9406154	-7.561362185	0.006772457	Arthropoda	Maxillopoda	Harpacticoida
ESV_3467	18.5935807	-7.694831339	0.007930195	Arthropoda	Maxillopoda	Harpacticoida
ESV_521	76.6032471	-9.736413139	0.008315891	Arthropoda	Maxillopoda	Harpacticoida
ESV_470	65.0941528	-9.501838978	0.008437428	Arthropoda	Maxillopoda	Harpacticoida
ESV_1462	61.8655953	-9.428423421	0.008437781	Arthropoda	Ostracoda	Podocopida
ESV_1472	72.0028085	-9.647368398	0.008437781	Arthropoda	Maxillopoda	unclassified_Copepoda
ESV_2062	15.7749104	-7.458691586	0.008549254	Arthropoda	Maxillopoda	Harpacticoida
ESV_2161	74.4142555	-9.694986558	0.008565128	Arthropoda	Maxillopoda	Cyclopoida
ESV_20311	14.1299606	-7.299033738	0.008773536	Arthropoda	Maxillopoda	Harpacticoida
ESV_747	51.4517303	-9.162485222	0.009114502	Arthropoda	Maxillopoda	Harpacticoida
ESV_4181	12.0275859	-7.065998313	0.009288725	Arthropoda	Maxillopoda	Facetotecta
ESV_973	42.7815667	-8.896624923	0.009300025	Arthropoda	Maxillopoda	Cyclopoida
ESV_2142	48.0946177	-9.065497167	0.009550277	Arthropoda	Maxillopoda	Harpacticoida
ESV_6491	60.5274487	-9.397064247	0.009626364	Arthropoda	Maxillopoda	Harpacticoida
ESV_6561	38.4980507	-8.744396001	0.009688873	Arthropoda	Maxillopoda	Harpacticoida
ESV_948	50.7839092	-9.143983087	0.009798785	Arthropoda	Maxillopoda	Cyclopoida
ESV_1565	51.5990826	-9.166822149	0.011675826	Arthropoda	Maxillopoda	Cyclopoida
ESV_2113	10.2237296	-6.83342522	0.011981694	Arthropoda	Maxillopoda	Harpacticoida
ESV_4195	10.3376995	-6.847716305	0.012536479	Arthropoda	Maxillopoda	Harpacticoida
ESV_5231	16.2334101	-7.499184221	0.012782046	Arthropoda	Maxillopoda	Harpacticoida
ESV_1876	35.2661543	-8.617982995	0.013849263	Arthropoda	Maxillopoda	Cyclopoida
ESV_1117	32.8490322	-8.515261688	0.014496888	Arthropoda	Ostracoda	Podocopida
ESV_3555	9.48210916	-6.723772524	0.014636737	Arthropoda	Maxillopoda	unclassified_Copepoda
ESV_2588	8.36889105	-6.546760712	0.014671916	Arthropoda	Maxillopoda	Harpacticoida
ESV_871	10.8093701	-6.913169882	0.0156172	Arthropoda	Maxillopoda	Cyclopoida
ESV_1108	23.1557024	-8.010622556	0.01597164	Arthropoda	Ostracoda	Myodocopida
ESV_12311	22.4547177	-7.966050558	0.01597164	Arthropoda	Maxillopoda	Harpacticoida
ESV_4147	13.2799769	-7.209830828	0.01597164	Arthropoda	Maxillopoda	Harpacticoida
ESV_10501	12.4948251	-7.122353943	0.016727983	Arthropoda	Maxillopoda	Cyclopoida
ESV_2131	19.7052003	-7.779245504	0.017055483	Arthropoda	Maxillopoda	Cyclopoida
ESV_741	33.2785159	-8.534536398	0.017331364	Arthropoda	Ostracoda	Podocopida
ESV_1541	8.8712976	-6.629324096	0.017436783	Arthropoda	Maxillopoda	Harpacticoida
ESV_10251	9.14822351	-6.671707096	0.017969605	Arthropoda	Maxillopoda	Harpacticoida
ESV_1598	35.6849563	-8.634761178	0.018755536	Arthropoda	Maxillopoda	unclassified_Copepoda
ESV_6701	21.8712709	-7.929147108	0.018755536	Arthropoda	Maxillopoda	Harpacticoida
ESV_6781	12.4546913	-7.118507756	0.019323631	Arthropoda	Maxillopoda	Harpacticoida
ESV_3322	18.6118408	-7.697268945	0.019399018	Arthropoda	Maxillopoda	Cyclopoida
ESV_440	20.6670428	-7.848091116	0.019399018	Arthropoda	Ostracoda	Podocopida
ESV_2871	16.8018301	-7.549424727	0.019647744	Arthropoda	Maxillopoda	Siphonostomatoida
ESV_9691	17.4026772	-7.599409621	0.019787455	Arthropoda	Maxillopoda	Harpacticoida
ESV_10621	16.6159648	-7.532992451	0.020017929	Arthropoda	Maxillopoda	Harpacticoida
ESV_3892	19.4499503	-7.757425812	0.021168019	Arthropoda	Maxillopoda	Harpacticoida
ESV_1971	109.638176	-7.885926792	0.02135931	Arthropoda	Maxillopoda	Harpacticoida
ESV_6161	9.64867847	-6.751599166	0.022226782	Arthropoda	Maxillopoda	Harpacticoida
ESV_15091	7.07481598	-6.297196801	0.022407288	Arthropoda	Maxillopoda	Harpacticoida
ESV_3836	14.3479013	-7.321369788	0.022979369	Arthropoda	Maxillopoda	unclassified_Copepoda
ESV_2764	10.6569518	-6.893730174	0.023322584	Arthropoda	Maxillopoda	Harpacticoida
ESV_12241	9.01389538	-6.649826623	0.025533356	Arthropoda	Maxillopoda	Harpacticoida
ESV_2497	20.4657772	-7.832248761	0.027925601	Arthropoda	Maxillopoda	Harpacticoida
ESV_1786	7.23522334	-6.335605957	0.037243449	Arthropoda	Maxillopoda	Harpacticoida
ESV_1865	34.6820313	-8.593931541	0.037243449	Arthropoda	Maxillopoda	Harpacticoida
ESV_4757	6.65644305	-6.211970055	0.04292019	Arthropoda	Maxillopoda	Harpacticoida
ESV_1668	29.8463313	-8.377408809	0.042935157	Arthropoda	Maxillopoda	Calanoida
ESV_404	29.8800885	-8.378608397	0.042935157	Arthropoda	Ostracoda	Podocopida
ESV_2391	4.88847923	-5.771540292	0.045686986	Arthropoda	Maxillopoda	Harpacticoida
ESV_1443	25.7879098	-8.166303528	0.048738254	Arthropoda	Maxillopoda	Harpacticoida
ESV_1968	4.45774034	-5.630271711	0.049935971	Arthropoda	Maxillopoda	Harpacticoida
ESV_644	32.731268	-8.360870235	0.001766379	Bryozoa	Gymnolaemata	Cheilostomatida
ESV_1392	30.5530693	-7.295358478	0.001928734	Bryozoa	Stenolaemata	Cyclostomatida
ESV_469	35.9065615	-8.493203297	0.002246844	Bryozoa	Gymnolaemata	Cheilostomatida
ESV_375	37.3303976	-8.54924846	0.003844213	Bryozoa	Gymnolaemata	Cheilostomatida
ESV_78	299.718408	-5.861658498	0.005169087	Bryozoa	Gymnolaemata	Cheilostomatida
ESV_263	16.446886	-7.36699772	0.006004052	Bryozoa	Gymnolaemata	Cheilostomatida
ESV_883	24.4809545	-7.941205153	0.008892121	Bryozoa	Gymnolaemata	Cheilostomatida
ESV_1359	17.8186421	-7.482129667	0.011971161	Bryozoa	Gymnolaemata	Cheilostomatida
ESV_794	63.589128	-8.35386078	0.01631377	Bryozoa	Gymnolaemata	Cheilostomatida
ESV_648	98.7360864	-4.068492679	0.024265433	Bryozoa	Stenolaemata	Cyclostomatida
ESV_645	5.72426642	-5.851474943	0.049796519	Bryozoa	Gymnolaemata	Ctenostomatida
ESV_691	60.2509296	-23.44096195	1.46E-09	Bryozoa	Gymnolaemata	Cheilostomatida
ESV_781	243.87021	-11.4072515	3.00E-06	Bryozoa	Gymnolaemata	Cheilostomatida
ESV_722	153.86342	-8.574685374	3.88E-06	Bryozoa	Gymnolaemata	Cheilostomatida
ESV_4073	10.2392905	-6.829666879	0.009632005	Bryozoa	Gymnolaemata	Cheilostomatida
ESV_5098	5.35596947	6.65757464	0.019639057	Bryozoa	Gymnolaemata	Ctenostomatida
ESV_2575	7.77011215	-6.437863873	0.023207256	Bryozoa	Gymnolaemata	Cheilostomatida
ESV_1058	110.261269	-24.05853824	6.56E-10	Cnidaria	Anthozoa	Actiniaria
ESV_254	49.4076744	-22.88794987	3.12E-09	Cnidaria	Anthozoa	Actiniaria
ESV_1223	38.2014766	-22.08775168	9.85E-09	Cnidaria	Anthozoa	Scleractinia
ESV_127	168.278234	-10.72168832	5.26E-08	Cnidaria	Hydrozoa	Leptothecata
ESV_1255	46.4204224	-8.863950541	0.000336874	Cnidaria	Hydrozoa	Leptothecata
ESV_85	60.360727	-9.242264404	0.000877054	Cnidaria	Anthozoa	Actiniaria
ESV_1981	27.1854958	-8.094249178	0.001010228	Cnidaria	Hydrozoa	Leptothecata
ESV_2227	23.8851718	-7.907113659	0.001048265	Cnidaria	Hydrozoa	Leptothecata
ESV_48	818.498405	8.73666334	0.001781046	Cnidaria	Hydrozoa	Narcomedusae
ESV_2099	22.6507642	8.787832947	0.002034877	Cnidaria	Hydrozoa	Trachymedusae
ESV_1204	56.6187616	-9.148021508	0.002697346	Cnidaria	Anthozoa	Actiniaria
ESV_1660	23.1919211	-7.864034869	0.003408456	Cnidaria	Hydrozoa	Anthoathecata

ESV_1803	33.949187	-8.413845079	0.003671463	Cnidaria	Hydrozoa	Leptothecata
ESV_1530	41.1387914	-8.689073746	0.003732478	Cnidaria	Hydrozoa	Leptothecata
ESV_314	141.77197	-10.47370877	0.004736855	Cnidaria	Hydrozoa	Leptothecata
ESV_545	23.3188241	-7.872333106	0.00790409	Cnidaria	Hydrozoa	Anthoathecata
ESV_2154	16.953754	-6.44679162	0.012330798	Cnidaria	Hydrozoa	Leptothecata
ESV_112	354.431635	-6.814399668	0.017105968	Cnidaria	Anthozoa	Actiniaria
ESV_995	53.5857498	-4.972570131	0.023361986	Cnidaria	Scyphozoa	Coronatae
ESV_587	64.1522405	-5.588028985	0.026029271	Cnidaria	Anthozoa	Alcyonacea
ESV_196	29.5159072	-8.210917833	0.029155145	Cnidaria	Hydrozoa	Anthoathecata
ESV_4179	7.62878761	-6.26575523	0.033955046	Cnidaria	Hydrozoa	Leptothecata
ESV_4832	9.31342665	-6.549895598	0.038497304	Cnidaria	Hydrozoa	Leptothecata
ESV_2679	19.6867759	-4.369475878	0.044445564	Cnidaria	Hydrozoa	Leptothecata
ESV_621	12.168733	7.891423766	0.046883445	Cnidaria	Anthozoa	Actiniaria
ESV_5451	186.145934	-11.01750901	1.28E-08	Cnidaria	Hydrozoa	Anthoathecata
ESV_159	1061.99586	-7.450812652	5.79E-07	Cnidaria	Anthozoa	Scleractinia
ESV_139	37.6036787	-7.746290347	0.000736905	Cnidaria	Hydrozoa	Leptothecata
ESV_481	705.001548	8.015443423	0.000791306	Cnidaria	Hydrozoa	Narcomedusae
ESV_1738	35.7826204	-8.638274481	0.000822046	Cnidaria	Hydrozoa	Anthoathecata
ESV_2424	31.5927922	-8.459512487	0.003642481	Cnidaria	Hydrozoa	Anthoathecata
ESV_819	16.9180127	-7.557703265	0.005518651	Cnidaria	Hydrozoa	Anthoathecata
ESV_7311	6.63791608	-6.209474754	0.014798261	Cnidaria	Hydrozoa	Leptothecata
ESV_3385	9.97567077	-6.795072693	0.016268159	Cnidaria	Hydrozoa	Anthoathecata
ESV_22271	7.18502534	-6.321786946	0.021626727	Cnidaria	Hydrozoa	Leptothecata
ESV_4810	10.2919354	-6.841328801	0.025181757	Cnidaria	Hydrozoa	Leptothecata
ESV_268	233.67362	-11.19507868	1.02E-05	Entoprocta	Solitaria	Loxosomatidae
ESV_70	312.630857	-9.706315411	1.34E-05	Entoprocta	NA	Coloniales
ESV_395	48.7060171	-8.933846073	0.001906372	Entoprocta	Solitaria	Loxosomatidae
ESV_701	299.372998	-11.70306253	4.82E-07	Entoprocta	NA	Coloniales
ESV_449	100.28478	-7.782536532	4.66E-05	Entoprocta	Solitaria	Loxosomatidae
ESV_1209	90.3686496	-9.975155663	0.001859472	Entoprocta	Solitaria	Loxosomatidae
ESV_577	23.2276483	-8.016230091	0.003776884	Entoprocta	NA	Coloniales
ESV_279	141.472982	-4.537500793	0.027538998	Entoprocta	NA	Coloniales
ESV_755	60.5946999	-9.248488843	0.002952504	Gastrotricha	NA	Chaetonotida
ESV_1419	44.5586118	-8.955385333	0.00161714	Gastrotricha	NA	Chaetonotida
ESV_2243	15.7829284	-7.457714654	0.002669394	Gastrotricha	NA	Chaetonotida
ESV_2292	34.6478183	-8.592515072	0.01776807	Gastrotricha	NA	Chaetonotida
ESV_1088	53.1779426	-22.89643848	7.08E-10	Mollusca	Gastropoda	Caenogastropoda
ESV_1602	33.308364	-22.44430816	5.79E-09	Mollusca	Gastropoda	Heterobranchia
ESV_65	407.80319	-6.196065572	0.00026017	Mollusca	Polyplacophora	Neoloricata
ESV_338	110.843805	-5.675087372	0.000731823	Mollusca	Gastropoda	Caenogastropoda
ESV_1059	53.5269838	-9.068171952	0.000872936	Mollusca	Gastropoda	Caenogastropoda
ESV_125	174.506704	-10.77371273	0.000928973	Mollusca	Gastropoda	Heterobranchia
ESV_24	846.994929	-4.21481631	0.001957198	Mollusca	Bivalvia	Arcoida
ESV_416	63.0125289	-9.303821399	0.001995124	Mollusca	Bivalvia	Veneroida
ESV_980	67.8150099	-9.409602084	0.002284717	Mollusca	Gastropoda	Caenogastropoda
ESV_43	31.8018033	-8.318305299	0.002957629	Mollusca	Bivalvia	Pectinoida
ESV_252	28.6565598	-8.168847296	0.005667116	Mollusca	Gastropoda	Caenogastropoda
ESV_528	25.6539766	-8.006593529	0.006205196	Mollusca	Bivalvia	Veneroida
ESV_1362	15.850344	-7.310003175	0.006798378	Mollusca	Gastropoda	Caenogastropoda
ESV_1001	108.716542	-9.127777747	0.008200087	Mollusca	Gastropoda	Caenogastropoda
ESV_276	14.9877458	-7.227808081	0.015024727	Mollusca	Polyplacophora	Neoloricata
ESV_1	156.47577	-4.456645861	0.023079973	Mollusca	Bivalvia	Pectinoida
ESV_259	25.0823345	-7.976426013	0.023996087	Mollusca	Gastropoda	Heterobranchia
ESV_2546	9.13089847	-6.520293798	0.025250252	Mollusca	Gastropoda	Caenogastropoda
ESV_1104	11.5451594	-6.857615204	0.036189694	Mollusca	Gastropoda	Heterobranchia
ESV_1190	9.54968447	-6.585771059	0.038106968	Mollusca	Gastropoda	Caenogastropoda
ESV_1048	31.5483293	-8.306483266	0.044065986	Mollusca	Gastropoda	Heterobranchia
ESV_2521	498.553236	-26.31919701	7.05E-15	Mollusca	Gastropoda	Caenogastropoda
ESV_432	134.829366	-24.52489446	4.51E-11	Mollusca	Bivalvia	Pectinoida
ESV_219	280.37725	-25.54210241	5.35E-11	Mollusca	Polyplacophora	Neoloricata
ESV_693	168.175869	-24.80103248	2.02E-10	Mollusca	Bivalvia	Ostreoida
ESV_1034	135.40053	-24.53202782	3.02E-10	Mollusca	Bivalvia	Veneroida
ESV_1015	83.651278	-23.88650499	7.57E-10	Mollusca	Gastropoda	Heterobranchia
ESV_1815	50.8464003	-23.20401375	1.97E-09	Mollusca	Gastropoda	Heterobranchia
ESV_340	39.1836167	-22.85745508	3.14E-09	Mollusca	Gastropoda	Caenogastropoda
ESV_231	21.43639	-22.03729158	1.08E-08	Mollusca	Bivalvia	Veneroida
ESV_5281	25.3930389	-21.10525561	4.55E-08	Mollusca	Bivalvia	Veneroida
ESV_11	929.417387	-5.949311072	0.001609005	Mollusca	Bivalvia	Pectinoida
ESV_241	294.55559	-6.414970307	0.002991597	Mollusca	Bivalvia	Arcoida
ESV_185	43.0463643	-8.904560339	0.011105852	Mollusca	Gastropoda	Vetigastropoda
ESV_4413	4.31799049	6.347147857	0.032212866	Mollusca	Bivalvia	Veneroida
ESV_2609	22.7039926	-20.97015467	5.41E-08	Nematozoa	Chromadorea	Monhysterida
ESV_1370	24.6080419	-7.950411922	0.000599979	Nematozoa	Chromadorea	Chromadorida
ESV_444	122.9602	-9.305521963	0.000723614	Nematozoa	Chromadorea	Chromadorida
ESV_639	46.1516517	-8.854877522	0.00136233	Nematozoa	Enoplea	Enoplida
ESV_944	21.9506366	-7.782793057	0.003362114	Nematozoa	Enoplea	Enoplida
ESV_1429	14.0992815	-7.146173574	0.003752896	Nematozoa	Enoplea	Enoplida
ESV_1302	15.0432131	-7.238612696	0.013709462	Nematozoa	Enoplea	Enoplida
ESV_2277	19.7923875	-7.635123588	0.017362995	Nematozoa	Chromadorea	unclassified_Chromadorea
ESV_800	6.62785934	-6.051259815	0.025754053	Nematozoa	Chromadorea	Desmodorida
ESV_966	13.5554989	-7.086511164	0.02697746	Nematozoa	Chromadorea	Araeolaimida
ESV_3851	7.00946313	-6.135862773	0.036622789	Nematozoa	Enoplea	Enoplida
ESV_1460	7.76951302	-6.286783166	0.038204773	Nematozoa	Chromadorea	Desmodorida
ESV_4279	7.64067901	-6.268005441	0.038362535	Nematozoa	Chromadorea	Chromadorida
ESV_3516	8.76654173	-6.460603854	0.039494779	Nematozoa	Chromadorea	Desmodorida
ESV_5738	8.72297478	-6.457723706	0.043342278	Nematozoa	Chromadorea	Monhysterida
ESV_1939	5.04710192	-5.661406588	0.044316897	Nematozoa	Chromadorea	Desmodorida
ESV_3511	4.01614917	-5.339644141	0.046854591	Nematozoa	Chromadorea	Desmodorida
ESV_511	272.534286	-11.56748135	1.29E-05	Nematozoa	Chromadorea	Desmodorida
ESV_519	219.495138	-11.25524367	2.22E-05	Nematozoa	Chromadorea	Desmodorida
ESV_14291	15.9101678	-7.472635467	0.000408012	Nematozoa	Enoplea	Enoplida
ESV_1129	94.7721985	-10.04323611	0.000628399	Nematozoa	Chromadorea	Desmodorida
ESV_13701	19.4710054	-7.762053672	0.00069706	Nematozoa	Chromadorea	Chromadorida
ESV_3028	18.2525	-7.668192842	0.000729753	Nematozoa	Enoplea	Enoplida

ESV_1136	55.9124957	-9.28160808	0.000736905	Nematozoa	Chromadorea	Desmodorida
ESV_1516	57.9855799	-9.335518907	0.000791418	Nematozoa	Chromadorea	Monhysterida
ESV_1713	51.0678313	-9.1521545	0.001470411	Nematozoa	Chromadorea	Desmodorida
ESV_6391	19.3669296	-7.753338114	0.00316158	Nematozoa	Enoplea	Enoplida
ESV_2992	12.8819722	-7.169681463	0.004880776	Nematozoa	Enoplea	Enoplida
ESV_4441	20.6331378	-7.846071021	0.005518651	Nematozoa	Chromadorea	Chromadorida
ESV_2980	19.0807262	-7.731330257	0.006348574	Nematozoa	Enoplea	Enoplida
ESV_4321	11.5113615	-7.004678552	0.011669259	Nematozoa	Chromadorea	Chromadorida
ESV_5251	8.90507982	-6.633297015	0.01597164	Nematozoa	Chromadorea	Chromadorida
ESV_3119	13.5727864	-7.241481907	0.016088784	Nematozoa	Chromadorea	Monhysterida
ESV_4036	8.79209587	-6.615554667	0.016473441	Nematozoa	Chromadorea	Desmodorida
ESV_4775	9.80219334	-6.771619201	0.017471269	Nematozoa	Chromadorea	Chromadorida
ESV_4647	11.4013	-6.991517881	0.017956238	Nematozoa	Chromadorea	Desmodorida
ESV_3230	11.1600631	-6.960531541	0.020108572	Nematozoa	Chromadorea	Desmodorida
ESV_1474	80.7541635	-7.446935484	0.026370852	Nematozoa	Chromadorea	Desmodorida
ESV_489	93.0530339	-23.82852948	9.56E-10	Nemertea	Anopla	Palaeonemertea
ESV_2897	8.72892741	-20.63170546	9.36E-08	Nemertea	Enopla	Monostilifera
ESV_600	97.337502	-9.931190371	0.000804799	Nemertea	Anopla	Heteronemertea
ESV_1044	55.4399239	-9.11785567	0.00226299	Nemertea	Anopla	Palaeonemertea
ESV_2751	9.76855021	-6.61521585	0.015935454	Nemertea	Anopla	Heteronemertea
ESV_296	86.4183092	-23.92746861	7.57E-10	Nemertea	Anopla	Palaeonemertea
ESV_498	29.186328	-8.344127552	0.017467863	Nemertea	Enopla	unclassified_Enopla
ESV_582	188.222506	-8.045364374	0.04342023	Nemertea	Anopla	Palaeonemertea
ESV_565	75.6994782	-23.55819478	1.37E-09	Platyhelminthes	Rhabditophora	Prolecithophora
ESV_509	58.0345158	-23.19444752	2.02E-09	Platyhelminthes	Rhabditophora	Macrostomida
ESV_439	28.1489566	-21.85207092	1.34E-08	Platyhelminthes	Rhabditophora	Macrostomida
ESV_1168	26.8805101	-21.67253505	1.76E-08	Platyhelminthes	Rhabditophora	Macrostomida
ESV_113	600.047573	-11.59337954	1.83E-05	Platyhelminthes	Rhabditophora	Polycladida
ESV_725	43.2613864	-8.76263699	0.000107398	Platyhelminthes	Rhabditophora	Rhabdocoela
ESV_309	168.593883	-10.72374314	0.000837597	Platyhelminthes	Rhabditophora	Rhabdocoela
ESV_180	47.4700779	-8.896578676	0.003567453	Platyhelminthes	Rhabditophora	Macrostomida
ESV_282	126.61413	-9.547591527	0.005796492	Platyhelminthes	Rhabditophora	Polycladida
ESV_570	35.6744222	-8.484735202	0.005825506	Platyhelminthes	Rhabditophora	Prolecithophora
ESV_2361	30.0026803	-8.232870241	0.005829951	Platyhelminthes	Rhabditophora	Rhabdocoela
ESV_1343	31.7408564	-8.316431229	0.006423506	Platyhelminthes	Rhabditophora	unclassified_Rhabditophora
ESV_372	32.2939516	-8.341585945	0.006563361	Platyhelminthes	Rhabditophora	Rhabdocoela
ESV_1483	30.334972	-8.251199905	0.011063932	Platyhelminthes	Rhabditophora	Rhabdocoela
ESV_287	165.578858	-7.183589998	0.016363584	Platyhelminthes	Rhabditophora	Polycladida
ESV_1281	33.9248763	-8.412025932	0.017977789	Platyhelminthes	Rhabditophora	Macrostomida
ESV_1094	18.2816247	-7.520732415	0.019451618	Platyhelminthes	Rhabditophora	Rhabdocoela
ESV_1120	12.5082939	-6.972162184	0.029243674	Platyhelminthes	Rhabditophora	Rhabdocoela
ESV_270	33.6479291	-4.291602866	0.040111341	Platyhelminthes	Rhabditophora	Polycladida
ESV_3250	8.66000037	-6.447028271	0.047665982	Platyhelminthes	Rhabditophora	Rhabdocoela
ESV_977	132.141473	-24.5105149	3.66E-11	Platyhelminthes	Rhabditophora	Rhabdocoela
ESV_1109	95.6707459	-24.06784646	6.37E-10	Platyhelminthes	Rhabditophora	Rhabdocoela
ESV_1583	73.0000376	-23.702663	1.02E-09	Platyhelminthes	Rhabditophora	Rhabdocoela
ESV_2481	44.3277916	-23.02384977	2.49E-09	Platyhelminthes	Rhabditophora	Proseriata
ESV_1063	74.1190278	-21.98925625	1.13E-08	Platyhelminthes	Rhabditophora	Rhabdocoela
ESV_1131	8.85921197	-20.84690192	6.78E-08	Platyhelminthes	Rhabditophora	Polycladida
ESV_3091	113.434949	-10.30342139	5.30E-05	Platyhelminthes	Rhabditophora	Rhabdocoela
ESV_420	313.000119	-11.76719984	0.000124934	Platyhelminthes	Rhabditophora	Macrostomida
ESV_1642	16.6622221	-7.538663945	0.000986973	Platyhelminthes	Rhabditophora	Macrostomida
ESV_1801	65.0329095	-9.500144601	0.001186605	Platyhelminthes	Rhabditophora	Macrostomida
ESV_1933	49.6187293	-9.110238459	0.001341437	Platyhelminthes	Rhabditophora	Prolecithophora
ESV_1548	54.7978315	-9.252665782	0.001384227	Platyhelminthes	Rhabditophora	Prolecithophora
ESV_12811	47.1571816	-9.037304463	0.002041017	Platyhelminthes	Rhabditophora	Macrostomida
ESV_11681	24.7781842	-8.108782324	0.003927279	Platyhelminthes	Rhabditophora	Macrostomida
ESV_13431	23.9343201	-8.058774913	0.004700614	Platyhelminthes	Rhabditophora	unclassified_Rhabditophora
ESV_1597	22.9691338	-8.000188337	0.004952308	Platyhelminthes	Rhabditophora	Rhabdocoela
ESV_2821	14.8468385	-7.372191468	0.005518651	Platyhelminthes	Rhabditophora	Polycladida
ESV_3635	14.8045403	-7.364617537	0.006816316	Platyhelminthes	Rhabditophora	Rhabdocoela
ESV_774	67.4994349	-9.554353743	0.007877697	Platyhelminthes	Rhabditophora	Rhabdocoela
ESV_307	59.1558795	-9.364007415	0.009775249	Platyhelminthes	Rhabditophora	Rhabdocoela
ESV_7251	13.6368718	-7.248085613	0.009902416	Platyhelminthes	Rhabditophora	Rhabdocoela
ESV_3845	15.5294092	-7.436023041	0.013849263	Platyhelminthes	Rhabditophora	Macrostomida
ESV_1164	14.2525035	-7.310927205	0.014798261	Platyhelminthes	Rhabditophora	Prolecithophora
ESV_2563	12.4955141	-7.120612126	0.018490085	Platyhelminthes	Rhabditophora	Macrostomida
ESV_2943	11.3374344	-6.978074637	0.021511588	Platyhelminthes	Rhabditophora	Rhabdocoela
ESV_2322	10.6268591	-6.886748939	0.02353747	Platyhelminthes	Rhabditophora	Polycladida
ESV_4462	7.25447546	-6.339077911	0.02353747	Platyhelminthes	Rhabditophora	Macrostomida
ESV_4402	8.73186235	-6.604023264	0.027013938	Platyhelminthes	Rhabditophora	Rhabdocoela
ESV_1572	10.934808	-6.93069803	0.039395956	Platyhelminthes	Rhabditophora	Macrostomida
ESV_4111	6.61949066	-6.209170566	0.04436627	Platyhelminthes	Rhabditophora	Macrostomida
ESV_42	1664.69552	-9.675264567	1.20E-05	Porifera	Demospongiae	Poecilosclerida
ESV_107	1072.41793	-9.671777894	2.88E-05	Porifera	Demospongiae	Poecilosclerida
ESV_183	267.751158	-7.660408114	4.63E-05	Porifera	Demospongiae	Dendroceratida
ESV_20	5888.98316	-7.458363302	8.73E-05	Porifera	Demospongiae	Poecilosclerida
ESV_1437	60.489455	-9.245388244	0.000613783	Porifera	Demospongiae	Dendroceratida
ESV_518	70.35402	-9.462536635	0.000953591	Porifera	Demospongiae	unclassified_Demospongiae
ESV_324	57.0102677	-9.15931974	0.002433729	Porifera	Homoscleromorpha	Homosclerophorida
ESV_83	583.984026	-5.540314133	0.005392998	Porifera	Demospongiae	Poecilosclerida
ESV_322	27.8815142	-8.128074152	0.006794335	Porifera	Demospongiae	Dendroceratida
ESV_477	90.3968425	-7.907066273	0.006948918	Porifera	Calcarea	Clathrinida
ESV_150	15.3883946	-7.270237427	0.00786884	Porifera	Demospongiae	Axinellida
ESV_566	81.55699	-6.607877391	0.008588076	Porifera	Demospongiae	Poecilosclerida
ESV_530	31.940513	-8.3250157	0.009346926	Porifera	Demospongiae	Poecilosclerida
ESV_255	70.3352124	-7.067362908	0.00985606	Porifera	Demospongiae	Axinellida
ESV_376	80.9235031	-9.664572941	0.011151398	Porifera	Demospongiae	Poecilosclerida
ESV_328	64.0102485	-6.256723798	0.011484147	Porifera	Calcarea	Clathrinida
ESV_1446	10.2402316	6.982493216	0.011774343	Porifera	Demospongiae	Dictyoceratida
ESV_2363	8.34803754	7.347701812	0.014095865	Porifera	Demospongiae	Suberitida
ESV_1116	14.2000043	-7.154891901	0.014105464	Porifera	Demospongiae	Dendroceratida
ESV_1029	13.8587232	-7.11665371	0.017842384	Porifera	Calcarea	Clathrinida
ESV_765	7.12885138	7.120023536	0.017977789	Porifera	Demospongiae	Dictyoceratida

ESV_3149	7.54655883	7.202487727	0.018255402	Porifera	Demospongiae	Suberitida
ESV_611	78.6466913	-5.071794117	0.020478301	Porifera	Demospongiae	Dictyoceratida
ESV_1041	15.6948004	-7.301156102	0.021805243	Porifera	Calcarea	Clathrinida
ESV_994	32.4225311	-6.424457736	0.022709773	Porifera	Homoscleromorpha	Homosclerophorida
ESV_1098	98.5459413	-5.35246971	0.022842209	Porifera	Calcarea	Clathrinida
ESV_2192	37.6860824	-8.562638503	0.023996087	Porifera	Calcarea	Clathrinida
ESV_273	41.9682042	-6.963768436	0.02763887	Porifera	Demospongiae	Poecilosclerida
ESV_2018	7.90452274	-6.316951903	0.035213235	Porifera	Calcarea	Clathrinida
ESV_2836	8.9919859	-6.495588804	0.040464813	Porifera	Demospongiae	Verongiida
ESV_5301	161.266383	-24.78165955	2.02E-10	Porifera	Demospongiae	Poecilosclerida
ESV_895	40.0648002	-22.87594792	3.10E-09	Porifera	Demospongiae	Dictyoceratida
ESV_1145	107.680028	-22.77745986	3.50E-09	Porifera	Demospongiae	Biemnida
ESV_1368	87.7741282	-22.69827675	3.91E-09	Porifera	Homoscleromorpha	Homosclerophorida
ESV_337	33.1818214	-22.62797914	4.33E-09	Porifera	Calcarea	Clathrinida
ESV_1831	626.308851	-7.122409505	1.54E-06	Porifera	Demospongiae	Dendroceratida
ESV_1501	404.650315	-12.13783539	2.08E-06	Porifera	Demospongiae	Axinellida
ESV_831	294.552261	-11.67971813	5.62E-06	Porifera	Demospongiae	Poecilosclerida
ESV_11161	69.7804539	-9.601839581	6.57E-05	Porifera	Demospongiae	Dendroceratida
ESV_525	374.23975	-6.937523595	0.000110106	Porifera	Homoscleromorpha	Homosclerophorida
ESV_66	2299.80879	-6.416029362	0.000275738	Porifera	Demospongiae	Poecilosclerida
ESV_436	334.828478	-11.86447536	0.000353663	Porifera	Demospongiae	Dendroceratida
ESV_14461	30.6670148	8.850000181	0.000408012	Porifera	Demospongiae	Dictyoceratida
ESV_249	29.1842336	9.103380862	0.000742128	Porifera	Demospongiae	Dictyoceratida
ESV_1520	48.3789832	-9.073159826	0.000772093	Porifera	Demospongiae	Dendroceratida
ESV_2731	78.7936832	-9.777201174	0.000905244	Porifera	Demospongiae	Poecilosclerida
ESV_422	816.760324	-4.734649379	0.000979238	Porifera	Demospongiae	Poecilosclerida
ESV_913	122.552417	-10.41463324	0.00119455	Porifera	Demospongiae	Poecilosclerida
ESV_1075	21.6188975	-7.914989833	0.001377103	Porifera	Calcarea	Leucosolenida
ESV_4860	12.5135009	-7.118752197	0.001881539	Porifera	Homoscleromorpha	Homosclerophorida
ESV_887	126.40148	-6.810759568	0.004408562	Porifera	Demospongiae	Poecilosclerida
ESV_992	120.139277	-5.93582263	0.005051931	Porifera	Demospongiae	Poecilosclerida
ESV_23631	9.02919409	7.411067978	0.005507226	Porifera	Demospongiae	Suberitida
ESV_465	242.428732	-6.372560529	0.011100992	Porifera	Demospongiae	Poecilosclerida
ESV_298	268.935662	-3.346609959	0.012590931	Porifera	Demospongiae	Poecilosclerida
ESV_1484	39.285306	9.532061885	0.0156172	Porifera	Demospongiae	Hadromerida
ESV_10411	24.6060067	-8.098178503	0.020383319	Porifera	Calcarea	Clathrinida
ESV_1017	56.0269009	9.060808876	0.021511588	Porifera	Demospongiae	unclassified_Demospongiae
ESV_1625	52.5158497	-6.238302061	0.022682644	Porifera	Homoscleromorpha	Homosclerophorida
ESV_2976	5.76022895	-6.002664715	0.024069876	Porifera	Homoscleromorpha	Homosclerophorida
ESV_5693	6.73982866	-6.236541122	0.025792799	Porifera	Homoscleromorpha	Homosclerophorida
ESV_3853	8.29800466	-6.53188322	0.031525872	Porifera	Homoscleromorpha	Homosclerophorida
ESV_6398	5.0610231	-5.81566008	0.043686836	Porifera	Demospongiae	Dendroceratida
ESV_58	12.497127	5.443881917	0.046757041	Porifera	Demospongiae	Dictyoceratida
ESV_292	27.6291607	-8.116465122	0.002789828	Scalidophora	NA	Cyclorhagida
ESV_3712	13.6142435	-7.093782769	0.017362995	Scalidophora	NA	Cyclorhagida
ESV_160	127.439172	8.156879797	4.59E-05	Tunicata	Appendicularia	Copelata
ESV_345	252.125274	12.26437492	8.35E-05	Tunicata	Thaliacea	Salpida
ESV_172	66.7488867	10.34713144	0.000123878	Tunicata	Appendicularia	Copelata
ESV_1830	31.5644772	8.619868072	0.000849245	Tunicata	Appendicularia	Copelata
ESV_1898	20.6557493	8.005071489	0.002227451	Tunicata	Thaliacea	Doliolida
ESV_2141	17.2351325	8.393734269	0.002768428	Tunicata	Appendicularia	Copelata
ESV_3015	9.3600433	7.513030686	0.010239703	Tunicata	Appendicularia	Copelata
ESV_1188	8.32395015	-6.389324938	0.033955046	Tunicata	Ascidiacea	Stolidobranchia
ESV_1601	183.464648	7.079513043	0.001881539	Tunicata	Appendicularia	Copelata
ESV_3638	5.05768587	6.575224233	0.023045996	Tunicata	Ascidiacea	Enterogona